NOVA SCHOOL OF SCIENCE & TECHNOLOGY

DEPARTAMENT OF CHEMISTRY

Afonso José Reis Bernardes

BSc in Biochemistry

NEW FIGHT AGAINST TUBERCULOSIS USING PHARMACEUTICAL IONIC LIQUIDS

MASTER IN BIOORGANIC CHEMISTRY

NOVA University, Lisbon

October, 2022

DEPARTAMENT OF CHEMISTRY

NEW FIGHT AGAINST TUBERCULOSIS USING PHARMACEUTICAL IONIC LIQUIDS

AFONSO JOSÉ REIS BERNARDES

BSc in Biochemistry

Adviser: Doctor Miguel Santos
CHARM, Chemistry Department, NOVA School of Science and Technology

Co-adviser: Professor Doctor Luís Branco
Assistant professor, CHARM, Chemistry Department, NOVA School of Science and Technology

Examination Committee:

Chair: Professor Paula Branco,
Full Professor, Chemistry Department, NOVA School of Science and Technology

Rapporteurs: Professor Maria Manuel Marques,
Assistant Professor, Chemistry Department, NOVA School of Science and Technology

Adviser: Doctor Miguel Santos,
CHARM, Chemistry Department, Chemistry Department, NOVA School of Science and Technology

MASTER IN BIOORGANIC CHEMISTRY

NOVA University Lisbon
October 2022

Acknowledgments

Em primeiro, aos meus orientadores, Dr. Miguel Santos e Prof. Doutor Luís Branco por me aceitarem neste projeto que tanto me desafiou. Apesar de todos os inconvenientes, conseguiram orientar-me e encontram oportunidades para expandir o tema e exporem-me a outras áreas. Apesar da corrida que foi setembro e outubro, não me arrependo da tese que escolhi e sinto que aprendi tanto.

Um agradecimento especial ao Francisco Faísca por ter paciência para aturar as minhas frustrações com problemas e tanto me ter ajudado neste processo.

Um agradecimento ao Zeljko Petrovski por me ajudar com dúvidas e por tantas discussões interessantes.

A todo o pessoal dos laboratórios 410, 406 e 305 por tantos momentos especiais e por toda a entreajuda que tanto agradeço.

A todos os meus amigos, tanto da faculdade como fora por manterem a minha sanidade (ou gastarem-na) e por me ajudarem e apoiarem nestes momentos.

Por fim, a toda a minha família com o seu apoio constante e em especial à minha avó Natalina Silva que será para sempre lembrada.

ABSTRACT

Tuberculosis (TB) is to this day a disease that threatens public health, being the second major cause of infectious disease related deaths. Only in 2020, caused the death of 1.5 million people in highly populated or developing countries. The treatment of this disease involves multi-drug formulations including rifampicin as one of the prominent drugs used. This drug has a low bioavailability, and it is also hepatotoxic. However, rifampicin can be ionized, being an excellent target for the development of organic salts and ionic liquids (OSILs) based on this active pharmaceutical ingredient (Rif-OSIL). The ionization of this drug as well as the combination with highly polar counter-ions considerably increased its water solubility at least 450 times compared to the neutral API reported value. In parallel, it is observed a reducing in the octanol/water partition coefficient as a clear indication about the improvement of the API permeability. All Rif-OSILs based on cationic or anionic approaches were characterized by ^{1}H and ^{13}C NMR, FTIR and elemental analysis to prove the desired chemical structures. *In vivo* toxicity assays were performed in zebrafish (*Danio rerio*) to evaluate the impacts in toxicity of the drug (Rif and Rif-OSILs) when bioavailability is increased. From these assays, both catalase and glutathione-*S*-transferase were inhibited by the rifampicin organic salt, but no statistically relevant oxidative damage in the form of lipid peroxidation was observed. Another problem of rifampicin involves the low action local concentration for effective treatment. Dry powders for inhalation from both original rifampicin and the most promissory Rif-OSIL were produced through Supercritical CO_2-assisted Spray Drying and then they were tested in Andersen-Cascade Impactor to assess aerodynamic properties. Two protocols were used, one of which produced powders capable of reaching the alveoli, in which infection by *Mycobacterium tuberculosis* occurs. This work opens good perspectives to use Rif-OSILs as a sustainable and more effective therapeutic strategy for the treatment of tuberculosis.

Keywords: Rifampicin, organic salt and ionic liquid, tuberculosis, bioavailability, *in vivo* toxicity, dry powders.

RESUMO

Tuberculose (TB) é até hoje uma doença que ameaça a saúde pública, sendo a segunda maior causa de mortes relacionadas com doenças infeciosas. Só em 2020, causou a morte de 1,5 milhões de pessoas em países em desenvolvimento ou com alta densidade populacional. O tratamento desta doença envolve múltiplos fármacos, sendo um dos principais a rifampicina. Este fármaco tem uma biodisponibilidade baixa, e é também hepatotóxico. No entanto, pode ser ionizado, sendo um excelente alvo para o desenvolvimento de sais orgânicos e líquidos iónicos (OSIL) baseados neste ingrediente farmacêutico ativo (Rif-OSIL). A ionização da rifampicina, bem como a combinação com contra-iões altamente polares, aumentou consideravelmente a sua solubilidade em água pelo menos 450 vezes em comparação com o valor do API neutro reportado. Em paralelo, observa-se uma redução no coeficiente de partição octanol/água que dá uma clara indicação sobre a melhoria da permeabilidade do API. Todos os Rif-OSILs foram caracterizados por RMN ^{1}H e ^{13}C, IV e análise elementar para provar as estruturas químicas desejadas. Foram realizados ensaios de toxicidade in vivo em peixes zebra (*Danio rerio*) para avaliar os impactos na toxicidade do fármaco (Rif e Rif-OSILs) quando a biodisponibilidade é aumentada. A partir destes ensaios, tanto a catalase como a glutationa-*S*-transferase foram inibidas pelo Rif-OSIL testado, mas não foi observado qualquer dano oxidativo estatisticamente relevante sob a forma de peroxidação lipídica. Outro problema da rifampicina envolve a baixa concentração local de ação para um tratamento eficaz. O dry powders para inalação tanto da rifampicina original como do Rif-OSIL mais promissor foram produzidos através de Supercritical CO_2-assisted Spray Drying e depois foram testados num Andersen-Cascade Impactor para avaliar as propriedades aerodinâmicas. Foram utilizados dois protocolos, um dos quais produziu pós capazes de atingir os alvéolos, nos quais ocorre a infeção por *Mycobacterium tuberculosis*. Este trabalho abre boas perspetivas para a utilização de Rif-OSILs como estratégia terapêutica sustentável e mais eficaz para o tratamento da tuberculose.
Palavras chave: Rifampicina, sais orgânicos e líquidos iónicos, tuberculose, biodisponibilidade, toxicidade *in vivo*, dry powders.

CONTENTS

LIST OF FIGURES

LIST OF TABLES

List of Abreviations

^{13}C NMR	Carbon nuclear magnetic resonance
^{1}H NMR	Proton nuclear magnetic resonance
API	Active pharmaceutical ingredient
API-OSIL	Active pharmaceutical ingredient as an organic salt or ionic liquid
COSY	Correlated spectroscopy
CAT	Catalase
DMSO	Dimethylsulfoxide
DPF	Dry powder formulation
equiv.	Molar equivalent
FPF	Fine particle fraction
GSD	Geometric standard deviation
GST	Glutathione-*S*-transferase
GPx	Glutathione peroxidase
HMBC	Heteronuclear multiple bond correlation spectroscopy
HSQC	Heteronuclear single quantum coherence spectroscopy
Hz	Hertz
IR	Infrared spectroscopy
LPO	Lipid peroxidation
MMAD	Mass median aerodynamic diameter
MDR-TB	Multidrug-resistant tuberculosis

NMR	Nuclear magnetic resonance
OSIL	Organic salts and ionic liquids
PBS	Phosphate buffer solution
Rif	Rifampicin
SOD	Superoxide dismutase
XDR-TB	Extremely drug-resistant tuberculosis

1

INTRODUCTION

1.1 Tuberculosis

Mycobacterium tuberculosis infection, which typically affects the lungs, is the primary cause of the deadly disease tuberculosis. Over 80% of cases are centered in Africa and Asia, prominently in developing countries with low capacity for medical assistance for this kind of infection, represented in Figure 1.1 [1]. According to the World Health Organization (WHO) [2], only in 2020, tuberculosis claimed the lives of 1.5 million people, being the primary cause of death by infectious disease before the COVID-19 Pandemic.

This disease is spread in the form of an aerosol by patients that develop active tuberculosis. In a typical infection, the bacteria travels into the lungs through the aerosolized particles and stays dormant, being called latent tuberculosis at this stage. A patient with this condition has a 10% chance in a lifetime to develop active tuberculosis [3]. Depending on risk factors like smoking and the patient being infected with HIV/AIDS, this probability increases considerably, and the disease evolves into the deadly and extremely contagious active tuberculosis [2].

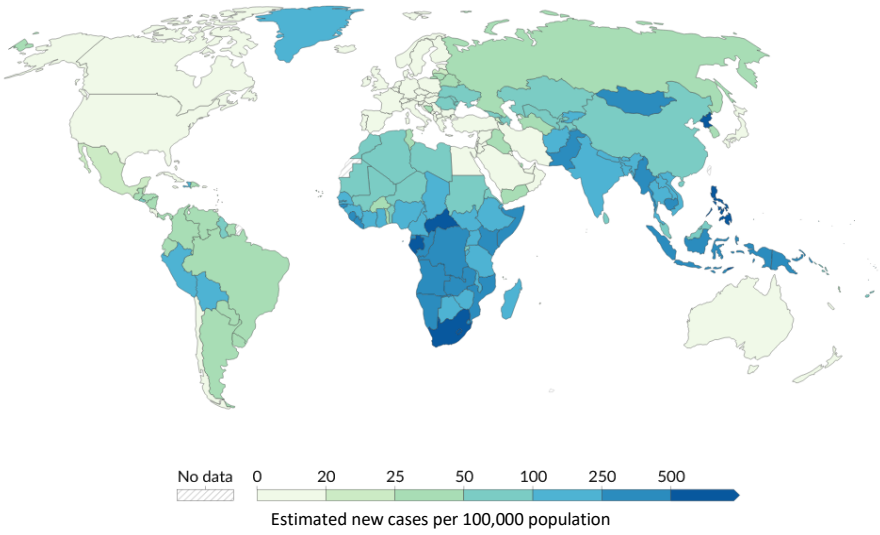

Figure 1.1 - Map of tuberculosis incidence in 2020 [4].

Symptoms of active tuberculosis include chronic coughing, fever, chills, night sweats, and fatigue, symptoms that resemble a common cold, so this disease is not only difficult to treat, but also difficult to diagnose from symptoms alone. Clinical diagnosis of tuberculosis involves an x-ray of the lungs in search of specific structures, called granulomas, and a culture of sputum of the infected [5].

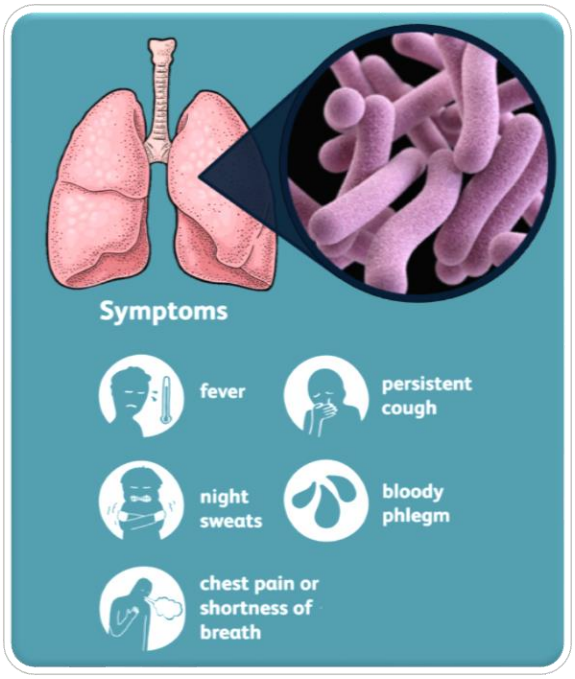

Figure 1.2 - Symptoms of tuberculosis (image taken from [6]).

The most optimal method to combat such a deadly disease would be a vaccine. Unfortunately, the only licensed vaccine for tuberculosis is BCG (bacille Calmette-Guerin), one-hundred-year vaccine administrated in infants to prevent severe forms of tuberculosis [7]. While a plethora of vaccines is being researched and in clinical trials, a short and effective treatment is still to be put in place. If the treatment is not efficient, resistant strains can emerge. These are called multidrug-resistant tuberculosis (MDR-TB) and extremely drug-resistant tuberculosis (XDR-TB).

Nowadays, the search for new drugs for the treatment of both tuberculosis and drug-resistant tuberculosis is extensive and usually based on screening compounds that present antibiotic activity without understanding the mechanism of such activity [8]. Knowing a specific mechanism in bacteria helps the development of a drug that can disrupt it effectively. In the case of *Mycobacterium tuberculosis*, three main targets are currently used: electron transport chain, cell wall synthesis, and transcription/translation machinery [9]. Unfortunately, the mycobacterium is known to bypass disrupted mechanisms or develop resistance if treatment is not completed [10]. While research is being conducted to discover new drug targets, optimization of already applied pharmaceutical ingredients is imperative and necessary.

1.2 Treatment of tuberculosis

The treatment of tuberculosis is a difficult and strenuous task, particularly for developing countries with limited access to health care, by involving a 6-month chemotherapy treatment with four standard first-line antimicrobial drugs: rifampicin, ethambutol, pyrazinamide, and isoniazid, shown in figure 3 [11]. This treatment was developed gradually toward the end of the 20th century: ethambutol in the 1960s, rifampicin, and isoniazid in the 1970s, and pyrazinamide in the 1980s [11].

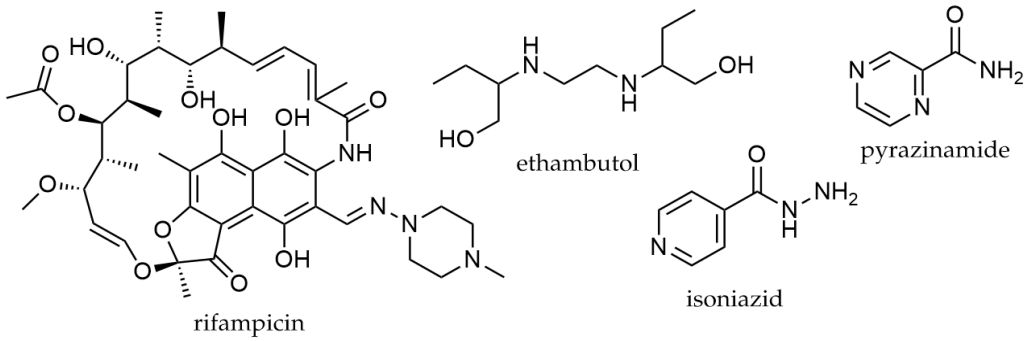

Figure 1.3 - Chemical structures of rifampicin, ethambutol, isoniazid, and pyrazinamide.

Although this method has been effective for decades, there are pressing issues centered on drug side effects and lengthy treatment courses [9][12]. Many drugs used for the treatment of tuberculosis entail serious side effects like headaches, lack of coordination, temporary discoloration, and nausea, to name a few examples [13]. These side effects, in combination with lengthy treatment, combine into a high dropout rate. Incomplete therapy opens the way to MDR-TB and XDR-TB, which are considered serious public health threats. The reported successful treatment rate for MDR-TB is 55% and only 30% for XDR-TB cases [9]. Even with specific care for these resistant variations, the WHO reports that cases of MDR-TB keep growing year by year, as shown in Figure 1.4. The decline observed in 2020 is due to the COVID-19 pandemic's associated precautions and lack of adequate evaluations [14].

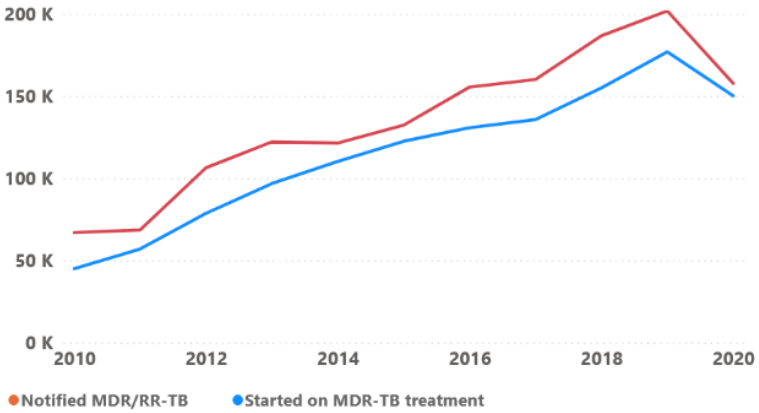

Figure 1.4 - Notified cases and enrolment in treatment of multidrug-resistant tuberculosis by WHO [15].

1.3 Active pharmaceutical ingredients (API)

An active pharmaceutical ingredient is the drug's main component that is used to produce a certain effect in the organism when administered. These compounds are the basis for pharmaceuticals to treat so many diseases and conditions and must be extensively studied for side effects and correct dosage, as well as their mechanism of action, toxicity, administration, bioavailability, dosage vs effect balance, among many other properties.

Bioavailability can be described as the capacity of an API to reach systemic circulation and to be available in its site of action. The Biopharmaceutics Categorization System (BCS) is a classification system that emphasizes bioavailability and is intended to help and expedite pharmacological development. It considers the API's aqueous solubility and intestinal permeability, being divided in four classes, as represented in Figure 1.5 [16].

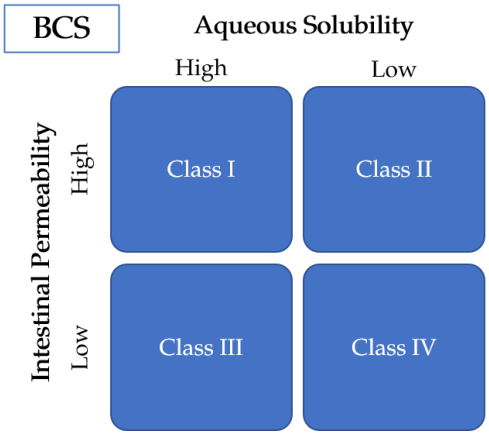

Figure 1.5 - Different classes within the Biopharmaceutics Classification System [16].

A prevalent problem in drug development is polymorphism, where the same compound presents different crystalline forms that can have different characteristics like bioavailability [17]. Changes in synthetic methodology or production can be implemented to reduce physicochemical differences or prevent the formation of different polymorphs but this can be a strenuous and expensive process for pharmaceutical industry.

1.3.1 Antibacterial drugs

Antibacterial drugs or antibiotics are active pharmaceutical ingredients that are used to impeach or retard the growth and spread of bacteria [18]. These can be specific for certain strains of microorganisms, or of broad spectrum and for application against diverse strains. There are varied mechanisms antibacterial drugs can be used against bacteria, depicted in Figure 1.6. For example, the first isolated antibacterial drugs, known as penicillins, inhibit the completion of the synthesis of peptidoglycans, responsible for cell wall assembly. This way, this cell wall weakens, and the osmotic balance of the cell is hampered [19]. Furthermore,

water flows inside the cell without a mechanism to stop it, causing lysis and death [19]. This is a mechanism of one class but many others affecting other parts of the cell's survival mechanisms such as protein synthesis, fatty acid metabolism or DNA and RNA transcription have been reported [20]. In this thesis, we will focus on rifampicin, an ansamycin with the latter mechanism of action.

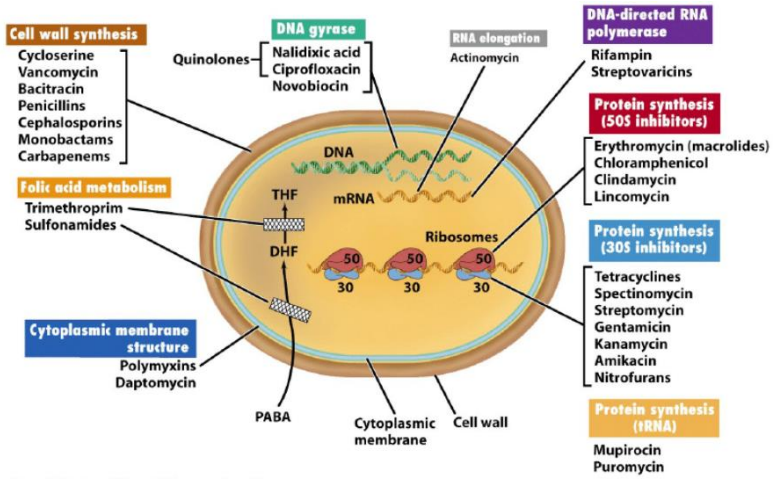

Figure 1.6 - Classes of antibiotics and respective mechanisms of action [20].

1.3.2 Ansamycins

Ansamycin was a name given in 1973 by Prelog and Oppolzer to a series of coloured compounds that had both a chromophore, in the form of an aromatic ring, and an aliphatic chain that connected opposing positions of this aromatic ring [21]. This group can be subdivided in two, separating the compounds with a benzene ring and those with a naphthalene one. This difference in aromatic ring also changes the type of activity associated with each compound. Ansamycins with benzene rings are mainly associated with anti-tumoral activity, while the naphthalene ones are associated with antimicrobial or antiviral activities [20](Figure 1.7). The most known compounds from the latter group are the rifamycins, in where rifampicin is included.

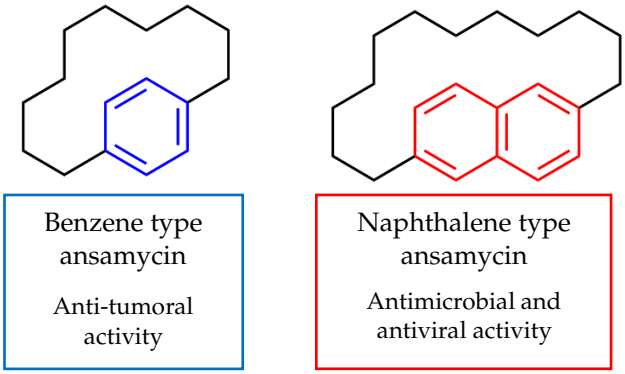

Figure 1.7 - Types of ansamycins and corresponding activities [20].

1.3.3 Rifampicin

Rifampicin is a commonly used drug in the treatment of bacterial infections discovered in 1957 and later produced and distributed in 1968. This drug was isolated from *Amycolatopsis rifamycinica*, and since its discovery it has been used in the treatment of tuberculosis as a first line drug.

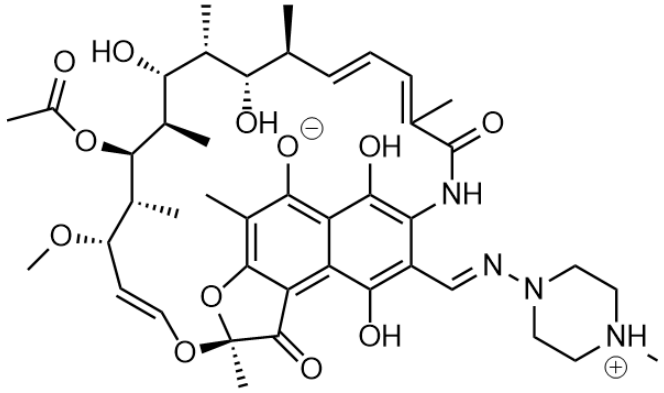

Figure 1.8 - Chemical structure of rifampicin.

Rifampicin is classified as a class II drug in the BCS system (low solubility, high intestinal permeability) but reported data suggests it can be classified as a class IV drug (low solubility, low intestinal permeability)[22]. Its solubility depends on the local pH and it's a typical zwitterionic drug. A zwitterionic compound is a compound with equal number of positive and negative charges that in total equates to formal charge zero. At pH lower than 2, anionic alkoxyl group (pKa=1.7 [23]) protonates into an alcohol group, obtaining a formal positive charge which significantly raises rifampicin's solubility. This also applies to pH higher than 8 when the protonated piperazine ring deprotonates (pKa = 7.9 [23]) to obtain a formal negative charge [23]. Unfortunately, this means that rifampicin possesses good solubility in the stomach and intestines, but very low solubility in the serum. However, if an approach could allow rifampicin to be ionized in these conditions, bioavailability of this API would increase considerably.

1.3.4 Mechanism of action of rifampicin

This drug inhibits the transcription of RNA by bonding to the RNA polymerase. It binds directly to the exit of RNA on the polymerase and prevents elongation beyond three nucleotides [24]. This interaction is centred in multiple hydrogen bonds between alcohol and ester groups of rifampicin and diverse groups from the amino acids, illustrated in Figure 1.9 [25]. The binding is strong and, most often than not, will cause the death of the bacteria through blocking its ability to transcribe DNA. Unfortunately, the most common resistance to this drug is developed after only one mutation, which changes a serine into a leucine, affecting the

interactions highlighted by a red circle in Figure 1.9 [26]. This change not only removes one hydrogen bond from the interaction completely, but also impeaches the other interaction made by the same atom considering leucine has a longer side chain than serine. This diminishes the strength of the interaction between rifampicin and the RNA Polymerase and turns this drug ineffective [20].

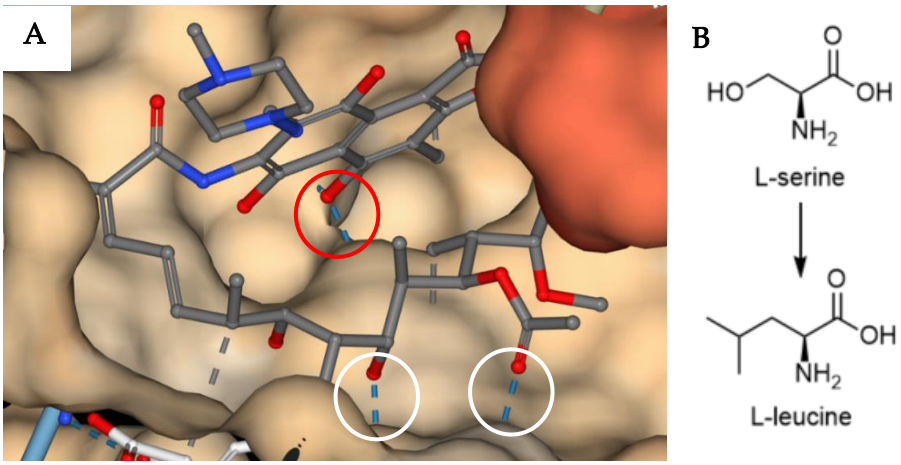

Figure 1.9 - A) Three-dimensional structure of rifampicin and interactions in binding site in *Mycobacterium smegmatis* [25]; B) Chemical structures of L-serine and L-leucine.

1.4 Organic salts and ionic liquids (OSIL's)

Ionic liquids are organic salts with melting points usually under 100 ºC [27]. These compounds are constituted by exclusively organic cations and organic or inorganic anion. In this thesis, the term ionic liquid will be seldomly used because low melting point organic salts were not obtained.

This area of science has increased in popularity dramatically since the start of the century and has maintained its importance [28]. A steady number of publications and patents have been reported as of late, illustrated in Figure 1.10, representing an interesting and promising area of study.

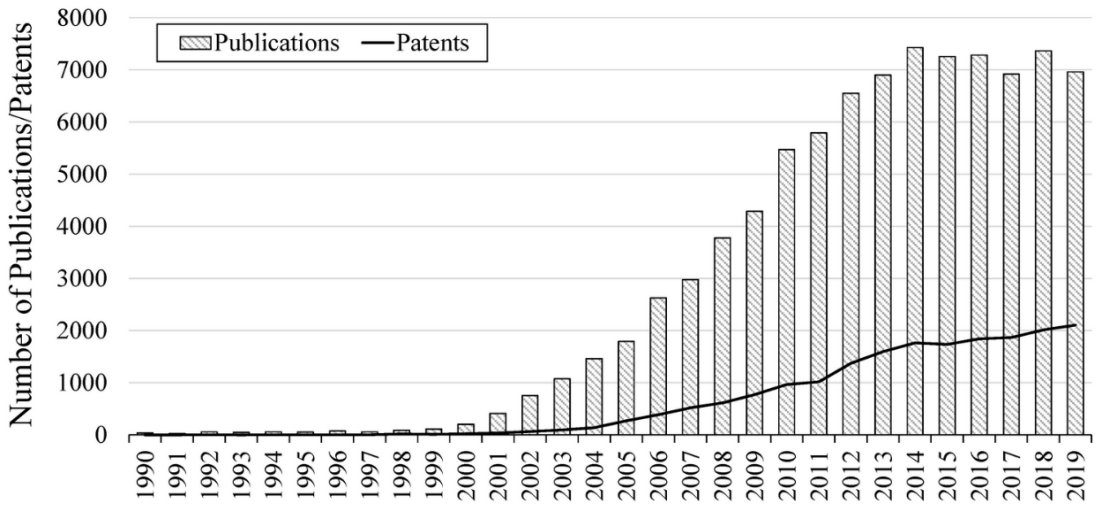

Figure 1.10 - Plot of publications and patents related to ionic liquids per year between 1990 and 2019 (taken from SciFinder^{TM} database containing the concept "ionic liquid")

The earliest discovery of such compounds is dated back to 1914 reported by Paul Walden that neutralized triethylamine with nitric acid and formed a low melting point salt represented by [Et_3NH][NO_3] [29]. This was the first case that was reported of a protic ionic liquid, that Walden found interesting due to the relation between its high conductivity and their molecular size [29]. Unfortunately, the potential of these discoveries was mostly unnoticed until, in 2000, when this subclass was rediscovered by Hiroyuki Ohno [30]. OSILs have greatly evolved since these times, having applications in rather diverse areas like organic chemistry, electrochemistry, biochemistry, and medicinal chemistry, being used as solvents, catalysts and much more (Figure 1.11).

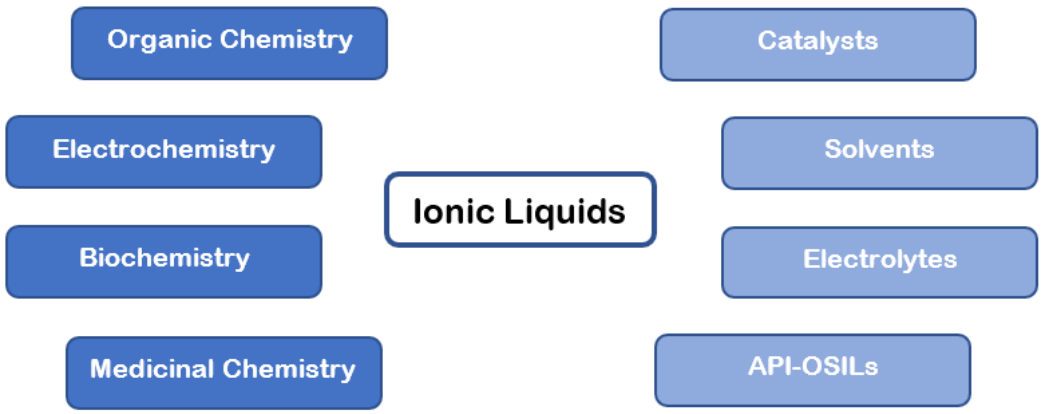

Figure 1.11 - Main scientific areas for applications of OSILs.

There are three main generations of OSIL research shown in Figure 1.12. The first generation focuses on the discovery of new ionic liquids and characterization of those novel liquids. In this generation, the formation of an ionic liquid was more like a coincidence and so those same ionic compounds would need to be studied. In the second generation, a variety of reported cations and anions are used to produce OSILs and in so obtain compounds appropriate to the application desired. Third generation research centers on obtaining compounds with improved biological properties by incorporating APIs as one or more components of novel OSILs, as to overcome pharmaceutically relevant issues or enhance activity starting from a determined molecule with biological activity with the capacity to form OSILs [31]. These novel compounds are known as Active Pharmaceutical Ingredients as Organic Salts or Ionic Liquids.

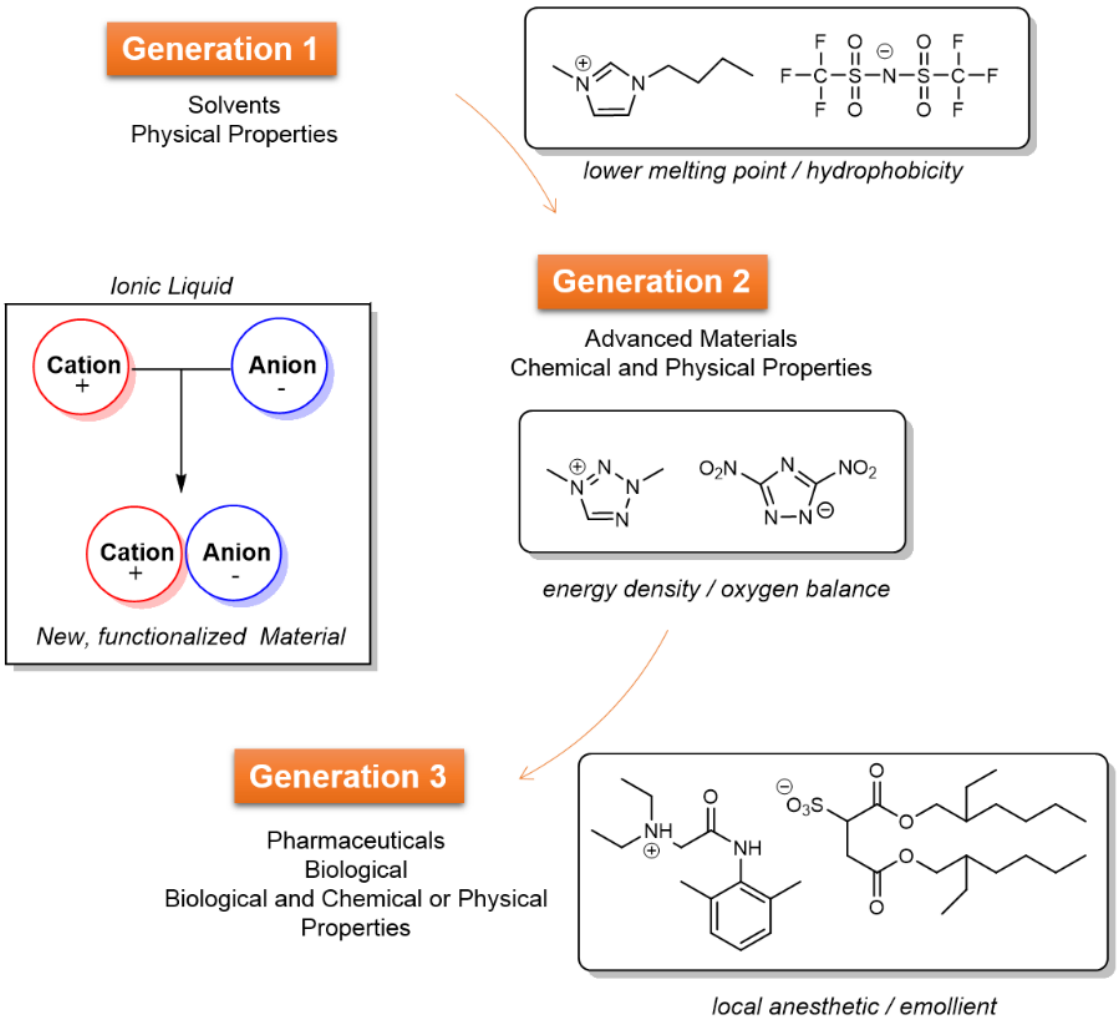

Figure 1.12 – Generations of OSIL research and examples of developed compounds ([32] adapted from [33]).

1.5 Organic salts and ionic liquids based on active pharmaceutical ingredients (API-OSILs)

In recent years, diverse organic salts and ionic liquids have been applied in the pharmaceutical field. These ionic compounds can be applied in the form of alternative solvents for API synthesis preventing solvent losses and turn processes overall greener [31]. Furthermore, they can be used as crystallizing solvents to produce specific polymorphs with increased bioavailability and shelf life. These applications involve the processes of synthesizing and producing the APIs, but these can be applied in the formulations for drug administration [31].

OSILs can be used as cosolvents for APIs, improving water solubility by forming an API/OSIL aggregate. This can be done instead of using organic cosolvents like ethanol, methanol or DMSO. The OSIL can behave as an hydrotrope, having a similar behavior to a surfactant, or forming micellar structures around the API. Jesus, A et al. 2019 [34] and 2021 [35] showed promising results with this approach, improving water solubility of the tested APIs while no significant increase in cytotoxicity was observed.

Another approach involves the synthesis of API-OSILs where at least one constituting ion is an active pharmaceutical ingredient. Turning the API into these ionic compounds improves properties like aqueous solubility and permeability considerably. Furthermore, the formation of these salts can reduce the melting point of the API and form an ionic liquid that negates any problems related to polymorphism. Ferraz et al. [36] reports the synthesis of ampicillin based API-OSILs allowing a remarkable improvement in the original API's solubility at least 10 times [37]. Furthermore, body temperature ionic liquids were obtained which present a competitive alternative for the original marketed drug due to lower cytotoxicity and higher antiproliferative activity [38]. This approach can also produce compounds with lower water solubility due to lipophilic counter-ions. This alternative approach can remediate high water solubility problems such as low permeability and fast drug excretion.

Regarding the improvement of antibiotics, our group has researched the properties of β-lactam (amoxicillin and penicillin G hydrolysates, and ampicillin) [39], [40] and fluoroquinolone (ciprofloxacin, norfloxacin, and mefloquine) [41]–[44] API-OSILs and their biological activities against resistant and non-resistant bacteria strains. It was demonstrated that properties such as 1-octanol/water partition coefficient and water and PBS solubility could be modulated through counter-ion choice. In the case of the β-lactam-based OSILs, a synergistic interaction let to a considerable increase in antimicrobial activities against drug resistant strains of *Staphylococcus aureus* and *Escherichia coli* in comparison with the original drug.

1.6 Biological studies using zebrafish as an animal model

Toxicity and activity studies are critical to drug development and approval. Biological models are a valuable tool frequently used in these studies, where studies using the zebrafish (*Danio rerio*) model are among the most popular. Despite obvious anatomical differences with humans, these fish maintain very similar physiological and genetic similarities, including 70% of human disease genes [45]. Toxicity and activity studies using this fish as a model are extensively reported in literature for drug development, including development of new antibacterial and anti-cancer agents [46], [47]. Furthermore, these animals are easily genetically modified and have a well-characterized genome. In addition, they are easy to maintain in the laboratory [48].

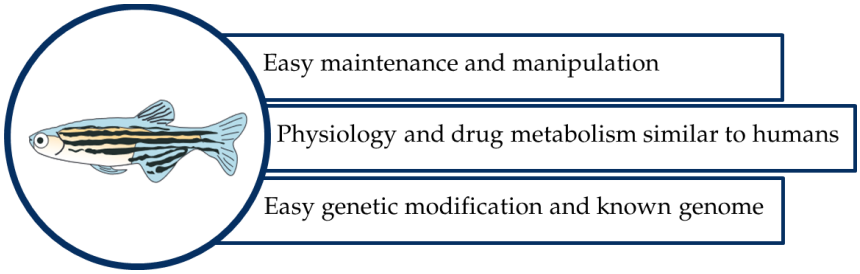

Figure 1.13 - Advantages of using zebrafish as animal model [49].

1.6.1 Oxidative stress biomarkers

Oxidative stress describes a disproportion between the organism's ability to metabolize reactive oxygen species (ROS) and their respective production or repair the resulting damage [50]. Dysregulation in this equilibrium due to exposure to toxic compounds may result in extensive tissue and biomolecular damage [51]. Monitoring biomarkers related to oxidative stress, such as catalase, superoxide dismutase (SOD), glutathione-S-transferase, and lipid peroxidation (LPO), can indicate whether a given compound is toxic and to what degree [50].

Glutathione-S-transferases (GSTs) are a group of metabolic enzymes responsible for catalysing a detoxification reaction [52]. This reaction is the nucleophilic attack by reduced glutathione on xenobiotics with electrophilic carbon, nitrogen, or sulphur atoms [53]. This phase II biotransformation reaction not only prevents these groups from reacting with important biomolecules but also increases the solubility of the compound to facilitate removal from the cell by specific transporters [54]. Later, the xenobiotic is turned into mercapturic acid and removed from the organism through urine or bile [52], [54].

Superoxide dismutase (SOD) is responsible for catalysing the dismutation of superoxide radical into molecular oxygen and hydrogen peroxide [55]. This still reactive hydrogen peroxide can then be neutralized by several enzymes, including catalase (CAT) and glutathione peroxidase [56]. Xenobiotics can cause an imbalance in this process, diminishing the organism's ability to metabolize these ROSs, and causing oxidative damage [56]. One type of

oxidative damage is lipid peroxidation. The excess of ROS in the cell from exposure to xenobiotics can initiate radical-driven chain reactions that result in membrane lipid peroxidation [57]. These lipids can then decompose into a variety of highly cytotoxic products, malonaldehyde being one such products [58]. This compound can be monitored to evaluate the extent of oxidative damage caused by xenobiotics.

Relevant alterations in these biomarkers can correlate with drug toxicity and present as excellent indicators for drug development.

1.7 Dry powder formulations

Pulmonary delivery is a premium method of treating lung diseases, from common asthma to lung cancer [59]. Due to the lung's physiognomy (high blood flow, low enzymatic activity, and a thin absorption membrane [60,61]), this kind of administration increases the treatment's efficiency through local drug delivery. This approach not only avoids first-pass metabolism in the liver but also allows a lower dosage that entails lesser systemic side effects [60,62]. This latter point was particularly important due to rifampicin's known liver toxicity [63].

In this work, in order to deliver the drug into the lungs, dry powder formulations were produced. Spray drying is the standard technique to obtain such dry powders which revolve around the atomization of a liquid solution into fine droplets through a spray nozzle to produce fine dry particles [64]. Several variations of this technique have been developed by the scientific community, some of which reaching the commercial stage [65]. One such developed process was supercritical CO_2-assisted spray drying. This green and sustainable technique uses supercritical carbon dioxide to aid the drying process as a cosolvent [64]. Supercritical CO_2 is obtained from an increase in temperature and pressure past the critical temperature and pressure points, as evidenced by Figure 1.14 [66].

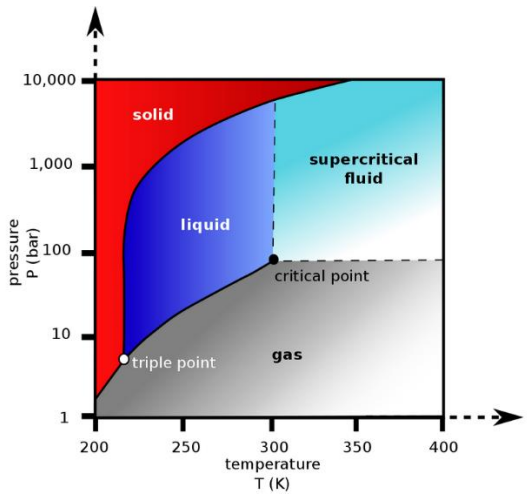

Figure 1.14 - Phase diagram of CO_2.

A supercritical fluid presents as both a gas and a liquid and possesses properties from both states such as the diffusion properties of a gas and the solvating properties of a liquid [67]. Supercritical CO_2 has been particularly useful in applications such as extractions, where the high solvating properties and the ease in its removal from extracted compounds shine while being a green and sustainable process by avoiding organic solvents [68].

In Supercritical CO_2 - assisted Spray Drying, supercritical CO_2 is a cosolvent for a casting solution. When this expanded mixture is atomized through a nozzle, the droplets formed through this process subdivide due to the vaporization of CO_2 caused by the sudden change in pressure [64]. Thus, the drying process is more efficient, and the dry particles produced are finer and better suited for inhalation [64]. In fact, SASD provides a green and sustainable one-step process to produce fine dry powders, although optimization of working variables is central to obtaining good results. Such variables can range from temperature, pressure, and the phase's behaviour to the nozzle's diameter or the cyclone's efficiency, proving to be a fine balance between physics, chemistry, and engineering [65].

To produce dry powder formulations, excipients needed to be chosen. Trehalose is a disaccharide commonly used as an excipient in pharmacologic formulations and is used as a stabilizer for the APIs but is known to be slightly hygroscopic which diminishes the dispersibility for inhalation [66]. L-Leucine is used in lower quantity in tandem with trehalose to serve as a dispersion enhancer that prevents hydration of the powder [66]. So far, there are no reports either using SASD as a process applied to rifampicin, or trehalose used as an excipient in this kind of formulation, proving to be an interesting approach in rifampicin dry powder formulations.

Figure 1.15 - SASD apparatus.

2

EXPERIMENTAL SECTION

2.1 Reagents and Equipment

Most reagents are listed below and were acquired from several chemical suppliers and used without further purification. The remaining reagents were previously synthesized within the group.

Reagents acquired from Carbosynth (Switzerland):

- Rifampicin (96.5%)

Reagents acquired from Sigma-Aldrich (USA):

- Amberlyst® 15 (H) (capacity of 1,25 meq/mL) ion exchange resin
- L-Leucine (>98%)
- Methanesulfonic acid (>99%)
- *Para*-toluenesulfonic acid monohydrate (99%)

Reagents acquired from Merck (Germany):

- Sodium 1-hexanesulfonate (>99%)

Reagents acquired from TCI (China):

- D-(+)-Trehalose Dihydrate (>98%)
- Choline Chloride (>98%)
- 1-Bromododecane (98%)
- 2-(Dimethylamino)ethanol (99%)
- 1-Methylimidazole (>99%)
- Sodium 1-propanenesulfonate (98%)
- Sodium 1-nonanesulfonate (98%)

Reagents acquired from Thermo Scientific (USA):

- 1-Bromobutane (98%)

Reagents acquired from Alfa Aesar (USA):

- Amberlyst® 26 (OH) (capacity of 0.8 meq/mL) ion exchange resin
- 1-Bromohexane (99%)
- 1-Bromooctane (>98%)
- N-Methyldiethanolamine (98%)

All synthesis of the different compounds were performed with glass and plastic available current laboratory materials.

Common use equipment in the lab included a rotary evaporator (Rotavapor R-100 BUCHI, Switzerland), a Schlenk line (Edwards RV5 vacuum pump, USA), an analytical balance (Sartorious R200 D, Germany) and a lab microwave (Monowave 450, Aston Paar)

Nuclear magnetic resonance (NMR) spectra were obtained via Bruker ARX400 400MHz at 298K and analyzed with MestreNova. The ^{1}H and ^{13}C spectra of all compounds with rifampicin were acquired in deuterated dimethylsulfoxide (DMSO-*d6*) and the remaining spectra were in deuterated water (D_2O). Both deuterated solvents were acquired from Eurisotop. Chemical shifts are reported upfield in parts per million (ppm). IR spectra were obtained in a Perkin Elmer Spectrum Two FT-IR spectrophotometer with a Universal ATR Sampler accessory. UV-Vis spectra were obtained in a CARY 100 Bio spectrophotometer.

The elemental analysis assays were performed in a Thermo Finnigan-CE Instruments Flash EA 1112 CHNS series under standard conditions (T combustion reactor 900 C T GC column furnace 65 C, O_2 flow 250 mL/min), He flow 130 mL/min, multiseparation SS GC column, at the REQUIMTE Analysis Lab, Department of Chemistry in NOVA School of Science.

2.2 Methods

2.2.1 Solubility assays

The solubility assays of the Rif-OSILs were performed in water and PBS at 37 ºC. This assay consisted in adding Milli-Q water into a measured amount of compound until it dissolved. The dissolution is determined by observation. For each compound, duplicate assays were performed, and the results are presented as averages.

2.2.2 Partition coefficient assays (K_{OW})

Partition coefficient indicates a measure of lipophilicity and hydrophilicity of a compound. By stirring two immiscible phases, in this case water and 1-octanol, with our studied compound it's possible to determine the octanol/water partition coefficient (K_{ow}) by comparing the quantity of compound in each phase. The protocol for the determination of this constant was obtained from Gard et al. [69].

$$K_{OW} = \frac{(A_i \times df_i - A_f \times df_f) \times V_{water}}{A_f \times df_f \times V_{octanol}}$$

A_i and A_f are the absorbances of the aqueous layer before and after extraction. V_{water} and $V_{octanol}$ are the volumes of the water and 1-octanol phases. Finally, df_i and df_f are the dilution factors used to find A_i and A_f. We can simplify this expression by considering all dilution factors and phase volumes are equivalent. Although the method is accurate, due to rifampicin's lack of water solubility, most assays used octanol as starting and ending phase. Therefore, the expression needed to be adapted to the following.

$$K_{OW} = \frac{A_f \times df_f \times V_{water}}{(A_i \times df_i - A_f \times df_f) \times V_{octanol}}$$

In this expression A_i and A_f become the absorbances of the 1-octanol phase. A solution of 1 mg/mL of compound was made using 1-octanol saturated with water. 1 mL of this solution and 1 mL of water saturated with 1-octanol was stirred for 2 hours. The mixture was then centrifuged, and an aliquot of the octanol phase was taken. The starting solution's absorbance was compared to the final absorbance using the latter expression. All absorbances were determined at 339 nm in a CARY 100 Bio UV-Vis spectrophotometer.

2.2.3 *In vivo* toxicity assays in zebrafish

2.2.3.1 Experiment design

The selected biological model was zebrafish (*Danio rerio*), obtained from a national commercial supplier (Aquaplante, Portugal). The fish were acclimated to laboratory conditions for two days before the exposure assays. Housing conditions for the fish involved 10 L plastic containers with filtered de-chlorinated tap water with pH = 7.1±0.2 at 22±1ºC, photoperiod 12h light and 12h dark, and steady aeration above 6mg O_2/L. Furthermore, the fish were fed daily with Tetra brand dry flakes.

The assays involved a total of 38 fish that were exposed to two different compounds (rifampicin and cholinium rifampicinate [$N_{1,1,1,2OH}$][Rif]) at three different concentrations: 0.25 mg/L, 1.25 mg/L, and 2.5 mg/L. Assays using rifampicin contained 1 mL of methanol to dissolve the API before adding it to the aquarium water resulting in a concentration of 0.0001% v/v (a control with the same concentration of methanol was done as well). The fish were collected after 96 hours of exposure and then euthanized and conserved by freezing at -80 ºC.

2.2.3.2 Sample treatment

The fish were homogenized to obtain the cytosolic fraction using a Tissue Homogenizer (Tissue Master 125, Omni) in 2 mL of phosphate buffer saline solution (PBS: 140 mM NaCl (Panreac, Spain), 10 mM Na_2HPO_4 (Sigma Aldrich, USA), 3 mM KCl (Merck, Germany), 2 mM KH_2PO_4 (Sigma-Aldrich, USA), pH=7.4) and transferred to microtubes (2 mL). Then, the samples were centrifuged at 15,000×g for 15 minutes at 4 ºC (VWR, Hitachi Koki Co., Ltd). The microtubes were then stored at -80 ºC.

2.2.3.3 Bradford assay

In accordance with Bradford's procedure, Bradford assays were carried out [50]. Six successive dilutions were prepared in PBS using Bovine Serum Albumin - BSA (NzyTech, 98%) as a standard, from a 4 mg/mL stock solution to build a calibration curve ranging from 0 to 2 mg/mL. Then it was added 10 µL of BSA standard into standard wells, and 190 µL of Bradford reagent in a 96-well microplate (Greiner bio-one, Germany). Remaining wells were filled with 10 µL of diluted supernatant sample solution (1:20) and 190 µL of Bradford reagent. Absorbance was read at 595 nm in a microplate reader (BIO-RAD Benchmark microplate reader). For each sample total protein concentration was determined using the previously referred calibration curve to normalize the biomarker results.

2.2.3.4 Catalase assay

The catalase activity assays were performed using a method adapted from Aebi [70] for microplates [71]. This method is based on the reaction of hydrogen peroxide with methanol catalysed by catalase that produces formaldehyde. This latter compound is quantified colorimetrically with 4-amino-3-hydrazino-5-mercapto-1,2,4-triazole (Purpald). This compound forms a bicyclic heterocycle in the presence of aldehydes which after oxidation are purple. The assay was performed in a 96 well microplate (Greiner bio-one, Germany). Several formaldehyde standards with concentrations between 0 and 75mM were prepared from a stock solution of 4.25 mM formaldehyde (Sigma-Aldrich, USA). In each well were added 100 µL of assay buffer, 30 µL of methanol (Scharlab, Spain) and 20 µL of formaldehyde standard or supernatant sample. The reaction started with the addition of a diluted hydrogen peroxide solution (3.5mM, Sigma Aldrich, USA) to all wells and incubated for 20 minutes at room temperature. 30 µL of potassium hydride 10M (Chem-lab, Belgium) was added to all wells to stop the reaction, followed by the addition of 30 µL of Purpald (Sigma-Aldrich, USA). The microplate was covered and incubated for 10 minutes on a shaker at room temperature and 10 µL of potassium periodate (Sigma-Aldrich, USA) was added following the incubation. The microplate was covered once again and incubated for 5 minutes in the same previously referred conditions. The absorbances were read at 540 nm in a microplate reader (VICTOR Nivo™, PerkinElmer, USA). Through the determined calibration line, total enzyme activity was obtained. Results are expressed in relation to the total protein concentration of the sample.

2.2.3.5 Glutathione-*S*-transferase assay

The glutathione-*S*-transferase (GST) assays were performed according to a method described by Habig et al. [72] and optimized for 96-well microplates. In this assay, 1-chloro-2,4-dinitrobenzene (CDNB) is used as a substrate which is compatible with a broad range of GST isoenzymes. After conjugation of the thiol group with the substrate, an increase in absorbance at 340 nm is observed. 180 µL of a reaction mixture (100 µL of 200 mM reduced glutathione; 100 µL of 100mM CDNB (Sigma- Aldrich, USA); 9.8 mL PBS (Sigma-Aldrich, USA)) was added to the wells of the microplate (Greiner Bio-one, Germany) with 20 µL of supernatant sample. Absorbance was read 6 times in 1-minute intervals in a microplate reader (VICTOR Nivo™, PerkinElmer, USA) to obtain total enzyme activity. Results are expressed in relation to the total protein concentration of the sample.

2.2.3.6 Lipid peroxidation assay

The lipid peroxidation (LPO) assays were performed according to the TBARS (thiobarbituric acid reactive substances) protocol [73]. To 2 mL microtubes it was added 5 µL of

malonaldehyde standard or supernatant sample, 45 µL of phosphate buffer, 12.5 µL of sodium dodecyl sulphate (Merk, Germany) solution (8.1%), 93.5 µL of trichloroacetic acid (Panreac, Spain) solution (20%, pH 3.5), 93.5 µL of thiobarbituric acid (Sigma-Aldrich, USA) solution (1%), and 50.5 µL of Milli-Q ultrapure water. Each microtube was centrifuged at 2,000 rpm for 1 minute, the lids were punctured with a needle and were incubated in boiling water for 10 minutes. Then the tubes were put on ice to cool and 62.5 µL of Milli-Q ultrapure water were added to each one. 150 µL of the contents of the microtubes were transferred into a 96-well microplate wells in duplicates. Absorbance was read at 530 nm with a microplate reader (VICTOR Nivo^{TM}, PerkinElmer, USA). A calibration curve was built using the MDA standards (range: 0 - 0.1 µM) for quantification. Results are expressed in relation to the total protein concentration of the sample.

2.2.3.7 Statistical analysis

The statistical analysis of the results was done using Prism software (GraphPad Prism version 8.0.1; Dotmatics) at a significance level of 5%. The homogeneity of variances was tested through Levene's test. In case of failure, Kruskal-Wallis ANOVA nonparametric test was used instead.

2.2.4 Methodology involving dry powder formulations

2.2.4.1 Particle preparation

A casting solution composed by 8.08% (w/v) trehalose, 0.43% (w/v) leucine and 0.43% (w/v) of rifampicin or Rif-OSIL was prepared with 85% (v/v) distilled water and 15% (v/v) ethanol. The particles were produced using the supercritical CO_2- assisted spray-drying (SASD) apparatus represented previously in figure 11. Briefly, liquefied CO_2 was pumped at 25 mL/min using an HPLC pump (Knauer HPLC pump K-501) and heated in an oil bath at 80 ºC. In parallel, the casting solution was pumped at a rate of 3.5 mL/min, also using a high-pressure pump (Knauer Smartline pump 1000). Both streams were delivered into the static mixer (3/16 model 37-03-075 Chemieer, 4.8 mm diameter, 191 mm length and 27 helical mixing elements), which was enrolled by a heating tape (85±5ºC), controlled by a Shinko FCS-13A temperature controller. A near-equilibrium mixture was achieved by the CO_2 solubilization into the liquid solution in the static mixer. Then, it was atomized into a precipitator through a 150µm internal diameter nozzle. At the same time, a flow of heated compressed air (T_{Air}=100 ºC and $F_{Air,in}$=30 m^3/h) entered the precipitator to evaporate the liquid solvent. The particles where then separated from the CO_2-solvent flow by a high-efficiency cyclone and collected in a glass vessel.

The process's yield can be calculated as follows:

$$\eta_{SASD}(\%) = \frac{total\ mass\ \ after\ SASD\ (g)}{total\ mass\ before\ SASD\ (g)} \times 100$$

Dry powder API loading determines the percentage of API that composes the powder produced. This parameter can be calculated as follows:

$$API\ Loading(\%) = \frac{quantificated\ API\ mass\ (mg)}{total\ dry\ powder\ mass\ (mg)} \times 100$$

Dry powder API entrapment determines the percentage of API that composes the powder comparing the theoretical amount, taking yield into consideration. This parameter can be calculated as follows:

$$API\ Entrapment(\%) = \frac{quantificated\ API\ mass\ (mg)}{theoretical\ API\ mass\ (mg)} \times 100$$

2.2.4.2 Powder flowability

The aerodynamic performance of the formulations was assessed using an aluminium Andersen Cascade Impactor apparatus (ACI, Copley). 30 mg of dry powder was loaded into three hydroxypropylmethylcellulose capsules nº3 (Aerovaus) and the capsules were individually placed into a previously weighed dry powder inhaler (DPI) that was coupled to the ACI device. Each plate of the cascade impactor was covered by a filter (Glass Microfiber filter MFV1080, Filter Lab) that is weighted before and after the experiment. The DPI punctured the capsule prior to the inhalation, and a high-capacity pump was used to simulate an intake of breath according to the European pharmacopoeia [46]. After the intake, several aerodynamic parameters can be calculated from the amount deposited in each plate: mass median aerodynamic diameter (MMAD), fine particle fraction (FPF), and geometric standard deviation (GSD). Firstly, MMAD characterizes the size of the particles that reached the impactor, excluding those deposited in the throat, representing the diameter of 50% the particles. Secondly, FPF is the portion of the delivered particles sized below 5 μm, as determined by the interpolation of the percentage of the particles with smaller sizes than this value. Finally, the GSD measures the distribution of sizes of the particles, and it can be calculated using the following equation (d_{84} and d_{16} - diameters corresponding to 84 % and 16 % of the cumulative distribution, respectively):

$$GSD = \sqrt{\frac{d_{84}}{d_{16}}}$$

2.3 Reactions

2.3.1 Counter-ions

Anionic Counter-ions

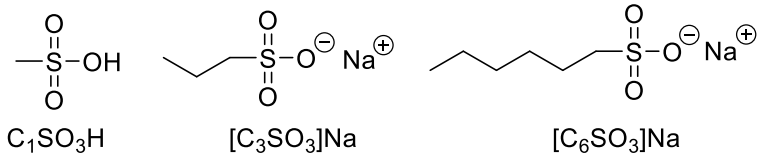

C_1SO_3H $[C_3SO_3]Na$ $[C_6SO_3]Na$

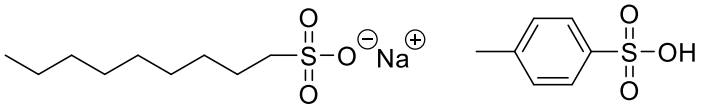

$[C_9SO_3]Na$ $TolSO_3H$

Cationic Counter-ions

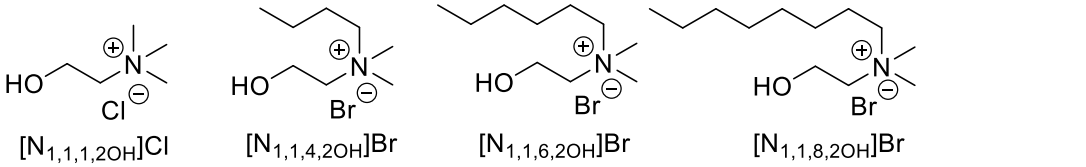

$[N_{1,1,1,2OH}]Cl$ $[N_{1,1,4,2OH}]Br$ $[N_{1,1,6,2OH}]Br$ $[N_{1,1,8,2OH}]Br$

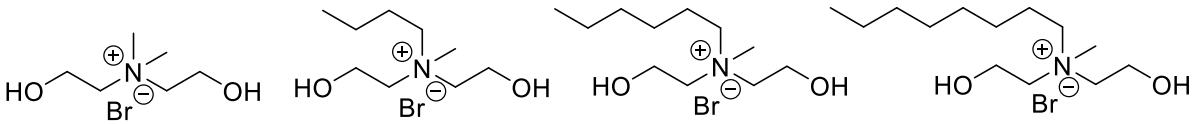

$[N_{1,1,2OH,2OH}]Br$ $[N_{1,4,2OH,2OH}]Br$ $[N_{1,6,2OH,2OH}]Br$ $[N_{1,8,2OH,2OH}]Br$

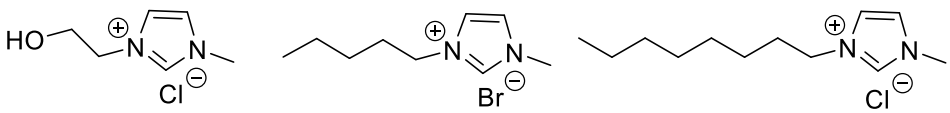

$[C_2OHMIM]Cl$ $[C_4MIM]Br$ $[C_8MIM]Cl$

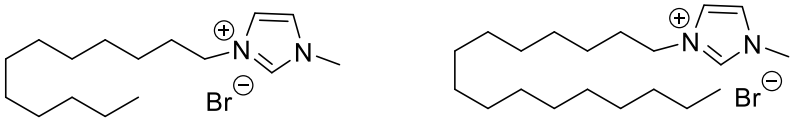

$[C_{12}MIM]Br$ $[C_{16}MIM]Br$

2.3.2 OSILs synthesized from rifampicin

Cationic Approach

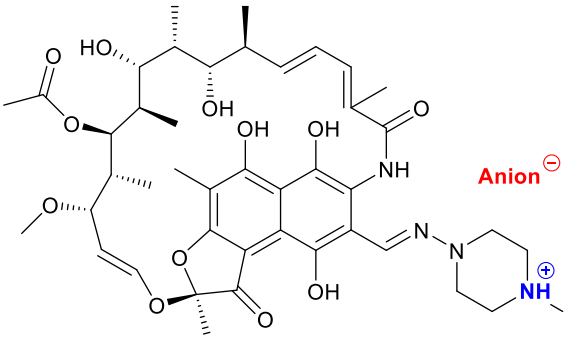

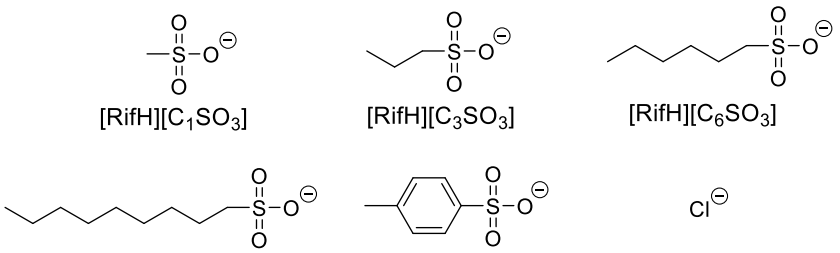

[RifH][C_1SO_3] [RifH][C_3SO_3] [RifH][C_6SO_3]

[RifH][C_9SO_3] [RifH][$TolSO_3$] [RifH]Cl

Anionic Approach

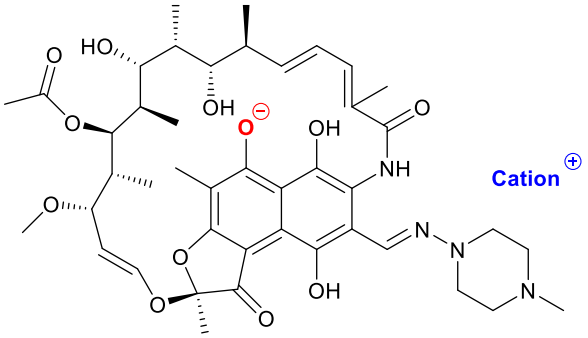

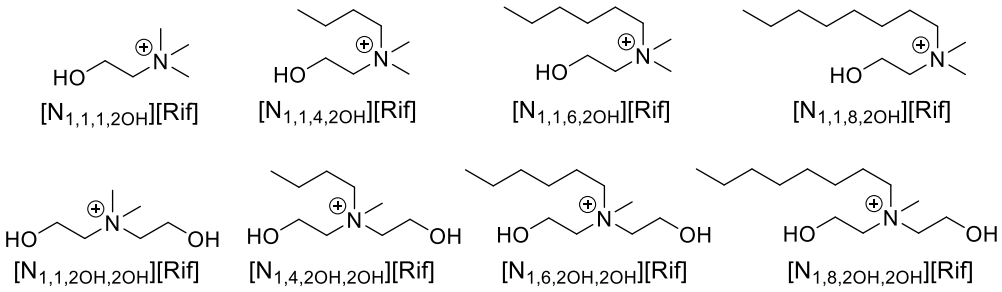

[$N_{1,1,1,2OH}$][Rif] [$N_{1,1,4,2OH}$][Rif] [$N_{1,1,6,2OH}$][Rif] [$N_{1,1,8,2OH}$][Rif]

[$N_{1,1,2OH,2OH}$][Rif] [$N_{1,4,2OH,2OH}$][Rif] [$N_{1,6,2OH,2OH}$][Rif] [$N_{1,8,2OH,2OH}$][Rif]

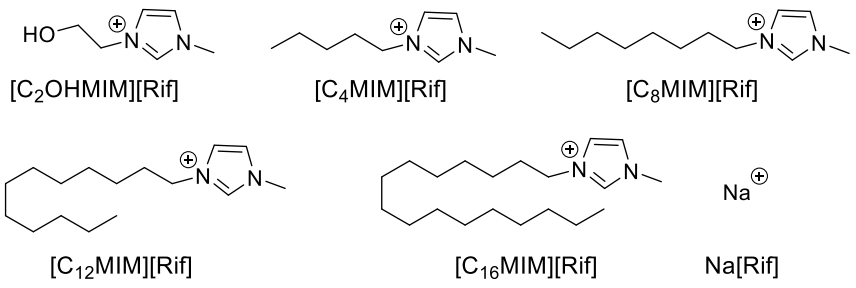

[C_2OHMIM][Rif] [C_4MIM][Rif] [C_8MIM][Rif]

[$C_{12}MIM$][Rif] [$C_{16}MIM$][Rif] Na[Rif]

2.3.3 Synthesis of counter-ions

While some of the counter-ions were purchased from several chemical suppliers or had already been synthesized within the group, a few were synthesized as part of this work, as described below.

Counter-ions acquired from chemical suppliers (respective suppliers previously mentioned in 2.1): methanesulfonic acid ([C_1SO_3]H), sodium propanesulfonate ([C_3SO_3]Na); sodium hexanesulfonate ([C_6SO_3]Na), sodium nonanesulfonate ([C_9SO_3]Na), *para*-toluenesulfonic acid (TolSO_3H) and choline chloride ([$N_{1,1,1,2OH}$]Cl).

Counter-ions previously synthesised within the group were [C_2OHMIM]Br, [C_8MIM]Br and [C_{16}MIM]Br and the remaining counter-ions were synthesized as part of this work.

2.3.3.1 Synthesis of 3-butyl-1-methyl-1H-imidazol-3-ium bromide ([C_4MIM]Br)

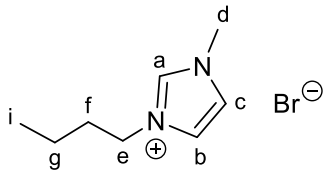

154 mg (1.88 mmol, 1 equiv.) of 1-methylimidazole, 322 mg (2.35 mmol, 1.25 equiv.) of 1-bromobutane and 5 mL of acetonitrile were measured into a vial ready for microwave. The reaction took a total of 2 hours at 120 ºC until completion was observed through NMR spectroscopy. The desired product was obtained as a light brown oil (394.2 mg; 95.9% yield).

^{1}H NMR (400 MHz, D_2O) δ 8.73 (s, 1H, H_a), 7.51 (s, 1H, H_c), 7.46 (s, 1H, H_b), 4.23 (t, *J* = 7.2 Hz, 3H, H_e), 2.10 (s, 3H, H_d), 1.88 (s, 2H, H_f) 1.35 (m, 2H, H_g), 0.95 (m, 3H, H_i)

2.3.3.2 Synthesis of 3-dodecyl-1-methyl-1H-imidazol-3-ium bromide ([C_{12}MIM]Br)

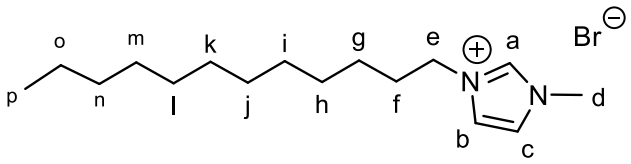

0,66 mL (685 mg, 8.35 mmol, 1 equiv.) of 1-methylimidazole and 2.10 mL (2.18 g, 8.77 mmol, 1.05 equiv.) of 1-bromododecane were measured into a vial ready for microwave. This *in neat* reaction took 8 mins at 130 ºC, with 1200 rpm stirring. The product was washed with ethylic ether to remove excess bromoalkane, dissolved with acetonitrile and concentrated under

vacuum. A considerable amount of product was lost in the evaporation step due to the formation of bubbles. The desired product was obtained as a white wax (1.53 g; 55.3%).

^{1}H NMR (400 MHz, DMSO-*d6*) δ 9.17 (s, 1H, H_a), 7.79 (t, *J* = 1.8 Hz, 1H, H_c), 7.72 (t, *J* = 1.8 Hz, 1H, H_b), 4.15 (t, *J* = 7.2 Hz, 3H, H_e) 3.85 (s, 3H, H_d), 3.32 (s, 2H, H_f) 1.23 (m, 18H, H_g, H_h, H_i, H_j, H_k, H_l, H_m, H_n, and H_o), 0.84 (t, *J* = 7.2, 3H, H_p)

2.3.3.3 Synthesis of *N* - (2 - hydroxyethyl) - *N*, *N* - dimethylbutan - 1 - aminium bromide ([N1,1,4,2OH]Br)

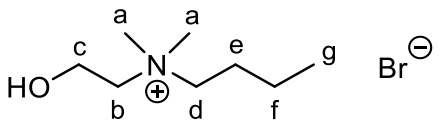

1.12 mL (1.00 g, 11.11 mmol, 1 equiv.) of 2-(dimethylamino)ethan-1-ol, 2.46 mL (3.07 g, 22.44 mmol, 2 equiv.) of 1-bromobutane and 4 mL of acetonitrile were added to a microwave ready vial. The reaction took 20 minutes at 120 ºC with 1200 rpm stirring. The reaction mixture was concentrated, washed with diethyl ether, and dried under vacuum. The desired product was obtained as a white powder (2.50 g; 98.6% yield).

^{1}H NMR (400 MHz, D_2O) δ 4.04 (s, 2H, H_c), 3.49 (t, J = 5.0 Hz, 2H, H_b), 3.38 (m, 2H, H_d), 3.14 (s, 6H, H_a), 1.77 (p, J = 7.5 Hz, H_e), 1.39 (h, J = 7.3 Hz, 2H, H_f), 0.96 (t, J = 7.4 Hz, 3H, H_g)

2.3.3.4 Synthesis of *N* - (2 - hydroxyethyl) - *N*, *N* - dimethylhexan - 1 - aminium bromide ([N1,1,6,2OH]Br)

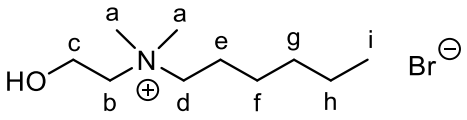

315.0 mg (3.53 mmol, 1 equiv.) of 2-(dimethylamino)ethan-1-ol, 1 mL (1170 mg, 7.07 mmol, 2 equiv.) of 1-bromohexane and 4 mL of acetonitrile were added to a microwave ready vial. The reaction took 20 minutes at 120 ºC with 1200 rpm stirring. The reaction mixture was concentrated, washed with diethyl ether, and dried under vacuum. The desired product was obtained as a white powder (841.3 mg; 93.7% yield).

^{1}H NMR (400 MHz, D_2O) δ 4.04 (s, 2H, H_c), 3.55-3.45 (m, 2H, H_b), 3.40-3.35 (m, 2H, H_d), 3.14 (s, 6H, H_a), 1.85-1.70 (m, 2H, H_e), 1.40-1.25 (m, 6H, H_f, H_g and H_h), 0.95-0.85 (m, 3H, H_i)

2.3.3.5 Synthesis of *N* - (2 - hydroxyethyl) - N , N - dimethyloctan - 1 - aminium bromide ([N1,1,8,2OH]Br)

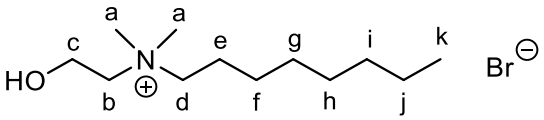

1.12 mL (1.0 g, 11.22 mmol, 1 equiv.) of 2-(dimethylamino)ethan-1-ol, 3.87 mL (4.33 g, 22.44 mmol, 2 equiv.) of 1-bromooctane and 4 mL of acetonitrile were added into a microwave ready vial. The reaction took 20 minutes at 120 ºC with 1200 rpm stirring. The reaction mixture was concentrated, washed with diethyl ether, and dried over vacuum. The desired product was obtained as a white powder (2.42 g; 76.3% yield).

^{1}H NMR (400 MHz, D_2O) δ 4.04 (s, 2H, H_c), 3.53-3.45 (m, 2H, H_b), 3.40-3.32 (m, 2H, H_d), 3.14 (s, 6H, H_a), 1.85-1.70 (m, 2H, H_e), 1.40-1.25 (m, 10H, H_f, H_g, H_h, H_i and H_j), 0.90-0.80 (m, 3H, H_k)

2.3.3.6 Synthesis of 2-hydroxy-*N*-(2-hydroxyethyl)-*N*,*N*-dimethylethan-1-aminium bromide ([N1,1,2OH,2OH]Br)

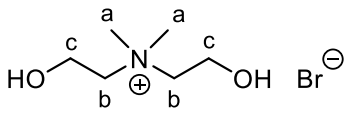

1.12 mL (1.00 g, 11.22 mmol, 1 equiv.) of 2-(dimethylamino)ethan-1-ol, 1.59 mL (2.8 g, 22.44 mmol, 2 equiv.) of 2-bromoethan-1-ol, and 4 mL of acetonitrile were added to a microwave ready vial. The reaction took 20 minutes at 120 ºC with 1200 rpm stirring. The reaction mixture was concentrated, washed with diethyl ether, and dried over vacuum. The desired product was obtained as a light brown oil (1.32 g; 54.8% yield).

^{1}H NMR (400 MHz, D_2O) δ 4.10-4.05 (m, 4H, H_c), 3.60 (t, J = 4.3 Hz, 4H, H_b), 3.23 (s, 6H, H_a)

2.3.3.7 Synthesis of *N,N*-bis(2-hydroxyethyl)-*N*-methylbutan-1-aminium bromide ([N1,4,2OH,2OH]Br)

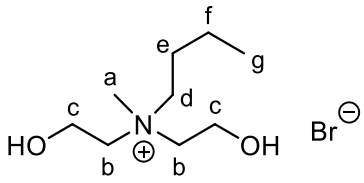

0.96 mL (1.00 g, 8.22 mmol, 1 equiv.) of 2,2'-(methylazanediyl)bis(ethan-1-ol), 1.80 mL (2.50 g, 16.44 mmol, 2 equiv.) of 1-bromobutane into a microwave ready vial. The reaction took 35 minutes at 120 ºC with 1200 rpm stirring. The reaction mixture was washed with diethyl ether and dried over vacuum. The desired product was obtained as a colourless oil (2.00 g; 95.1% yield).

^{1}H NMR (400 MHz, D_2O) δ 3.98 (s, 4H, H_c), 3.70-3.53 (m, 4H, H_b), 3.40-3.33 (m, 2H, H_d), 3.10 (s, 3H, H_a), 1.69 (p, J = 8.3 Hz, 2H, H_e), 1.32 (h, J = 7.6 Hz, 2H, H_f), 0.89 (t, J = 7.5 Hz, 3H, H_g)

2.3.3.8 Synthesis of *N,N*-bis(2-hydroxyethyl)-*N*-methylhexan-1-aminium bromide ([N1,6,2OH,2OH]Br)

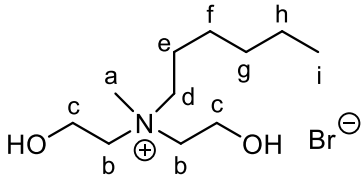

0.96 mL (1.00 g, 8.22 mmol, 1 equiv.) of 2,2'-(methylazanediyl)bis(ethan-1-ol), 1.80 mL (2.25 g, 16.44 mmol, 2 equiv.) of 1-bromohexane into a microwave ready vial. The reaction took 45 minutes at 120 ºC with 1200 rpm stirring. The reaction mixture was washed with diethyl ether and dried over vacuum. The desired product was obtained as a colourless oil (2.13 g; 91.3% yield).

^{1}H NMR (400 MHz, D_2O) δ 4.10-4.00 (m, 4H, H_c), 3.55-3.65 (m, 4H, H_b), 3.40-3.50 (m, 2H, H_d) 3.18 (s, 3H, H_a), 1.75-1.85 (m, 2H, H_e), 1.42-1.30(m, 6H, H_f, H_g and H_h), 0.90 (t, 3H, H_i)

2.3.3.9 Synthesis of *N,N*-bis(2-hydroxyethyl)-*N*-methyloctan-1-aminium bromide [N1,8,2OH,2OH]Br)

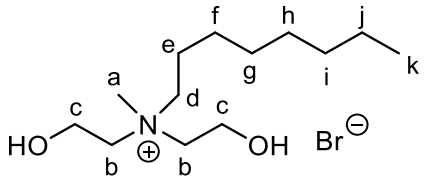

0.96 mL (1.00 g, 8.22 mmol, 1 equiv.) of 2,2'-(methylazanediyl)bis(ethan-1-ol), 1.80 mL (2.25 g, 16.44 mmol, 2 equiv.) of 1-bromooctane into a microwave ready vial. The reaction took 60 minutes at 120 °C with 1200 rpm stirring. The reaction mixture was washed with diethyl ether and dried over vacuum. The desired product was obtained as white wax (2.24 g; 87.2% yield).

^{1}H NMR (400 MHz, D_2O) δ 4.04 (m, 4H, H_c), 3.60-3.50 (m, 4H, H_b), 3.50-3.40 (m, 2H, H_d), 3.17 (s, 3H, H_a), 1.85-1.70 (m, 2H, H_e), 1.40-1.25 (m, 10H, H_f, H_g, H_h, H_i and H_j), 0.93-0.80 (m, 3H, H_k)

2.3.4 Cationic Approach

2.3.4.1 General synthesis of cationic rifampicin

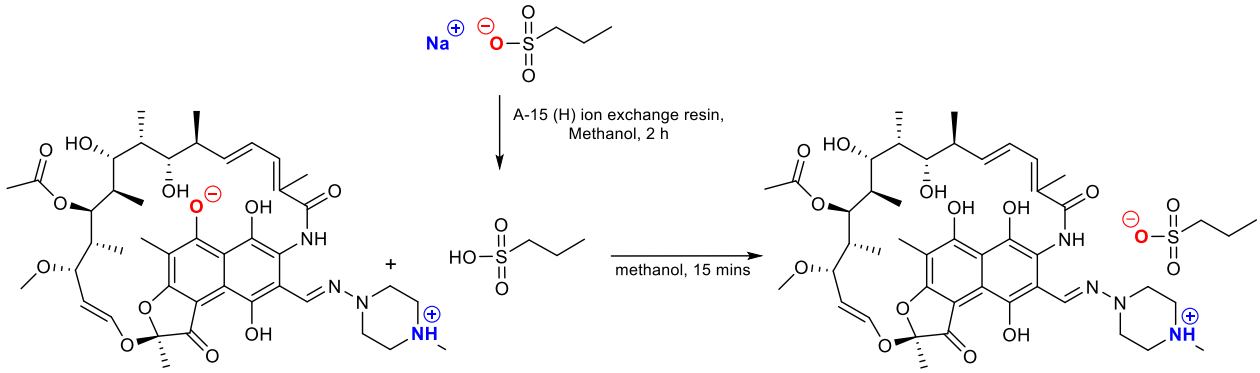

Rifampicin

The desired anions were either in the form of a sodium salt or in acid form. If the anion is in acid form, we dilute it and add it dropwise to rifampicin dissolved in methanol and let stir for 15 minutes. If the anion is in sodium salt form, it's dissolved in methanol and stirred in an anionic exchange resin (Amberlyst® 26(OH)) for 2 hours to form the acids of the respective anions [74]. After the filtration of the resin, the acids were added dropwise to rifampicin dissolved in methanol. This way we do not need purification steps apart from drying. The products formed were red powders with a variation in shade and obtained in high yields.

2.3.4.2 Rifampicinium methanesulfonate [RifH][C_1SO_3]

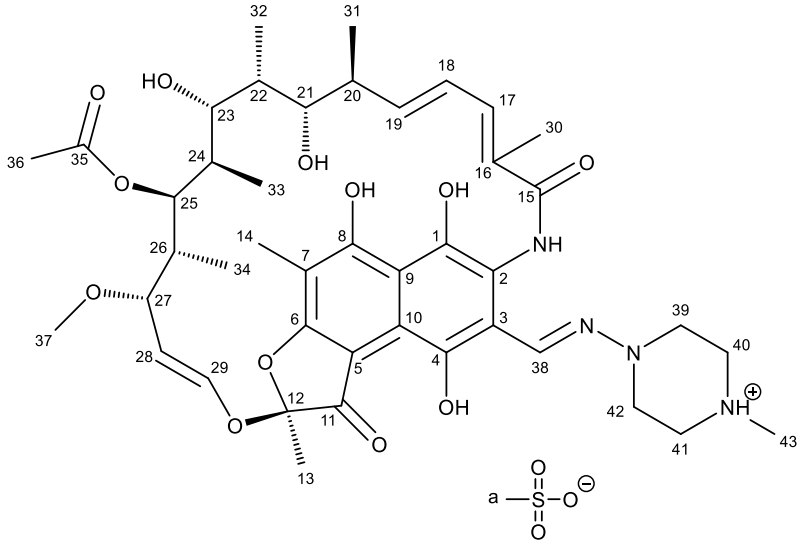

35.1 mg of methanesulfonic acid (0.365 mmol, 1 equiv.) and 300 mg (0.365 mmol, 1 equiv.) of rifampicin were used. The product was obtained in the form of a red powder.

^{1}H NMR (400 MHz, DMSO-*d6*) δ 9.68 (s, 1H, OH_1), 8.18 (s, 1H, H_{38}), 6.71 (dd, *J* = 14.9, 11.3 Hz, 1H, H_{18}), 6.49 (d, *J* = 11.0 Hz, 1H, H_{17}), 6.32 (d, *J* = 12.8 Hz, 1H, H_{29}), 5.96 (dd, *J* = 15.6, 5.3 Hz, 1H, H_{19}), 5.03 (d, *J* = 10.9 Hz, 1H, H_{25}), 4.97 (dd, *J* = 12.8, 8.1 Hz, 1H, H_{28}), 3.70 (d, *J* = 9.2 Hz, 1H, H_{21}), 3.75-3.63 (m, 2H, H_{39a} and H_{42a}), 3.60-3.42 (m, 2H, H_{40a} and H_{41a}), 3.28 (d, *J* = 8.1, 1H, H_{27}), 3.18-3.06 (m, 2H, H_{40b} and H_{41b}), 3.00-2.84 (m, 3H, H_{39b}, H_{42b} and H_{23}), 2.90 (m, 3H, H_{37}), 2.85 (s, 3H, H_{43}), 2.34 (s, 3H, H_a), 2.28-2.18 (m, 1H, H_{20}), 2.09 (s, 3H, H_{36}), 2.01 (s, 3H, H_{30}), 1.98 (s, 3H, H_{14}), 1.73 (s, 3H, H_{13}), 1.58-1.53 (m, 1H, H_{22}), 1.30-1.21 (m, 1H, H_{24}), 1.00-0.92 (m, 1H, H_{26}), 0.89 (d, *J* = 6.9 Hz, 3H, H_{32}), 0.82 (d, *J* = 7.0 Hz, 3H, H_{31}), 0.45 (d, *J* = 6.8 Hz, 3H, H_{33}), -0.42 (d, *J* = 6.8 Hz, 3H, H_{34})

^{13}C NMR (101 MHz, DMSO-*d6*) δ 173.17, 169.49, 168.54, 147.03, 143.09, 136.50, 134.55, 129.19, 123.69, 119.22, 119.07, 117.03, 112.58, 108.93, 104.84, 75.87, 75.83, 73.18, 70.60, 55.99, 55.84, 51.09, 42.01, 38.50, 37.92, 32.80, 21.59, 20.59, 20.07, 18.52, 17.31, 10.86, 8.49, 7.54.

IR (ATR) υ_{max} (cm^{-1}) 3429 (N-H and O-H st), 2972 (C-H st), 2936 (C-H st), 2883 (C-H st), 1725 (C=O st), 1647 (C=N asymmetric st), 1564 (aromatic C-H), 1456, 1374, 1328, 1216, 1158, 1039, 973, 802, 770, 724, 643, 552, 524, 496

Elemental analysis calcd (%) for [RifH][C_1SO_3] ● H_2O: C 56.84, H 7.06, N 6.22; found C 56.40, H 6.88, N 5.98

2.3.4.3 Rifampicinium propane-1-sulfonate [RifH][C_3SO_3]

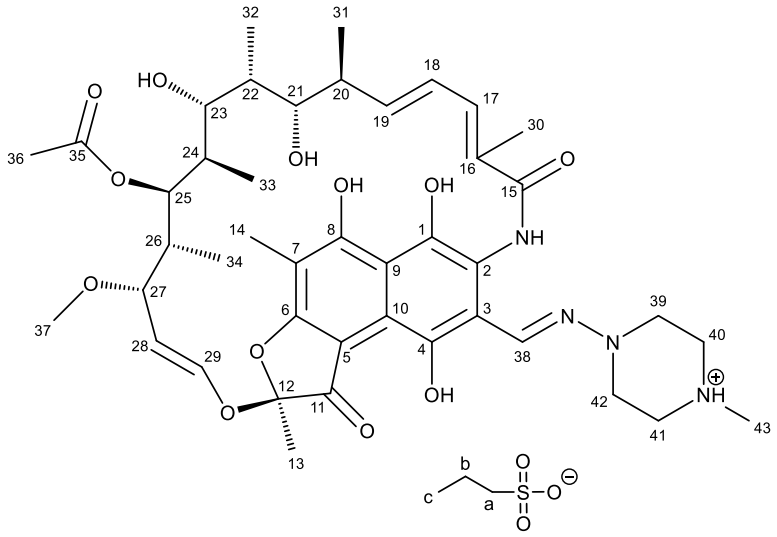

53.34 mg (0.365 mmol, 1 equiv.) sodium propane-1-sulfonate, 0.644 mL (1.095 mmol, 3 equiv.) Amberlyst© A-15(H^+) ion exchange resin and 300 mg (0.365 mmol, 1 equiv.) of rifampicin were used. A red powder was obtained.

^{1}H NMR (400 MHz, DMSO-*d6*) δ 9.69 (s, 1H, OH_1), 8.19 (s, 1H, H_{38}), 6.75 (dd, *J* = 15.3, 11.4 Hz, 1H, H_{18}), 6.48 (d, *J* = 11.0 Hz, 1H, H_{17}), 6.32 (d, *J* = 12.7 Hz, 1H, H_{29}), 5.98 (dd, *J* = 15.6, 5.3 Hz, 1H, H_{19}), 5.04 (d, *J* = 10.9 Hz, 1H, H_{25}), 4.98 (dd, *J* = 12.8, 8.1 Hz, 1H, H_{28}), 3.71 (d, *J* = 9.2 Hz, 1H, H_{21}), 3.78-3.62 (m, 2H, H_{39a} and H_{42a}), 3.58-3.43 (m, 2H, H_{40a} and H_{41a}), 3.29 (d, *J* = 8.2 Hz, 1H, H_{27}), 3.20-3.04 (m, 2H, H_{40b} and H_{41b}), 3.00-2.80 (m, 3H, H_{39b}, H_{42b} and H_{23}), 2.91 (s, 3H, H_{37}), 2.86 (s, 3H, H_{43}), 2.44-2.37 (m, 2H, H_a), 2.28-2.18 (m, 1H, H_{20}), 2.09 (s, 3H, H_{36}), 2.01 (s, 3H, H_{30}), 1.99 (s, 3H, H_{14}), 1.74 (s, 3H, H_{13}), 1.62-1.52 (m, 3H, H_{22} and H_b), 1.32-1.21 (m, 1H, H_{24}), 1.00-0.92 (m, 1H, H_{26}), 0.92-1.85 (m, 6H, H_{32}, H_c), 0.82 (d, *J* = 7.0 Hz, 3H, H_{31}), 0.46 (d, *J* = 6.8 Hz, 3H, H_{33}), -0.40 (d, *J* = 6.8 Hz, 3H, H_{34})

^{13}C NMR (101 MHz, DMSO-*d6*) δ 173.03, 169.49, 168.31, 146.87, 143.07, 142.05, 136.57, 134.31, 129.45, 118.74, 117.04, 112.71, 108.89, 104.47, 75.88, 73.21, 70.72, 55.81, 53.48, 51.09, 42.02, 40.15, 39.94, 39.73, 39.52, 39.31, 39.10, 38.89, 38.49, 37.93, 32.80, 21.63, 20.60, 20.12, 18.48, 17.34, 13.48, 10.91, 8.49, 7.54.

IR (ATR) υ_{max} (cm^{-1}) 3433 (N-H and O-H st), 2970 (C-H st), 2940 (C-H st), 2879 (C-H st), 1726 (C=O st), 1646 (C=N asymmetric st), 1564 (aromatic C-H), 1526, 1456, 1374, 1329, 1218, 1145, 1091, 1028, 973, 896, 771, 723, 601, 522, 496

Elemental analysis calcd (%) for [RifH][C_3SO_3] ● H_2O: C 56.94, H 7.16, N 6.06; found C 57.25, H 7.10, N 5.81

2.3.4.4 Rifampicinium hexane-1-sulfonate [RifH][C_6SO_3]

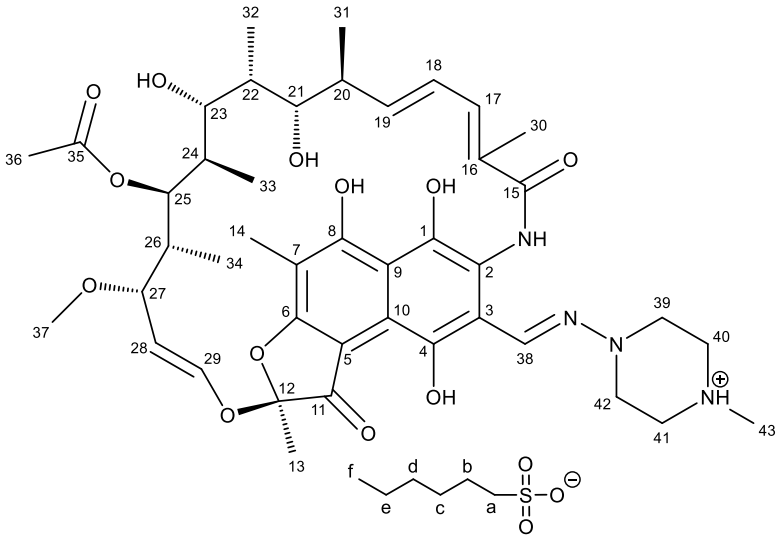

68.7 mg (0.365, 1 equiv.) of sodium hexane-1-sulfonate, 0.644 mL (1.095 mmol, 3 equiv.) Amberlyst© A-15(H^+) ion exchange resin and 300 mg (0.365 mmol, 1 equiv.) of rifampicin were used. A red powder was obtained.

^{1}H NMR (400 MHz, DMSO-*d6*) δ 9.70 (s, 1H, OH_1), 8.18 (s, 1H, H_{38}), 6.82-6.70 (m, 1H, H_{18}), 6.46 (d, *J* = 11.0 Hz, 1H, H_{17}), 6.30 (d, *J* = 12.8 Hz, 1H, H_{29}), 5.97 (dd, *J* = 15.7, 5.5 Hz, 1H, H_{19}), 5.03 (d, *J* = 10.9 Hz, 1H, H_{25}), 4.97 (dd, *J* = 12.8, 8.1 Hz, 1H, H_{28}), 3.71 (d, *J* = 9.6 Hz, 1H, H_{21}), 3.75-3.62 (m, 2H, H_{39a} and H_{42a}), 3.58-3.42 (m, 2H, H_{40a} and H_{41a}), 3.28 (d, *J* = 8.1 Hz, 1H, H_{27}), 3.20-3.06 (m, 2H, H_{40b} H_{41b}), 3.00-2.80 (m, 3H, H_{39b}, H_{42b} and H_{23}), 2.90 (s, 3H, H_{37}), 2.84 (s, 3H, H_{43}), 2.44-2.37 (m, 2H, H_a), 2.28-2.18 (m, 1H, H_{20}), 2.07 (s, 3H, H_{36}), 2.00 (s, 3H, H_{30}), 1.98 (s, 3H, H_{14}), 1.72 (s, 3H, H_{13}), 1.59-1.46 (m, 3H, H_{22} and H_b), 1.34-1.18 (m, 7H, H_{24}, H_c, H_d and H_e), 1.01-0.93 (m, H, H_{26}), 0.93-0.80 (m, 9H, H_{32}, H_f and H_{31}), 0.46 (d, *J* = 6.8 Hz, 3H, H_{33}), -0.40 (d, *J* = 6.8 Hz, 3H, H_{34})

^{13}C NMR (101 MHz, DMSO-*d6*) δ 172.94, 169.48, 168.05, 146.72, 143.39, 143.03, 136.85, 129.85, 118.84, 117.09, 113.02, 108.86, 75.96, 73.26, 70.90, 55.79, 51.54, 47.27, 42.00, 38.47, 37.93, 32.81, 31.11, 28.05, 25.03, 21.95, 20.16, 17.36, 13.89, 10.97, 8.60, 8.51, 7.48

IR (ATR) υ_{max} (cm^{-1}) 3429 (N-H and O-H st), 2964 (C-H st), 2934 (C-H st), 2875 (C-H st), 1725 (C=O st), 1647 (C=N asymmetric st), 1564 (aromatic C-H), 1456, 1374, 1329, 1217, 1157, 1091, 1033, 973, 945, 895, 802, 771, 723, 601, 522, 494

Elemental analysis calcd (%) for [RifH][C_6SO_3] ● $2H_2O$: C 57.03, H 7.33, N 5.87; found C 57.41, N 7.47, H 5.46

2.3.4.5 Rifampicinium nonane-1-sulfonate [RifH][C9SO3]

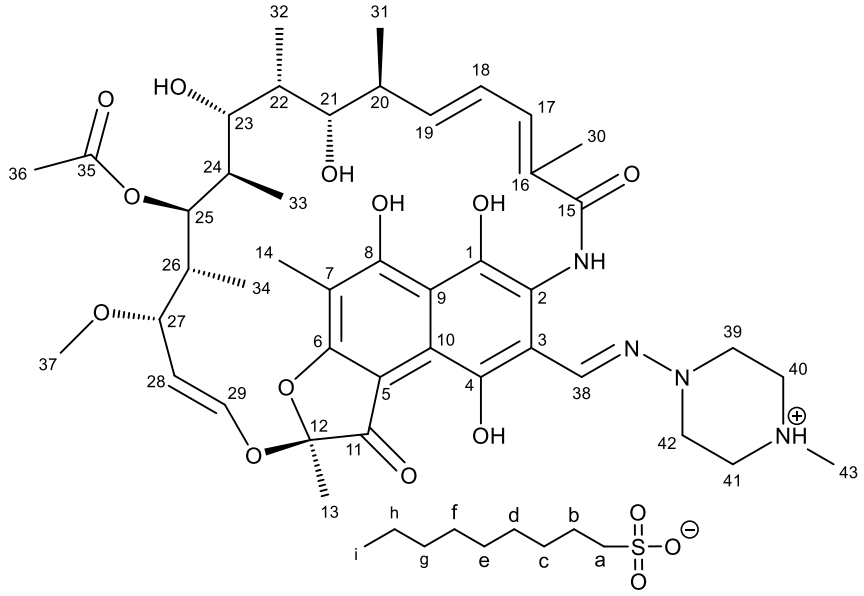

88.6 mg (0.365, 1 equiv.) of sodium nonane-1-sulfonate, 0.644 mL (1.095 mmol, 3 equiv.) of Amberlyst© A-15(H^+) ion exchange resin and 300 mg (0.365 mmol, 1 equiv.) of rifampicin were used. A red powder was obtained.

^{1}H NMR (400 MHz, DMSO-*d6*) δ 9.70 (s, 1H, OH_1), 8.19 (s, 1H, H_{38}), 6.78-6.65 (m, 1H, H_{18}), 6.48 (d, *J* = 11.1 Hz, 1H, H_{17}), 6.31 (d, *J* = 12.7 Hz, 1H, H_{29}), 5.98 (dd, *J* = 15.6, 5.2 Hz, 1H, H_{19}), 5.03 (d, *J* = 10.9 Hz, 1H, H_{25}), 4.97 (dd, *J* = 12.8, 8.1 Hz, 1H, H_{28}), 3.69 (d, *J* = 10.0 Hz, 1H, H_{21}), 3.75-3.62 (m, 2H, H_{39a} and H_{42a}), 3.60-3.42 (m, 2H, H_{40a} and H_{41a}), 3.28 (d, *J* = 8.1 Hz, 1H, H_{27}), 3.20-3.06 (m, 2H, H_{40b} and H_{41b}), 3.02-2.82 (m, 3H, H_{39b}, H_{42b} and H_{23}), 2.90 (s, 3H, H_{37}), 2.85 (s, 3H, H_{43}), 2.44-2.37 (m, 2H, H_a), 2.28-2.18 (m, 1H, H_{20}), 2.09 (s, 3H, H_{36}), 2.00 (s, 3H, H_{30}), 1.98 (s, 3H, H_{14}), 1.73 (s, 3H, H_{13}), 1.59-1.46 (m, 3H, H_{22} and H_b), 1.34-1.18 (m, 13H, H_{24}, H_c, H_d, H_e, H_f, H_g, and H_h), 1.00-0.80 (m, 10H, H_{31}, H_{32}, H_i and H_{26}), 0.46 (d, *J* = 6.8 Hz, 3H, H_{33}), -0.41 (d, *J* = 6.8 Hz, 3H, H_{34})

^{13}C NMR (101 MHz, DMSO-*d6*) δ 173.20, 169.48, 168.50, 147.04, 143.10, 136.59, 134.49, 129.26, 123.81, 119.16, 119.05, 117.06, 112.70, 108.94, 104.82, 75.85, 73.19, 70.63, 55.84, 51.52, 47.17, 42.01, 38.50, 37.92, 32.80, 31.27, 28.87, 28.65, 28.35, 25.03, 22.06, 21.59, 20.59, 20.08, 17.29, 13.91, 10.87, 8.49, 7.51.

IR (ATR) υ_{max} (cm^{-1}) 3437 (N-H and O-H st), 2927 (C-H st), 2854 (C-H st), 1726(C=O st), 1645 (C=N asymmetric st), 1564 (aromatic C-H), 1525, 1456, 1374, 1329, 1215, 1159, 1033, 974, 802, 723, 601, 522, 496

Elemental analysis calcd (%) for [RifH][C_9SO_3] ● $2H_2O$: C 58.61, H 7.68, N 5.48; found C 58.52, N 7.74, H 5.25

2.3.4.6 Rifampicinium *para*-toluenesulfonate [RifH][TolSO3]

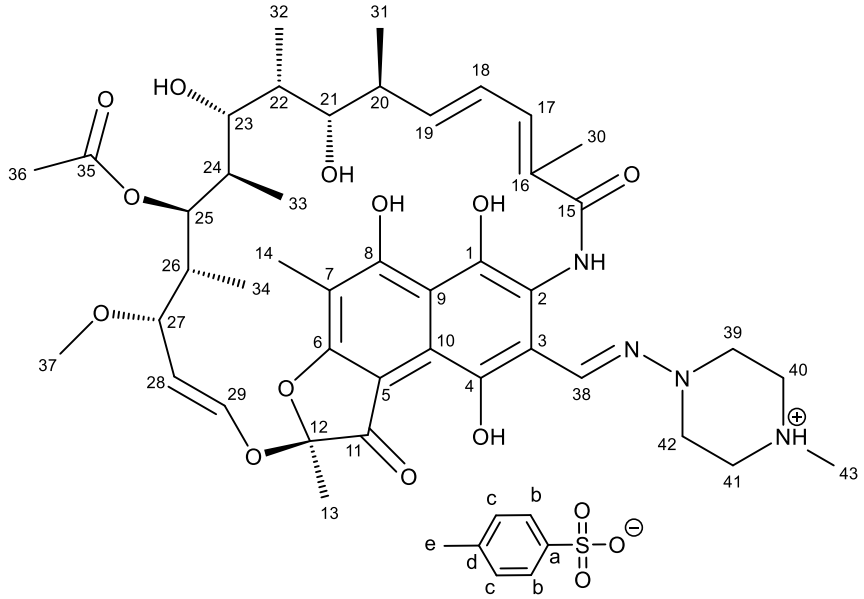

46.22 mg (0.243 mmol, 1 eq.) *para*-toluenesulfonic acid monohydrate, 200 mg of rifampicin (0.243 mmol, 1 eq.) dissolved in 6 mL of methanol. A red powder was obtained.

^{1}H NMR (400 MHz, DMSO-*d6*) δ 9.62 (s, 1H, OH_1)8.19 (s, 1H, H_{38}), 7.49 (d, *J* = 8.1 Hz, 2H, H_b), 7.12 (d, *J* = 7.8 Hz, 2H, H_c), 6.71 (dd, *J* = 15.6, 11.1 Hz, 1H, H_{18}), 6.50 (d, *J* = 11.1 Hz, 1H, H_{17}), 6.33 (d, *J* = 12.7 Hz, 1H, H_{29}), 5.99 (dd, *J* = 15.6, 5.3 Hz, 1H, H_{19}), 5.04 (d, *J* = 10.9 Hz, 1H, H_{25}), 4.98 (dd, *J* = 12.8, 8.1 Hz, 1H, H_{28}), 3.70 (d, *J* = 9.3 Hz, 1H, H_{21}), 3.78-3.63 (m, 2H, H_{39a} and H_{42a}), 3.61-3.43 (m, 2H, H_{40a} and H_{41a}), 3.30 (d, *J* = 8.2 Hz, 1H, H_{27}), 3.22-3.07 (m, 2H, H_{40b} and H_{41b}), 3.00-2.80 (m, 3H, H_{39b}, H_{42b} and H_{23}), 2.91 (s, 3H, H_{37}), 2.86 (s, 3H, H_{43}), 2.29 (s, 3H, H_e), 2.28-2.20 (m, 1H, H_{20}), 2,1 (s, 3H, H_{36}), 2,02 (s, 3H, H_{30}), 1,99 (s, 3H, H_{14}), 1,74 (s, 3H, H_{13}), 1.60-1.51 (m, 1H, H_{22}), 1.32-1.22 (m, 1H, H_{24}), 1.01-0,93 (m, 1H, H_{26}), 0,9 (d, *J* = 6.9 Hz, 3H, H_{32}), 0,82 (d, *J* = 7.0 Hz, 3H, H_{31}), 0,46 (d, *J* = 6.8 Hz, 3H, H_{33}), -0,42 (d, *J* = 6.8 Hz, 3H, H_{34})

^{13}C NMR (101 MHz, DMSO-*d6*) δ 173.19, 169.50, 168.59, 147.07, 145.47, 143.12, 142.56, 137.75, 136.43, 134.63, 129.11, 128.08, 125.47, 123.60, 119.15, 117.02, 112.54, 111.18, 108.95, 104.92, 103.68, 75.82, 73.17, 70.56, 55.86, 51.16, 42.01, 38.50, 37.92, 32.79, 21.61, 20.75, 20.60, 20.08, 17.30, 10.85, 8.50, 7.57.

IR (ATR) υ_{max} (cm^{-1}) 3428 (N-H and O-H st), 2973 (C-H st), 2936 (C-H st), 2883 (C-H st), 1721 (C=O st), 1646 (C=N asymmetric st), 1564 (aromatic C-H), 1455, 1374, 1330, 1316, 1159, 1159, 1120, 1032, 1009, 973, 802, 770, 682, 567, 495

Elemental analysis calcd (%) for [RifH][TolSO3] ● H_2O: C 58.75, H 6.88, N 5.73; found C 59.27, H 7.73, N 5.53

2.3.4.7 Rifampicin hydrochloride [RifH]Cl

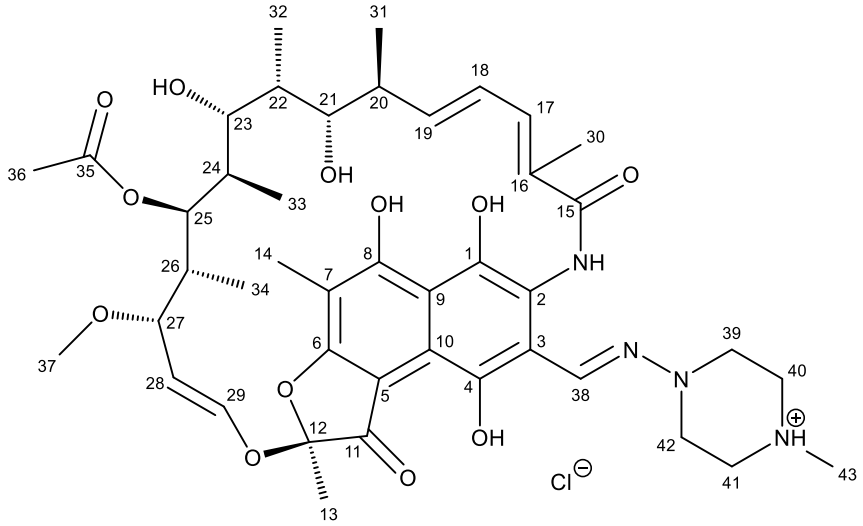

2.43 mL of a 0.1 M aqueous hydrochloric acid solution was added dropwise to 300 mg of rifampicin (0.365 mmol, 1 eq.) dissolved in 6 mL of methanol. The product was dried, and a red powder was obtained in quantitative yield.

^{1}H NMR (400 MHz, DMSO-*d6*) δ 8.20 (s, 1H, H_{38}), 6.70-6.60 (m, 1H, H_{18}), 6.52 (d, *J* = 11.1 Hz, 1H, H_{17}), 6.34 (d, *J* = 12.7 Hz, 1H, H_{29}), 5.98 (dd, *J* = 15.5, 5.0 Hz, 1H, H_{19}), 5.03 (d, *J* = 11.6 Hz, 1H, H_{25}), 5.00-4.90 (m, 1H, H_{28}), 3.69 (d, *J* = 9.2 Hz, 1H, H_{21}), 3.75-3.60 (m, 2H, H_{39a} and H_{42a}), 3.60-3.40 (m, 2H, H_{40a} and H_{41a}), 3.29 (d, *J* = 8.1, 1H, H_{27}), 3.18-3.00 (m, 2H, H_{40b} and H_{41b}), 2.95-2.85 (m, 3H, H_{39b}, H_{42b} and H_{23}), 2.90 (m, 3H, H_{37}), 2.79 (s, 3H, H_{43}), 2.28-2.18 (m, 1H, H_{20}), 2.11 (s, 3H, H_{36}), 2.02 (s, 3H, H_{30}), 1.99 (s, 3H, H_{14}), 1.74 (s, 3H, H_{13}), 1.60-1.50 (m, 1H, H_{22}), 1.30-1.21 (m, 1H, H_{24}), 1.00-0.90 (m, 1H, H_{26}), 0.89 (d, *J* = 6.8 Hz, 3H, H_{32}), 0.82 (d, *J* = 7.0 Hz, 3H, H_{31}), 0.46 (d, *J* = 6.8 Hz, 3H, H_{33}), -0.44 (d, *J* = 6.7 Hz, 3H, H_{34})

IR (ATR) υ_{max} (cm^{-1}) 3393 (N-H and O-H st), 2977 (C-H st), 2936 (C-H st), 2883 (C-H st), 2822 (C-H st), 1717 (C=O st), 1648 (C=N asymmetric st), 1586, 1546, 1501, 1435, 1373, 1346, 1289, 1142, 1061, 997, 975, 893, 771, 628

2.3.5 Anionic Approach

2.3.5.1 General synthesis of anionic rifampicin

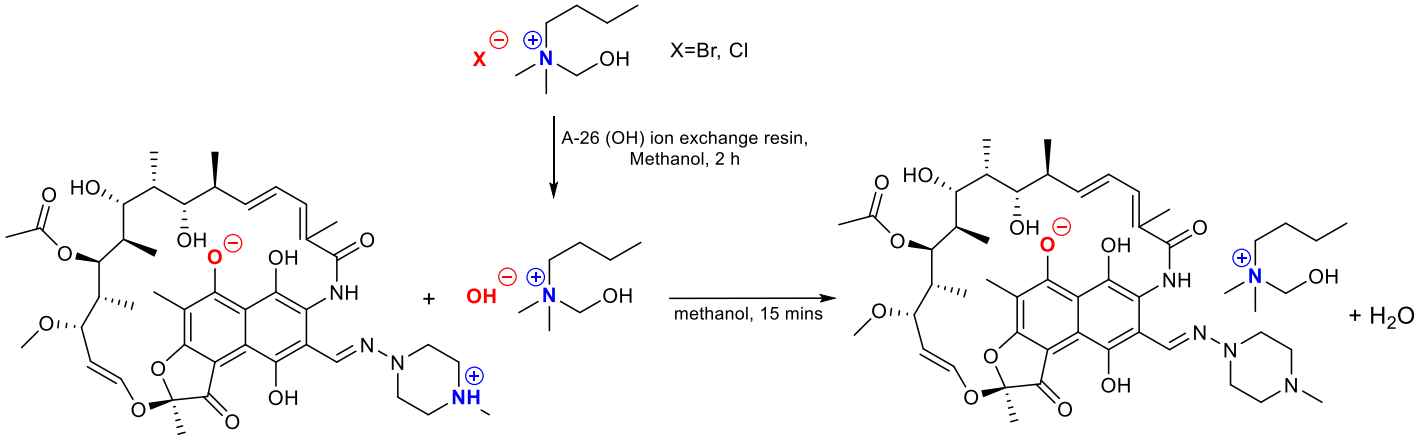

Rifampicin

The desired cations were in the form of halide salts, which were dissolved in methanol and stirred with an anionic exchange resin (Amberlyst® 26 (OH)) for 2 hours to form the corresponding hydroxide cations [74]. After the filtration of the resin, the hydroxide cations were added dropwise to rifampicin dissolved in methanol. The product was then concentrated under vacuum. Once again, this way we do not need purification steps apart from removing the solvent. The products formed were red powders with a variation in shade and obtained in high yields.

2.3.5.2 2 - hydroxy - *N, N, N* -trimethylethan - 1 - aminium bromide rifampicinate [$N_{1,1,1,2OH}$][Rif]

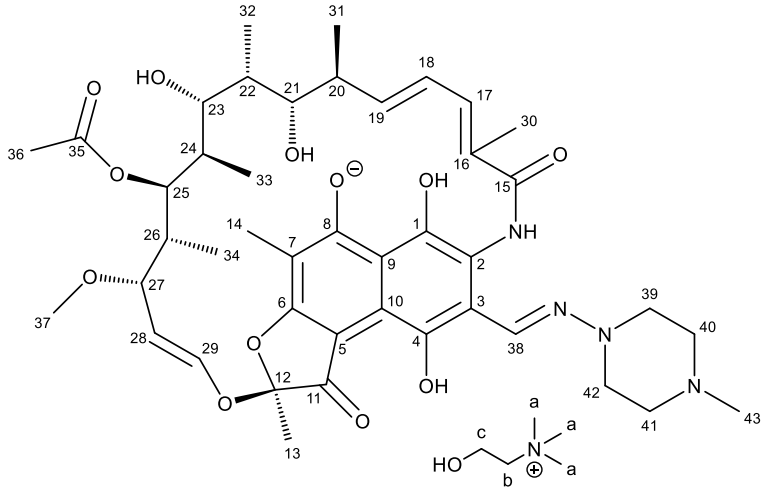

Following the previously described protocol, from 66.4 mg (0.476 mmol, 1.00 equiv.) of [$N_{1,1,1,2OH}$][Cl],1.785 mL (1.428 mmol, 3.00 equiv.) of anionic exchange resin and 434.85 mg (0.476 mmol, 1.00 equiv.) of rifampicin we obtained a dark red powder.

^{1}H NMR (400 MHz, DMSO-*d6*) δ 15.49 (s, 1H, OH_4), 12.46 (s, 1H, NH_{15}), 9.07 (s, 1H, OH_1), 7.99 (s, 1H, H_{38}), 6.98 (dd, *J* = 15.9, 10.8 Hz, 1H, H_{18}), 6.30-6.15 (m, 2H, H_{17} and H_{29}), 5.85 (dd, *J* = 16.0, 6.6 Hz, 1H, H_{19}), 5.26 (s, 1H, OH_c), 5.07 (d, *J* = 10.8 Hz, 1H, H_{25}), 4.93 (dd, *J* = 12.8, 8.2 Hz, 1H, H_{28}), 4.86 (d, *J* = 3.6 Hz, 1H, OH_{21}), 4.32 (s, *J* = 8.0 Hz, 1H, OH_{23}), 3.82 (m, 2H, H_c), 3.72 (d, *J* = 8.9 Hz, 1H, H_{21}), 3.38 (m, 3H, H_b), 3.23 (d, *J* = 8.3 Hz, 1H, H_{27}), 3.10 (s, 9H, H_a), 2.98 (m, 4H, H_{39} H_{42}), 2.90 (s, 3H, H_{37}), 2.84 (t, 1H, H_{23}), 2.56 (s, 4H, H_{40} H_{41}), 2.29 (s, 3H, H_{43}), 2.16 (m, 1H, H_{20}), 1.97 (s, 3H, H_{36}), 1.91 (s, 3H, H_{30}), 1.89 (s, 3H, H_{14}), 1.62 (s, 3H, H_{13}), 1.60-1.51 (m, 1H, H_{22}), 1.32-1.22 (m, 1H, H_{24}), 1.01-0,93 (m, 1H, H_{26}), 0.90-0.80 (m, 6H, H_{31} and H_{32}), 0.44 (d, *J* = 6.8 Hz, 3H, H_{33}), -0.24 (d, *J* = 6.8 Hz, 3H, H_{34})

^{13}C NMR (101 MHz, DMSO-*d6*) δ 184.50, 183.91, 171.58, 169.61, 165.93, 148.43, 144.88, 142.87, 138.09, 133.60, 132.35, 131.89, 127.21, 117.40, 116.99, 116.81, 116.00, 113.83, 108.56, 100.71, 98.44, 76.52, 76.13, 73.59, 71.90, 66.97, 66.95, 66.92, 55.61, 55.15, 53.79, 53.19, 53.16, 53.12, 50.21, 45.57, 37.89, 32.99, 22.12, 20.68, 17.86, 11.47, 8.92, 8.57, 7.48.

IR (ATR) υ_{max} (cm^{-1}) 3346 (N-H and O-H st), 2967 (C-H st), 2937 (C-H st), 2879 (C-H st), 1723 (C=O st), 1644 (C=N asymmetric st), 1585 (aromatic C-H), 1431, 1372, 1225, 1142, 1061, 997, 948, 891, 770, 626, 470

Elemental analysis calcd (%) for [$N_{1,1,1,2OH}$][Rif] ● $2H_2O$: C 59.55, H 7.76, N 7.60; found C 59.92, H 7.86, N 7.28

2.3.5.3 *N*-(2-hydroxyethyl)-*N*,*N*-dimethylbutan-1-aminium rifampicinate [N1,1,4,2OH][Rif]

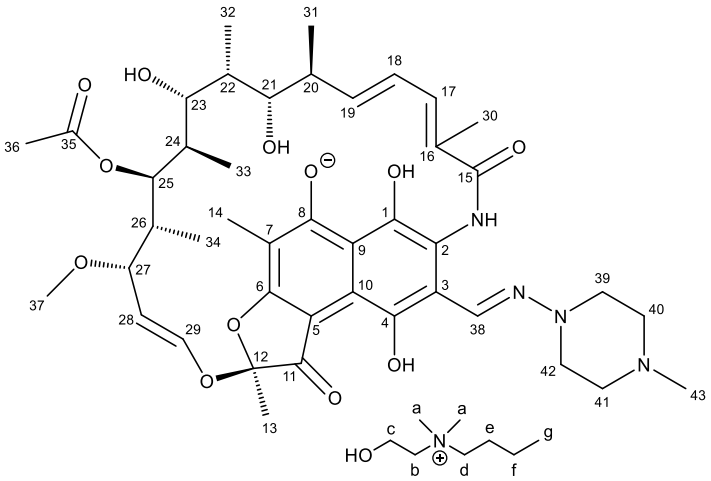

Following the previously described protocol, from 83.6 mg (0.370 mmol, 1.00 equiv.) of [N1,1,4,2OH][Br], 1,39 mL (1.110 mmol, 3.00 equiv) of anionic exchange resin and 337.94 mg (0.370 mmol, 1.00 equiv.) of rifampicin we obtained a dark red powder.

^{1}H NMR (400 MHz, DMSO-*d6*) δ 15.49 (s, 1H, OH_4), 12.46 (s, 1H, NH_{15}), 9.10 (s, 1H, OH_1), 7.99 (s, 1H, H_{38}), 6.98 (dd, *J* = 16.0, 10.8 Hz, 1H, H_{18}), 6.27-6.18 (m, 2H, H_{29} and H_{17}), 5.86 (dd, *J* = 15.8, 6.5 Hz, 1H, H_{19}), 5.25 (t, *J* = 4.9 Hz, 1H, OH_c), 5.08 (d, *J* = 10.8 Hz, 1H, H_{25}), 4.93 (dd, *J* = 12.8, 8.2 Hz, 1H, H_{28}), 4.84 (d, *J* = 3.6 Hz, 1H, OH_{21}), 4.30 (d, *J* = 8.0 Hz, 1H, OH_{23}), 3.82 (s, 2H, H_c), 3.77-3.69 (m, 1H, H_{21}), 3.40-3.21 (m, 5H, H_b, H_{27} and H_d), 3.05 (s, 6H, H_a), 3.01-2.95 (m, 4H, H_{39} H_{42}), 2.91 (s, 3H, H_{37}), 2.85 (t, *J* = 9.3 Hz, 1H, H_{23}), 2.24 (s, 3H, H_{43}), 2.21-2.11 (m, 1H, H_{20}), 1.98 (s, 3H, H_{36}), 1.92 (s, 3H, H_{30}), 1.90 (s, 3H, H_{14}), 1.71-1.61 (m, 2H, H_e), 1.63 (s, 3H, H_{13}), 1.62-1.53 (m, 1H, H_{22}), 1.23-1.39 (m, 3H, H_{24} and H_f), 1.10-1.01 (m, 1H, H_{26}), 0.97-0.82 (m, 9H, H_{31}, H_{32} and H_g), 0.45 (d, *J* = 6.8 Hz, 3H, H_{33}), -0.23 (d, *J* = 6.8 Hz, 3H, H_{34})

^{13}C NMR (101 MHz, DMSO-*d6*) δ 184.47, 183.93, 171.58, 169.58, 165.91, 148.42, 144.91, 142.83, 138.07, 132.34, 131.86, 127.23, 117.42, 113.87, 108.54, 100.72, 98.41, 76.50, 76.13, 73.59, 71.90, 64.61, 63.92, 55.60, 54.93, 53.51, 50.79, 49.94, 45.21, 37.90, 32.99, 23.76, 22.09, 20.64, 19.19, 17.83, 13.48, 11.47, 8.91, 8.57, 7.46.

IR (ATR) υ_{max} (cm^{-1}) 3358 (N-H and O-H st), 2967 (C-H st), 2936 (C-H st), 2879 (C-H st), 1724 (C=O st), 1648 (C=N asymmetric st), 1586 (aromatic C-H), 1430, 1372, 1225, 1143, 1061, 997, 972, 891, 944, 770, 736, 626, 466.

Elemental analysis calcd (%) for [N1,1,4,2OH][Rif] ● 2H_2O: C 60.76, H 8.04, N 6.71; found C 61.00, H 8.13, N 6.97

2.3.5.4 *N*- (hydroxyethyl) - *N,N*- dimethylhexan -1- aminium rifampicinate [$N_{1,1,6,2OH}$][Rif]

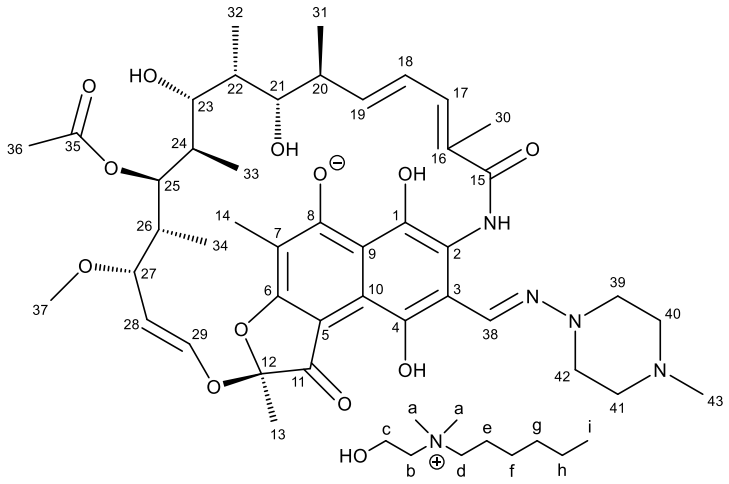

Following the previously described protocol, from 94.52 mg (0.372 mmol, 1.00 equiv.) of [$N_{1,1,6,2OH}$][Br], 1,395 mL (1.116 mmol, 3.00 equiv.) of anionic exchange resin and 339.97 mg (0.372 mmol, 1.00 equiv.) of rifampicin we obtained a dark red powder.

^{1}H NMR (400 MHz, DMSO-*d6*) δ 15.50 (s, 1H, OH_4), 12.47 (s, 1H, NH_{15}), 9.09 (s, 1H, OH_1), 7.99 (s, 1H, H_{38}), 6.99 (dd, *J* = 15.9, 10.8 Hz, 1H, H_{18}), 6.27-6.18 (m, 2H, H_{29} and H_{17}), 5.86 (dd, *J* = 15.9, 6.6 Hz, 1H, H_{19}), 5.25 (s, 1H, OH_c), 5.08 (d, *J* = 10.8 Hz, 1H, H_{25}), 4.93 (dd, *J* = 12.8, 8.2 Hz, 1H, H_{28}), 4.86 (d, *J* = 3.6 Hz, 1H, OH_{21}), 4.30 (d, *J* = 8.0 Hz, 1H, OH_{23}), 3.82 (s, 2H, H_c), 3.73 (d, *J* = 8.9 Hz, 1H, H_{21}), 3.40-3.21 (m, 5H, H_{27}, H_b and H_d), 3.04 (s, 6H, H_a), 3.02-2.97 (m, 4H, H_{39} and H_{42}), 2.91 (s, 3H, H_{37}), 2.85 (t, *J* = 9.3 Hz, 1H, H_{23}), 2.28 (s, 3H, H_{43}), 2.21-2.11 (m, 1H, H_{20}), 1.98 (s, 3H, H_{36}), 1.92 (s, 3H, H_{30}), 1.90 (s, 3H, H_{14}), 1.71-1.61 (m, 2H, H_e), 1.63 (s, 3H, H_{13}), 1.62-1.53 (m, 1H, H_{22}), 1.23-1.39 (m, 3H, H_{24}, H_f, H_g and H_h), 1.10-1.01 (m, 1H, H_{26}), 0.97-0.82 (m, 9H, H_{31}, H_{32} and H_i), 0.45 (d, *J* = 6.8 Hz, 3H, H_{33}), -0.23 (d, *J* = 6.8 Hz, 3H, H_{34})

^{13}C NMR (101 MHz, DMSO-*d6*) δ 184.46, 183.96, 171.59, 169.57, 165.93, 148.43, 144.94, 142.83, 138.08, 132.33, 131.88, 127.27, 117.44, 116.96, 116.85, 115.91, 113.89, 108.53, 100.73, 98.42, 76.50, 76.13, 73.59, 71.91, 64.61, 64.12, 55.60, 54.92, 53.37, 50.77, 49.81, 37.91, 32.97, 30.63, 25.41, 22.08, 21.84, 21.69, 20.66, 20.63, 17.82, 13.80, 11.46, 8.91, 8.57, 7.45.

IR (ATR) υ_{max} (cm^{-1}) 3356, 2935, 2879, 1724, 1647, 1586, 1430, 1372, 1225, 1143, 1061, 998, 971, 891, 770, 736, 625, 467

Elemental analysis calcd (%) for [$N_{1,1,6,2OH}$][Rif] ● $2H_2O$: C 61.74, H 8.20, N 6.43; found C 61.67, H 8.30, N 6.78

2.3.5.5 *N*- (hydroxyethyl) - *N,N*- dimethyloctan - 1 - aminium rifampicinate [$N_{1,1,8,2OH}$][Rif]

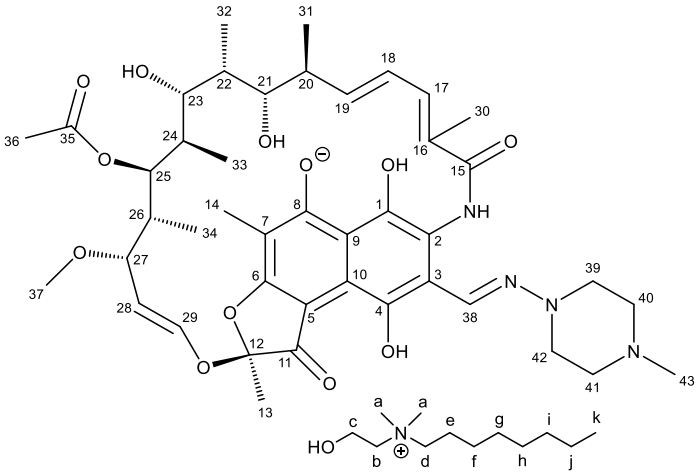

Following the previously described protocol, from 98.50 mg (0.367 mmol, 1.00 equiv.) of [$N_{1,1,8,2OH}$][Br], 1.376 mL (1.101 mmol, 3.00 equiv.) of anionic exchange resin and 335.77 mg (0.367 mmol, 1.00 equiv.) of rifampicin we obtained a dark red powder.

^{1}H NMR (400 MHz, DMSO-*d6*) δ 15.48 (s, 1H, OH_4), 12.46 (s, 1H, NH_{15}), 9.10 (s, 1H, OH_1), 7.98 (s, 1H, H_{38}), 6.97 (dd, *J* = 15.9, 10.8 Hz, 1H, H_{18}), 6.27-6.18 (m, 2H, H_{29} H_{17}), 5.85 (dd, *J* = 16.0, 6.5 Hz, 1H, H_{19}), 5.23 (s, 1H, OH_c), 5.07 (d, *J* = 10.8 Hz, 1H, H_{25}), 4.93 (dd, *J* = 12.8, 8.2 Hz, 1H, H_{28}), 4.84 (d, *J* = 3.6 Hz, 1H, OH_{21}), 4.30 (d, *J* = 8.0 Hz, 1H, OH_{23}), 3.81 (s, 2H, H_c), 3.72 (d, *J* = 8.9 Hz, 1H, H_{21}), 3.40-3.21 (m, 5H, H_{27}, H_b and H_d), 3.03 (s, 6H, H_a), 3.02-2.97 (m, 4H, H_{39} and H_{42}), 2.90 (s, 3H, H_{37}), 2.84 (t, *J* = 8.9 Hz, 1H, H_{23}), 2.23 (s, 3H, H_{43}), 2.21-2.11 (m, 1H, H_{20}), 1.97 (s, 3H, H_{36}), 1.91 (s, 3H, H_{30}), 1.89 (s, 3H, H_{14}), 1.71-1.61 (m, 2H, H_e), 1.63 (s, 3H, H_{13}), 1.62-1.53 (m, 1H, H_{22}), 1.39-1.23 (m, 11H, H_{24}, H_f, H_g, H_h, H_i and H_j), 1.10-1.01 (m, 1H, H_{26}), 0.97-0.82 (m, 9H, H_{31}, H_{32} and H_i), 0.44 (d, *J* = 6.8 Hz, 3H, H_{33}), -0.24 (d, *J* = 6.8 Hz, 3H, H_{34})

^{13}C NMR (101 MHz, DMSO-*d6*) δ 184.47, 183.93, 171.59, 169.58, 165.91, 148.42, 144.91, 142.84, 138.08, 132.34, 131.87, 127.24, 117.43, 116.96, 116.83, 115.94, 113.87, 108.54, 100.72, 98.42, 76.50, 76.13, 73.59, 71.90, 64.60, 64.12, 55.60, 54.93, 53.55, 50.78, 49.97, 45.23, 37.90, 32.98, 31.15, 28.44, 25.77, 22.09, 22.03, 21.75, 20.65, 17.83, 13.94, 11.47, 8.91, 8.56, 7.45.

IR (ATR) υ_{max} (cm^{-1}) 3348, 2932, 2879, 1724, 1648, 1586, 1431, 1372, 1225, 1062, 997, 971, 891, 770, 625, 466

Elemental analysis calcd (%) for [$N_{1,1,8,2OH}$][Rif] ● $2H_2O$: C 62.94, H 8.29, N 6.29; found C 62.30, H 8.46, N 6.60

2.3.5.6 2 - hydroxy - *N*- (2 - hydroxyethyl) - *N,N*- dimethylethan - 1 - aminium rifampicinate [N1,1,2OH,2OH][Rif]

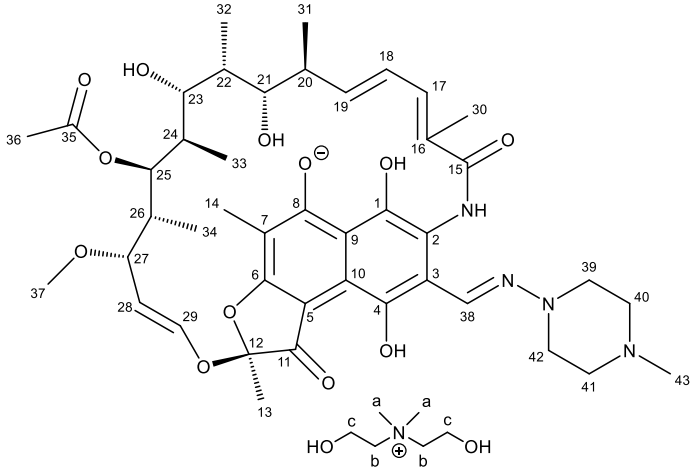

Following the previously described protocol, from 79.24 mg (0.367 mmol, 1.00 equiv.) of [N1,1,2OH,2OH][Br], 1.376 mL (1.101 mmol, 3.00 equiv.) of anionic exchange resin and 338.42 mg (0.367 mmol, 1.00 equiv.) of rifampicin we obtained a dark red powder.

^{1}H NMR (400 MHz, DMSO-*d6*) δ 15.49 (s, 1H, OH_4), 12.46 (s, 1H, NH_{15}), 9.07 (s, 1H, OH_1), 7.98 (s, 1H, H_{38}), 6.98 (dd, *J* = 16.0, 10.8 Hz, 1H, H_{18}), 6.27-6.16 (m, 2H, H_{29} and H_{17}), 5.85 (dd, *J* = 15.9, 6.6 Hz, 1H, H_{19}), 5.25 (t, *J* = 4.8 Hz, 2H, OH_c), 5.07 (d, *J* = 10.8 Hz, 1H, H_{25}), 4.93 (dd, *J* = 12.8, 8.2 Hz, 1H, H_{28}), 4.85 (d, *J* = 3.6 Hz, 1H, OH_{21}), 4.29 (d, *J* = 8.1 Hz, 1H, OH_{23}), 3.83 (s, 4H, H_c), 3.73 (d, *J* = 8.8 Hz, 1H, H_{21}), 3.50-3.40 (m, 4H, H_b), 3.23 (d, *J* = 8.3 Hz, 1H, H_{27}), 3.11 (s, 6H, H_a), 3.02-2.93 (m, 4H, H_{39} and H_{42}), 2.90 (s, 3H, H_{37}), 2.84 (t, *J* = 9.4 Hz, 1H, H_{23}), 2.28 (s, 3H, H_{43}), 2.21-2.11 (m, 1H, H_{20}), 1.97 (s, 3H, H_{36}), 1.91 (s, 3H, H_{30}), 1.89 (s, 3H, H_{14}), 1.62 (s, 3H, H_{13}), 1.62-1.53 (m, 1H, H_{22}), 1.39-1.28 (m, 1H, H_{24}), 1.10-1.00 (m, 1H, H_{26}), 0.92-0.80 (m, 6H, H_{31} and H_{32}), 0.44 (d, *J* = 6.8 Hz, 3H, H_{33}), -0.24 (d, *J* = 6.8 Hz, 3H, H_{34})

^{13}C NMR (101 MHz, DMSO-*d6*) δ 184.46, 183.98, 171.61, 169.58, 165.95, 148.43, 144.95, 142.83, 138.10, 134.28, 132.32, 131.89, 127.26, 117.44, 116.96, 116.86, 115.91, 113.90, 108.54, 100.75, 98.43, 76.50, 76.13, 73.59, 71.92, 65.85, 65.82, 65.80, 55.61, 54.99, 53.35, 51.55, 49.79, 44.98, 38.56, 37.92, 32.97, 22.08, 20.64, 17.82, 11.46, 8.91, 8.58, 7.46.

IR (ATR) υ_{max} (cm^{-1}) 3336, 2973, 2937, 2883, 1722, 1646, 1554, 1431, 1373, 1224, 1143, 1060, 997, 971, 891, 770, 736, 626, 456

Elemental analysis calcd (%) for [N1,1,2OH,2OH][Rif] ● 2.5H_2O: C 59.04, H 7.66, N 6.51, C 58.78, H 7.85, N 7.00

2.3.5.7 *N* , *N* - bis(2 - hydroxyethyl) - *N* - methylbutan - 1 - aminium rifampicinate [N1,4,2OH,2OH][Rif]

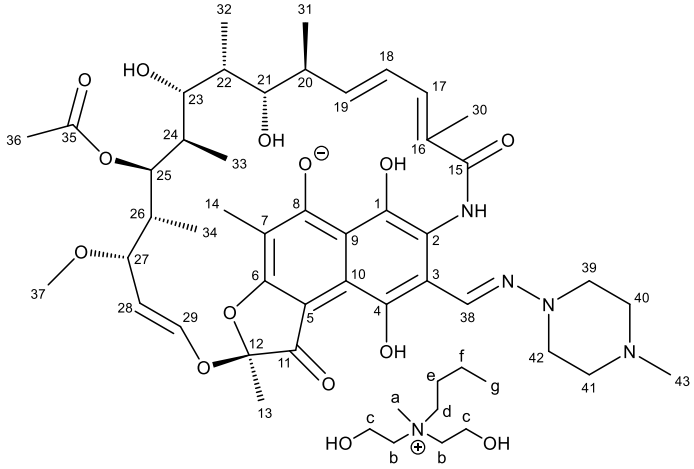

Following the previously described protocol, from 93.5 mg (0.365 mmol, 1.00 equiv.) of [N1,4,2OH,2OH][Br], 1.369 mL (1.095 mmol, 3.00 equiv.) of anionic exchange resin and 333,73 mg (0.365 mmol, 1.00 equiv.) of rifampicin we obtained a dark red powder.

^{1}H NMR (400 MHz, DMSO-*d6*) δ 15.47 (s, 1H, OH_4), 12.45 (s, 1H, NH_{15}), 9.11 (s, 1H, OH_1), 7.97 (s, 1H, H_{38}), 6.97 (dd, *J* = 15.9, 10.8 Hz, 1H, H_{18}), 6.27-6.16 (m, 2H, H_{29} and H_{17}), 5.85 (dd, *J* = 15.9, 6.6 Hz, 1H, H_{19}), 5.23 (t, *J* = 4.7 Hz, 2H, OH_c), 5.07 (d, *J* = 10.8 Hz, 1H, H_{25}), 4.93 (dd, *J* = 12.8, 8.2 Hz, 1H, H_{28}), 4.83 (d, *J* = 3.6 Hz, 1H, OH_{21}), 4.30 (d, *J* = 8.0 Hz, 1H, OH_{23}), 3.81 (s, 4H, H_c), 3.72 (d, *J* = 8.9 Hz, 1H, H_{21}), 3.50-3.40 (m, 4H, H_b), 3.23 (d, *J* = 8.3 Hz, 1H, H_{27}), 3.06 (s, 3H, H_a), 3.00-2.93 (m, 4H, H_{39} and H_{42}), 2.90 (s, 3H, H_{37}), 2.84 (t, *J* = 9.4 Hz, 1H, H_{23}), 2.46 (s, 4H, H_{40} and H_{41}), 2.21 (s, 3H, H_{43}), 2.21-2.11 (m, 1H, H_{20}), 1.97 (s, 3H, H_{36}), 1.91 (s, 3H, H_{30}), 1.89 (s, 3H, H_{14}), 1.70-1.63 (m, 2H, H_e), 1.62 (s, 3H, H_{13}), 1.60-1.53 (m, 1H, H_{22}), 1.39-1.22 (m, 3H, H_{24} and H_f), 1.10-1.00 (m, 1H, H_{26}), 0.96-0.80 (m, 9H, H_{31}, H_{32} and H_g), 0.44 (d, *J* = 6.8 Hz, 3H, H_{33}), -0.24 (d, *J* = 6.8 Hz, 3H, H_{34})

^{13}C NMR (101 MHz, DMSO-*d6*) δ 184.47, 183.92, 171.58, 169.58, 165.90, 148.41, 144.89, 142.83, 138.09, 133.85, 132.33, 131.87, 127.20, 117.42, 116.95, 116.81, 115.95, 113.85, 108.53, 100.71, 98.41, 76.50, 76.12, 73.58, 71.89, 63.21, 62.22, 55.60, 54.79, 53.63, 50.05, 48.98, 45.35, 38.58, 37.89, 32.98, 23.57, 22.09, 20.65, 19.19, 17.82, 13.49, 11.46, 8.90, 8.56, 7.45.

IR (ATR) υ_{max} (cm^{-1}) 3323, 2964, 2937, 2883, 1725, 1647, 1430, 1373, 1225, 1061, 997, 972, 891, 770, 626, 464

Elemental analysis calcd (%) for [N1,4,2OH,2OH][Rif] ● $2H_2O$: C 60.87, H 8.07, N 6.38; found C 60.39, H 8.09, N 6.77

2.3.5.8 *N,N* - bis(2 - hydroxyethyl) - *N* - methylhexan - 1 - aminium rifampicinate [N1,6,2OH,2OH][Rif]

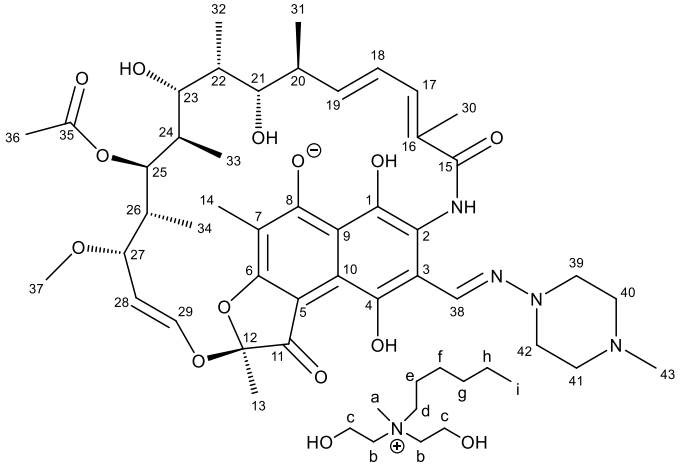

Following the previously described protocol, from 115.20 mg (0.405 mmol, 1.00 equiv.) of [N1,6,2OH,2OH][Br], 1,513 mL (1.215 mmol, 3 equiv.) of anionic exchange resin and 370.60 mg (0.405 mmol, 1.00 equiv.) of rifampicin we obtained a dark red powder.

^{1}H NMR (400 MHz, DMSO-*d6*) δ 15.49 (s, 1H, OH_4), 12.46 (s, 1H, NH_{15}), 9.08 (s, 1H, OH_1), 7.98 (s, 1H, H_{38}), 6.98 (dd, *J* = 15.9, 10.8 Hz, 1H, H_{18}), 6.27-6.16 (m, 2H, H_{29} and H_{17}), 5.85 (dd, *J* = 15.9, 6.6 Hz, 1H, H_{19}), 5.23 (t, *J* = 4.9 Hz, 2H, OH_c), 5.07 (d, *J* = 10.8 Hz, 1H, H_{25}), 4.93 (dd, *J* = 12.8, 8.2 Hz, 1H, H_{28}), 4.85 (d, *J* = 3.6 Hz, 1H, OH_{21}), 4.29 (d, *J* = 8.1 Hz, 1H, OH_{23}), 3.81 (s, 4H, H_c), 3.73 (d, *J* = 8.8 Hz, 1H, H_{21}), 3.50-3.40 (m, 4H, H_b), 3.23 (d, *J* = 8.3 Hz, 1H, H_{27}), 3.06 (s, 3H, H_a), 3.00-2.93 (m, 4H, H_{39} and H_{42}), 2.90 (s, 3H, H_{37}), 2.84 (t, *J* = 9.4 Hz, 1H, H_{23}), 2.27 (s, 3H, H_{43}), 2.21-2.11 (m, 1H, H_{20}), 1.97 (s, 3H, H_{36}), 1.91 (s, 3H, H_{30}), 1.89 (s, 3H, H_{14}), 1.70-1.63 (m, 2H, H_e), 1.62 (s, 3H, H_{13}), 1.60-1.53 (m, 1H, H_{22}), 1.40-1.21 (m, 7H, H24 H_f, H_g and H_i), 1.10-1.00 (m, 1H, H_{26}), 0.91-0.81 (m, 9H, H_{31}, H_{32} and H_g), 0.44 (d, *J* = 6.8 Hz, 3H, H_{33}), -0.24 (d, *J* = 6.8 Hz, 3H, H_{34})

^{13}C NMR (101 MHz, DMSO-*d6*) δ 184.46, 183.96, 171.60, 169.57, 165.93, 148.43, 144.95, 142.83, 138.09, 132.32, 131.88, 127.26, 117.44, 116.96, 116.86, 115.90, 113.89, 108.53, 100.74, 98.42, 76.50, 76.13, 73.59, 71.92, 63.20, 62.43, 55.60, 54.79, 53.37, 49.80, 48.96, 45.00, 38.56, 37.91, 32.97, 30.63, 25.42, 22.08, 21.85, 21.50, 20.63, 17.82, 13.79, 11.45, 8.91, 8.57, 7.45.

IR (ATR) υ_{max} (cm^{-1}) 3319, 2969, 2935, 2879, 1725, 1646, 1505, 1430, 1373, 1225, 1143, 1060, 997, 972, 891, 770, 626

Elemental analysis calcd (%) for [N1,6,2OH,2OH][Rif] ● 1.5H_2O: C 61.64, H 8.13, N 6.15; found C 61.58, H 8.23, N 6.65

2.3.5.9 *N,N* - bis(2-hydroxyethyl) - *N* - methyloctan - 1 - aminium rifampicinate [$N_{1,8,2OH,2OH}$][Rif]

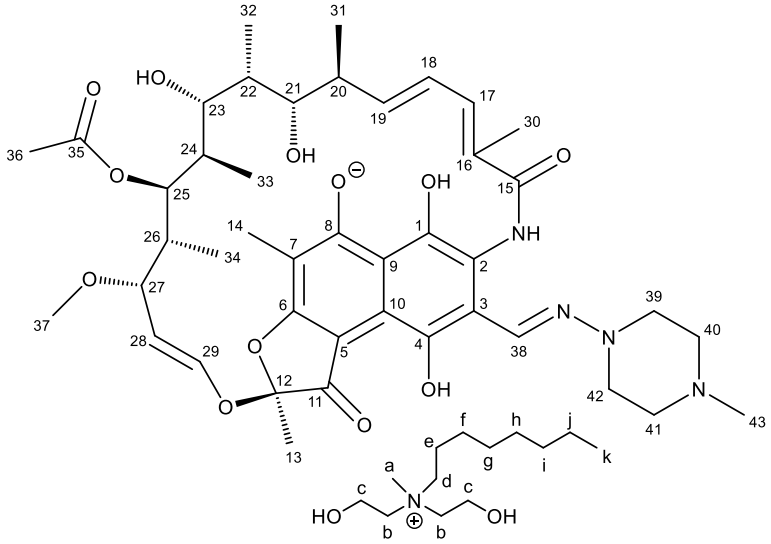

Following the previously described protocol, from 123.50 mg (0.395 mmol, 1.00 equiv.) of [$N_{1,8,2OH,2OH}$][Br], 1.481 mL (1.185 mmol, 3.00 equiv.) of anionic exchange resin and 361.61 mg (0.395 mmol, 1.00 equiv.) of rifampicin we obtained a dark red powder.

^{1}H NMR (400 MHz, DMSO-*d6*) δ 15.49 (s, 1H, OH_4), 12.46 (s, 1H, NH_{15}), 9.08 (s, 1H, OH_1), 7.98 (s, 1H, H_{38}), 6.98 (dd, J = 16.0, 10.8 Hz, 1H, H_{18}), 6.27-6.16 (m, 2H, H_{29} and H_{17}), 5.85 (dd, J = 15.9, 6.6 Hz, 1H, H_{19}), 5.23 (t, J = 5.0 Hz, 2H, OH_c), 5.07 (d, J = 10.8 Hz, 1H, H_{25}), 4.93 (dd, J = 12.8, 8.2 Hz, 1H, H_{28}), 4.85 (d, J = 3.6 Hz, 1H, OH_{21}), 4.29 (d, J = 8.1 Hz, 1H, OH_{23}), 3.81 (d, J = 4.9 Hz, 4H, H_c), 3.72 (d, J = 8.9 Hz, 1H, H_{21}), 3.50-3.40 (m, 4H, H_b), 3.23 (d, J = 8.3 Hz, 1H, H_{27}), 3.06 (s, 3H, H_a), 3.00-2.93 (m, 4H, H_{39} and H_{42}), 2.90 (s, 3H, H_{37}), 2.84 (t, J = 9.0 Hz, 1H, H_{23}), 2.46 (s, 4H, H_{40} and H_{41}), 2.26 (s, 3H, H_{43}), 2.21-2.11 (m, 1H, H_{20}), 1.97 (s, 3H, H_{36}), 1.91 (s, 3H, H_{30}), 1.89 (s, 3H, H_{14}), 1.70-1.63 (m, 2H, H_e), 1.62 (s, 3H, H_{13}), 1.60-1.53 (m, 1H, H_{22}), 1.39-1.20 (m, 11H, H_{24}, H_f, H_g, H_h, H_i and H_j), 1.10-1.00 (m, 1H, H_{26}), 0.96-0.80 (m, 9H, H_{31}, H_{32} and H_k), 0.44 (d, J = 6.8 Hz, 3H, H_{33}), -0.24 (d, J = 6.8 Hz, 3H, H_{34})

^{13}C NMR (101 MHz, DMSO-*d6*) δ 184.46, 183.95, 171.59, 169.56, 165.93, 148.43, 144.94, 142.82, 138.08, 134.21, 132.32, 131.88, 127.26, 117.43, 116.95, 116.85, 115.91, 113.89, 108.53, 100.73, 98.41, 76.50, 76.13, 73.59, 71.91, 63.19, 62.43, 55.60, 54.79, 53.39, 49.83, 48.96, 45.03, 38.56, 37.91, 32.97, 31.15, 28.44, 25.78, 22.08, 22.03, 21.56, 20.63, 17.82, 13.94, 11.46, 8.91, 8.57, 7.45.

IR (ATR) υ_{max} (cm^{-1}) 3335, 2964, 2931, 2879, 1725, 1646, 1506, 1431, 1373, 1225, 1144, 1061, 997, 972, 892, 770, 626, 468

Elemental analysis calcd (%) for [$N_{1,8,2OH,2OH}$][Rif] ● 1H_2O: C 62.54, H 8.44, N 6.13; found C 62.72, H 8.37, N 6.53

2.3.5.10 3-(2-hydroxyethyl)-1-methyl-1*H*-imidazol-3-ium rifampicinate [C2OHMIM][Rif]

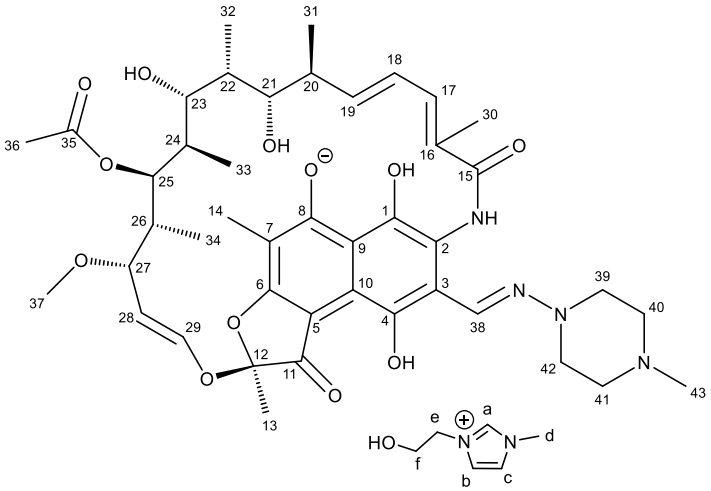

Following the previously described protocol, from 63.6 mg (0.390 mmol, 1.00 equiv.) of [C2OHMIM][Br], 1.463 mL (1.170 mmol, 3.00 equiv.) of anionic exchange resin and 321.8 mg (0.390 mmol, 1.00 equiv.) of rifampicin we obtained a dark red powder.

^{1}H NMR (400 MHz, DMSO-*d6*) δ 15.48 (s, 1H, OH_4), 12.45 (s, 1H, NH_{15}), 9.10 (s, 1H, OH_1), 9.07 (s, 1H, H_a), 7.98 (s, 1H, H_{38}), 7.71 (s, 1H, H_c), 7.68 (s, 1H, H_b), 6.97 (dd, *J* = 15.9, 10.8 Hz, 1H, H_{18}), 6.30-6.15 (m, 2H, H_{17} and H_{29}), 5.85 (dd, *J* = 16.0, 6.5 Hz, 1H, H_{19}), 5.2-5.12 (m, 1H, OH_f), 5.07 (d, *J* = 10.8 Hz, 1H, H_{25}), 4.93 (dd, *J* = 12.8, 8.1 Hz, 1H, H_{28}), 4.83 (d, *J* = 3.6 Hz, 1H, OH_{21}), 4.30 (d, *J* = 8.0 Hz, 1H, OH_{23}), 4.20 (t, *J* = 5.0 Hz, 2H, H_e), 3.86 (s, 3H, H_d), 3.77-3.69 (m, 3H, H_{21} and H_f), 3.23 (d, *J* = 8.3 Hz, 1H, H_{27}), 3.01-2.88 (m, 4H, H_{39} H_{42}), 2.90 (s, 3H, H_{37}), 2.84 (t, *J* = 9.4 Hz, 1H, H_{23}), 2.52-2.40 (m, 4H, H_{40} and H_{41}), 2.23 (s, 3H, H_{43}), 2.24-2.12 (m, 1H, H_{20}), 1.97 (s, 3H, H_{36}), 1.91 (s, 3H, H_{30}), 1.89 (s, 3H, H_{14}), 1.62 (s, 3H, H_{13}), 1.60-1.53 (m, 1H, H_{22}), 1.38-1.18 (m, 1H, H_{24}), 1.10-1.00 (m, 1H, H_{26}), 0.94-0.80 (m, 6H, H_{32} and H_{31}), 0.44 (d, *J* = 6.8 Hz, 3H, H_{33}), -0.24 (d, *J* = 6.8 Hz, 3H, H_{34})

^{13}C NMR (101 MHz, DMSO-*d6*) δ 184.47, 183.90, 171.56, 169.58, 165.89, 148.38, 144.86, 142.81, 136.77, 132.34, 131.86, 127.12, 123.31, 122.63, 116.89, 116.78, 115.98, 113.82, 108.52, 100.69, 98.39, 76.50, 76.12, 73.58, 71.86, 59.29, 55.59, 53.73, 51.59, 50.16, 45.48, 38.58, 37.87, 35.63, 32.98, 22.07, 20.63, 17.81, 11.45, 8.87, 8.54, 7.43.

IR (ATR) υ_{max} (cm^{-1}) 2969, 2937, 2879, 1725, 1647, 1555, 1506, 1431, 1373, 1225, 1159, 1061, 997, 972, 891, 769, 623, 468

Elemental analysis calcd (%) for [C2OHMIM][Rif] ● $3H_2O$: C 58.67, H 7.31, N 8.77; found C 58.67, H 7.44, N 8.38

2.3.5.11 3-butyl-1-methyl-1*H*-imidazol-3-ium rifampicinate [C4MIM][Rif]

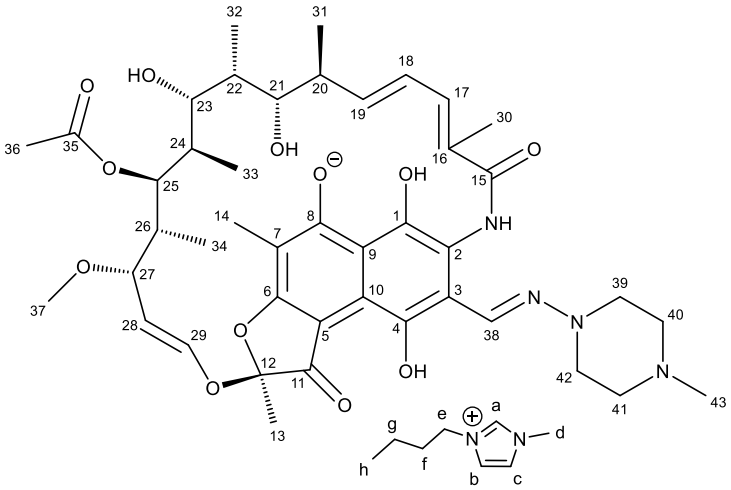

Following the previously described protocol, from 80.07 mg (0.365 mmol, 1.00 equiv.) of [C4MIM][Br], 1.4 mL (1.095 mmol, 3 equiv.) of anionic exchange resin and 333.0 mg (0.365 mmol, 1.00 equiv.) of rifampicin we obtained a dark red powder.

^{1}H NMR (400 MHz, DMSO-*d6*) δ 15.49 (s, 1H, OH_4), 12.46 (s, 1H, NH_{15}), 9.15-9.05 (m, 2H, OH_1 and H_a), 7.98 (s, 1H, H_{38}), 7.76 (s, 1H, H_c), 7.70 (s, 1H, H_b), 6.97 (dd, *J* = 15.9, 10.9 Hz, 1H, H_{18}), 6.23 (m, 2H, H_{17} and H_{29}), 5.86 (dd, *J* = 16.0, 6.6 Hz, 1H, H_{19}), 5.08 (d, *J* = 10.8 Hz, 1H, H_{25}), 4.94 (dd, *J* = 12.9, 8.2 Hz, 1H, H_{28}), 4.83 (s, 1H, OH_{21}), 4.31 (d, *J* = 8.0 Hz, 1H, OH_{23}), 4.16 (t, *J* = 7.2 Hz, 2H, H_e), 3.85 (s, 3H, H_d), 3.77-3.69 (m, 1H, H_{21}), 3.24 (d, *J* = 8.3 Hz, 1H, H_{27}), 3.01-2.88 (m, 4H, H_{39} and H_{42}), 2.91 (s, 3H, H_{37}), 2.85 (t, *J* = 9.4 Hz, 1H, H_{23}), 2.52-2.40 (m, 4H, H40 H_{41}), 2.22 (s, 3H, H_{43}), 2.24-2.12 (m, 1H, H_{20}), 1.98 (s, 3H, H_{36}), 1.92 (s, 3H, H_{30}), 1.90 (s, 3H, H_{14}), 1.81-1.72 (p, *J* = 7.5 Hz, 2H, H_f), 1.63 (s, 3H, H_{13}), 1.60-1.53 (m, 1H, H_{22}), 1.38-1.18 (m, 3H, H_{24} and H_g), 1.10-1.00 (m, 1H, H_{26}), 0.94-0.80 (m, 9H, H_{32}, H_h and H_{31}), 0.44 (d, *J* = 6.8 Hz, 3H, H_{33}), -0.24 (d, *J* = 6.8 Hz, 3H, H_{34})

^{13}C NMR (101 MHz, DMSO-*d6*) δ 184.48, 183.93, 171.58, 169.59, 165.93, 148.41, 144.90, 142.84, 138.10, 136.48, 133.87, 132.34, 131.88, 127.19, 123.61, 122.25, 117.41, 116.94, 116.82, 115.96, 113.85, 108.54, 100.72, 98.42, 76.51, 76.12, 73.59, 71.89, 55.61, 53.62, 50.04, 48.49, 45.34, 37.90, 35.73, 32.98, 31.34, 22.10, 20.66, 18.76, 17.83, 13.26, 11.46, 8.90, 8.56, 7.46.

IR (ATR) υ_{max} (cm^{-1}) 3409, 2964, 2936, 2879, 1724, 1651, 1496, 1431, 1373, 1224, 1160, 1062, 997, 972, 944, 891, 769, 736, 623, 469

2.3.5.12 1-methyl-3-octyl-1*H*-imidazol-3-ium rifampicinate [C8MIM][Rif]

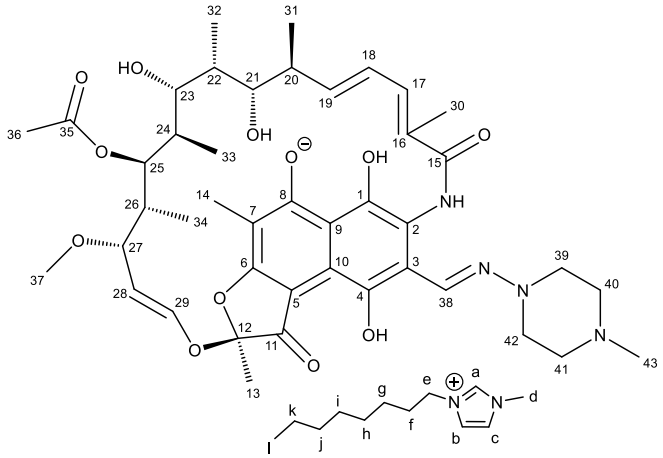

Following the previously described protocol, from 84,2 mg (0.365 mmol, 1.00 equiv.) of [C8MIM][Br], 1.369 mL (1.095 mmol, 3.00 equiv.) of anionic exchange resin and 333,0 mg (0.365 mmol, 1.00 equiv.) of rifampicin we obtained a dark red powder.

^{1}H NMR (400 MHz, DMSO-*d6*) δ 15.48 (s, 1H, OH_4), 12.45 (s, 1H, NH_{15}), 9.12-9.09 (m, 2H, OH_1 H_a), 7.97 (s, 1H, H_{38}), 7.75 (s, 1H, H_c), 7.68 (s, 1H, H_b), 6.97 (dd, *J* = 15.9, 10.8 Hz, 1H, H_{18}), 6.22 (m, 2H, H_{17} and H_{29}), 5.85 (dd, *J* = 15.9, 6.6 Hz, 1H, H_{19}), 5.07 (d, *J* = 10.8 Hz, 1H, H_{25}), 4.93 (dd, *J* = 12.8, 8.2 Hz, 1H, H_{28}), 4.83 (d, *J* = 3.6 Hz, 1H, OH_{21}), 4.30 (d, *J* = 8.0 Hz, 1H, OH_{23}), 4.13 (t, *J* = 7.2 Hz, 2H, H_e), 3.84 (d, *J* = 8.9 Hz, 1H, H_a), 3.75-3.69 (m, 1H, H_{21}), 3.23 (d, *J* = 8.3 Hz, 1H, H_{27}), 3.01-2.88 (m, 4H, H_{39} and H_{42}), 2.90 (s, 3H, H_{37}), 2.84 (t, *J* = 9.4 Hz, 1H, H_{23}), 2.52-2.40 (m, 4H, H_{40} and H_{41}), 2.21 (s, 3H, H_{43}), 2.24-2.12 (m, 1H, H_{20}), 1.98 (s, 3H, H_{36}), 1.91 (s, 3H, H_{30}), 1.89 (s, 3H, H_{14}), 1.81-1.72 (m, 2H, H_f), 1.62 (s, 3H, H_{13}), 1.60-1.53 (m, 1H, H_{22}), 1.38-1.18 (m, 11H, H_{24} H_g, H_h, H_i, H_j and H_k), 1.10-1.00 (m, 1H, H_{26}), 0.94-0.80 (m, 9H, H_{32}, H_l and H_{31}), 0.44 (d, *J* = 6.8 Hz, 3H, H_{33}), -0.24 (d, *J* = 6.8 Hz, 3H, H_{34})

^{13}C NMR (101 MHz, DMSO-*d6*) δ 184.46, 183.92, 171.57, 169.57, 165.92, 148.39, 144.89, 142.82, 138.10, 136.44, 133.88, 132.32, 131.87, 127.17, 123.57, 122.23, 117.41, 116.90, 116.82, 115.94, 113.85, 108.52, 100.70, 98.40, 76.50, 76.12, 73.58, 71.88, 55.59, 53.60, 50.03, 48.75, 45.31, 38.57, 37.88, 35.71, 32.97, 31.13, 29.35, 28.45, 28.31, 25.47, 22.07, 22.02, 20.63, 17.81, 13.90, 11.44, 8.88, 8.55, 7.43.

IR (ATR) υ_{max} (cm^{-1}) 3417, 2931, 1725, 1652, 1431, 1372, 1226, 1159, 1062, 998, 971, 891, 769, 623, 470

Elemental analysis calcd (%) for [C8MIM][Rif] ● $1H_2O$: C 64.01, H 7.99, N 8.42; found C 63.81, H 7.98, N 8.12

2.3.5.13 3-dodecyl-1-methyl-1H-imidazol-3-ium rifampicinate [C_{12}MIM][Rif]

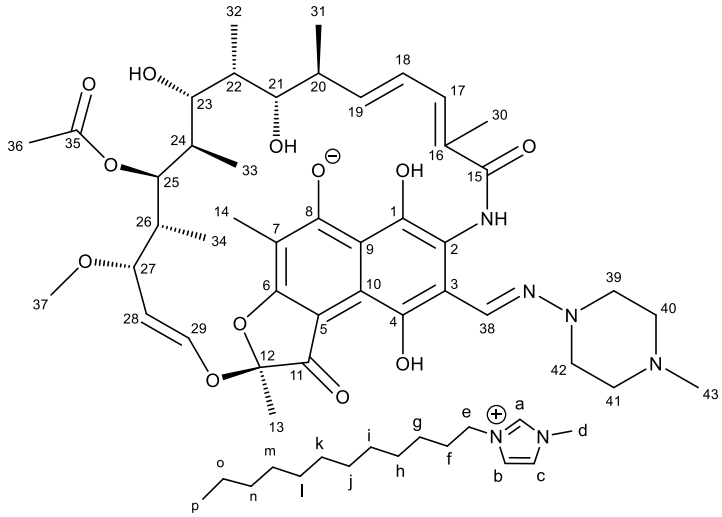

Following the previously described protocol, from 120.94 mg (0.365 mmol, 1.00 equiv.) of [C_{12}MIM][Br], 1.369 mL (1.095 mmol, 3.00 equiv.) of anionic exchange resin and 333.0 mg (0.365 mmol, 1.00 equiv.) of rifampicin we obtained a dark red powder.

^{1}H NMR (400 MHz, DMSO-*d6*) δ 15.48 (s, 1H, OH_4), 12.46 (s, 1H, NH_{15}), 9.15-9.05 (m, 2H, OH_1 H_a), 7.98 (s, 1H, H_{38}), 7.75 (s, 1H, H_c), 7.69 (s, 1H, H_b), 6.97 (dd, J = 16.0, 10.9 Hz, 1H, H_{18}), 6.25-6.15 (m, 2H, H_{17} and H_{29}), 5.85 (dd, J = 16.0, 6.5 Hz, 1H, H_{19}), 5.07 (d, J = 10.8 Hz, 1H, H_{25}), 4.93 (dd, J = 12.8, 8.2 Hz, 1H, H_{28}), 4.84 (d, J = 3.6 Hz, 1H, OH_{21}), 4.30 (d, J = 8.1 Hz, 1H, OH_{23}), 4.13 (t, J = 7.2 Hz, 2H, H_e), 3.84 (s, 3H, H_d), 3.72 (d, J = 8.8 Hz, 1H, H_{21}), 3.23 (d, J = 8.3 Hz, 1H, H_{27}), 3.02-2.88 (m, 4H, H_{39} and H_{42}), 2.90 (s, 3H, H_{37}), 2.84 (t, J = 9.3 Hz, 1H, H_{23}), 2.52-2.40 (m, 4H, H_{40} and H_{41}), 2.24 (s, 3H, H_{43}), 2.24-2.12 (m, 1H, H_{20}), 1.97 (s, 3H, H_{36}), 1.91 (s, 3H, H_{30}), 1.89 (s, 3H, H_{14}), 1.81-1.72 (m, 2H, H_f), 1.62 (s, 3H, H_{13}), 1.60-1.53 (m, 1H, H_{22}), 1.38-1.18 (m, 19H, H_{24}, H_g, H_h, H_i, H_j, H_k, H_l, H_m, H_n, and H_o), 1.10-1.00 (m, 1H, H_{26}), 0.94-0.80 (m, 9H, H_{32}, H_p and H_{31}), 0.44 (d, J = 6.7 Hz, 3H, H_{33}), -0.24 (d, J = 6.8 Hz, 3H, H_{34})

^{13}C NMR (101 MHz, DMSO-*d6*) δ 184.47, 183.90, 171.56, 169.57, 165.92, 148.39, 144.88, 142.83, 138.09, 136.45, 133.69, 132.33, 127.15, 123.57, 122.23, 116.90, 116.81, 115.96, 113.83, 108.52, 100.69, 98.40, 53.73, 50.14, 48.75, 45.47, 38.57, 37.87, 35.71, 32.98, 31.27, 29.35, 29.00, 28.98, 28.92, 28.80, 28.69, 28.36, 25.48, 22.09, 22.07, 20.64, 17.81, 13.92, 11.44, 8.88, 8.54, 7.43.

IR (ATR) υ_{max} (cm^{-1}) 3425, 2925, 2853, 1729, 1648, 1497, 1432, 1372, 1289, 1225, 1159, 1062, 998, 972, 891, 769, 736, 624, 470

Elemental analysis calcd (%) for [C_{12}MIM][Rif] • $2H_2O$: C 64.23, H 8.31, N 8.03; found C 63.88, H 8.36, N 7.58

2.3.5.14 3-hexadecyl-1-methyl-1*H*-imidazol-3-ium rifampicinate [C16MIM][Rif]

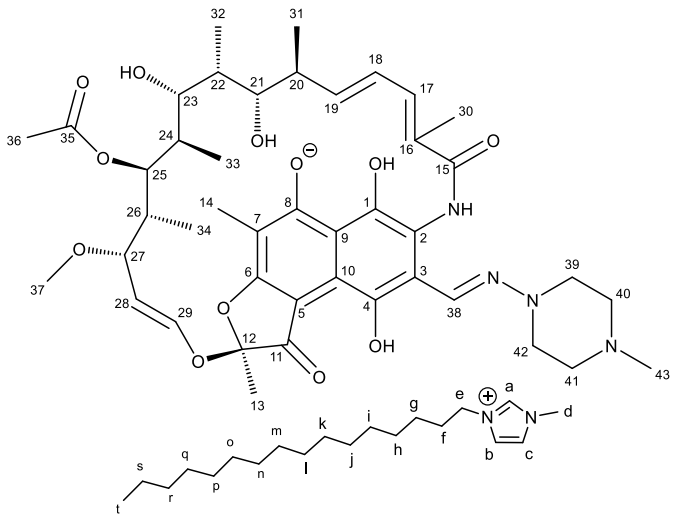

Following the previously described protocol, from 141.4 mg (0.365 mmol, 1.00 equiv.) of [C16MIM][Br], 1.369 mL (1.095 mmol, 3.00 equiv.) of anionic exchange resin and 333.0 mg (0.365 mmol, 1.00 equiv.) of rifampicin we obtained a dark red powder.

^{1}H NMR (400 MHz, DMSO-*d6*) δ 15.49 (s, 1H, OH_4), 12.46 (s, 1H, NH_{15}), 9.12 (s, 1H, OH_1), 9.09 (s, 1H, H_a), 7.99 (s, 1H, H_{38}), 7.76 (s, 1H, H_c), 7.69 (s, 1H, H_b), 6.98 (dd, *J* = 15.9, 10.8 Hz, 1H, H_{18}), 6.30-6.15 (m, 2H, H_{17} H_{29}), 5.85 (dd, *J* = 15.9, 6.6 Hz, 1H, H_{19}), 5.08 (d, *J* = 10.8 Hz, 1H, H_{25}), 4.94 (dd, *J* = 12.8, 8.2 Hz, 1H, H_{28}), 4.84 (d, *J* = 3.6 Hz, 1H, OH_{21}), 4.31 (d, *J* = 8.0 Hz, 1H, OH_{23}), 4.14 (t, *J* = 7.2 Hz, 2H, H_e), 3.85 (s, 3H, H_a), 3.77-3.69 (m, 1H, H_{21}), 3.24 (d, *J* = 8.2 Hz, 1H, H_{27}), 3.01-2.88 (m, 4H, H_{39} and H_{42}), 2.91 (s, 3H, H_{37}), 2.85 (t, *J* = 9.5 Hz, 1H, H_{23}), 2.52-2.40 (m, 4H, H_{40} and H_{41}), 2.23 (s, 3H, H_{43}), 2.24-2.12 (m, 1H, H_{20}), 1.98 (s, 3H, H_{36}), 1.92 (s, 3H, H_{30}), 1.90 (s, 3H, H_{14}), 1.63 (s, 3H, H_{13}), 1.60-1.53 (m, 1H, H_{22}), 1.40-1.15 (s, 26H, H_{24}, H_g, H_h, H_i, H_j, H_k, H_l, H_m, H_n, H_o, H_p, H_q, H_r and H_s), 1.10-1.00 (m, 1H, H_{26}), 0.94-0.80 (m, 9H, H_{32}, H_{31} and H_t), 0.44 (d, *J* = 6.8 Hz, 3H, H_{33}), -0.23 (d, *J* = 6.8 Hz, 3H, H_{34})

^{13}C NMR (101 MHz, DMSO-*d6*) δ 184.46, 183.93, 171.57, 169.56, 165.93, 148.40, 144.92, 142.82, 138.08, 133.99, 132.33, 131.86, 127.19, 123.57, 122.23, 117.41, 116.90, 116.83, 115.92, 113.86, 108.51, 100.70, 98.40, 76.50, 76.12, 73.59, 71.89, 55.59, 53.54, 49.96, 48.75, 45.23, 38.55, 37.88, 35.71, 32.97, 31.27, 29.36, 29.02, 28.99, 28.93, 28.81, 28.68, 28.36, 25.48, 22.07, 20.63, 17.79, 13.92, 11.43, 8.88, 8.54, 7.42.

IR (ATR) υ_{max} (cm^{-1}) 3429, 2924, 2853, 1729, 1649, 1497, 1434, 1372, 1226, 1159, 1062, 998, 972, 892, 769, 624, 471

Elemental analysis calcd (%) for [C16MIM][Rif] ● $1H_2O$: C 65.69, N 8.66, H 7.60; found C 66.99, H 8.61, N 7.32

2.3.5.15 Sodium rifampicinate Na[Rif]

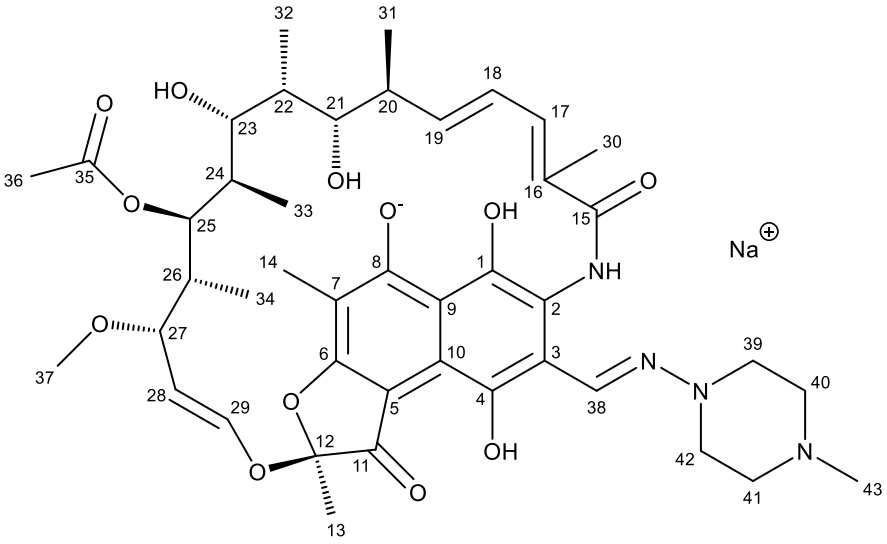

3.65 mL of a 0.1 M aqueous sodium hydroxide solution was added dropwise to 300 mg of rifampicin (0.365 mmol, 1 eq.) dissolved in 6 mL of methanol. The product was dried, and a red powder was obtained in quantitative yield.

^{1}H NMR (400 MHz, DMSO-*d6*) δ 15.47 (s, 1H, OH_4), 12.45 (s, 1H, NH_{15}), 9.15 (s, 1H, OH_1), 7.97 (s, 1H, H_{38}), 6.96 (dd, J = 15.9, 10.8 Hz, 1H, H_{18}), 6.30-6.15 (m, 2H, H17 H_{29}), 5.84 (dd, J = 15.9, 6.5 Hz, 1H, H_{19}), 5.07 (d, J = 10.7 Hz, 1H, H_{25}), 4.92 (dd, J = 12.8, 8.2 Hz, 1H, H_{28}), 4.84 (d, J = 3.6 Hz, 1H, OH_{21}), 4.32 (s, J = 8.0 Hz, 1H, OH_{23}), 3.72 (d, J = 8.9 Hz, 1H, H_{21}), 3.23 (d, J = 8.3 Hz, 1H, H_{27}), 3.00-2.80 (m, 4H, H_{39} H_{42}), 2.90 (s, 3H, H_{37}), 2.90-2.80 (m, 1H, H_{23}), 2.50-2.30 (m, 4H, H_{40} H_{41}), 2.17 (s, 3H, H_{43}), 2.25-2.15 (m, 1H, H_{20}), 1.97 (s, 3H, H_{36}), 1.91 (s, 3H, H_{30}), 1.89 (s, 3H, H_{14}), 1.62 (s, 3H, H_{13}), 1.60-1.50 (m, 1H, H_{22}), 1.40-1.30 (m, 1H, H_{24}), 1.10-1.00 (m, 1H, H_{26}), 0.90-0.80 (m, 6H, H_{31} H_{32}), 0.44 (d, J = 6.8 Hz, 3H, H_{33}), -0.24 (d, J = 6.8 Hz, 3H, H_{34})
IR (ATR) υ_{max} (cm^{-1}) 3393, 2977, 2883, 2822, 1717, 1648, 1586, 1546, 1501, 1435, 1373, 1346, 1289, 1225, 1142, 1061, 997, 975, 893, 771, 628

3

RESULTS AND DISCUSSION

3.1 Counter-ion synthesis

While most of the selected counter-ions were available in the laboratory, either purchased or previously prepared, eight of them were synthesized. More specifically, two imidazolium and six ammonium halides were prepared by alkylation of methylimidazole and the corresponding tertiary amines, respectively. It is important to emphasize that these reactions have been optimized in a microwave apparatus. The microwave process presented some advantages comparing to conventional reflux synthesis such as faster reactions times and easy purification steps. In this context, the possibility to optimize the synthetic protocols for the preparation of counter-ions by microwave process have been developed.

The first model reaction in microwave conditions was the synthesis of 1-dodecyl-3-methylimidazolium bromide [C_{12}MIM]Br. The protocol for this reaction was previously tested in our laboratories. The final pure product was proof after characterization by ^{1}H-NMR spectra, as indicated in Figure 3.1.

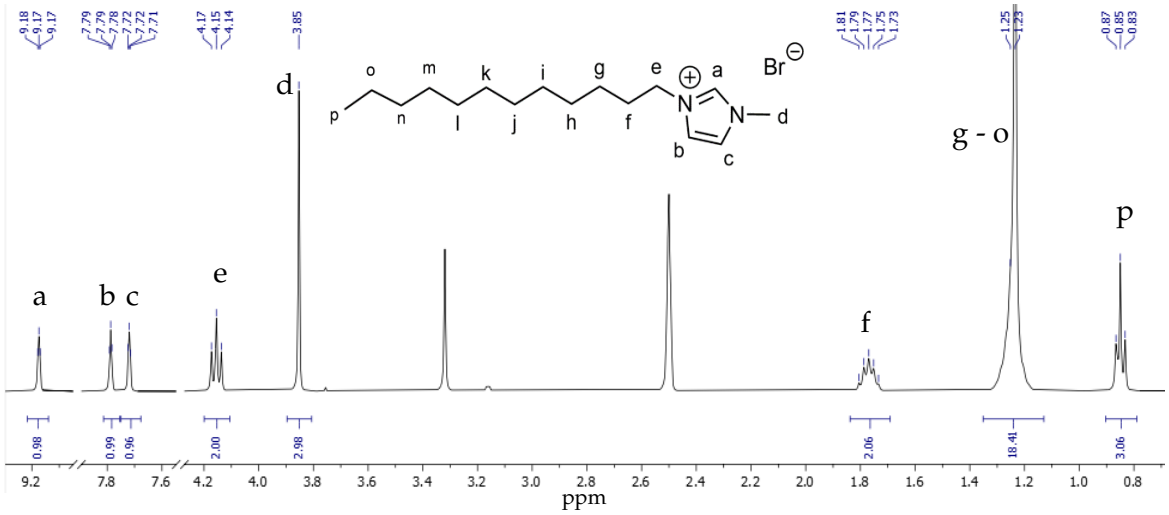

Figure 3.1 - ^{1}H-NMR spectrum of [C_{12}MIM]Br in DMSO-d_6

After purification, all peaks and correspondent predicted integrals can be attributed considering the chemical structure of the product. In these types of reactions, the formation of the desired product can be proved by the presence of the signals from the alkyl chain, even though the product was purified by washing with diethyl ether. As the product is an organic salt, it is easily separated from the nonpolar alkyl bromides that were used for its synthesis.

The yield was rather low at 55% due to low reactivity, incomplete reaction as well as difficult evaporation. No efforts were made to further improve the reaction yield. The product possesses a detergent behaviour through the water evaporation process, causing loss of yield. Lyophilization was carried out after several attempts to concentrate the product.

From this first reaction we concluded that water should not be an option for dissolution unless the salt didn't dissolve in any other polar solvent, and the reaction needed to be tracked by NMR to guarantee the reaction's completion.

In the case of the synthesis of 1-butyl-3-methyl-imidazolium bromide [C_4MIM]Br, acetonitrile was selected as solvent, and the reaction was checked by ^{1}H-NMR as indicated in Figure 3.2. After 120 min of reaction, the conversion to the desired product was almost complete with a small percentage of impurities easily removed after purification.

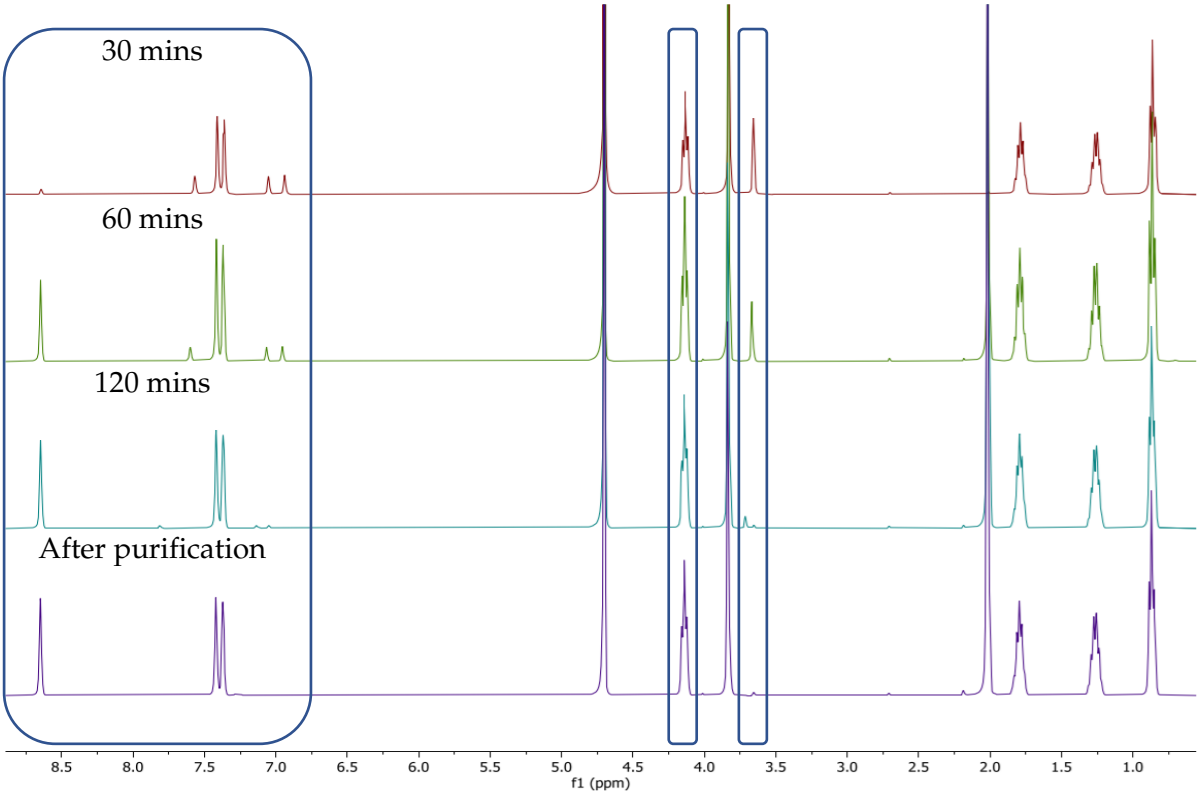

Figure 3.2 - Comparison of spectra from different reaction times of [C_4MIM]Br synthesis.

The synthesis of choline derivative salts was performed starting from commercially available tertiary amines with a final alkylation step with selected bromo-alkane. In general, the desired ammonium salt was obtained in moderate to high yield according to the reactivity of the respective alkylating agent. The reactions of [$N_{1,1,4,2OH}$]Br, [$N_{1,1,6,2OH}$]Br and [$N_{1,1,2OH,2OH}$]Br had overall good reactivity, finishing after 20 minutes with high yields except the latter where the low yield is due to human error.

In its turn, the synthesis of the cation family [$N_{1,x,2OH,2OH}$], with x=4, 6 and 8, had to account for the reduced reactivity of 2,2'-(methylazanediyl)bis(ethan-1-ol) because the nitrogen's free electrons can make intra and intermolecular hydrogen bonds. One of the problems we encountered with this reaction was in the tracking. When the reaction was stopped, the product would solidify in the vial and if it was put in the microwave again, the mixture would not be stirred until the temperature reached the melting point, and the product would visibly turn yellow. We suspect that without stirring, the part of the mixture that is exposed to the microwave radiation overheat and the alkyl bromide starts to react with alcohol groups. To avoid this from happening the vial should be heated to fuse the product to allow an efficient stirring since the beginning of the reaction.

3.2 Spectroscopic attribution of rifampicin

Prior to the synthesis of the desired final compounds, it was crucial to perform the total attribution of our drug, rifampicin, by NMR and FTIR spectroscopies. As rifampicin is not a new molecule, we based our attributions in literature and then confirmed these attributions with bidimensional NMR experiments. The referred spectra will be in Appendix 1, 2, 3, 4 and 5 that are 1H NMR, 13C NMR, COSY, HSQC and HMBC, respectively.

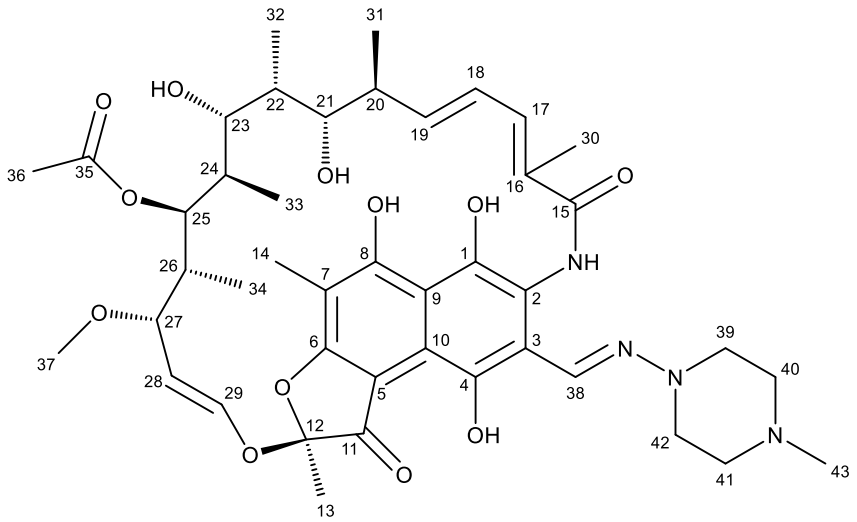

Figure 3.3 – Chemical structure of rifampicin and respective carbon numbering.

In this work, attribution of all ^{1}H NMR signals of rifampicin total was needed considering changes in shifts of signals can indicate interactions that are important for this work. This is particularly crucial in this thesis as rifampicin was combined with both anions and cations, due to its zwitterionic nature.

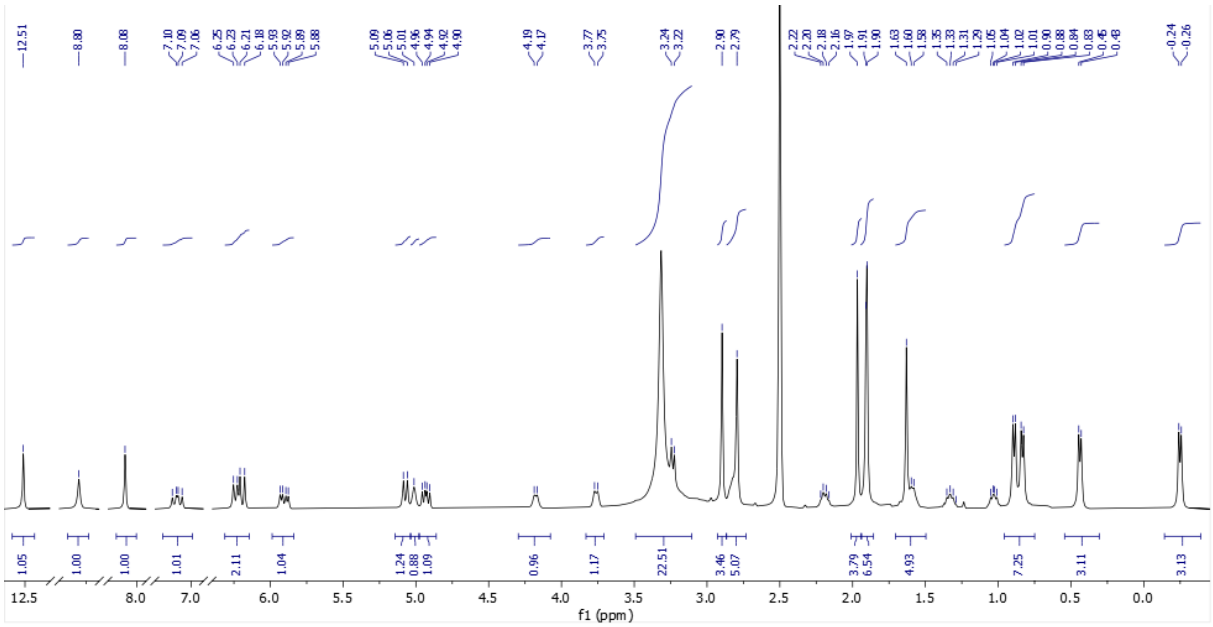

Figure 3.4 - ^{1}H-NMR spectrum of rifampicin in DMSO-*d6*.

An easy start for the attribution of this complex spectra is observing the signals in the 9.0-5.0 ppm range. These are attributed mainly to protons in double bonds. We acknowledged every signal in this range integrated to 1 proton, except for the signals between 6.3-6.1 ppm. These integrate to two protons and is composed of a superimposition of two signals. All the following attributions are either based or corroborated by literature [75]. In Figure 3.5, we observe the COSY correlation between the proton 18 with both protons 17 and 19. We can distinguish between these two signals considering H-17 presents as a doublet and H-19 as a doublet of doublets. From these we can attribute H-30, H-19 and H-20. By process of elimination, protons H-29 and H-28 can be identified due to the COSY correlation. To distinguish between these signals, H-29 is the doublet at δ 6.20 and then we attribute H-28, which in turn, couples with H-27. Hence H-28 is the double of doublets at δ 4.93 ppm.

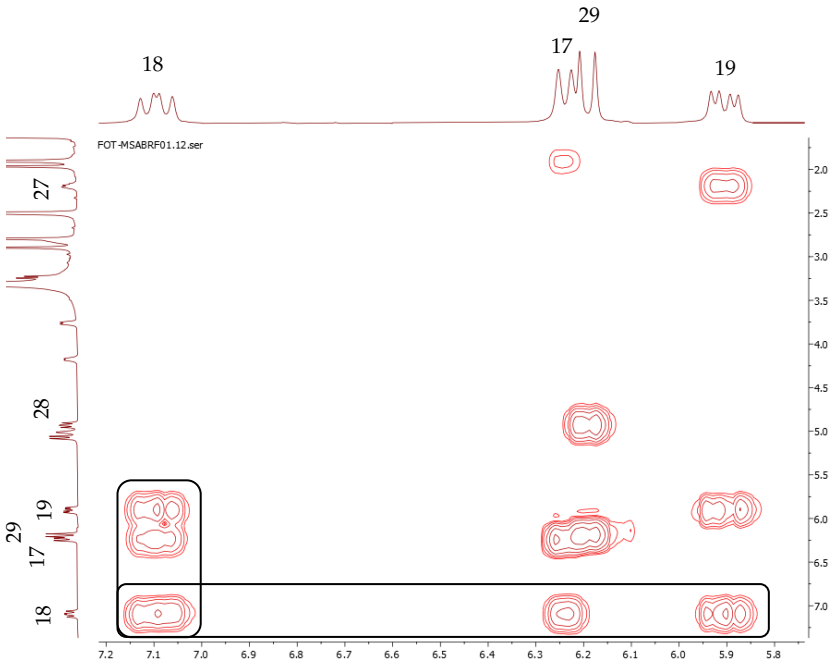

Figure 3.5 - Expansion of COSY correlation of rifampicin.

Moving on to Figure 3.6, it is possible to observe that H-28 has a COSY correlation with proton 27, that then has a weak correlation with proton 26. Proton 26 correlates to methyl group 34 and proton 25. From proton 25, we do not have more correlations, which can be due to the three-dimensional orientation of the molecule. Based on literature [50], we proceeded to look into attributing the respective carbon signal with HSQC and looking for a correlation in the HMBC. Unfortunately, carbon 25 only has a new correlation: methyl group 33 that we can attribute due to the integration. However, methyl group 33 has a COSY correlation with proton 24. Continuing the COSY correlation chain, proton 24 has correlation with superposition of 43 and 23. Please note this signal is comprised of a methyl group and single proton, considering the integration is for four protons. This superposition only has one more correlation with a non-carbon bonding proton. The only possible correlation is alcohol group 23. We can finalize the attribution of the side chain by using proton 20 that was attributed before. This proton correlates to proton 21 and methyl group 31. Proton 21 has a correlation with proton 22 but once again, with this signal, the COSY chain is broken.

The remaining signals were attributed by process of elimination and using literature. The signals from protons 39, 40, 41 and 42 that constitute the piperazine ring are superimposed by water and DMSO.

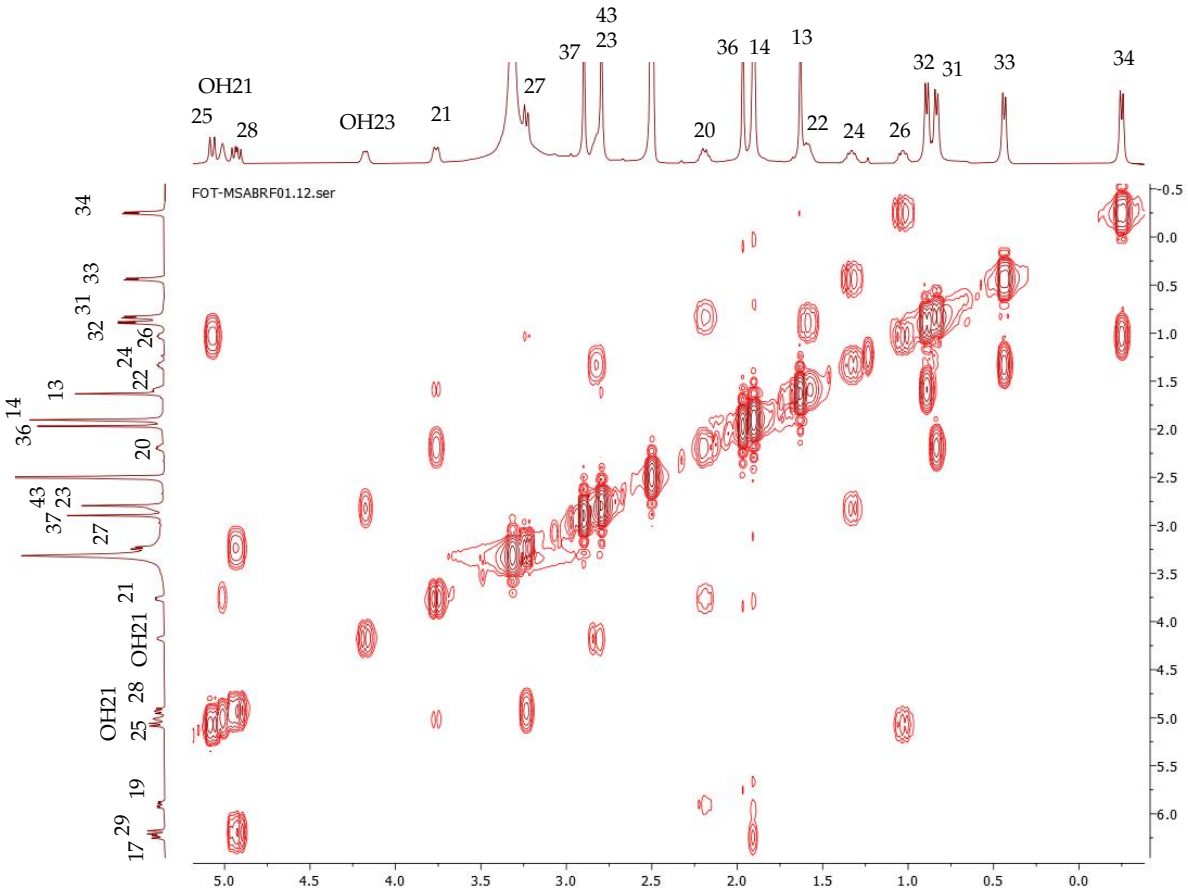

Figure 3.6 - COSY correlations rifampicin in DMSO-d_6

Following the complete identification of the ^{1}H-NMR spectra we turned to its FTIR spectrum. Considering literature reports from Liu et al.[76] and Agrawal et al. [77], a rough attribution of bands of this drug can be made (Figure 3.7): 3481 cm^{-1} is attributed to O-H and N-H bonds stretching vibrations, 3000-2800 cm^{-1} to C-H bonds stretching, 1726 cm^{-1} to C=O bond stretching, 1645 cm-1 to C=N bond stretching, and 1564 cm^{-1} to aromatic C=C bonds. Unfortunately, in this work, FTIR was not used as extensively as in other works by our group due to the complex nature of rifampicin's spectrum. However, FTIR spectroscopy can be used to identify ionization of the sulfonic acids into sulfonates upon combination with Rifampicin.

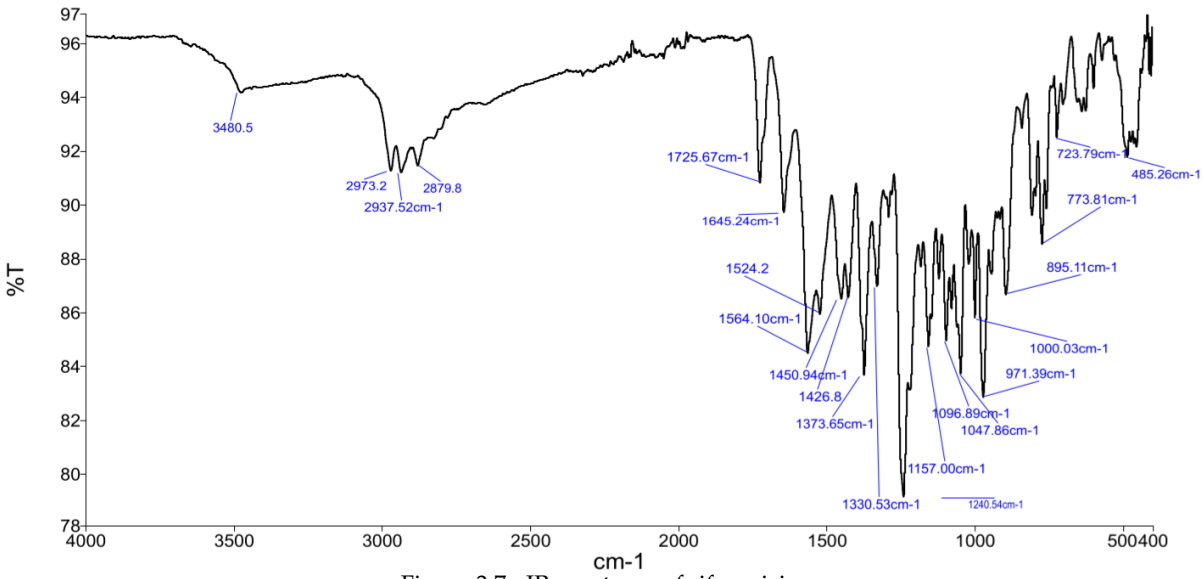

Figure 3.7 - IR spectrum of rifampicin.

3.3 Cationic approach for rifampicin-OSILs' synthesis

Rifampicin is a zwitterionic drug, allowing us to explore two different synthetic approaches. The cationic approach uses rifampicin as a cation combined with several anions associated to diverse anions. The synthesis of compounds in this approach occurred without major setbacks. The resin methodology previously developed and reported by the research group was found to be suitable in the case of Rifampicin, so there was no need for its optimization. In fact, as purification of the final product was not required with this methodology, all compounds were obtained in quantitative yields.

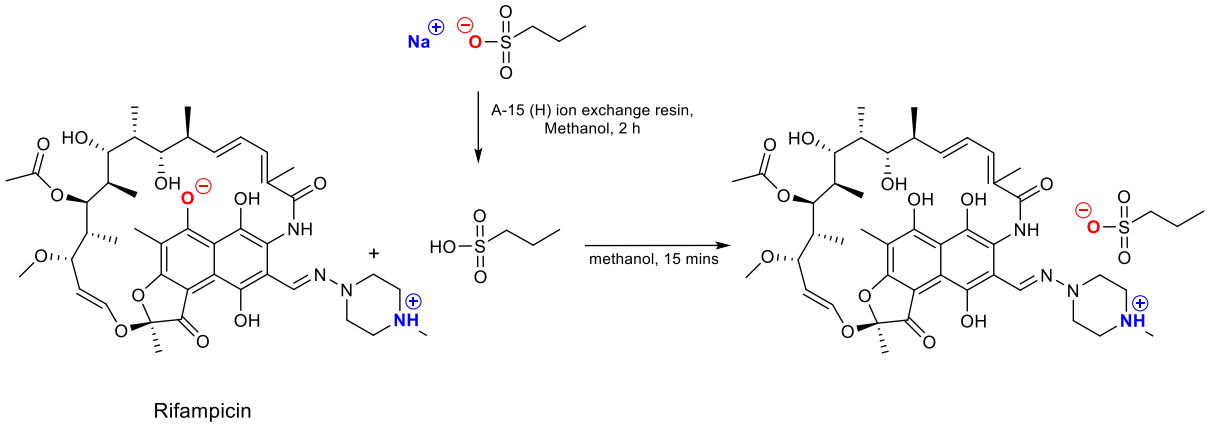

Figure 3.8 - Scheme of cationic approach synthesis.

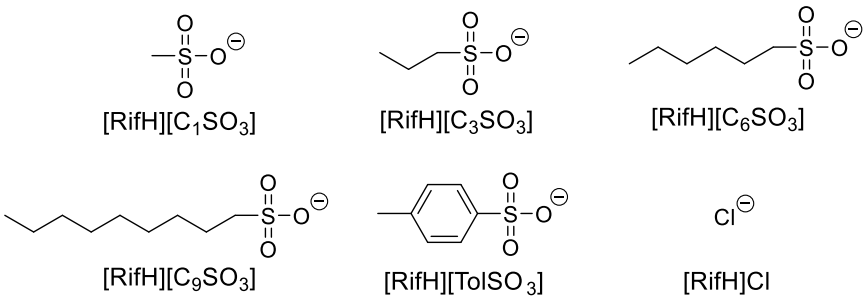

Figure 3.9 – Counter-ions used in the cationic approach

In this approach, direct protonation of rifampicin with sulfonic acids was performed (illustrated in Figure 3.8) to obtain Rif-OSILs with counter-ions represented in Figure 3.9. Successful synthesis of these compounds could be observed by both ^{1}H-NMR and FTIR.

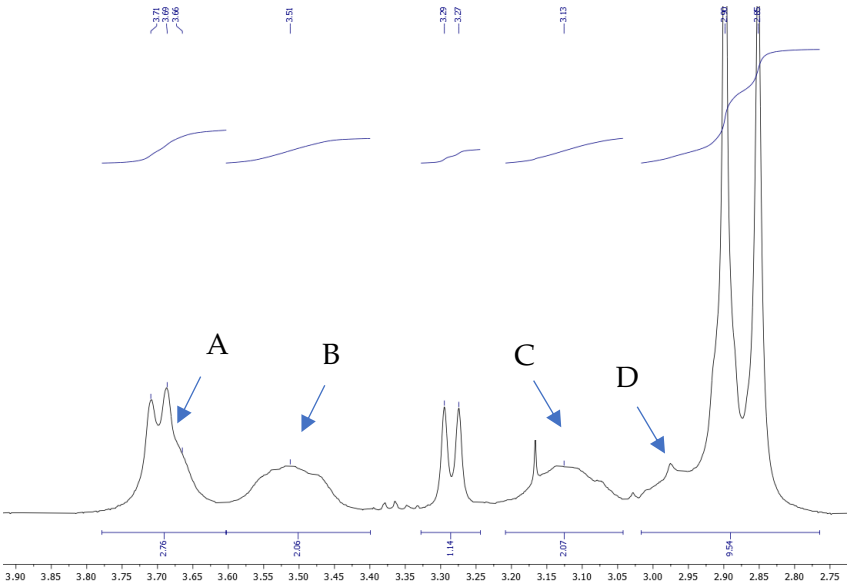

Figure 3.10 - Figure 11 — Expansion of ^{1}H-NMR spectra of [RifH][C_1SO_3].

In the case of ^{1}H-NMR, we could observe slight changes in chemical shifts of protons in the molecule as a whole, but the most compelling evidence is presented in figure 11. This figure demonstrates the formation of new signals, evidenced by the arrows, that we attribute to protons of the piperazine ring (protons 39, 40, 41, and 42). These could not be observed in rifampicin's spectra due to superimposition with water and deuterated DMSO. All signals integrate to two protons but in the HSQC correlation, it is observed a coupling between each signal and two separate carbons. With this observation, it is possible to conclude that each signal has two equivalent protons from different carbons.

In conclusion, signals A and D each possesses one proton from secondary carbons 39 and 42, and signals B and C have each one proton from 40 and 41. This significant change not

only is consistent with an interaction between our drug and the desired counter-ion, but also a possible change in the structure of the drug to accommodate this counter-ion.

Another method to prove this interaction is IR spectroscopy. Rifampicin is a complex compound where the changes in the IR spectrum are not obvious. In particular, the ammonium group in the piperazine ring does not present a distinct observable band. As an alternative, we can track the counter-ion ionization itself in the cases where this is possible, for example in the case of NMR spectra from [RifH][TolSO3]. In this case, it is possible to compare the spectra of different possible components of the formulation. In Figure 3.11, it is clear that the bands of the starting reagent named *para*-toluenesulfonic acid (TolSO3H) are either absent in the product's spectra, e.g. 1100 cm^{-1}, or slightly deviated, e.g. 683 cm^{-1}. The bands in the spectrum of the ionized counter-ion sodium *para*-toluenesulfonate (Na[TolSO3]) are a better match for the new product's spectrum. With this comparison, it is proof of ionization of the counter-ion and, by extension, the ionization of our drug.

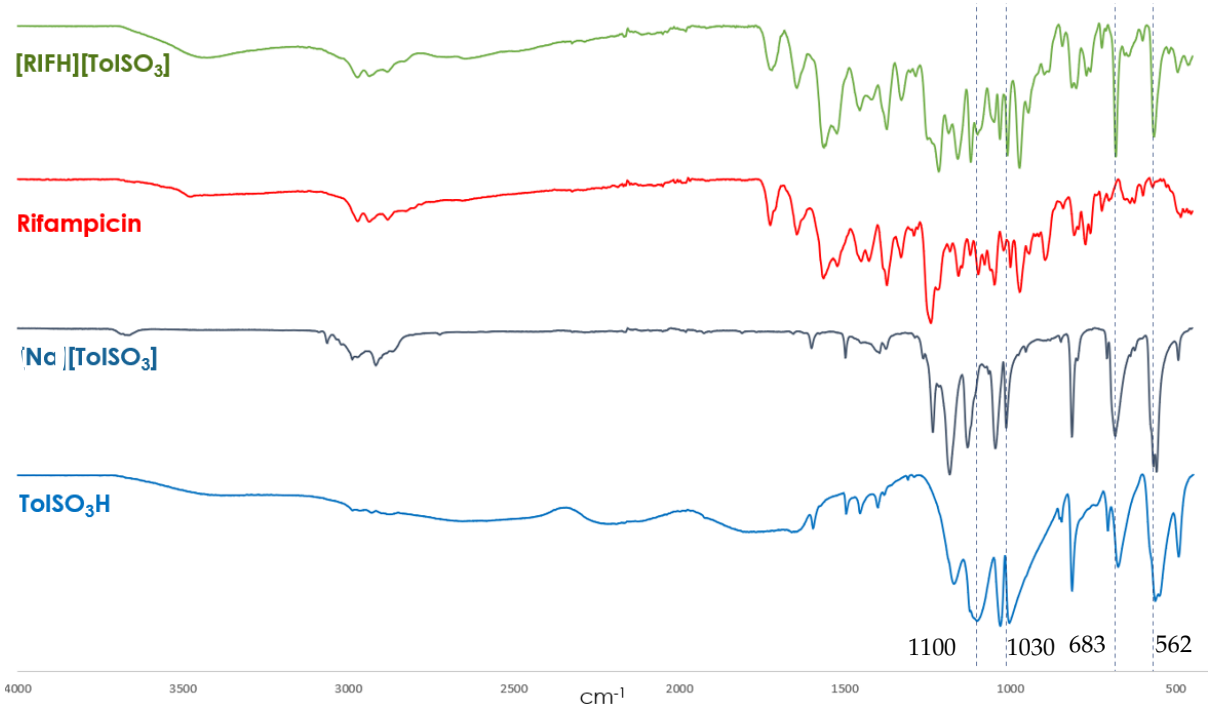

Figure 3.11 - Comparison of infrared spectra of [RifH][TolSO3] and possible components of the mixture.

In this approach, only sulfonates were used as counter-ions. This is due to the observation that the drug and the counter-ion separated. This fact was observed when PBS solubility studies were conducted and in order to corroborate our findings, the partition coefficient of [RifH][TolSO3] was performed. It is important to emphasize that this compound was selected due to both ions absorbing in the UV-Vis range.

After the experiment, rifampicin and the counter-ion are almost fully separated with most of rifampicin in the octanol phase. In Figure 3.12, the band at 221 nm is attributed to the

counter-ion *para*-toluenesulfonate that is in its majority in the aqueous phase after the experiment.

Due to these findings no more compounds were synthesised in this approach. The separation was to be expected considering the predicted pKa of the deprotonated alcohol is around 1.7 [23]. With such a low pKa, this alcohol deprotonates easily, making rifampicin's formal charge zero, separating from the counter-ion.

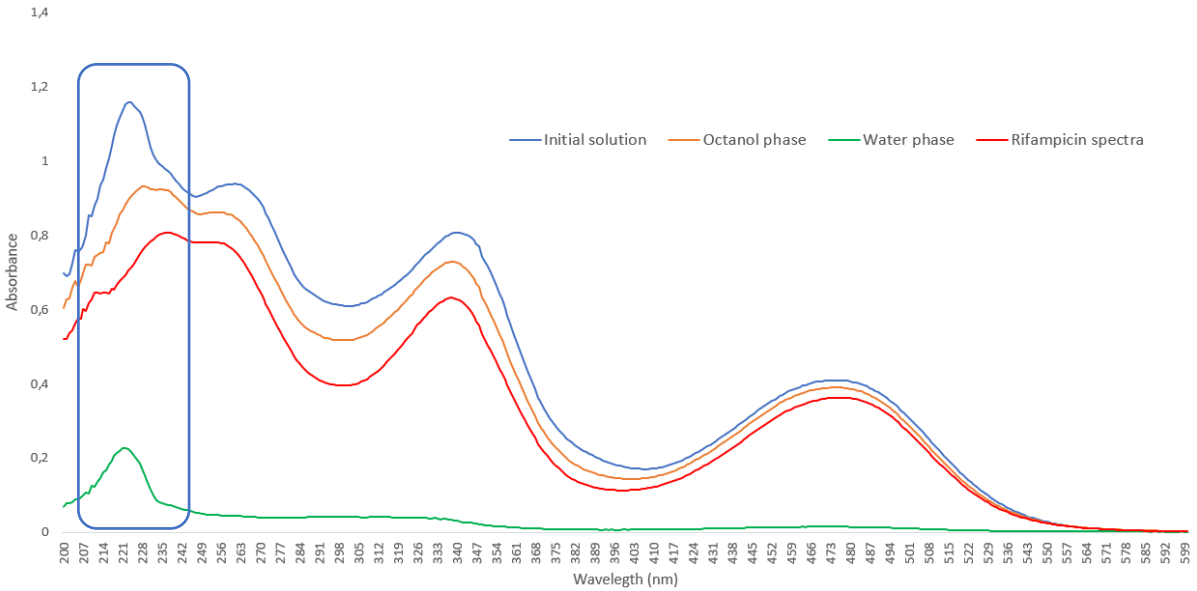

Figure 3.12 - Comparison of UV-Vis spectra from partition coefficient studies of [RifH][TolSO3].

3.4 Anionic approach for rifampicin-OSILs' synthesis

The anionic approach focuses on the use of rifampicin as an anion combined with diverse cations. We experimented with two major types of cations, methyl-imidazoles and ammoniums, compounds previously synthesised and used as counter-ions by the group [37], [78]. In parallel with the cationic approach, the synthetic protocols were already optimized by the group and were consistent throughout this work. A scheme of this process can be observed in Figure 3.13 while the selected counter-ions are represented in Figure 3.14.

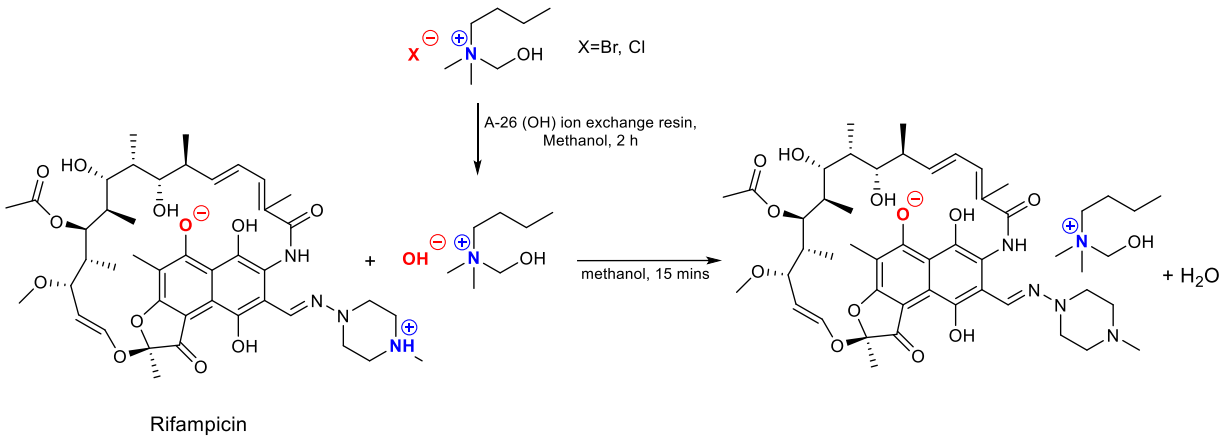

Figure 3.13 - Scheme of anionic approach synthesis

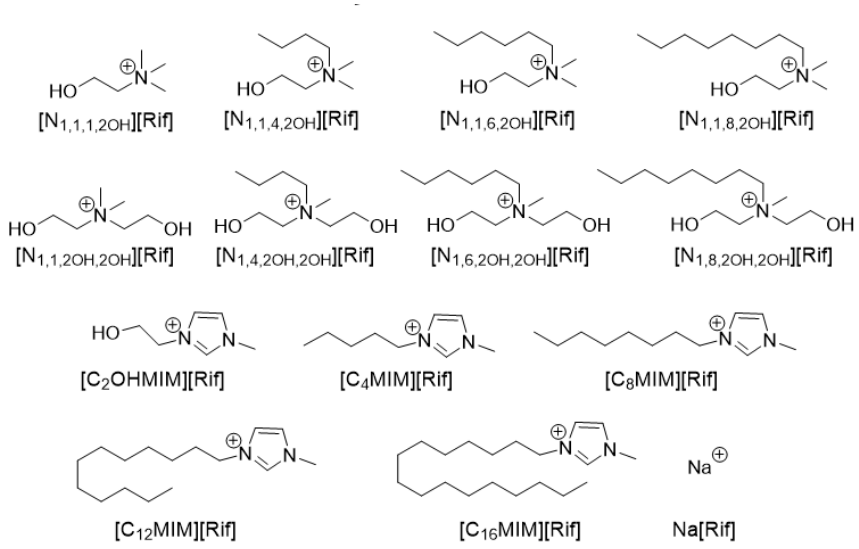

Figure 3.14 - Counter-ions used in the anionic approach.

For us to report these Rif-OSILs, proof of ionization must be provided to justify such an interaction. Unfortunately, these observations could not be made by IR, as only minor changes in the spectra could be observed, but such bands were not attributed to specific functional groups in the molecule to justify an interaction. Furthermore, the anionic approach used

a set of cations that are not protic, and in so, have a static positive charge. In other words, and as presented in Figure 3.13, the reaction consists of the deprotonation of Rifampicin's aromatic OH group by the selected cation hydroxides, which are very strong bases. This yields the desired Rif-OSILs and one molecule of water. These counter-ions have a fixed charge, and in so do not have a change in IR spectra with interaction with the API. In the case of ^{1}H-NMR spectroscopy, variations in the chemical shifts of peaks are observed. The signal at 9 ppm deviated slightly but it's a constant shift throughout spectra associated with this approach. Another example is related with the reported peak at 15.5 ppm in Figure 3.15. This signal is often overlooked in rifampicin's spectra throughout literature due to being a small and wide signal.

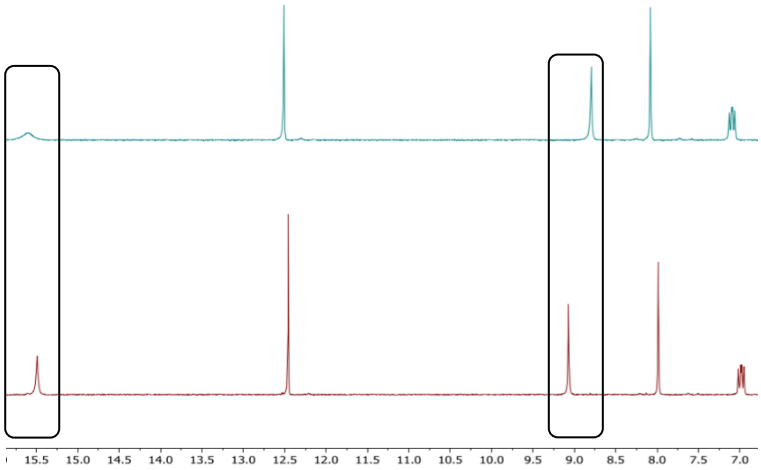

Figure 3.15 - Comparison of 1H-NMR of rifampicin and [N1,1,1,2OH][Rif].

In Figure 3.15, it is possible to consider that the peak changed significantly, and attribute it to proton from alcohol group 4 through HMBC correlations. This can be due to a change in the ring's resonance from the interaction between the deprotonated aromatic alcohol 8 and the cations, that slows the exchange of OH and obtains a signal with better resolution. Corroborating evidence of the interaction comes from an increase in the solubility of Rif-OSILs in comparison with rifampicin solubility referred to below.

3.5 Solubility in water and PBS solution

The solubility in water of an API is a focal point in drug development. It can determine how the API is absorbed, distributed and excreted.

Rifampicin showed an extremely low water solubility, due to its chemical structure and zwitterionic nature. In this context, the improvement of its water solubility is crucial in order to promote absorption as well as to achieve a more balanced permeability and a better diffusion. This augmented solubility could mean a lower liver toxicity but also a lower half-life, this being a delicate balance in drug development.

Holstege, C [79] reports a water solubility of rifampicin of 1.3 mg/mL at pH<6. In this work, this drug did not dissolve within our minimum solubility of 0.5 mg/mL at pH≈7 in both distilled water and PBS. All results are placed in Table 3.1 The most promising results are represented in Figure 3.16.

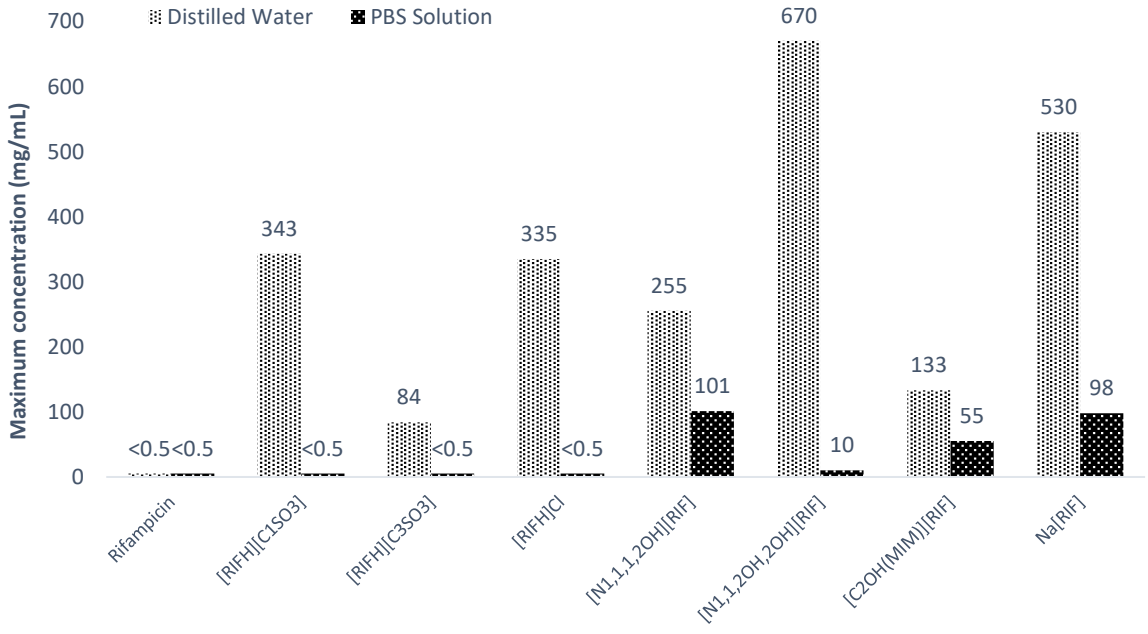

Figure 3.16 - Distilled water and PBS solubilities of rifampicin and most promising Rif-OSILs.

In the cationic approach, previously determined not to be ideal due instability of the Rif-OSIL, we obtained pronounceable increases in solubility with both [RifH][C_1SO_3] and [RifH][C_3SO_3]. [RifH][C_1SO_3] was extremely promising, obtaining a higher solubility than using an inorganic counter-ion, in this case, [RifH]Cl. When added to PBS solution, compounds of the cationic approach would form a suspension with a noticeable color change from the original dark red into a bright one. One of the possible explanations for this change derives from the separation of the Rif-OSILs due to the presence of ions in the PBS solution. These results, once again, turn our attention to the anionic approach.

In the anionic approach, we can observe a substantial increase in solubility with Rif-OSILs like [$N_{1,1,1,2OH}$][Rif], [$N_{1,1,2OH,2OH}$][Rif] and [C_2OHMIM][Rif]. However, only [$N_{1,1,2OH,2OH}$][Rif] showed a higher water solubility comparing to sodium salt, Na[Rif]. These results changed in the solubility studies in PBS solution. The highest PBS solubility is from [$N_{1,1,1,2OH}$][Rif], higher than the inorganic counterpart.

In both approaches different sizes of alkyl chains were tested, and as expected, considering rifampicin is nearly insoluble in water, the counter-ions that did not improve this solubility due to larger alkyl chains were insoluble. The solubility of compounds such as [C_{12}MIM][Rif] and [C_{16}MIM][Rif] were nearly zero. Even in extremely small quantities, a strong orange colour could be observed in the medium with the slightest dissolution. In the case of [C_{12}MIM][Rif] and [C_{16}MIM][Rif], no colour was observed at all. However, smaller alkyl chain counter-ions contribute for a variety of water solubility data that still increased API solubility slightly, such as [$N_{1,1,4,2OH}$][Rif] and [$N_{1,4,2OH,2OH}$][Rif]. Although these results can seem inconsequential, please note that pharmaceutical development is a fine balance and the slight differences these compounds produce in bioavailability can significantly alter the permeability and half-life of the API.

The Rif-OSIL [$N_{1,1,1,2OH}$][Rif] was considered the most promising compound and the first choice for complementary studies involving the toxicity assays and dry powder production. Further studies must be performed with [$N_{1,1,2OH,2OH}$][Rif] to ascertain the reasoning for such a difference between solubility profile in water and PBS.

Table 3.1 – Water and PBS solubility data at 37 ºC.

Compound	Solubility in water at 37 ºC (mg/mL)	Solubility in PBS at 37 ºC (mg/mL)	Compound	Solubility in water at 37 ºC (mg/mL)	Solubility in PBS at 37 ºC (mg/mL)
Rifampicin	<0.5	<0.5	**[$N_{1,1,2OH,2OH}$][Rif]**	670	10
[RifH][C_1SO_3]	343	<0.5	**[$N_{1,4,2OH,2OH}$][Rif]**	8	<0.5
[RifH][C_3SO_3]	84	<0.5	**[$N_{1,6,2OH,2OH}$][Rif]**	1	<0.5
[RifH][C_6SO_3]	<0.5	<0.5	**[$N_{1,8,2OH,2OH}$][Rif]**	<0.5	<0.5
[RifH][C_9SO_3]	<0.5	<0.5	**[C_2OHMIM][Rif]**	133	55
[RifH][TolSO$_3$]	<0.5	<0.5	**[C_4MIM][Rif]**	4	<0.5
[RifH]Cl	335	<0.5	**[C_8MIM][Rif]**	<0.5	<0.5
[$N_{1,1,1,2OH}$][Rif]	255	101	**[C_{12}MIM][Rif]**	<0.5	<0.5
[$N_{1,1,4,2OH}$][Rif]	12.0	6	**[C_{16}MIM][Rif]**	<0.5	<0.5
[$N_{1,1,6,2OH}$][Rif]	<0.5	<0.5	**Na[Rif]**	530	98
[$N_{1,1,8,2OH}$][Rif]	<0.5	<0.5			

3.6 1-Octanol/water partition coefficients (K_{ow})

Partition coefficient assays are a means to predict permeability properties of compounds. Compounds with K_{ow} lower than 1 are predominantly hydrophilic while the compounds with K_{ow} higher than 1 are predominantly lipophilic. In Table 3.2 are placed the results obtained from such assays. As compounds from the cationic approach were shown to separate in these assays they are not listed.

Table 3.2 - 1-octanol/water partition coefficient assays after 2 hours .

Compound	Octanol/Water Partition Coefficient	Compound	Octanol/Water Partition Coefficient
Rifampicin	4.5±0.4	[$N_{1,8,2OH,2OH}$][Rif]	>25[a]
[$N_{1,1,1,2OH}$][Rif]	1.9±0.1	[C_2OHMIM][Rif]	1.6±0.1
[$N_{1,1,4,2OH}$][Rif]	2.9±0.02	[C_4MIM][Rif]	3.7±0.3
[$N_{1,1,6,2OH}$][Rif]	8.9±0.9	[C_8MIM][Rif]	>25[a]
[$N_{1,1,8,2OH}$][Rif]	>25[a]	[C_{12}MIM][Rif]	>25[a]
[$N_{1,1,2OH,2OH}$][Rif]	1.8±0.03	[C_{16}MIM][Rif]	>25[a]
[$N_{1,4,2OH,2OH}$][Rif]	3.2±0.1	Na[Rif]	1.5±0.2
[$N_{1,6,2OH,2OH}$][Rif]	9.0±0.8		

Several K_{ow} values of the Rif-OSILs showed a considerable improvement of hydrophilicity of the API, from which, [C_2OHMIM][Rif] was the most promising. However, a lower K_{ow} was expected for these highly soluble Rif-OSILs, so an assay was done to understand the equilibrium process.

The assay tracked variation of partition coefficient as function of time. In a normal Kow assay, this function should show a stabilization between the two phases in the form of a logarithmic type curve into a stabilization at which point the Kow can be calculated. So, if a compound started in the 1-octanol phase, it would gradually transfer to the water phase and reach an equilibrium, as depicted in Figure 3.17.B.

However, the partition coefficient of the Rif-OSILs did not stabilize after several hours. This was particularly abnormal because the equilibrium curve was inverted, as represented in Figure 3.17.A. As the compound started in the 1-octanol phase, it quickly reached a maximum concentration in the water phase, indicated by the K_{ow} near to 1. Unexpectedly, the

concentration of compound in water started to decline as an increase of K_{ow} is observed. Due to this increase, this method is no longer applicable to rifampicin and Rif-OSILs.

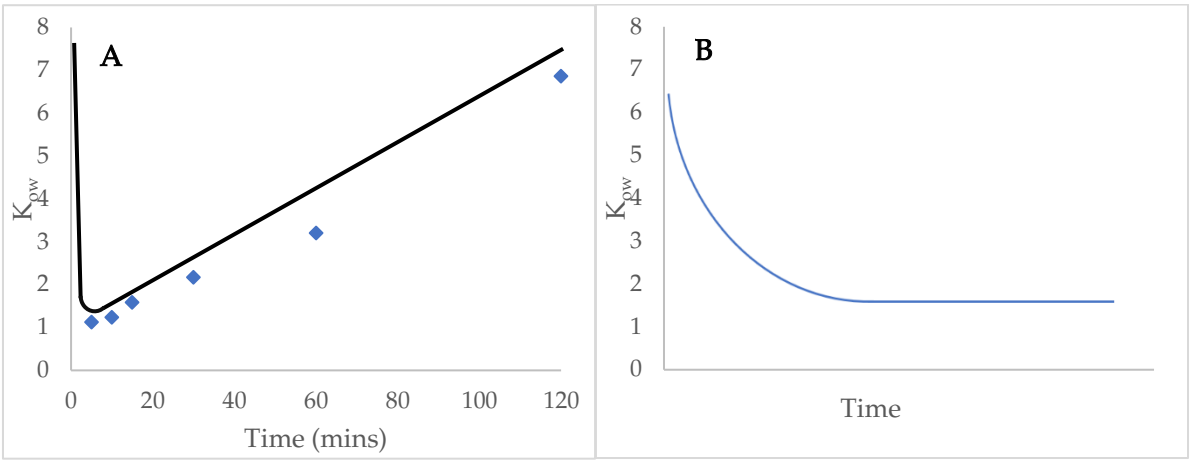

Figure 3.17 - A) Graphic of octanol/water partition coefficient of [C2OHMIM][Rif] as function of time (ilustrated trendline offset from data points for clarity); B) Expected trendline of partition coefficient as function of time.

The most likely cause for such an increase would be slow separation of rifampicin and respective counter-ion. This hypothesis was refuted when a ^{1}H-NMR spectrum of the K_{ow} water phase was analyzed. If separation was indeed occurring, a higher concentration of counter-ion should be observed in the water phase, and hence an increased counter-ion integral. When comparing integrals from both ions, no distinguishable difference was observed when compared with the original compound, in so refuting this hypothesis.

An alternative hypothesis would be a non-binding interaction between 1-octanol with the Rif-OSIL maintained by hydrogen bonds and Van der Waals interactions that would diminish the solubility of the compound when in the water phase. As the solubility of the compound decreased, the respective Kow would increase, as observed in Figure 3.17.

In conclusion, this method is ineffective to determine K_{ow} and it was only used to compare Rif-OSILs within this work. In further studies, membrane permeation studies should be considered as an alternative to K_{ow}.

3.7 *In vivo* toxicity assays in zebrafish

3.7.1 Glutathione-*S*-transferase (GST)

GST activity assays were assessed in the whole fish cytosolic fraction following exposure to two different compounds, the commercial rifampicin and Rif-OSIL [$N_{1,1,1,2OH}$][Rif] at three concentrations. The results are shown in Figure 3.18.

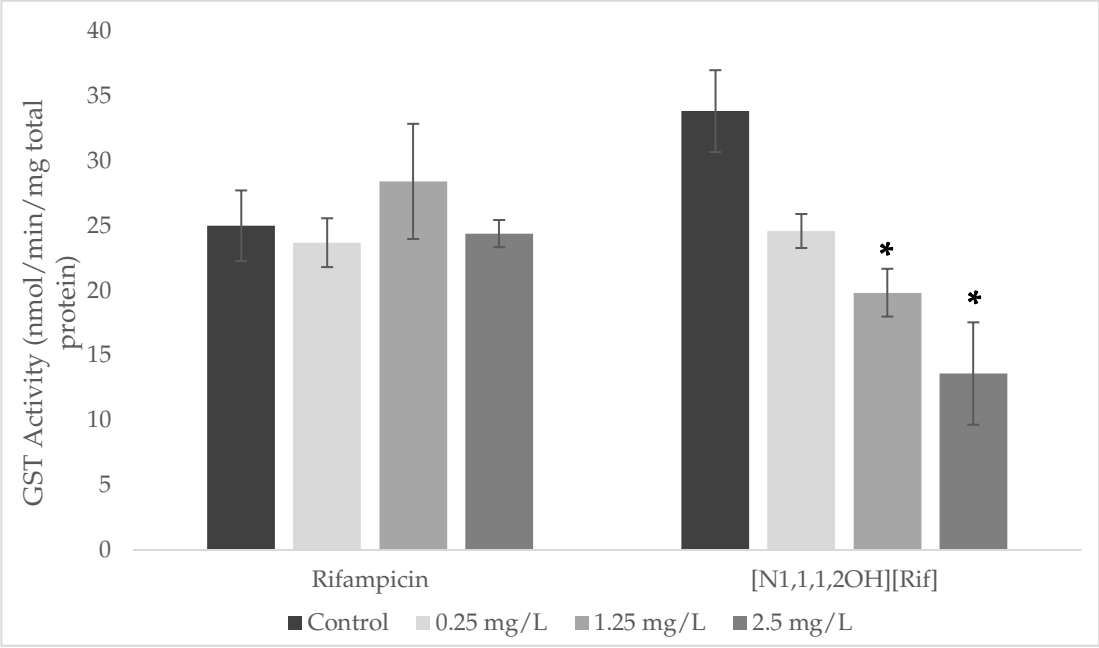

Figure 3.18 - GST activities in fish (asterisk represents statistically significant differences comparing with respective controls).

During the exposure assays no mortality was observed. Statistical analysis of the GST activity showed relevant differences ($p < 0.05$) between control fish and fish exposed to 1.25 mg/L and 2.5 mg/L of [$N_{1,1,1,2OH}$][Rif]. Rifampicin has been observed as a non-competitive inhibitor of some GST enzymes in zebrafish [80]. This apparent concentration-dependent decrease in Rif-OSIL activity can be related to a higher inhibition effect on GST activity due to the greater bioavailability of the tested compound.

3.7.2 Catalase (CAT)

CAT activity assays were performed in the whole fish cytosolic fraction after exposure to the two different compounds tested, the commercial rifampicin and Rif-OSIL [$N_{1,1,1,2OH}$][Rif] at three concentrations. CAT activity results are shown in Figure 3.19.

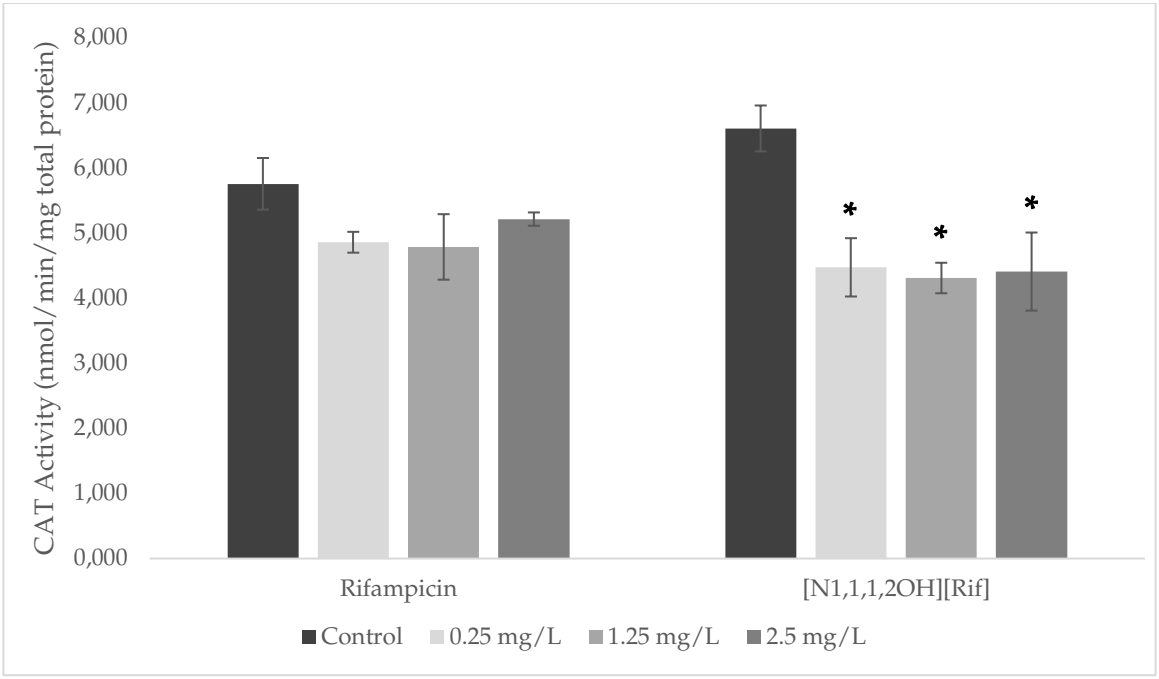

Figure 3.19 - CAT activities results (asterisk represents statistically significant differences comparing with respective controls).

As evidenced by the results, rifampicin, in the concentrations tested, does not cause a significant change in CAT activities compared to the respective controls, which may suggest that the compound does not cause oxidative stress. However, a relevant decrease in CAT activities in fish exposed to the several concentrations of Rif-OSIL is observed. Rifampicin is a very strong inducer of P-450 cytochrome, which can generate toxic metabolites that bind to hepatic macromolecules [81]. This can explain the reduction of activity of these enzymes due to higher bioavailability of the Rif-OSIL when comparing with rifampicin.

3.7.3 Lipid peroxidation (LPO) assays

LPO assays were performed in the whole fish cytosolic fraction after exposure to the two different compounds tested, the commercial rifampicin and Rif-OSIL [$N_{1,1,1,2OH}$][Rif] at three concentrations. LPO results (MDA content) are presented in Figure 3.20.

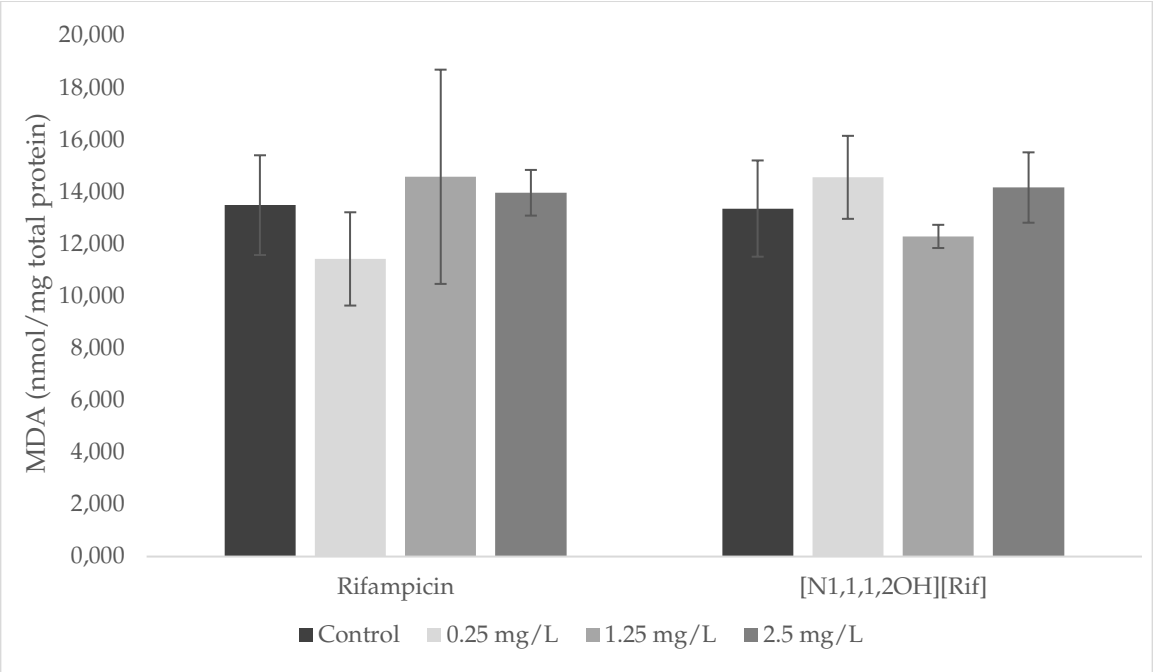

Figure 3.20 - LPO results (asterisk represents statistically significant differences comparing with control).

In general, the results of LPO (MDA content) show no changes in exposed fish to both compounds compared to the respective controls. The statistical analysis of Figure 3.20 indicate no substantial differences ($p < 0.05$) in lipid peroxidation between exposed fish and the respective controls, for both compounds tested. These results are congruent with assays done in albino rats reported by Olufusho et al. [82] which describes a statistical irrelevance in the increase of MDA when the animals were treated with rifampicin.

Despite the usefulness of the assays suggesting some interaction with oxidative stress enzymes (GST and CAT) for Rif-OSIL, this apparently does not appear to have caused oxidative stress or damage to cell membrane lipids as suggested by the results of the LPO. In conclusion, exposure to Rif-OSILs did not increase API toxicity, although these compounds considerably increased bioavailability. However, more assays must be done to, not only to further test more Rif-OSILs and their effects, but also other biomarkers can be performed such as superoxide dismutase (SOD) or glutathione peroxidase (GPx) to determine if other mechanisms are involved in the response to exposure to this drug or its respective Rif-OSILs.

3.8 Dry powder formulations

3.8.1 Production of Rif@DPFs and Rif-OSIL@DPFs

As *Mycobacterium tuberculosis* infection occurs in alveoli [83], finer dry powders with deep lung deposition are expected to obtain optimal tuberculosis treatment although, as of yet, no clinical trials of rifampicin administration via inhalation have been reported using expected therapeutic dosage. In these assays, subtherapeutic loading was used to obtain preliminary results of rifampicin dry powder formulations.

Rifampicin-loaded dry powder formulations (Rif@DPFs), composed of trehalose and leucine as excipient with rifampicin as the API is, so far, a novel approach on rifampicin solid powder formulations. The protocol to produce Rif@DPFs was adapted from Costa et al. [84]. However, since rifampicin is a poor water-soluble drug, the solvent mixture was adapted to water/acetonitrile (50:50, %v/v). For this experiment, a rifampicin entrapment of 91.2% was obtained from Rif@DPFs with 53.5% yield. Next, DPFs with a Rif-OSIL (Rif-OSIL@DPFs) were also produced. In this experiment, the protocol was not changed and a mixture of water/ethanol (85:15, %v/v) was used. [$N_{1,1,1,2OH}$][Rif] was chosen due to its high water and PBS solubilities and low partition coefficient that represents a good permeability. Furthermore, its counter-ion is FDA approved for pharmaceutical applications. The excipient, drug quantities and ratios were adapted from Mizoe et al. [85] that used mannitol as excipient. The Rif-OSIL@DPFs entrapment was 80.6% with 53.5% of process yield (Table 3.3).

Table 3.3 - Results from DPF production.

Formulation	Compound	Solvent mixture	Loading (%)	Entrapment (%)	Yield (%)
Rif@DPF *	**Rifampicin**	Water/Acetonitrile 50:50	4.3±0.04	91.2±1.8	50.3±0.8
Rif-OSIL@DPF *	**[$N_{1,1,1,2OH}$][Rif]**	Water/ethanol 85:15	3.91±0.01	81.9±0.2	53.5±2.7

*n=2 of independent batches

Table 3.3 shows that the process yield is around 50 % for both compounds. This yield is related to compound retainment in the apparatus or particles that were not collected by the cyclone. Regarding the compounds loading, determined by UV-Vis quantification, no major differences between assays were observed. Here, the main difference is in the design of the experiment. In fact, it is possible to obtain a similar loading for solid dosage forms produced

in a process with more water and lower amount of an organic solvent. Besides, ethanol is a greener organic solvent compared to acetonitrile.

3.8.2 Aerodynamic studies

Andersen-Cascade Impactor measures the flowability and aerodynamics of solid powders. This experiment simulates a breath intake to drive the powder through a series of progressively smaller filters. The distribution of the powder throughout these filters can correlate to how deep the powder would disperse through the lungs as depicted in Figure 3.21.

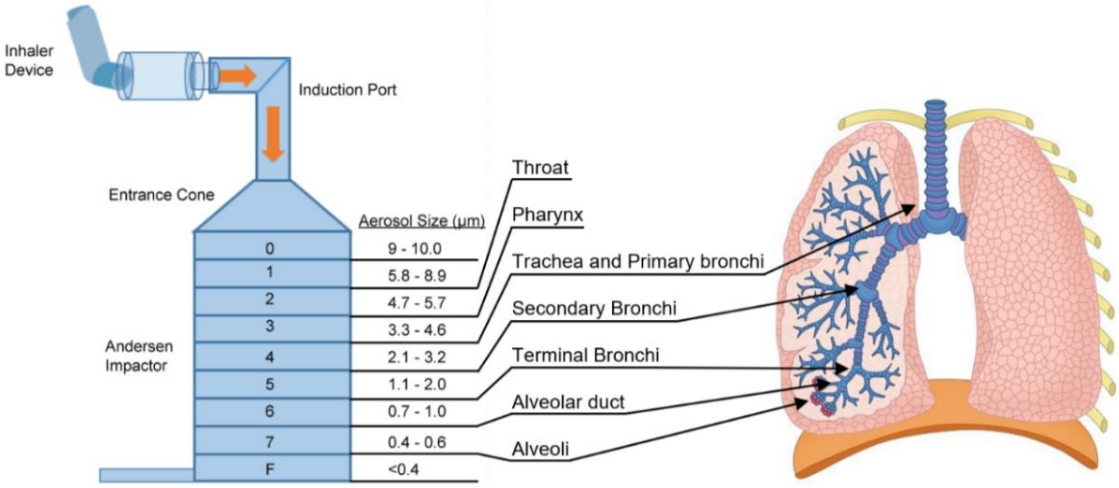

Figure 3.21 - Andersen-Cascade Impactor assay representation with lung dispersion correlation.

In Table 3.4 - Results from ACI assays.are represented the results from the ACI assays and powder distribution between stages is represented in Appendix 73. The powders from Rif@DPFs are overall finer and have better aerodynamics, as can be observed by a decrease in MMAD and an increase in FPF comparing with the Rif-OSIL@DPFs. This difference can be due to a better coating of the compound, a more efficient drying process, a lower hydration level or due to the disparity between the API polarities. Furthermore, this difference can be due to the lower amount of water percentage used in the solvent mixtures of the assays, that produce less hydrated and finer particles. Further testing is needed to ascertain the causes of such differences.

Table 3.4 - Results from ACI assays.

Formulation	Compound	MMAD (µm)	FPF (%)	GSD
Rif@DPF *	**Rifampicin**	1.08±0.08	56.8±0.00	2.13±0.05
Rif-OSIL@DPF *	**[$N_{1,1,1,2OH}$][Rif]**	2.62±0.12	45.75±6.55	2.21±0.15

Overall, both API formulations obtained promising results when compared with other techniques reported in literature, with average FPF of 50% [86]. However, the MMAD results make an important distinction between Rif@DPFs, which reach the alveoli duct, and Rif-OSIL@DPFs, which can only reach the secondary bronchi. This difference can be due to distinct API polarities that cause commercial rifampicin to act as a dispersing agent, improving the MMAD of the particles. Further assays must be made to improve Rif-OSIL@DPF particle sizes and optimize its production protocol. Furthermore, drug loading in these assays were minimal so further studies with higher drug loading need to be made to obtain therapeutic loading DPFs.

4

Conclusion and Future Perspectives

In this work, diverse organic salts were synthesized from rifampicin following two approaches based on the charge of the drug. All prepared compounds were analyzed by ^{1}H and ^{13}C NMR spectroscopy, FTIR, and elemental analysis. The cationic approach was shelved because the salts synthesized proved unstable in PBS solution. Nonetheless, the anionic approach showed the use of Rif-OSILs possessing higher water (at least 450 times) and PBS solubility comparing to original rifampicin solubility. The 1-octanol/water partition coefficient of these compounds could not be determined accurately due likely interaction between the compounds and 1-octanol.

Due to time constraints *in vivo* toxicity assays using zebrafish as animal model were only done for commercial rifampicin and prepared [$N_{1,1,1,2OH}$][Rif]. This compound was selected for being a pharmacologically approved counter-ion named choline with low toxicity and high PBS solubility that was expected to have promising results in these assays. This Rif-OSIL proved to inhibit the activity of both catalase and glutathione-*S*-transferase, but no increase in lipid peroxidation was observed.

Some compounds were then used to produce dry powders in order to explore an alternative administration process. These were prepared with a lab scale supercritical CO2 spray drying apparatus. Commercial rifampicin dry powders had better results than API-OSIL dry powders, reaching an FPF of 56.8% and an MMAD of 1.00. Comparing to the literature data, these were promising results for rifampicin dry powders, making API-OSIL dry powders interesting to study further to obtain better results with greener protocols.

The future work should involve the use of membranes for permeation studies as an alternative to 1-octanol/water partition coefficients, to proceed the in vivo toxicity assays. It is also important to evaluate the most promising Rif-OSILs against *Mycobacterium tuberculosis* or alternatively *Mycobacterium marinum or avium* using zebrafish as animal model. Finally, it is also expected to proceed the Rif-OSILs dry powder studies in order to optimize associated aerodynamics.

BIBLIOGRAPHY

[1] E. M. Zager and R. McNerney, "Multidrug-resistant tuberculosis," *BMC Infect Dis*, vol. 8, Jan. 2008, doi: 10.1186/1471-2334-8-10.

[2] World Health Organization, "Tuberculosis (TB)." https://www.who.int/news-room/fact-sheets/detail/tuberculosis (accessed Jul. 24, 2022).

[3] A. G. Mainous III and C. Pomerian, "Management of Antimicrobials in Infectious Diseases," in *Management of Antimicrobials in Infectious Diseases*, Humana Press, 2010, pp. 61–62. doi: 10.1007/978-1-60327-239-1.

[4] Our world in data, "Tuberculosis incidence." https://our-worldindata.org/grapher/incidence-of-tuberculosis-sdgs?time=latest (accessed Oct. 01, 2022).

[5] NHS Choices, "Diagnosis Tuberculosis (TB)." https://www.nhs.uk/conditions/tuberculosis-tb/diagnosis/ (accessed Aug. 27, 2022).

[6] Verywell Health, "When a Persistent Cough Could Indicate TB." https://www.verywellhealth.com/tuberculosis-symptoms-914924 (accessed Sep. 15, 2022).

[7] Simona Luca and Traian Mihaescu, "History of BCG vaccine.," *Maedica (Bucur)*, vol. 8, no. 1, pp. 53–58, 2013.

[8] L. Miesel, J. Greene, and T. A. Black, "Genetic strategies for antibacterial drug discovery," *Nat Rev Genet*, vol. 4, no. 6, pp. 442–456, 2003, doi: 10.1038/nrg1086.

[9] A. D. Bendre, P. J. Peters, and J. Kumar, "Tuberculosis: Past, present and future of the treatment and drug discovery research," *Current Research in Pharmacology and Drug Discovery*, vol. 2, p. 100037, 2021, doi: https://doi.org/10.1016/j.crphar.2021.100037.

[10] K. Arora *et al.*, "Respiratory Flexibility in Response to Inhibition of Cytochrome c Oxidase in Mycobacterium tuberculosis," *Antimicrob Agents Chemother*, vol. 58, no. 11, pp. 6962–6965, 2014, doi: 10.1128/AAC.03486-14.

[11] M. D. Iseman, "Tuberculosis therapy: Past, present and future," in *European Respiratory Journal, Supplement*, 2002, vol. 20, no. 36. doi: 10.1183/09031936.02.00309102.

[12] J. G. Jang and J. H. Chung, "Diagnosis and treatment of multidrug-resistant tuberculosis," *Yeungnam Univ J Med*, vol. 37, no. 4, pp. 277–285, 2020, doi: 10.12701/yujm.2020.00626.

[13] E. J. Forget and D. Menzies, "Adverse reactions to first-line antituberculosis drugs," *Expert Opin Drug Saf*, vol. 5, no. 2, pp. 231–249, 2006, doi: 10.1517/14740338.5.2.231.

[14] J. K. Louie *et al.*, "A decrease in tuberculosis evaluations and diagnoses during the COVID-19 pandemic," *International Journal of Tuberculosis and Lung Disease*, vol. 24, no. 8. International Union Against Tuberculosis and Lung Disease (The Union), pp. 860–862, Aug. 01, 2020. doi: 10.5588/ijtld.20.0364.

[15] World Health Organization, "Tuberculosis data." https://www.who.int/teams/global-tuberculosis-programme/data (accessed Oct. 01, 2022).

[16] L. Z. Benet, "The role of BCS (biopharmaceutics classification system) and BDDCS (biopharmaceutics drug disposition classification system) in drug development," *J Pharm Sci*, vol. 102, no. 1, pp. 34–42, 2013, doi: 10.1002/jps.23359.

[17] L. Yu, "Amorphous pharmaceutical solids: preparation, characterization and stabilization," *Adv Drug Deliv Rev*, vol. 48, no. 1, pp. 27–42, 2001, doi: https://doi.org/10.1016/S0169-409X(01)00098-9.

[18] World Health Organization, "Antibiotic resistance." https://www.who.int/news-room/fact-sheets/detail/antibiotic-resistance (accessed Aug. 20, 2022).

[19] R. R. Yocum, J. R. Rasmussen, and J. L. Strominger, "The mechanism of action of penicillin. Penicillin acylates the active site of Bacillus stearothermophilus D-alanine carboxypeptidase," *Journal of Biological Chemistry*, vol. 255, no. 9, pp. 3977–3986, 1980, doi: 10.1016/s0021-9258(19)85621-1.

[20] G. Bbosa, N. Mwebaza, J. Odda, D. Kyegombe, and M. Ntale, "Antibiotics/antibacterial drug use, their marketing and promotion during the post-antibiotic golden age and their role in emergence of bacterial resistance," *Health N Hav*, vol. 6, pp. 410–425, Sep. 2014, doi: 10.4236/health.2014.65059.

[21] A. Bryskier, "Ansamycins," in *Antimicrobial Agents: Antibacterials and Antifungals*, 1st ed., Washington, D.C.: ASM Press, 2005, pp. 906–912.

[22] T. T. Mariappan and S. Singh, "Positioning of Rifampicin in the Biopharmaceutics Classification System (BCS)," *Clin Res Regul Aff*, vol. 23, no. 1, pp. 1–10, Jan. 2006, doi: 10.1080/10601330500533990.

[23] M.J. O'Neil, "The Merck Index - An Encyclopedia of Chemicals, Drugs, and Biologicals.," 13th ed., NJ: Merck and Co.: Whitehouse Station, 2001, p. 1474.

[24] J. C. Palomino and A. Martin, "Drug Resistance Mechanisms in Mycobacterium tuberculosis," *Antibiotics*, vol. 3, no. 3, pp. 317–340, 2014, doi: 10.3390/antibiotics3030317.

[25] J. Peek *et al.*, "Rifamycin congeners kanglemycins are active against rifampicin-resistant bacteria via a distinct mechanism," *Nat Commun*, vol. 9, no. 1, p. 4147, 2018, doi: 10.1038/s41467-018-06587-2.

[26] B. P. Goldstein, "Resistance to rifampicin: a review," *J Antibiot (Tokyo)*, vol. 67, no. 9, pp. 625–630, 2014, doi: 10.1038/ja.2014.107.

[27] R. Ferraz, L. C. Branco, C. Prudêncio, J. P. Noronha, and . Petrovski, "Ionic Liquids as Active Pharmaceutical Ingredients," *ChemMedChem*, vol. 6, no. 6, pp. 975–985, 2011, doi: https://doi.org/10.1002/cmdc.201100082.

[28] A. J. Greer, J. Jacquemin, and C. Hardacre, "Industrial Applications of Ionic Liquids," *Molecules*, vol. 25, no. 21, 2020, doi: 10.3390/molecules25215207.

[29] P. Walden, "Ueber die Molekulargrösse und elektrische Leitfähigkeit einiger geschmolzenen Salze," *Proceedings of the Imperial Academy of Sciences*, vol. 8, no. 6, pp. 405–422, 1914.

[30] T. Welton, "Ionic liquids: a brief history," *Biophys Rev*, vol. 10, no. 3, pp. 691–706, 2018, doi: 10.1007/s12551-018-0419-2.

[31] S. N. Pedro, C. S. R. Freire, A. J. D. Silvestre, and M. G. Freire, "The Role of Ionic Liquids in the Pharmaceutical Field: An Overview of Relevant Applications," *Int J Mol Sci*, vol. 21, no. 21, 2020, doi: 10.3390/ijms21218298.

[32] Noémi Jordão, "Multi Stimuli-responsive Organic Salts: From preparation to functional device application," Faculdade de Ciências e Tecnologia, Universidade Nova de Lisboa, Lisboa, 2017.

[33] W. L. Hough *et al.*, "The third evolution of ionic liquids: active pharmaceutical ingredients," *New Journal of Chemistry*, vol. 31, no. 8, pp. 1429–1436, Jul. 2007, doi: 10.1039/B706677P.

[34] A. R. Jesus *et al.*, "Enhancement of water solubility of poorly water-soluble drugs by new biocompatible N-acetyl amino acid N-alkyl cholinium-based ionic liquids," *European Journal of Pharmaceutics and Biopharmaceutics*, vol. 137, pp. 227–232, 2019, doi: https://doi.org/10.1016/j.ejpb.2019.03.004.

[35] A. R. Jesus *et al.*, "New Non-Toxic N-alkyl Cholinium-Based Ionic Liquids as Excipients to Improve the Solubility of Poorly Water-Soluble Drugs," *Symmetry (Basel)*, vol. 13, no. 11, 2021, doi: 10.3390/sym13112053.

[36] R. Ferraz *et al.*, "Development of novel ionic liquids based on ampicillin," *Medchemcomm*, vol. 3, no. 4, pp. 494–497, Apr. 2012, doi: 10.1039/c2md00269h.

[37] C. Florindo *et al.*, "Evaluation of solubility and partition properties of ampicillin-based ionic liquids," *Int J Pharm*, vol. 456, no. 2, pp. 553–559, 2013, doi: 10.1016/j.ijpharm.2013.08.010.

[38] R. Ferraz *et al.*, "Antitumor Activity of Ionic Liquids Based on Ampicillin," *ChemMedChem*, vol. 10, no. 9, pp. 1480–1483, Sep. 2015, doi: 10.1002/cmdc.201500142.

[39] R. Ferraz *et al.*, "Synthesis and Antibacterial Activity of Ionic Liquids and Organic Salts Based on Penicillin G and Amoxicillin hydrolysate Derivatives against Resistant Bacteria," *Pharmaceutics*, vol. 12, no. 3, 2020, doi: 10.3390/pharmaceutics12030221.

[40] R. Ferraz *et al.*, "Antibacterial activity of Ionic Liquids based on ampicillin against resistant bacteria," *RSC Adv.*, vol. 4, no. 9, pp. 4301–4307, 2014, doi: 10.1039/C3RA44286A.

[41] M. M. Santos *et al.*, "Antimicrobial Activities of Highly Bioavailable Organic Salts and Ionic Liquids from Fluoroquinolones," *Pharmaceutics*, vol. 12, no. 8, 2020, doi: 10.3390/pharmaceutics12080694.

[42] C. Florindo *et al.*, "Novel organic salts based on fluoroquinolone drugs: Synthesis, bioavailability and toxicological profiles," *Int J Pharm*, vol. 469, no. 1, pp. 179–189, 2014, doi: https://doi.org/10.1016/j.ijpharm.2014.04.034.

[43] D. Madeira *et al.*, "Fluoroquinolone-Based Organic Salts and Ionic Liquids as Highly Bioavailable Broad-Spectrum Antimicrobials," *Proc West Mark Ed Assoc Conf*, vol. 78, no. 1, 2021, doi: 10.3390/IECP2020-08649.

[44] D. Silva *et al.*, "Novel Organic Salts Based on Mefloquine: Synthesis, Solubility, Permeability, and In Vitro Activity against Mycobacterium tuberculosis," *Molecules*, vol. 27, no. 16, 2022, doi: 10.3390/molecules27165167.

[45] F. R. Khan and S. S. Alhewairini, "Zebrafish (Danio rerio) as a Model Organism," in *Current Trends in Cancer Management*, L. Streba, D. I. Gheonea, and M. Schenker, Eds. Rijeka: IntechOpen, 2018, p. Ch. 1. doi: 10.5772/intechopen.81517.

[46] C. Parng, "In vivo zebrafish assays for toxicity testing," *Current opinion in drug discovery & development*, vol. 8, no. 1, pp. 100–106, 2005, [Online]. Available: http://europepmc.org/abstract/MED/15679177

[47] K. B. Ayaz Ahmed and V. Anbazhagan, "Synthesis of copper sulfide nanoparticles and evaluation of in vitro antibacterial activity and in vivo therapeutic effect in bacteria-infected zebrafish," *RSC Adv*, vol. 7, no. 58, pp. 36644–36652, 2017, doi: 10.1039/c7ra05636b.

[48] J. Yin, A.-P. Wang, W.-F. Li, R. Shi, H.-T. Jin, and J.-F. Wei, "Time-response characteristic and potential biomarker identification of heavy metal induced toxicity in zebrafish," *Fish Shellfish Immunol*, vol. 72, pp. 309–317, 2018, doi: https://doi.org/10.1016/j.fsi.2017.10.047.

[49] R. G. Leitão, M. P. Silva, M. S. Diniz, and M. Guerra, "Mapping the distribution of mercury (II) chloride in zebrafish organs by benchtop micro-energy dispersive X-ray fluorescence: A proof of concept," *Journal of Trace Elements in Medicine and Biology*, vol. 69, p. 126874, 2022, doi: https://doi.org/10.1016/j.jtemb.2021.126874.

[50] B. Matos, M. Martins, A. C. Samamed, D. Sousa, I. Ferreira, and M. S. Diniz, "Toxicity Evaluation of Quantum Dots (ZnS and CdS) Singly and Combined in Zebrafish (Danio rerio)," *Int J Environ Res Public Health*, vol. 17, no. 1, 2020, doi: 10.3390/ijerph17010232.

[51] H. Sies, C. Berndt, and D. P. Jones, "Oxidative Stress," *Annu Rev Biochem*, vol. 86, no. 1, pp. 715–748, 2017, doi: 10.1146/annurev-biochem-061516-045037.

[52] M. S. Moron, J. W. Depierre, and B. Mannervik, "Levels of glutathione, glutathione reductase and glutathione S-transferase activities in rat lung and liver," *Biochimica et Biophysica Acta (BBA) - General Subjects*, vol. 582, no. 1, pp. 67–78, 1979, doi: https://doi.org/10.1016/0304-4165(79)90289-7.

[53] J. D. Hayes, J. U. Flanagan, and I. R. Jowsey, "GLUTATHIONE TRANSFERASES," *Annu Rev Pharmacol Toxicol*, vol. 45, no. 1, pp. 51–88, Aug. 2004, doi: 10.1146/annurev.pharmtox.45.120403.095857.

[54] A. Tierbach, K. J. Groh, R. Schönenberger, K. Schirmer, and M. J.-F. Suter, "Glutathione S-Transferase Protein Expression in Different Life Stages of Zebrafish (Danio rerio)," *Toxicological Sciences*, vol. 162, no. 2, pp. 702–712, Apr. 2018, doi: 10.1093/toxsci/kfx293.

[55] V. C. Culotta, "Superoxide dismutase, oxidative stress, and cell metabolism," in *Current Topics in Cellular Regulation*, vol. 36, E. R. Stadtman and P. B. Chock, Eds. Academic Press, 2001, pp. 117–132. doi: https://doi.org/10.1016/S0070-2137(01)80005-4.

[56] A. Nandi, L.-J. Yan, C. K. Jana, and N. Das, "Role of Catalase in Oxidative Stress- and Age-Associated Degenerative Diseases," *Oxid Med Cell Longev*, vol. 2019, p. 9613090, 2019, doi: 10.1155/2019/9613090.

[57] Y. Jin *et al.*, "Oxidative stress response and gene expression with atrazine exposure in adult female zebrafish (Danio rerio)," *Chemosphere*, vol. 78, no. 7, pp. 846–852, 2010, doi: https://doi.org/10.1016/j.chemosphere.2009.11.044.

[58] B. Halliwell, "Oxidative damage, lipid peroxidation and antioxidant protection in chloroplasts," *Chem Phys Lipids*, vol. 44, no. 2, pp. 327–340, 1987, doi: https://doi.org/10.1016/0009-3084(87)90056-9.

[59] Y.-J. Son and J. T. McConville, "Preparation of sustained release rifampicin microparticles for inhalation," *J Pharm Pharmacol*, vol. 64, no. 9, pp. 1291–1302, Jul. 2012.

[60] R. P. Cabral *et al.*, "Design of experiments approach on the preparation of dry inhaler chitosan composite formulations by supercritical CO2-assisted spray-drying," *Journal of Supercritical Fluids*, vol. 116, pp. 26–35, Oct. 2016, doi: 10.1016/j.supflu.2016.04.001.

[61] M. Tavares *et al.*, "Development of PLGA dry powder microparticles by supercritical CO2-assisted spray-drying for potential vaccine delivery to the lungs," *Journal of Supercritical Fluids*, vol. 128, pp. 235–243, 2017, doi: 10.1016/j.supflu.2017.06.004.

[62] J. F. Pontes and A. Grenha, "Multifunctional Nanocarriers for Lung Drug Delivery," *Nanomaterials*, vol. 10, no. 2, 2020, doi: 10.3390/nano10020183.

[63] S. A. Tasduq, P. Kaiser, S. C. Sharma, and R. K. Johri, "Potentiation of isoniazid-induced liver toxicity by rifampicin in a combinational therapy of antitubercular drugs (rifampicin, isoniazid and pyrazinamide) in Wistar rats: A toxicity profile study," *Hepatology Research*, vol. 37, no. 10, pp. 845–853, 2007, doi: https://doi.org/10.1111/j.1872-034X.2007.00129.x.

[64] C. Moura, E. Costa, and A. Aguiar-Ricardo, "Optimization of Supercritical-CO2 Assisted Spray Drying for the Production of Inhalable composite particles," 2016.

[65] C. Costa, T. Casimiro, and A. Aguiar-Ricardo, "Optimization of Supercritical CO2-Assisted Atomization: Phase Behavior and Design of Experiments," *J Chem Eng Data*, vol. 63, no. 4, pp. 885–896, Apr. 2018, doi: 10.1021/acs.jced.7b00820.

[66] O. Adeoye, C. Costa, T. Casimiro, A. Aguiar-Ricardo, and H. Cabral-Marques, "Preparation of ibuprofen/hydroxypropyl- -cyclodextrin inclusion complexes using supercritical CO2-assisted spray drying," *Journal of Supercritical Fluids*, vol. 133, pp. 479–485, Mar. 2018, doi: 10.1016/j.supflu.2017.11.009.

[67] G. L. Weibel and C. K. Ober, "An overview of supercritical CO2 applications in microelectronics processing," *Microelectron Eng*, vol. 65, no. 1, pp. 145–152, 2003, doi: https://doi.org/10.1016/S0167-9317(02)00747-5.

[68] B. Díaz-Reinoso, A. Moure, H. Domínguez, and J. C. Parajó, "Supercritical CO2 Extraction and Purification of Compounds with Antioxidant Activity," *J Agric Food Chem*, vol. 54, no. 7, pp. 2441–2469, Apr. 2006, doi: 10.1021/jf052858j.

[69] M. K. Gard, E. G. Ennis, and J. H. Summerfield, "1-Octanol/Water Partition Coefficients of Dialkylated Methylimidazolium Halide Salts," *Glob. J. Sci. Front. Res. B Chem*, vol. 15, no. 6, 2015.

[70] H. Aebi, "[13] Catalase in vitro," in *Methods in Enzymology*, vol. 105, Academic Press, 1984, pp. 121–126. doi: https://doi.org/10.1016/S0076-6879(84)05016-3.

[71] M. S. Diniz *et al.*, "Ecotoxicity of ketoprofen, diclofenac, atenolol and their photolysis byproducts in zebrafish (Danio rerio)," *Science of the Total Environment*, vol. 505, pp. 282–289, Feb. 2015, doi: 10.1016/j.scitotenv.2014.09.103.

[72] W. H. Habig, M. J. Pabst, and W. B. Jakoby, "Glutathione S-Transferases: THE FIRST ENZYMATIC STEP IN MERCAPTURIC ACID FORMATION," *Journal of Biological Chemistry*, vol. 249, no. 22, pp. 7130–7139, 1974, doi: https://doi.org/10.1016/S0021-9258(19)42083-8.

[73] M. Uchiyama and M. Mihara, "Determination of malonaldehyde precursor in tissues by thiobarbituric acid test," *Anal Biochem*, vol. 86, no. 1, pp. 271–278, 1978, doi: https://doi.org/10.1016/0003-2697(78)90342-1.

[74] K. Fukumoto, M. Yoshizawa, and H. Ohno, "Room temperature ionic liquids from 20 natural amino acids," *J Am Chem Soc*, vol. 127, no. 8, pp. 2398–2399, Mar. 2005, doi: 10.1021/ja043451i.

[75] N. Marjanovi , A. ikoš, and S. Koštrun, "A new screening tool to determine chameleonic properties of macrocycles," *J Mol Struct*, vol. 1198, p. 126929, 2019, doi: https://doi.org/10.1016/j.molstruc.2019.126929.

[76] H. Liu, Z. Z. He, L. Yu, J. Ma, and X. P. Jin, "Improved solubility and stability of rifampicin as an inclusion complex of acyclic cucurbit[n]uril," *J Incl Phenom Macrocycl Chem*, vol. 101, no. 1–2, pp. 111–120, Oct. 2021, doi: 10.1007/s10847-021-01093-3.

[77] S. Agrawal, Y. Ashokraj, P. v. Bharatam, O. Pillai, and R. Panchagnula, "Solid-state characterization of rifampicin samples and its biopharmaceutic relevance," *European Journal of Pharmaceutical Sciences*, vol. 22, no. 2–3, pp. 127–144, Jun. 2004, doi: 10.1016/j.ejps.2004.02.011.

[78] A. R. Dias *et al.*, "Bioactivity of Ionic Liquids Based on Valproate in SH-SY5Y Human Neuroblastoma Cell Line," *Future Pharmacology*, vol. 2, no. 3, pp. 320–329, 2022, doi: 10.3390/futurepharmacol2030022.

[79] C. P. Holstege, "Rifampin," in *Encyclopedia of Toxicology (Third Edition)*, P. Wexler, Ed. Oxford: Academic Press, 2014, pp. 134–136. doi: https://doi.org/10.1016/B978-0-12-386454-3.00781-8.

[80] B. Bašica, I. Mihaljevi , N. Marakovi , R. Kova evi , and T. Smital, "Molecular characterization of zebrafish Gstr1, the only member of teleost-specific glutathione S- transferase class," *Aquatic Toxicology*, vol. 208, pp. 196–207, 2019, doi: https://doi.org/10.1016/j.aquatox.2019.01.005.

[81] S. K. Jatav *et al.*, "Spirulina maxima Protects Liver From Isoniazid and Rifampicin Drug Toxicity," *J Evid Based Complementary Altern Med*, vol. 19, no. 3, pp. 189–194, 2014, doi: 10.1177/2156587214530720.

[82] A. Olufunsho and A. Alade, "Investigation of lipid peroxidation as probable mechanism of rifampicin toxicity in vivo," *Ann Neurosci*, vol. 19, no. 2, pp. 68–70, Apr. 2012.

[83] G. Delogu, M. Sali, and G. Fadda, "The Biology of Mycobacterium Tuberculosis Infection," *Mediterr J Hematol Infect Dis*, vol. 5, no. 1, p. 2013070, 2013, doi: 10.4084/MJHID.2013.070.

[84] C. Costa *et al.*, "Inhalable hydrophilic molecule-loaded liposomal dry powder formulations using supercritical CO2 – assisted spray-drying," *Journal of CO2 Utilization*, vol. 53, p. 101709, 2021, doi: https://doi.org/10.1016/j.jcou.2021.101709.

[85] T. Mizoe, T. Ozeki, and H. Okada, "Application of a Four-fluid Nozzle Spray Drier to Prepare Inhalable Rifampicin-containing Mannitol Microparticles," *AAPS PharmSciTech*, vol. 9, no. 3, pp. 755–761, 2008, doi: 10.1208/s12249-008-9109-x.

[86] K. Berkenfeld, J. T. McConville, and A. Lamprecht, "Inhalable dry powders of rifampicin highlighting potential and drawbacks in formulation development for experimental tuberculosis aerosol therapy," *Expert Opinion on Drug Delivery*, vol. 17, no. 3. Taylor and Francis Ltd, pp. 305–322, Mar. 03, 2020. doi: 10.1080/17425247.2020.1720644.

A

Appendix

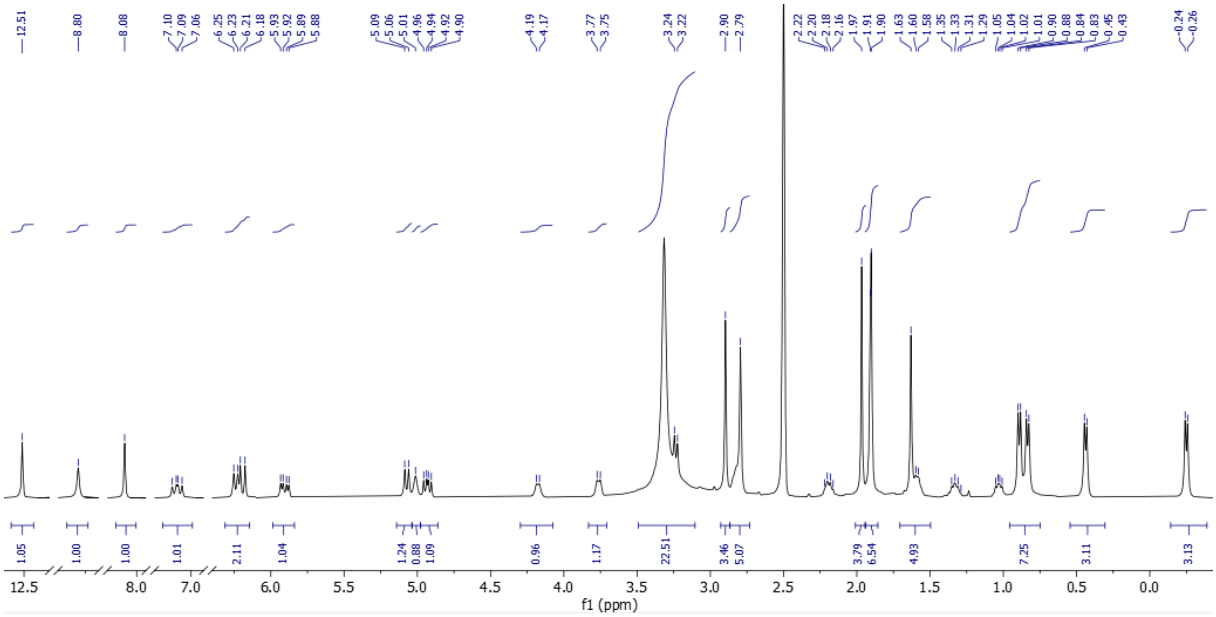

Appendix 1 - ^{1}H NMR spectrum of rifampicin in DMSO-*d*$_6$.

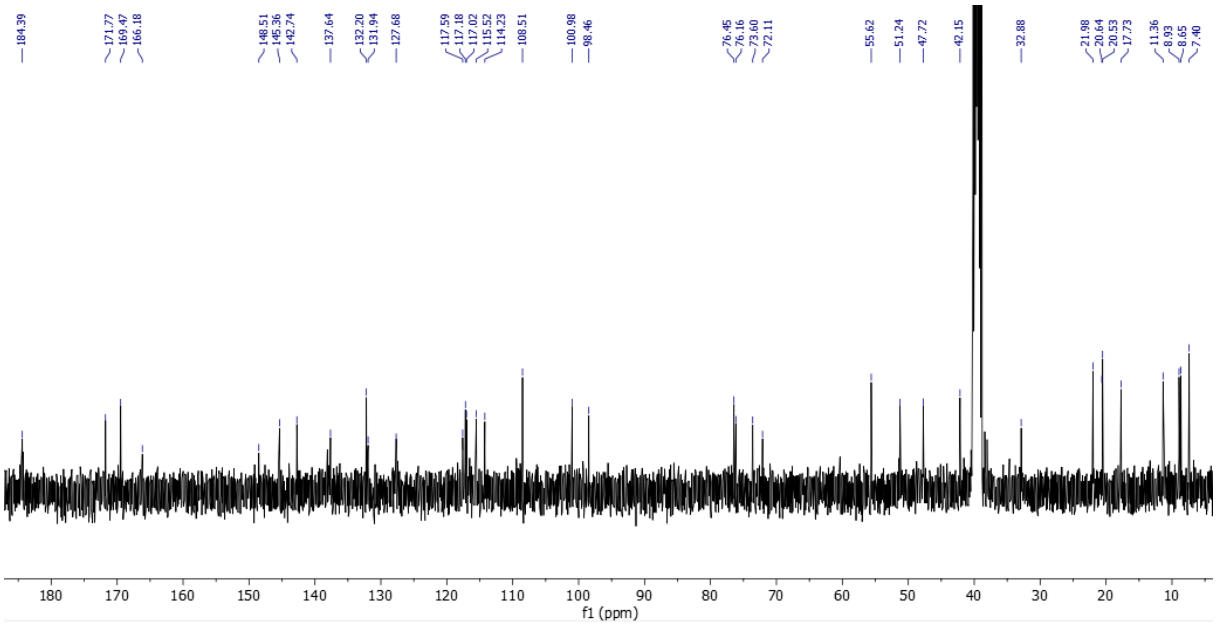

Appendix 2 - ^{13}C NMR spectrum of rifampicin in DMSO-*d*$_6$.

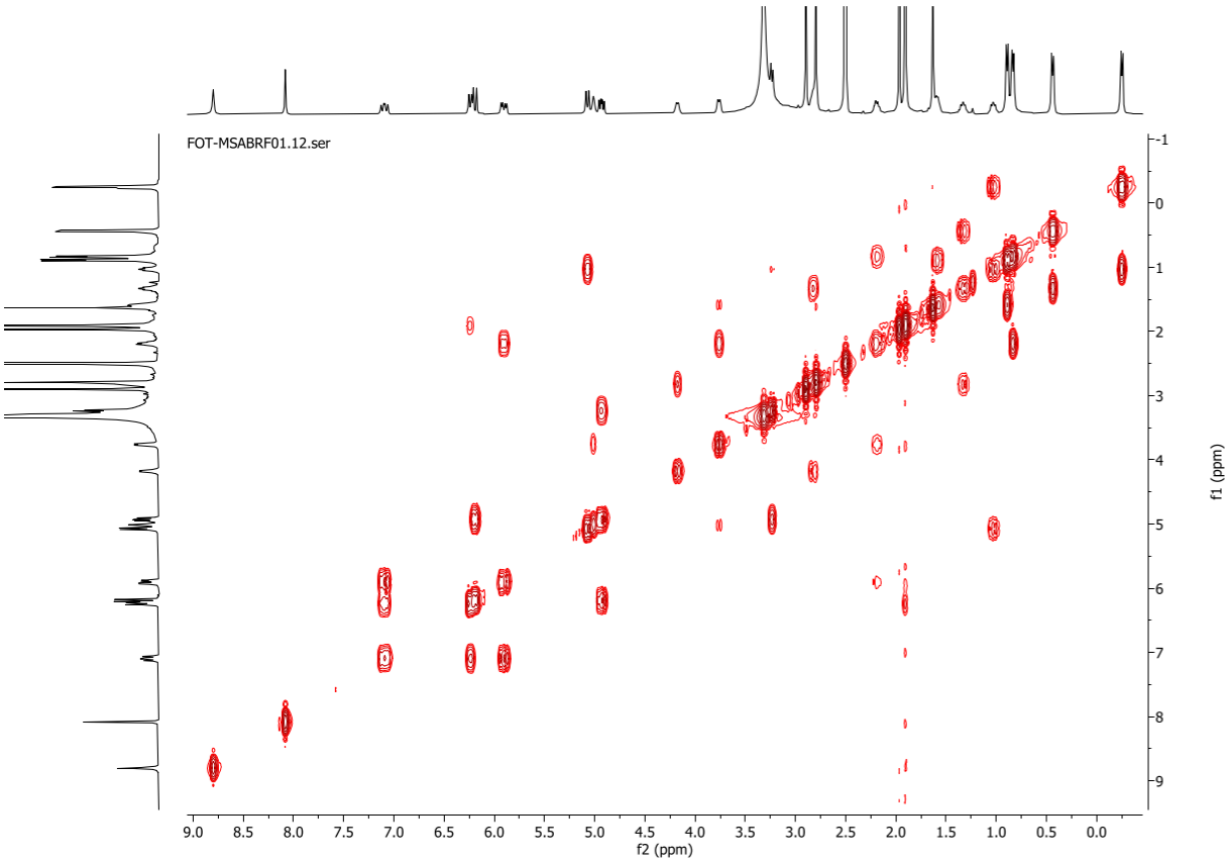

Appendix 3 - COSY correlations of rifampicin in DMSO-d_6.

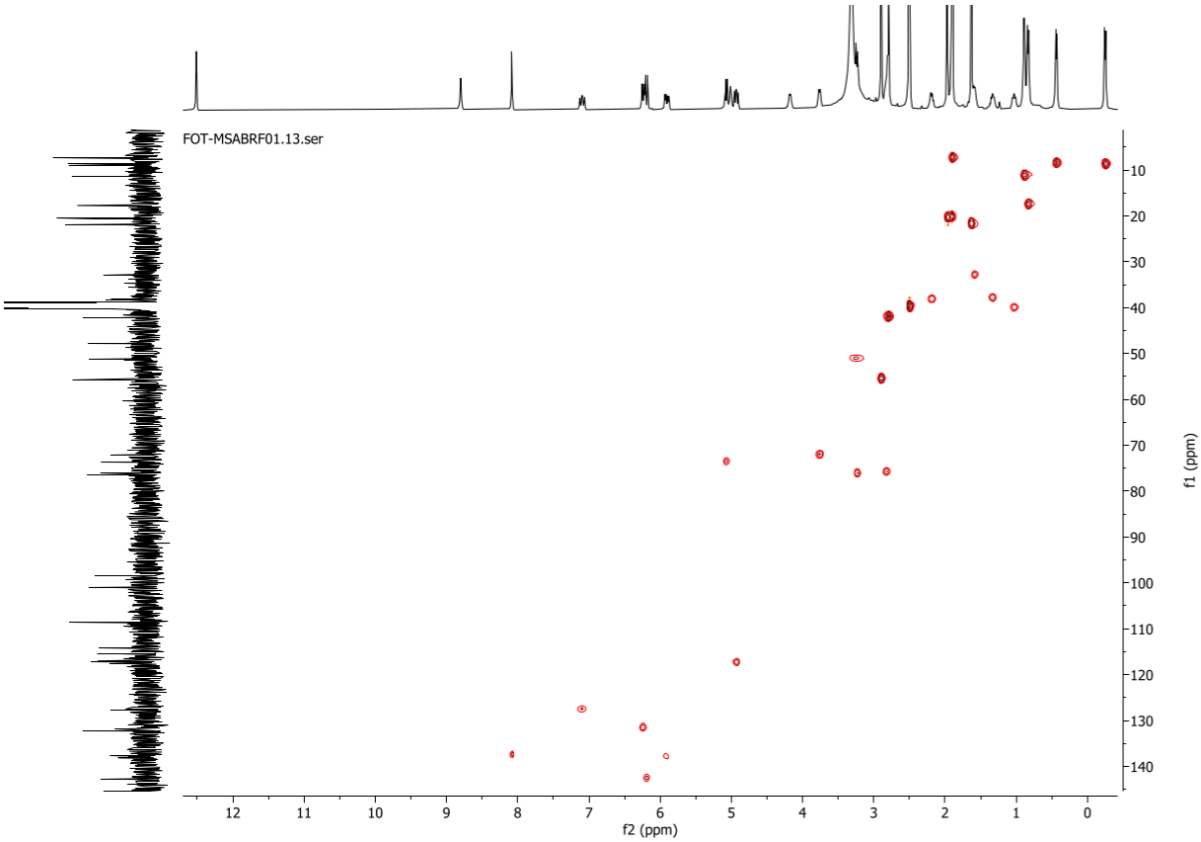

Appendix 4 - HSQC correlations of rifampicin in DMSO-*d6*.

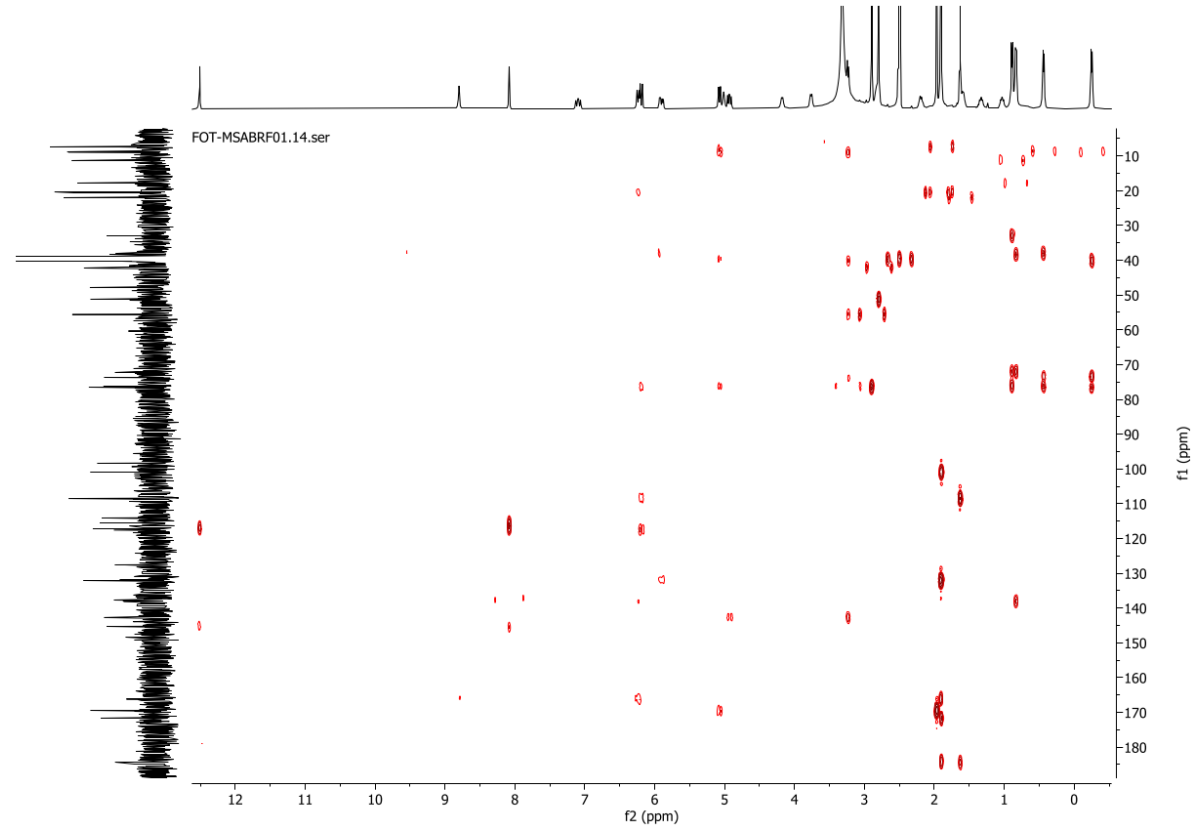

Appendix 5 - HMBC correlations of rifampicin in DMSO-*d6*

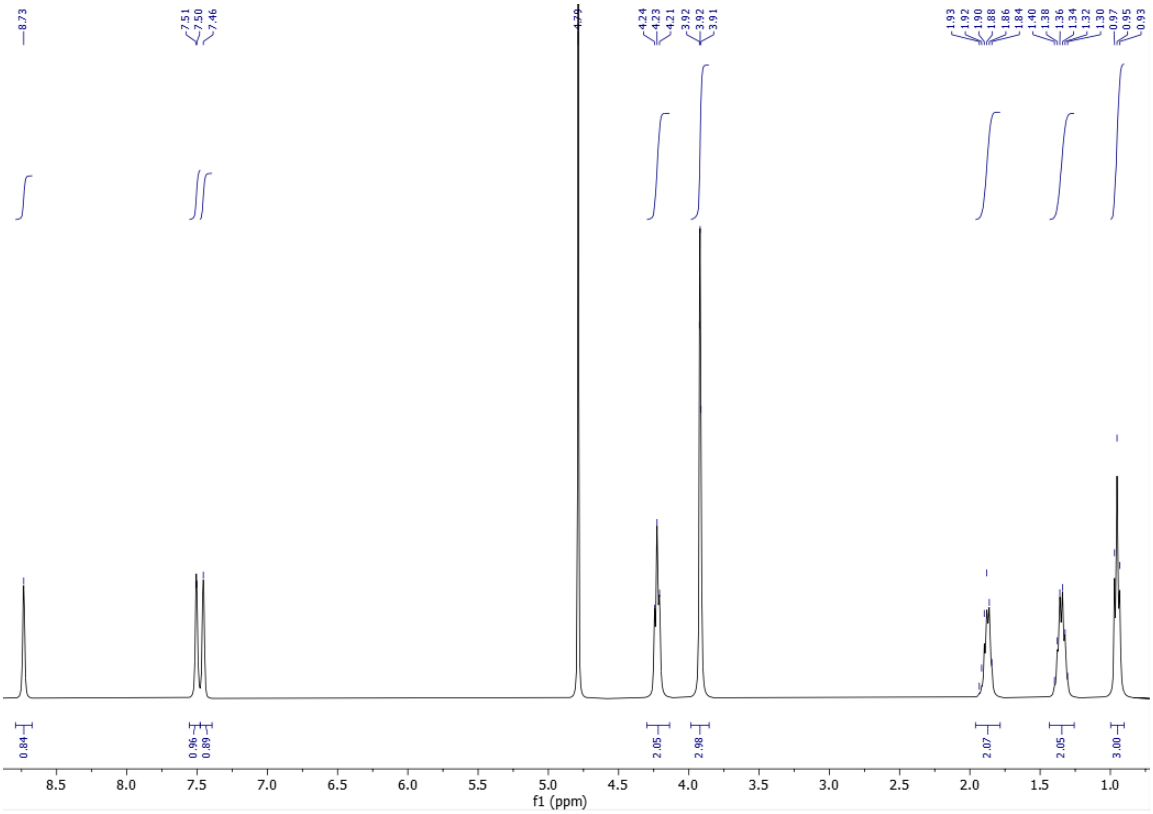

Appendix 6 - ^{1}H NMR spectrum of [C_4MIM]Br in D2O.

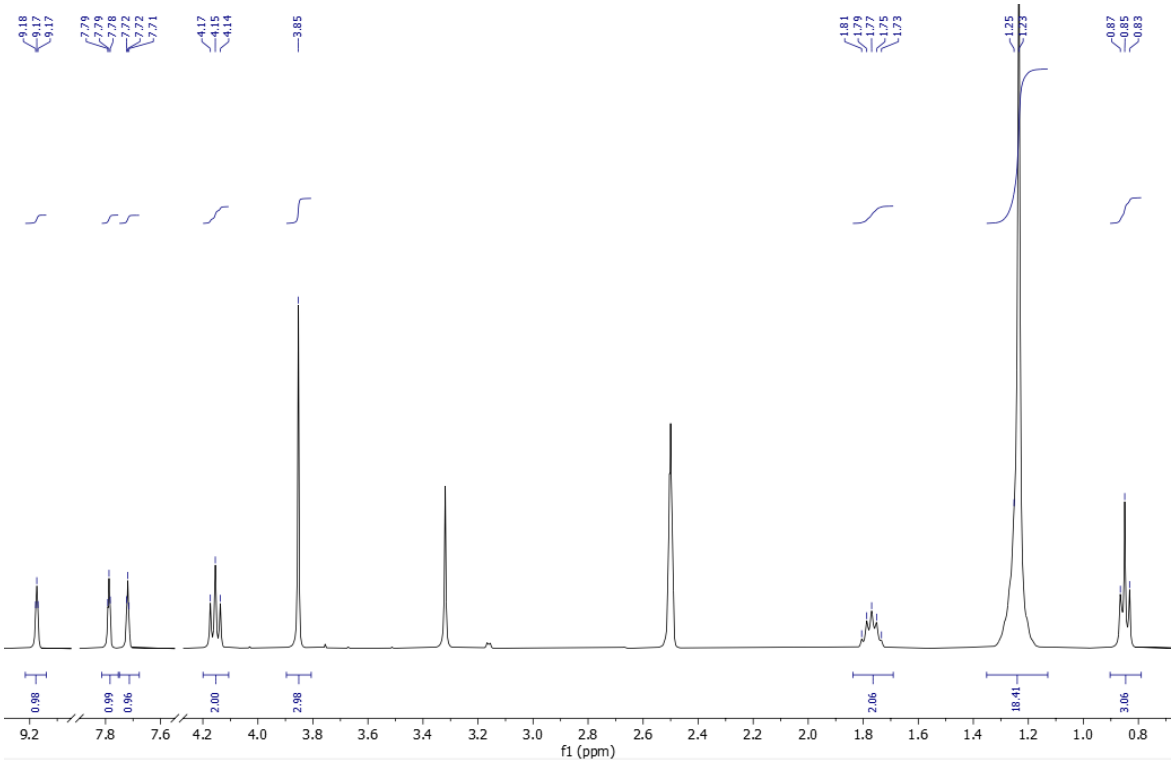

Appendix 7 - ^{1}H NMR spectrum of [C_{12}MIM]Br in DMSO-*d6*

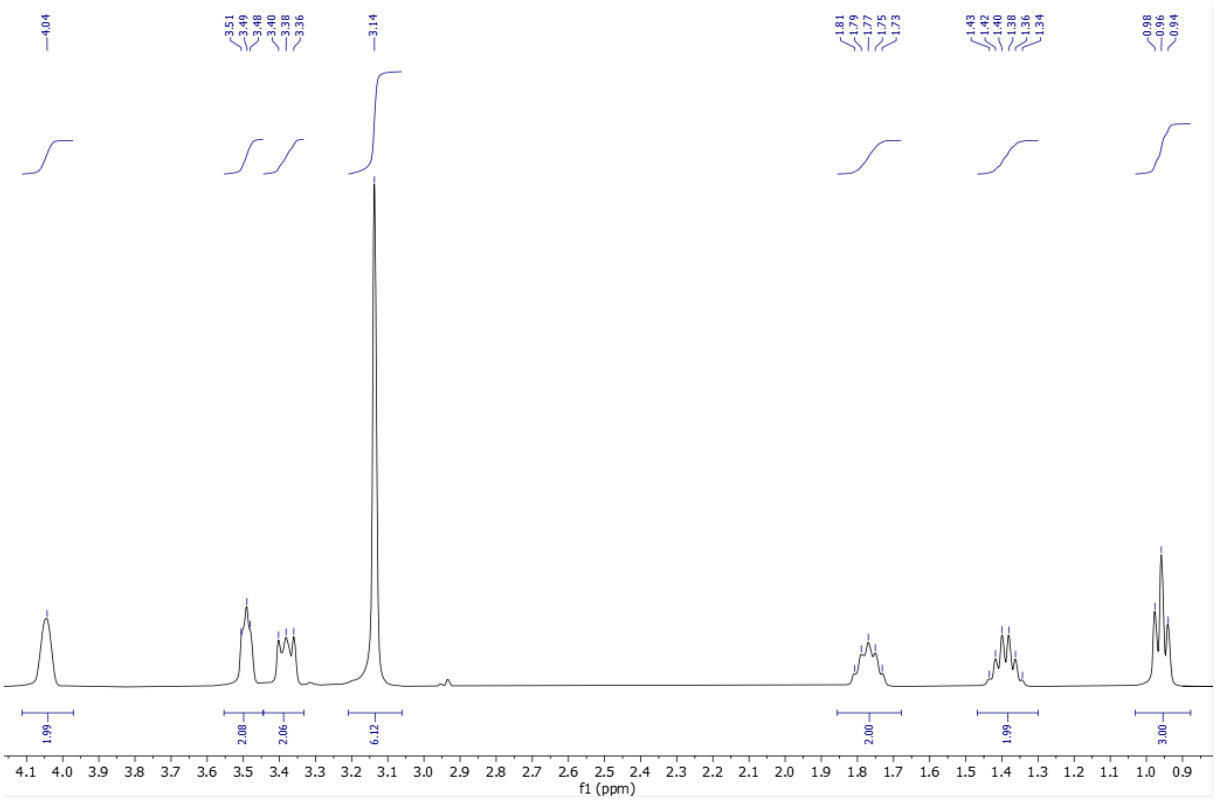

Appendix 8 - ^{1}H NMR spectrum of $[N_{1,1,4,2OH}]Br$ in D_2O.

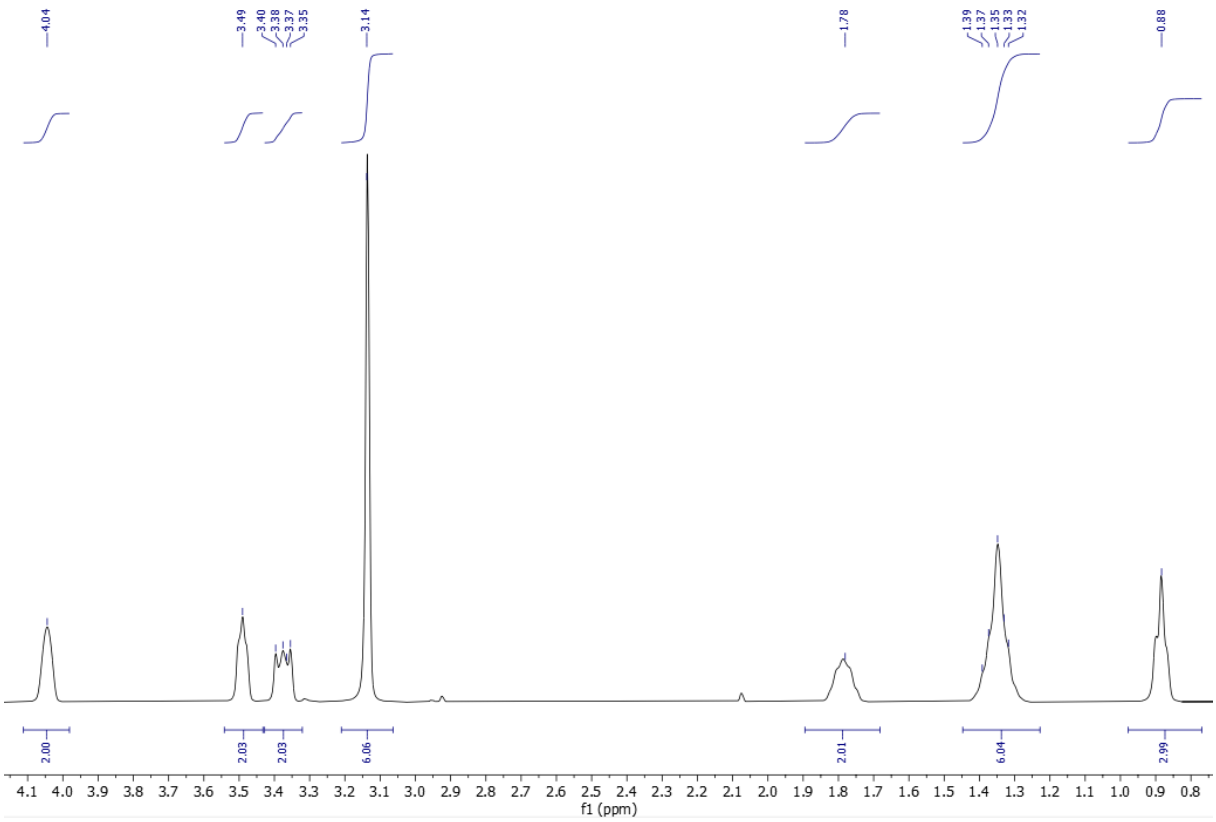

Appendix 9 - 1H NMR spectrum of $[N_{1,1,6,2OH}]Br$ in D_2O.

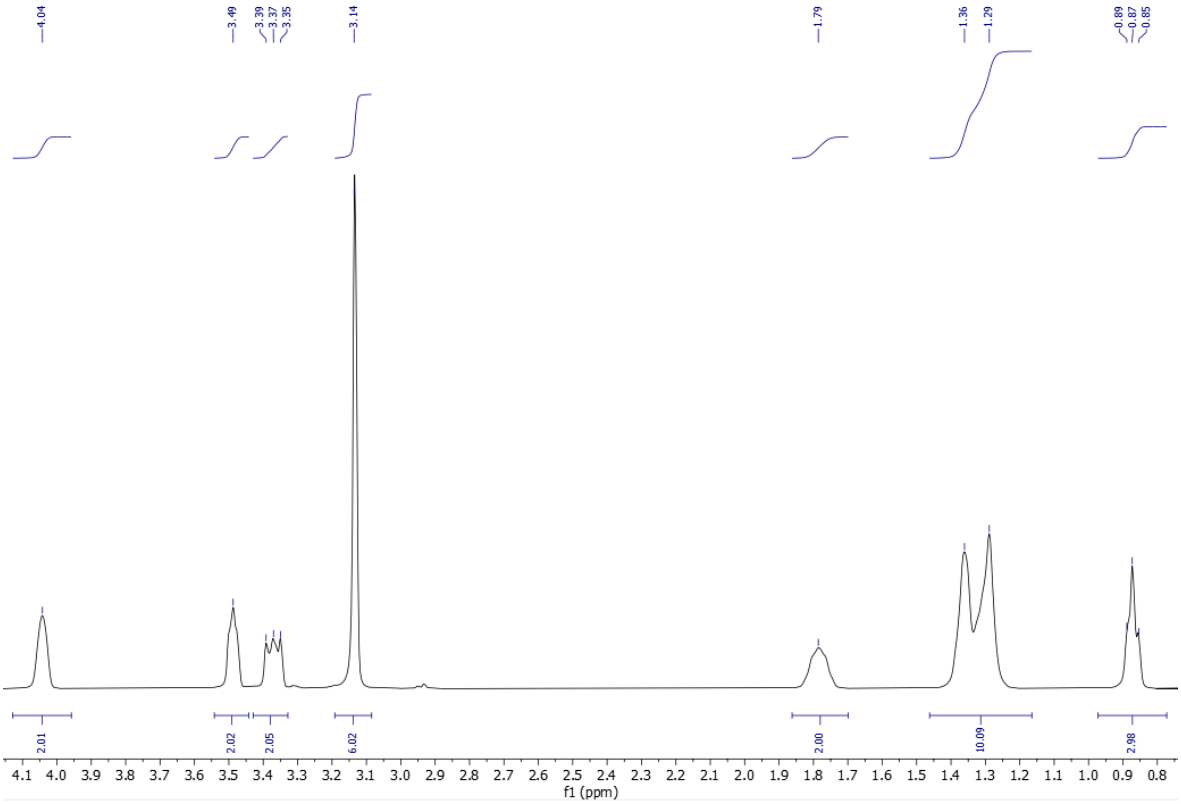

Appendix 10 - ^{1}H NMR spectrum of [$N_{1,1,8,2OH}$]Br in D_2O.

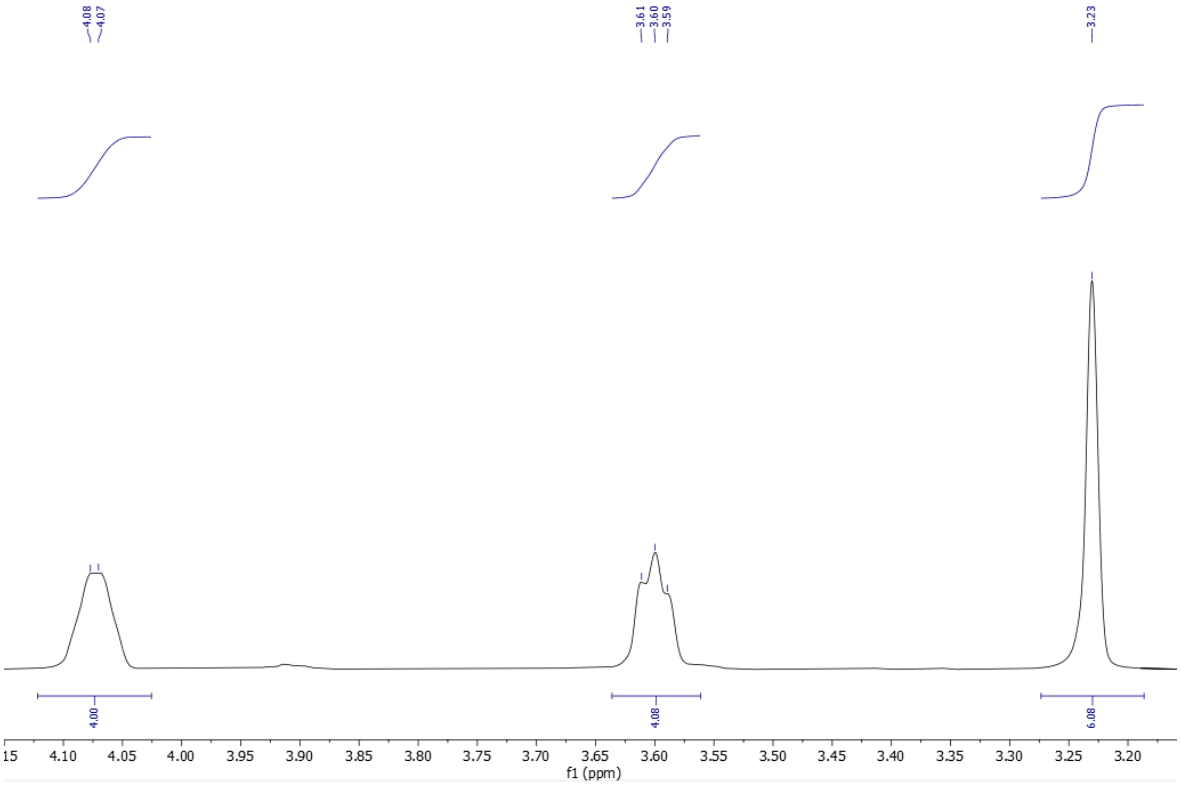

Appendix 11 - ^{1}H NMR spectrum of [$N_{1,1,2OH,2OH}$]Br in D_2O.

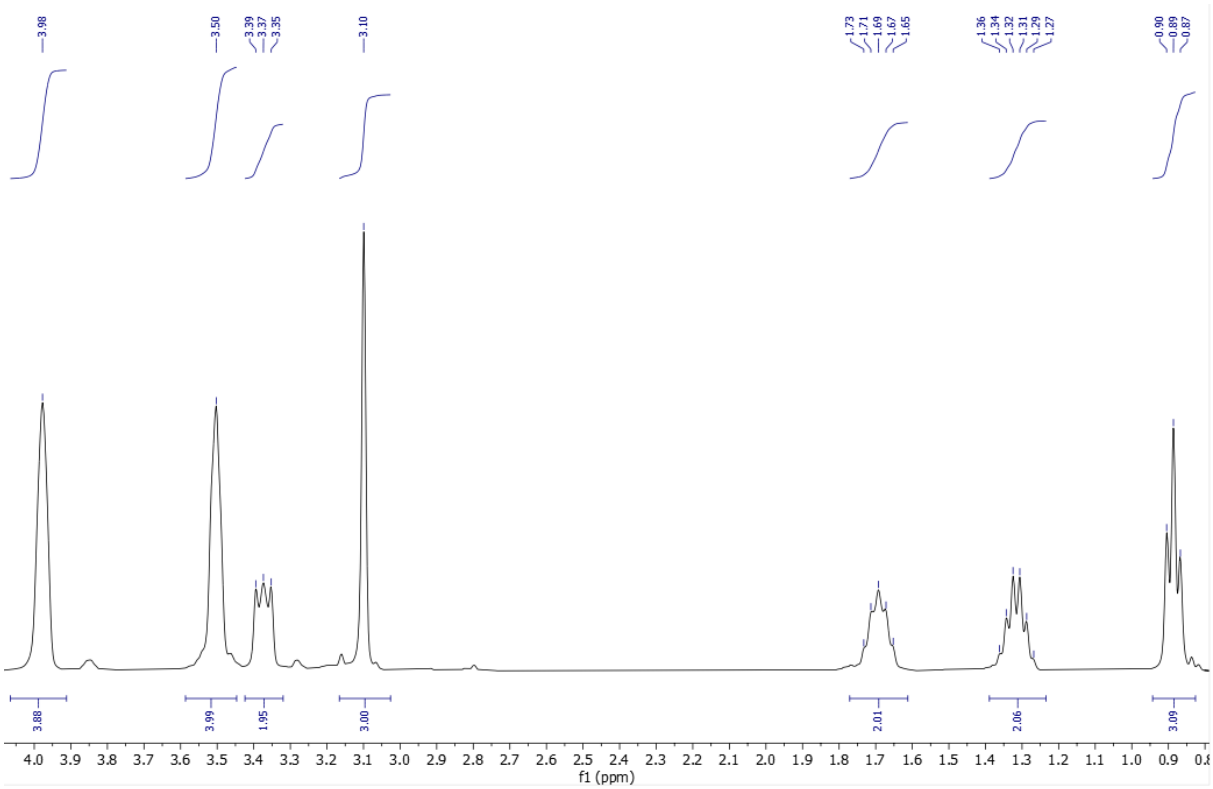

Appendix 12 - ^{1}H NMR spectrum of [N$_{1,4,2OH,2OH}$]Br in D$_2$O

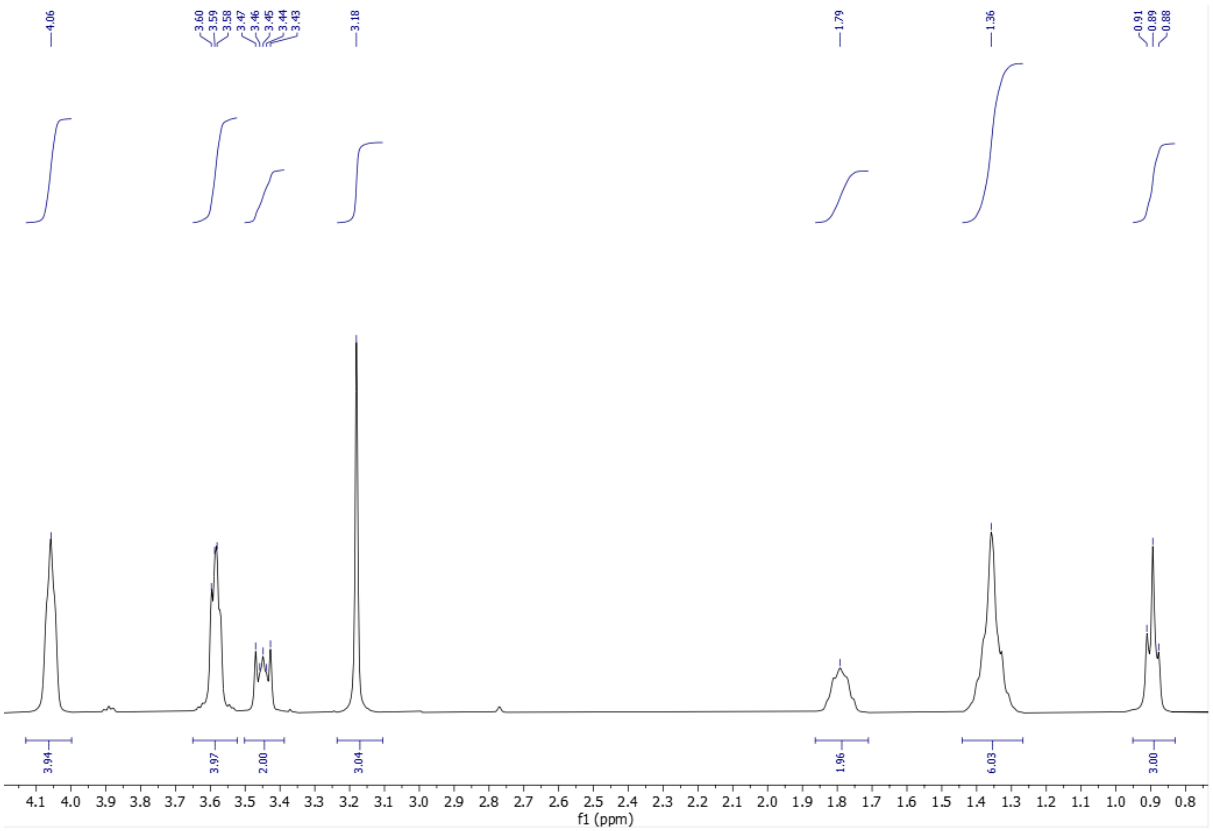

Appendix 13 - ^{1}H NMR spectrum of [N$_{1,6,2OH,2OH}$]Br in D$_2$O

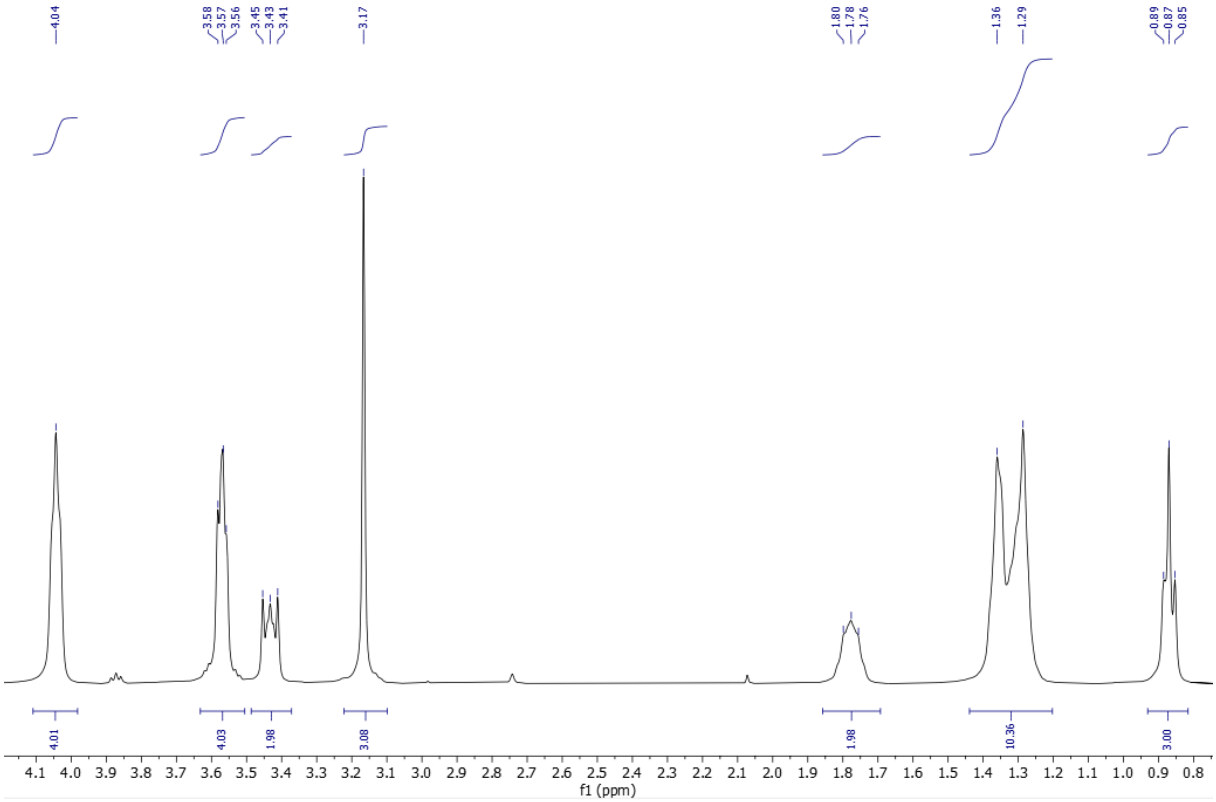

Appendix 14 - ^{1}H NMR spectrum of [$N_{1,8,2OH,2OH}$]Br in D_2O.

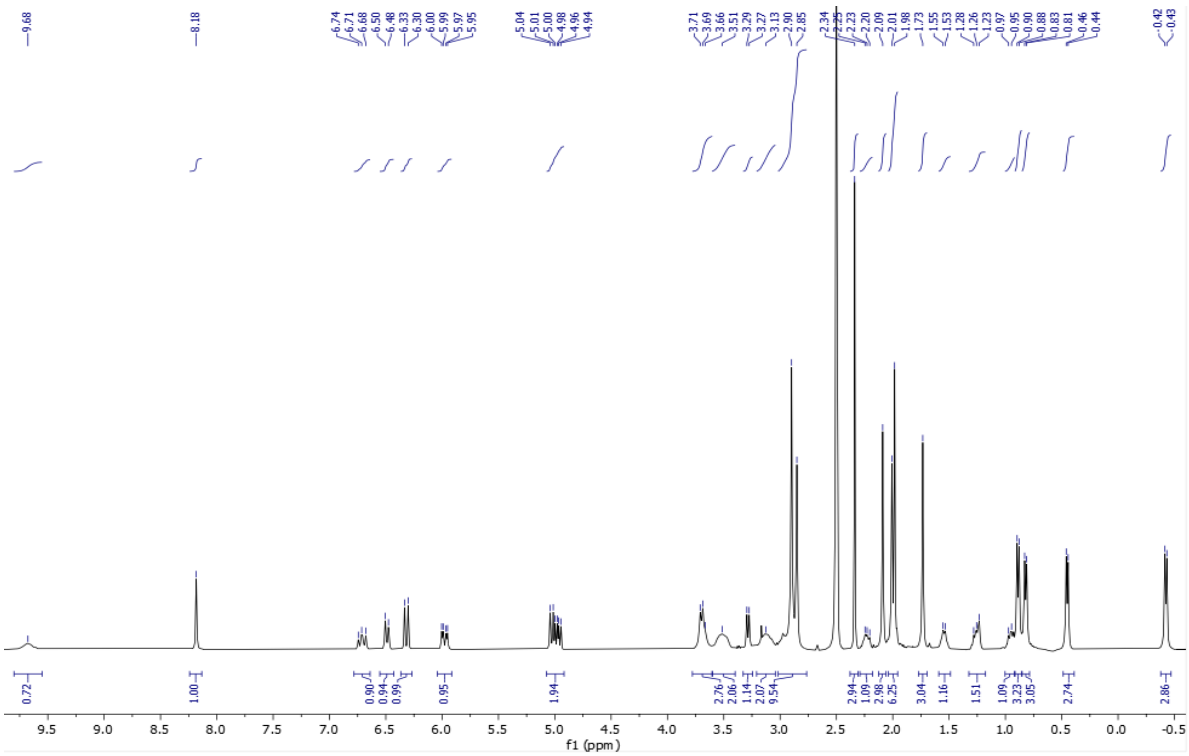

Appendix 15 - ^{1}H NMR spectrum of [RifH][C_1SO_3] in DMSO-*d_6*.

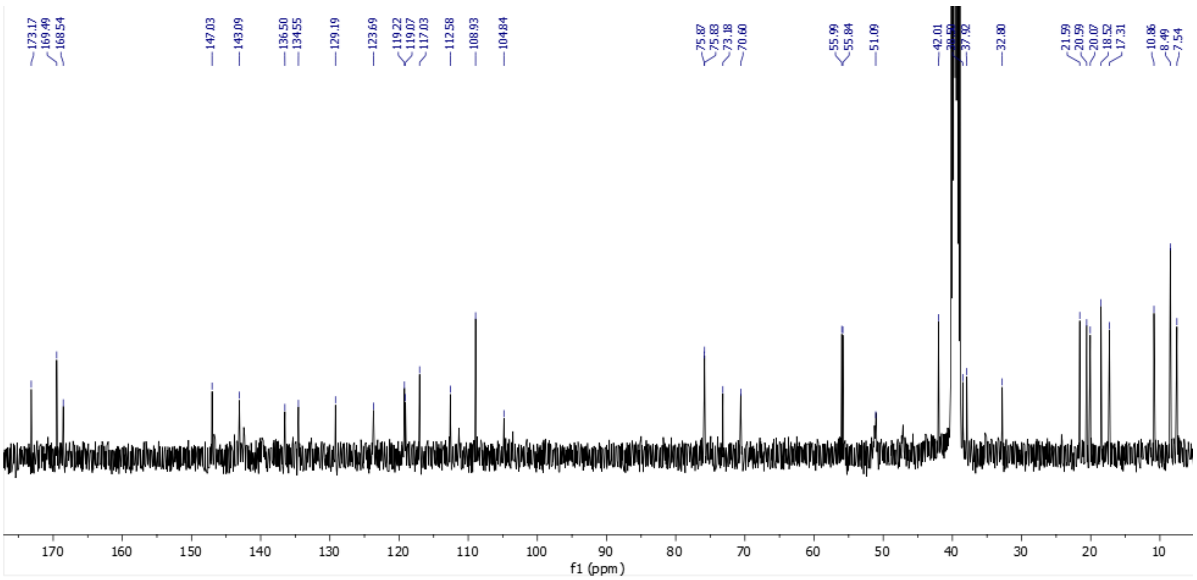

Appendix 16 - ^{13}C NMR spectrum of [RifH][C_1SO_3] in DMSO-*d6*.

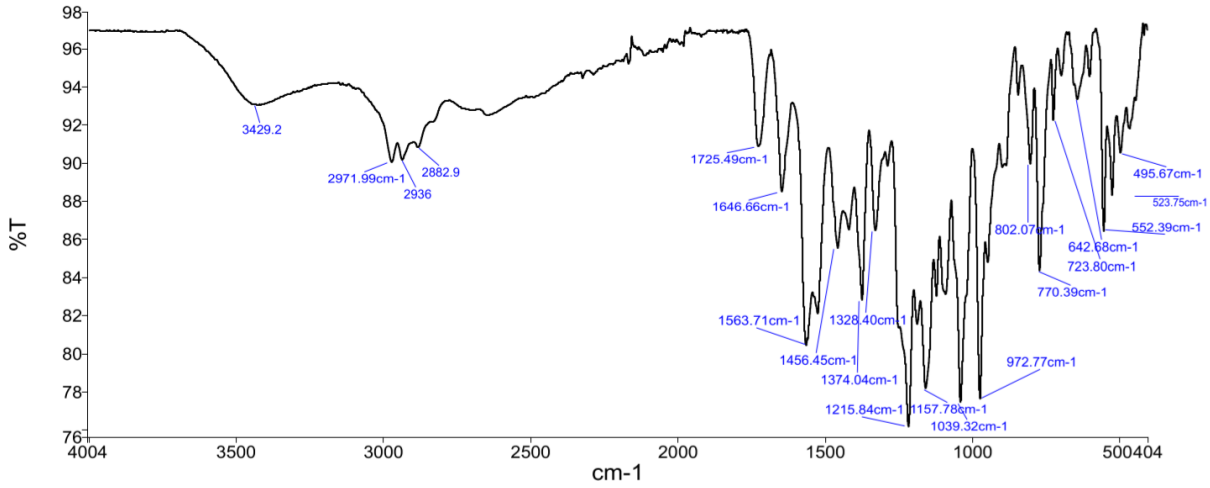

Appendix 17 – ATR-FTIR spectrum of [RifH][C_1SO_3].

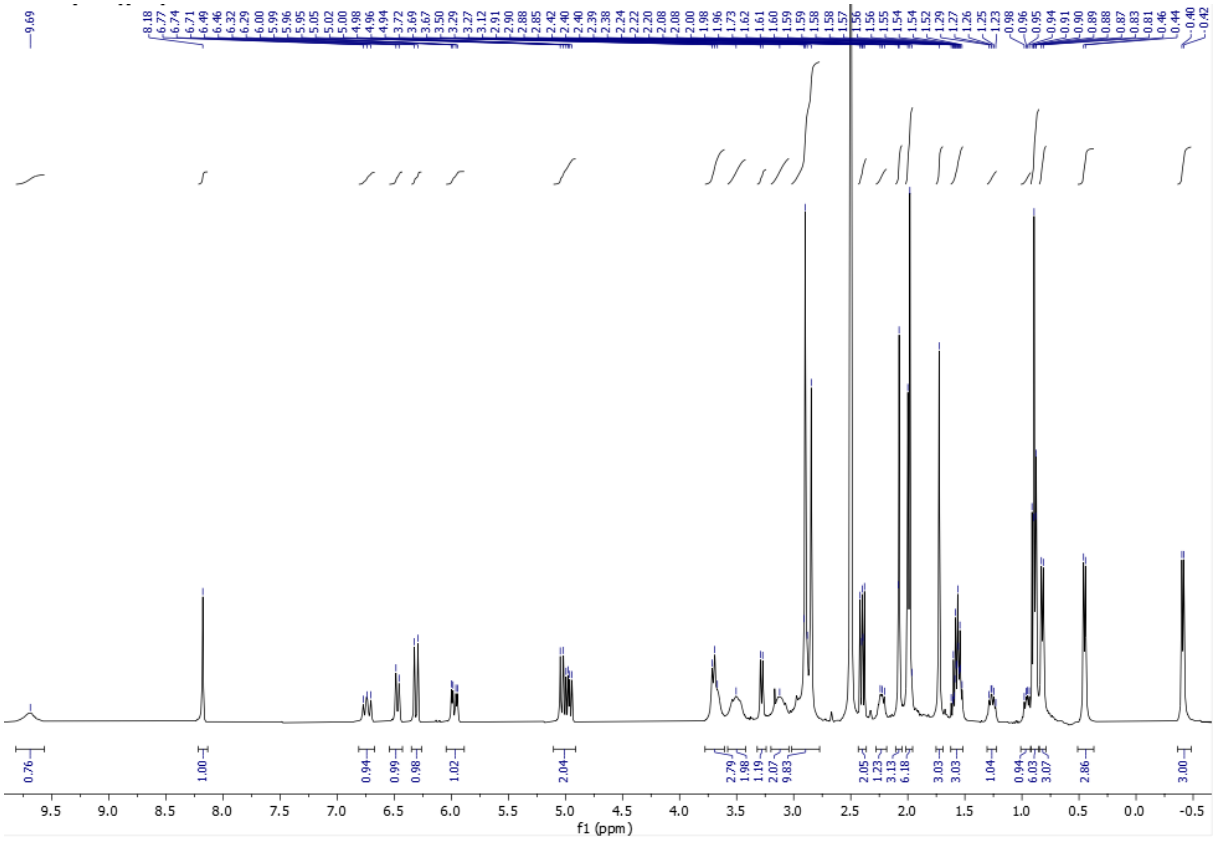

Appendix 18 - ^{1}H NMR spectrum of [RifH][C_3SO_3] in DMSO-*d*$_6$.

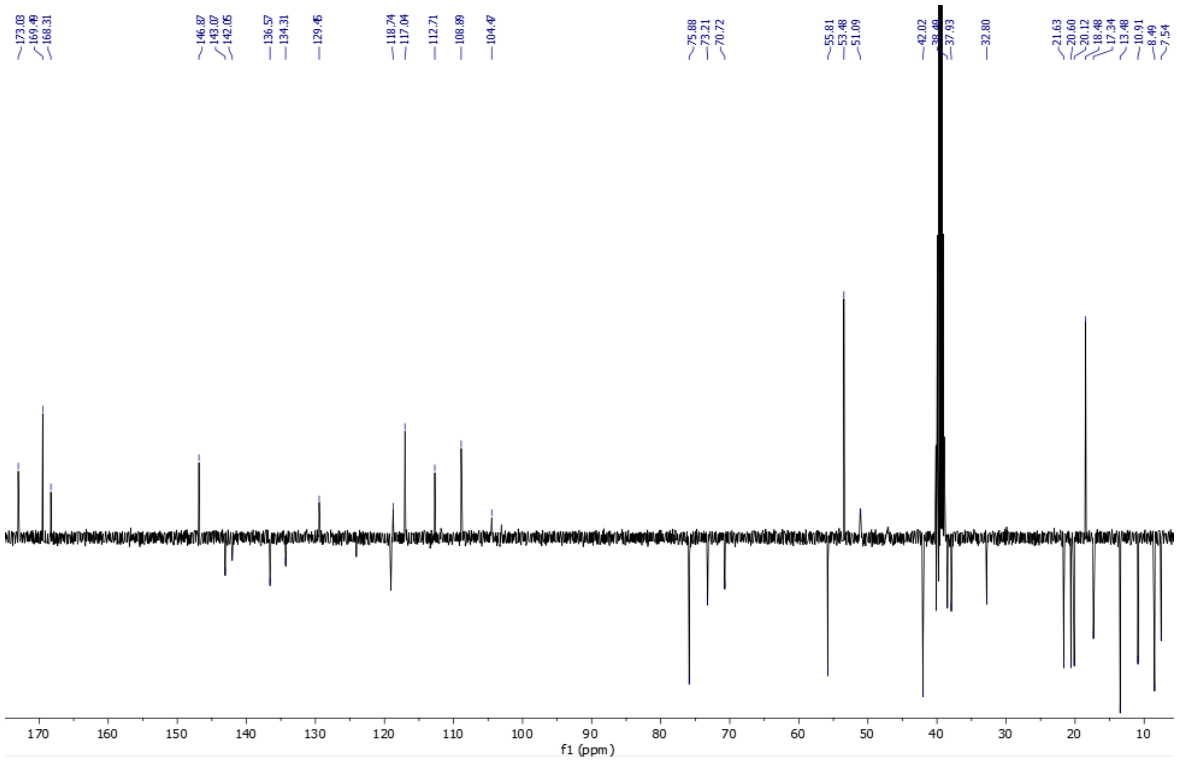

Appendix 19 - 13C NMR spectrum of [RifH][C_3SO_3] in DMSO-*d*$_6$.

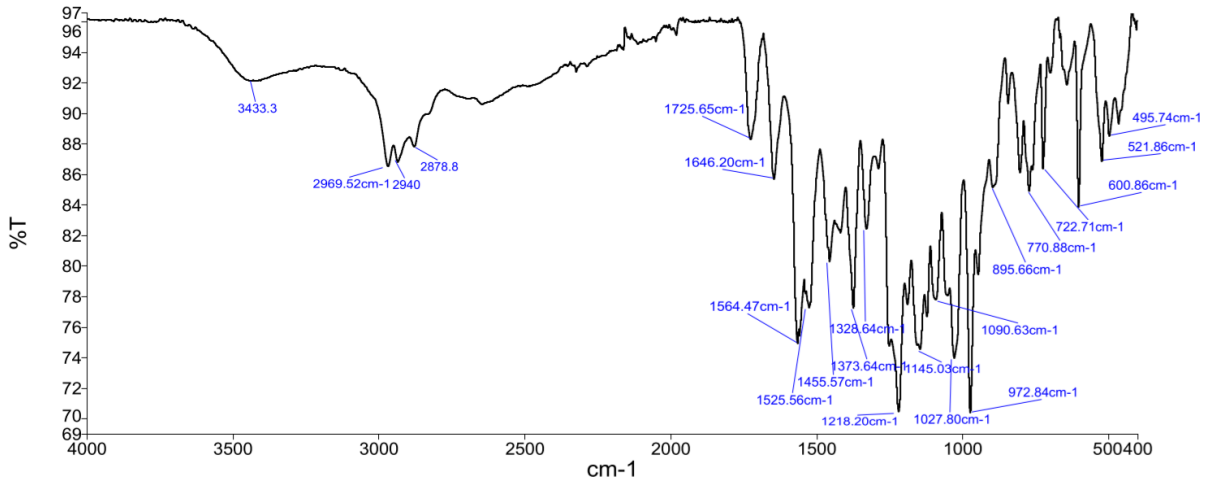

Appendix 20 - ATR-FTIR spectrum of [RifH][C_3SO_3].

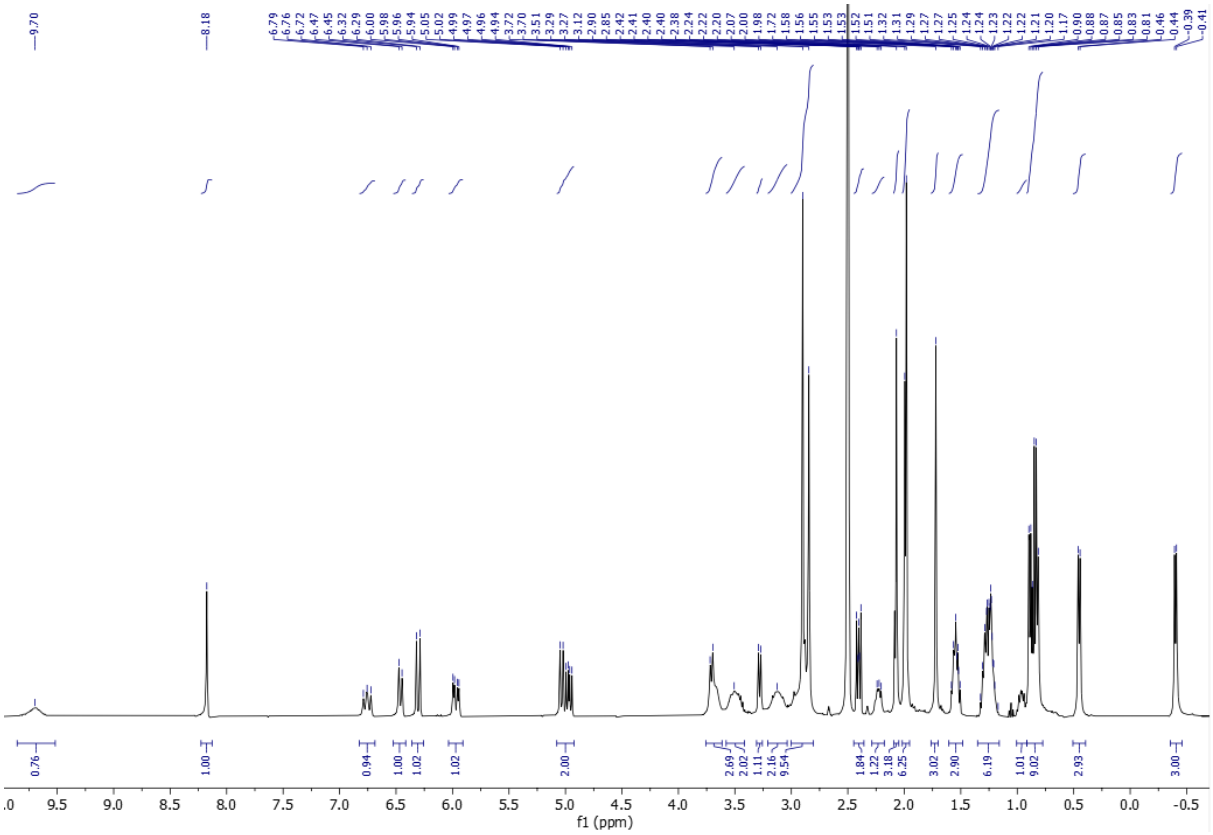

Appendix 21 - ^{1}H NMR spectrum of [RifH][C_6SO_3] in DMSO-*d6*.

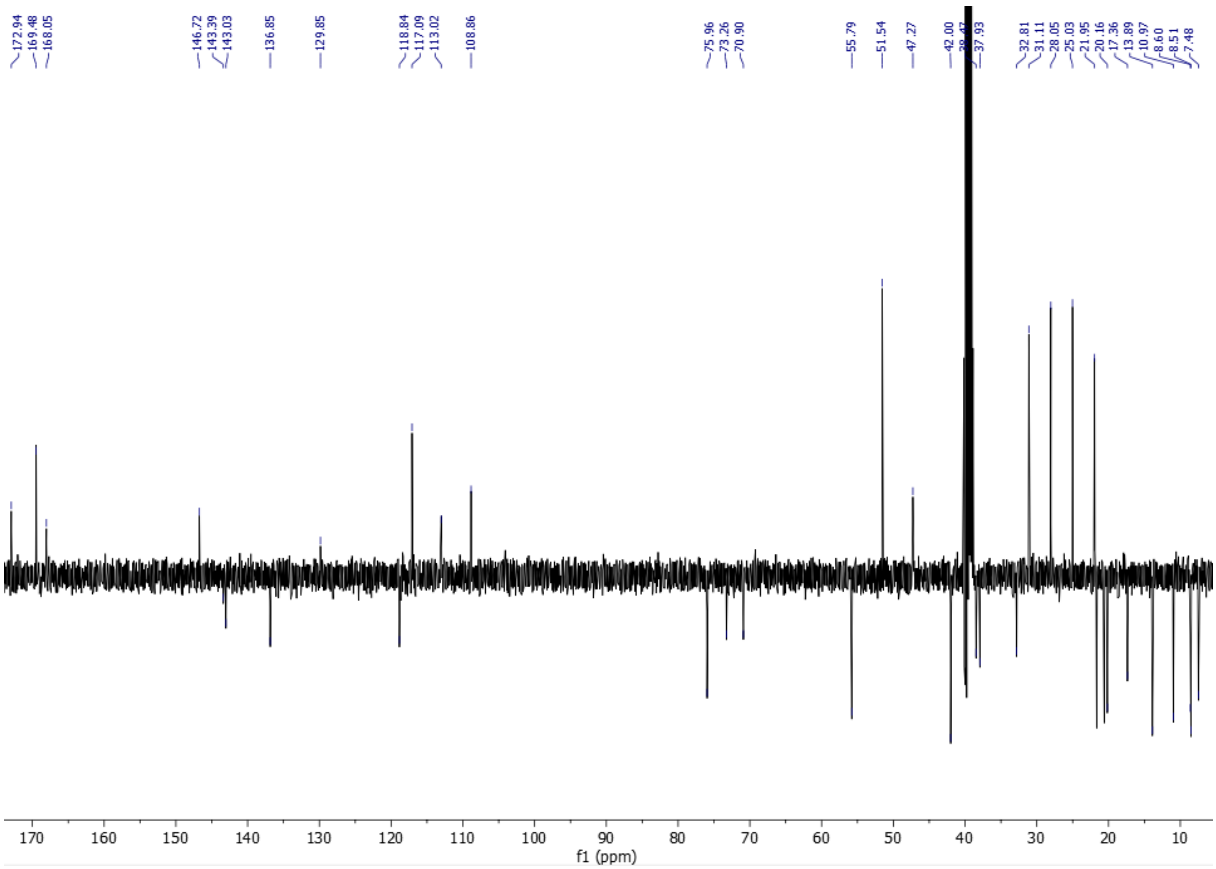

Appendix 22 - ^{13}C NMR spectrum of [RifH][C_6SO_3] in DMSO-*d*$_6$.

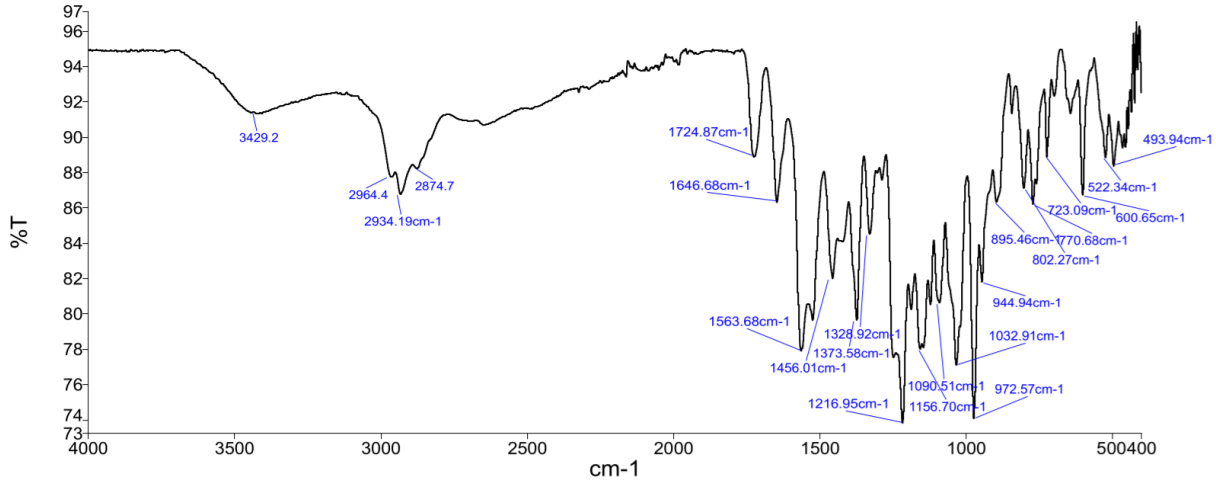

Appendix 23 - ATR-FTIR spectrum of [RifH][C_6SO_3].

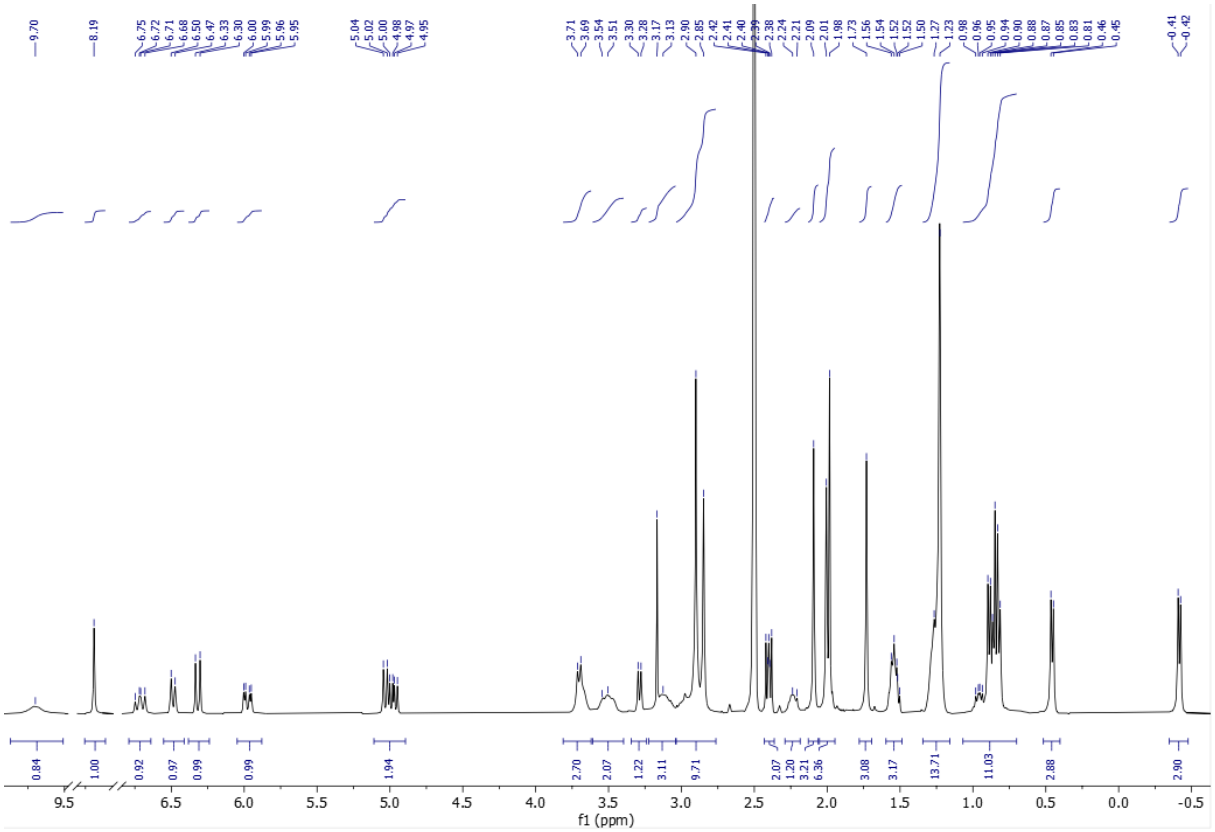

Appendix 24 - ^{1}H NMR spectrum of [RifH][C_9SO_3] in DMSO-*d6*.

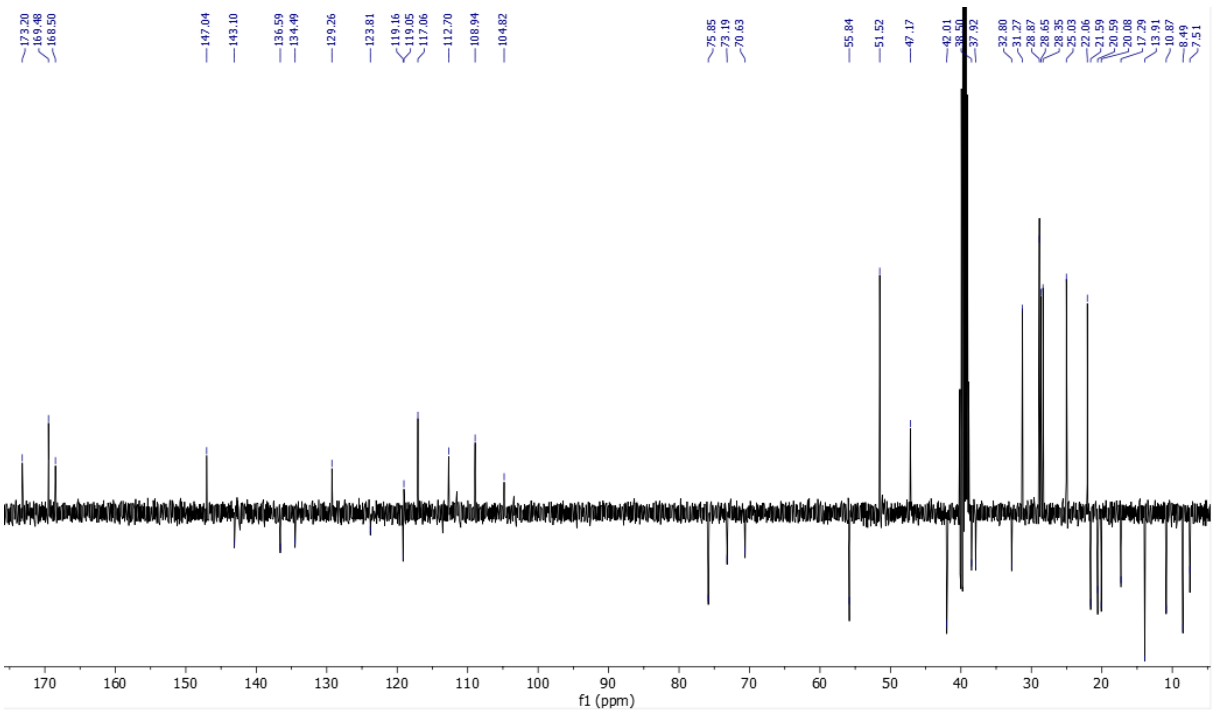

Appendix 25 - ^{13}C NMR spectrum of [RifH][C_9SO_3] in DMSO-*d6*

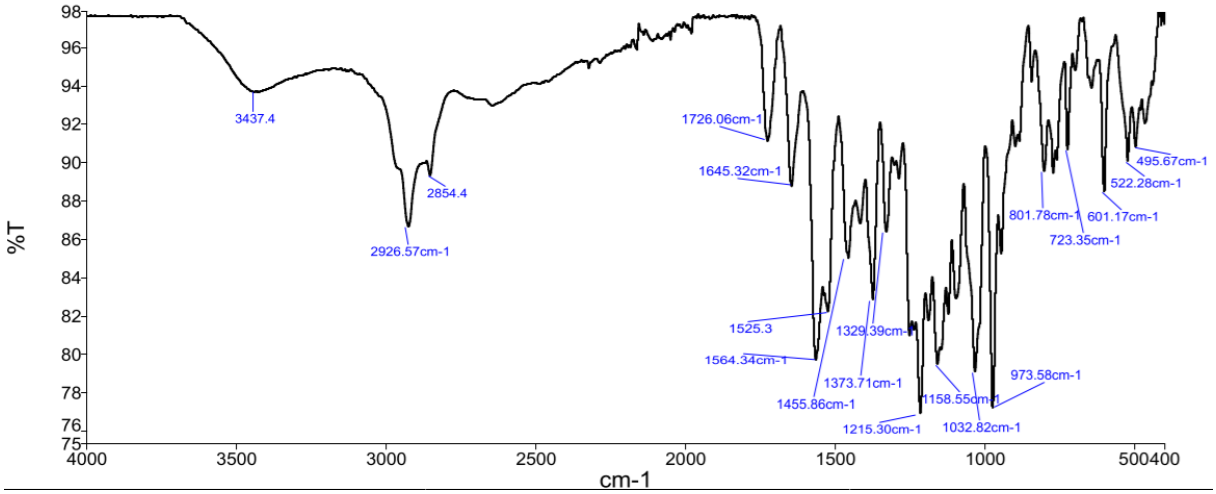

Appendix 26 - ATR-FTIR spectrum of [RifH][C_9SO_3].

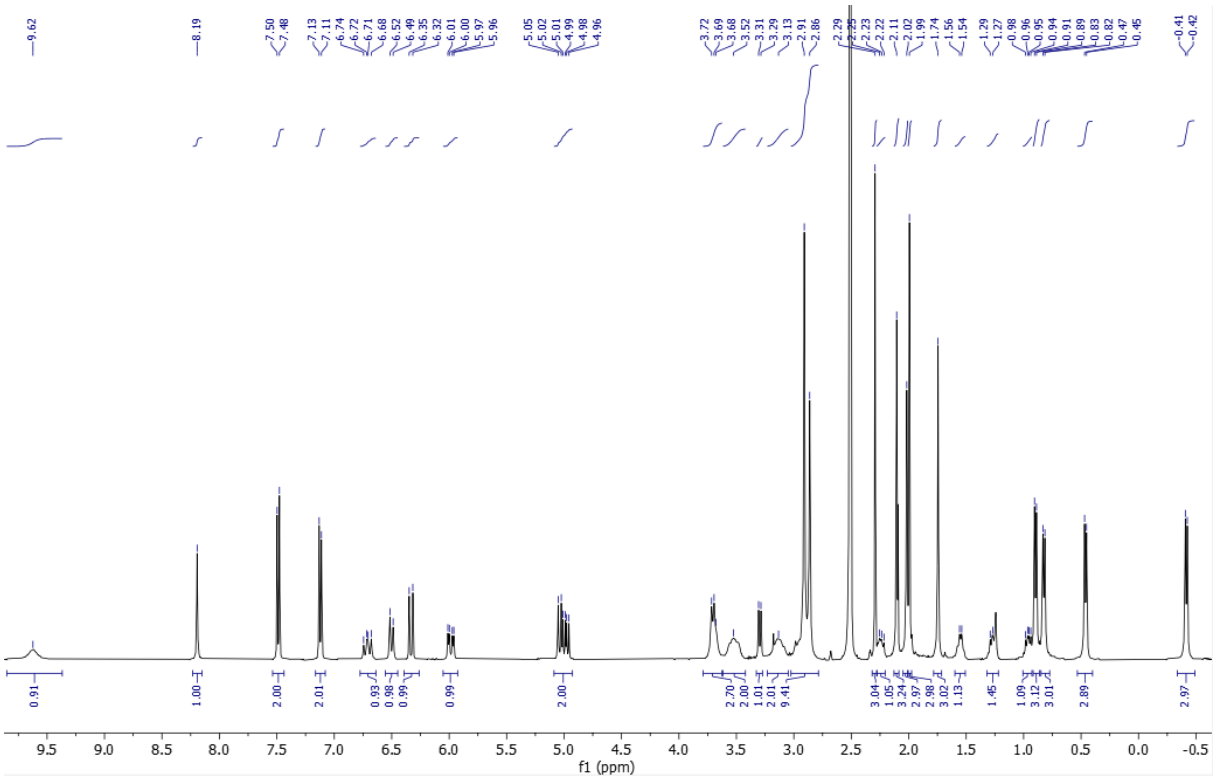

Appendix 27 - ^{1}H NMR spectrum of [RifH][$TolSO_3$] in DMSO-*d*$_6$.

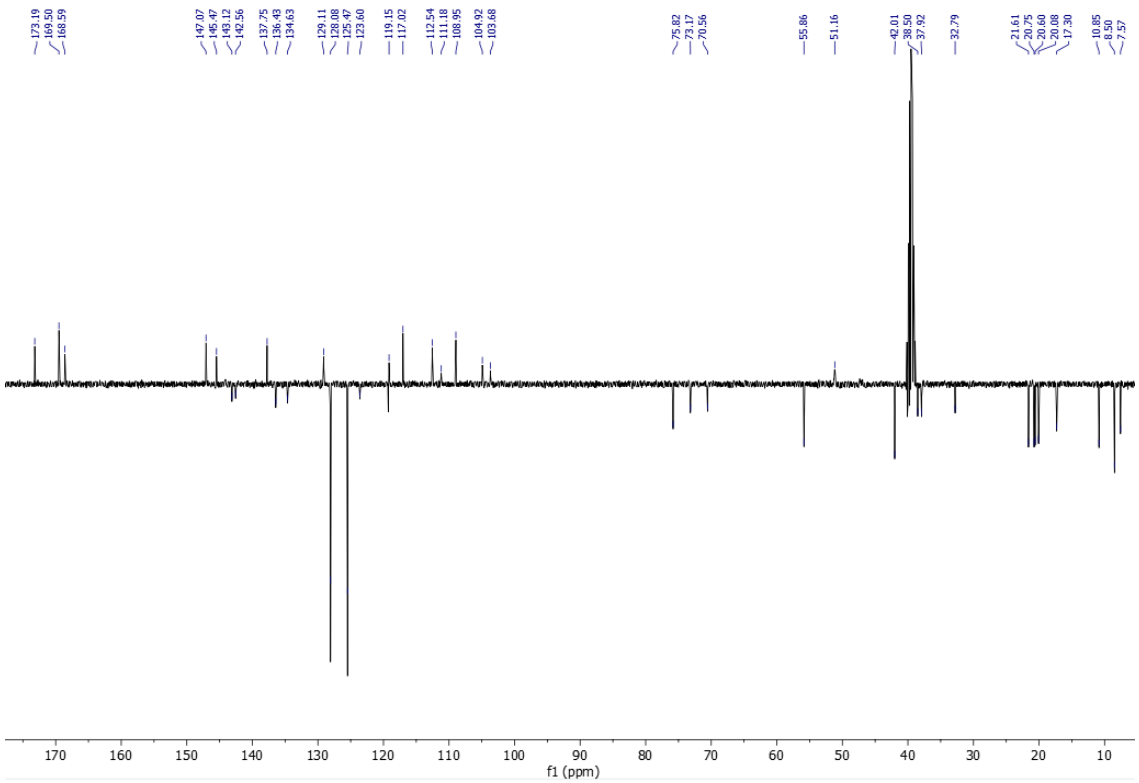

Appendix 28 - ^{13}C NMR spectrum of [RifH][TolSO3] in DMSO-*d6*.

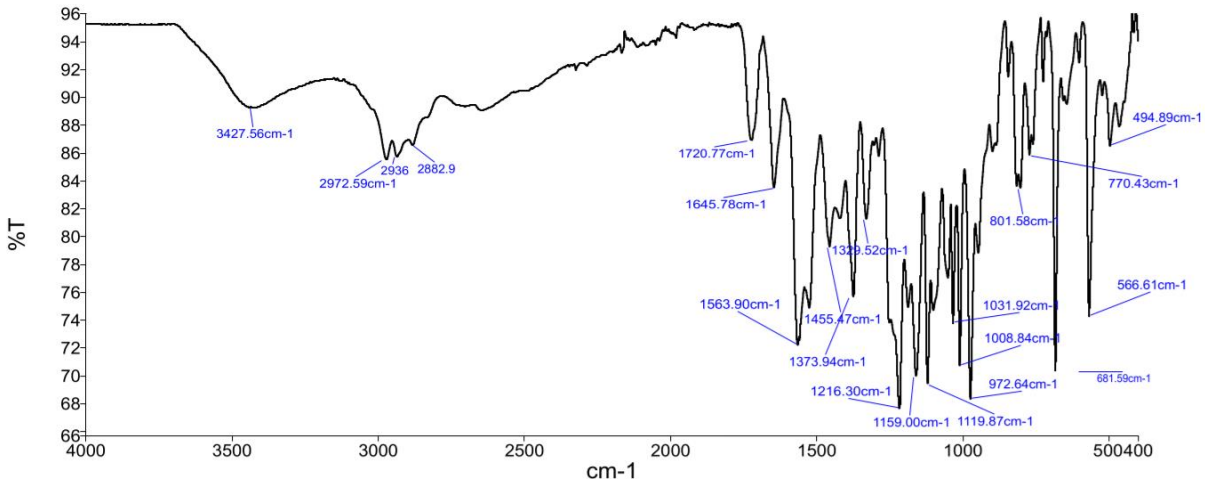

Appendix 29 - ATR-FTIR spectrum of [Rif][TolSO3].

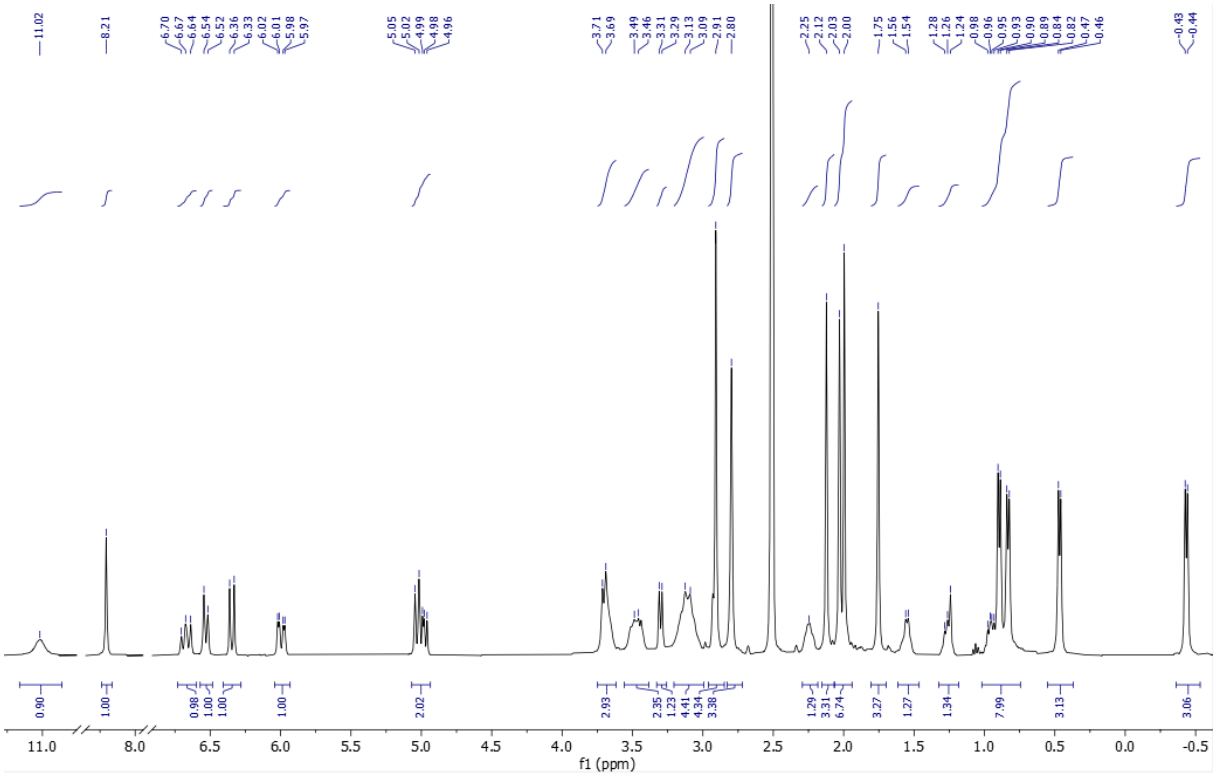

Appendix 30 - ^{1}H NMR spectrum of [RifH]Cl in DMSO-d_6.

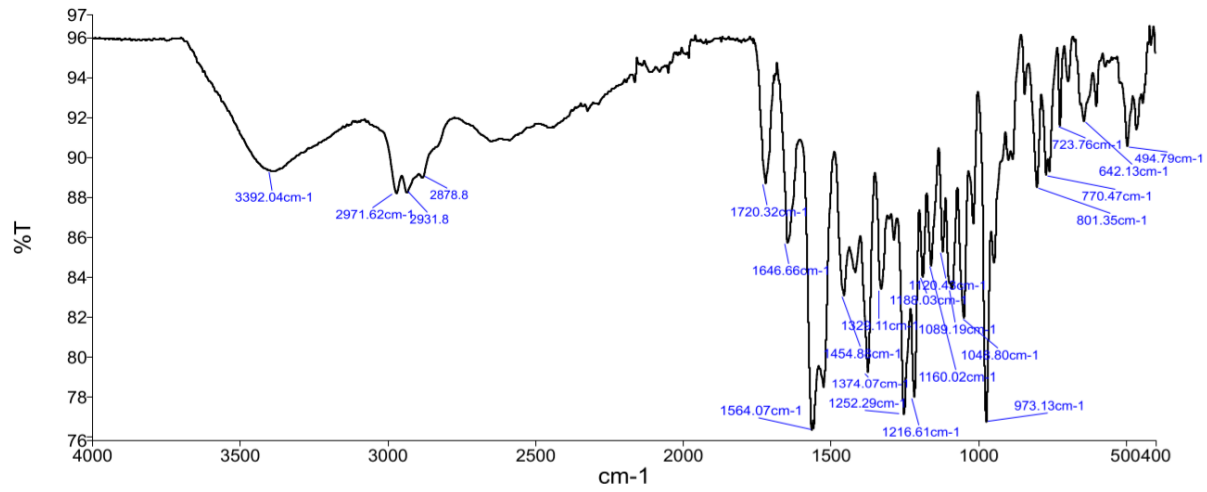

Appendix 31 - ATR-FTIR spectrum of [RifH]Cl.

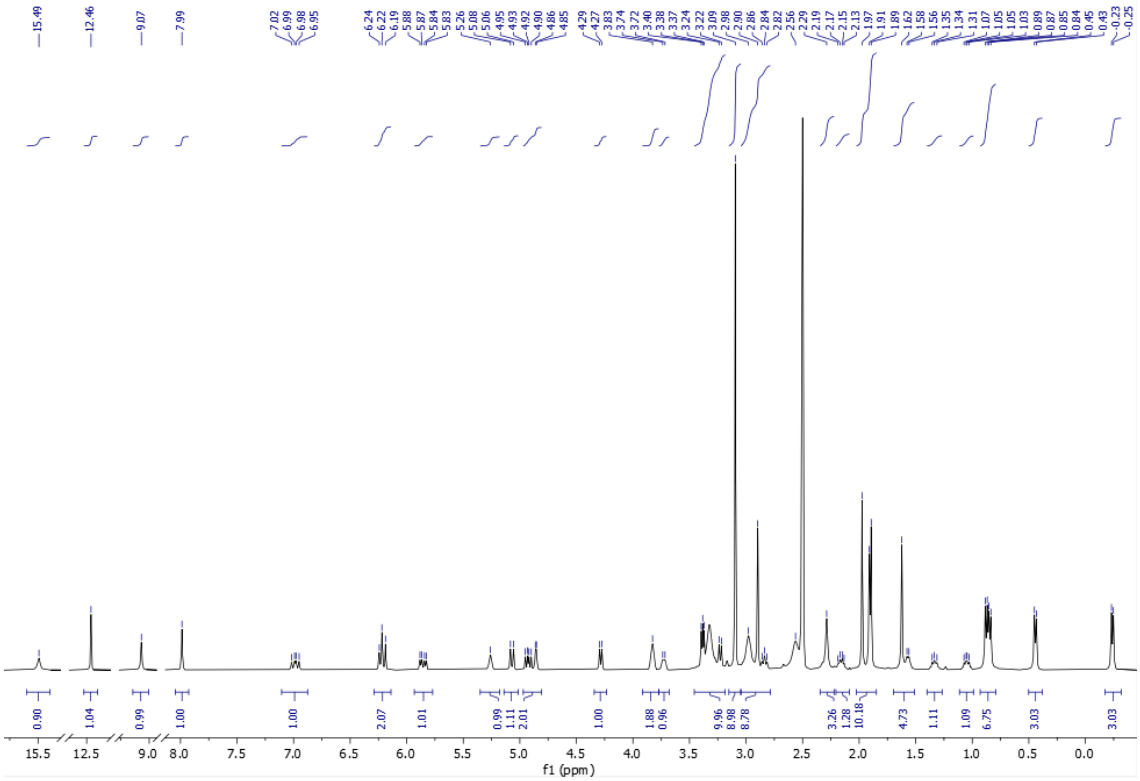

Appendix 32 - ^{1}H NMR spectrum of [$N_{1,1,1,2OH}$][Rif] in DMSO-*d*$_6$.

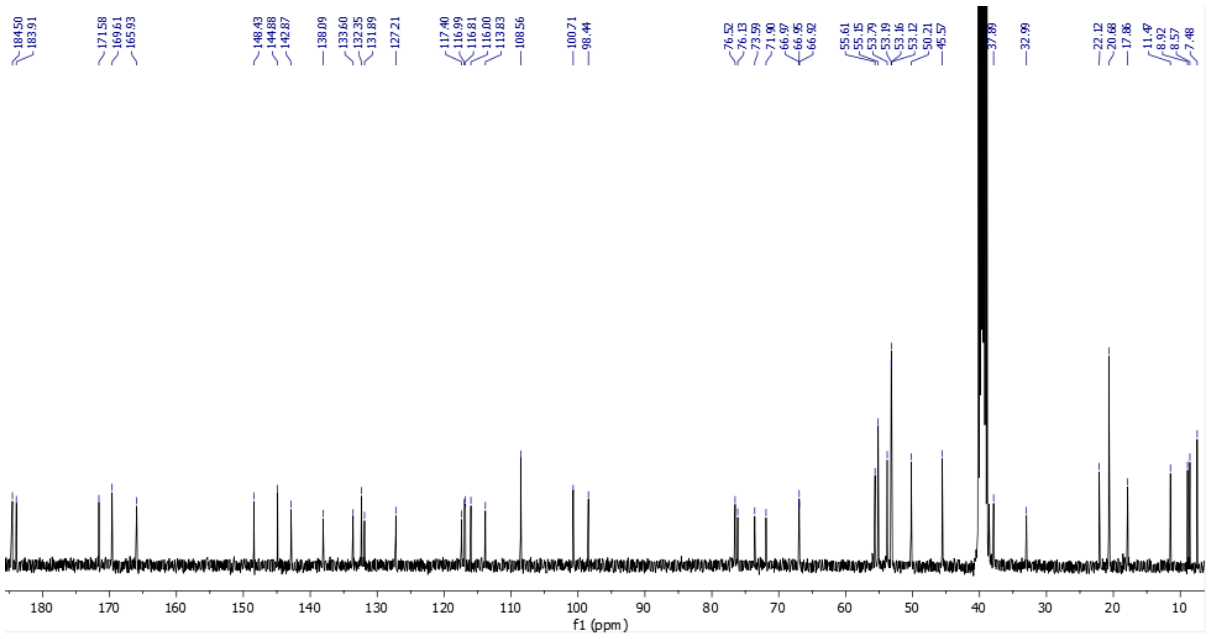

Appendix 33 - ^{13}C NMR spectrum of [$N_{1,1,1,2OH}$][Rif] in DMSO-*d*$_6$.

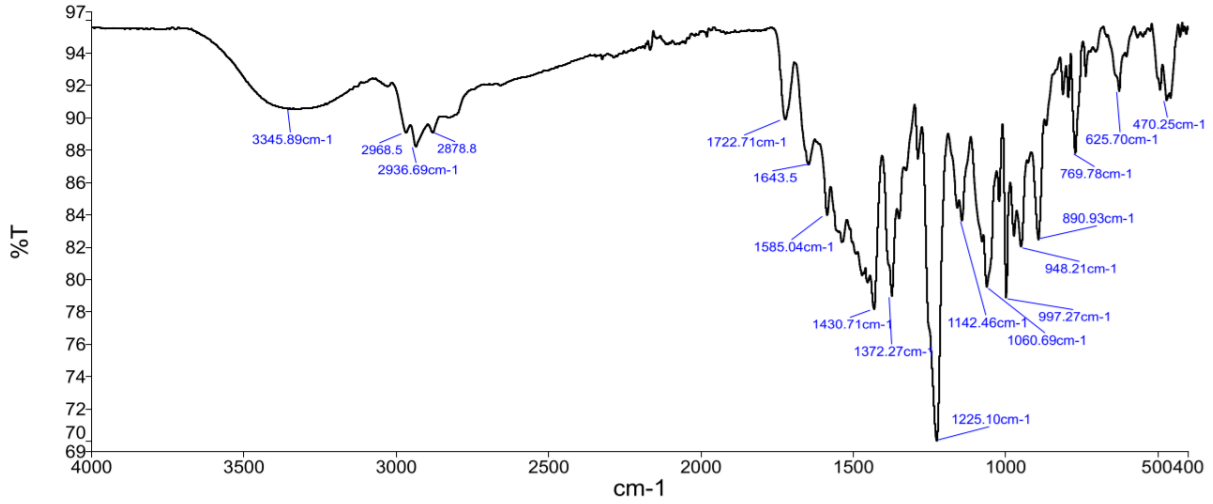

Appendix 34 - ATR-FTIR spectrum of [$N_{1,1,1,2OH}$][Rif].

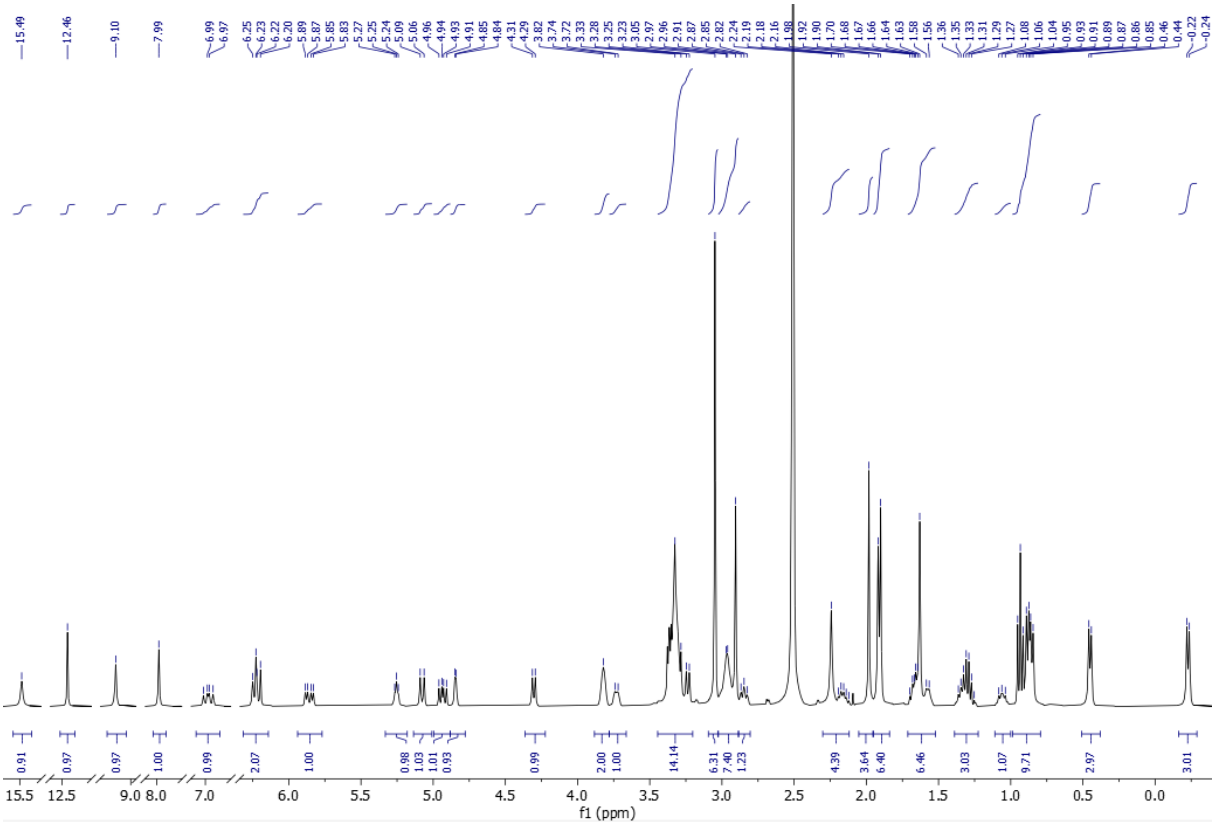

Appendix 35 - ^{1}H NMR spectrum of [$N_{1,1,4,2OH}$][Rif] in DMSO-*d*$_6$.

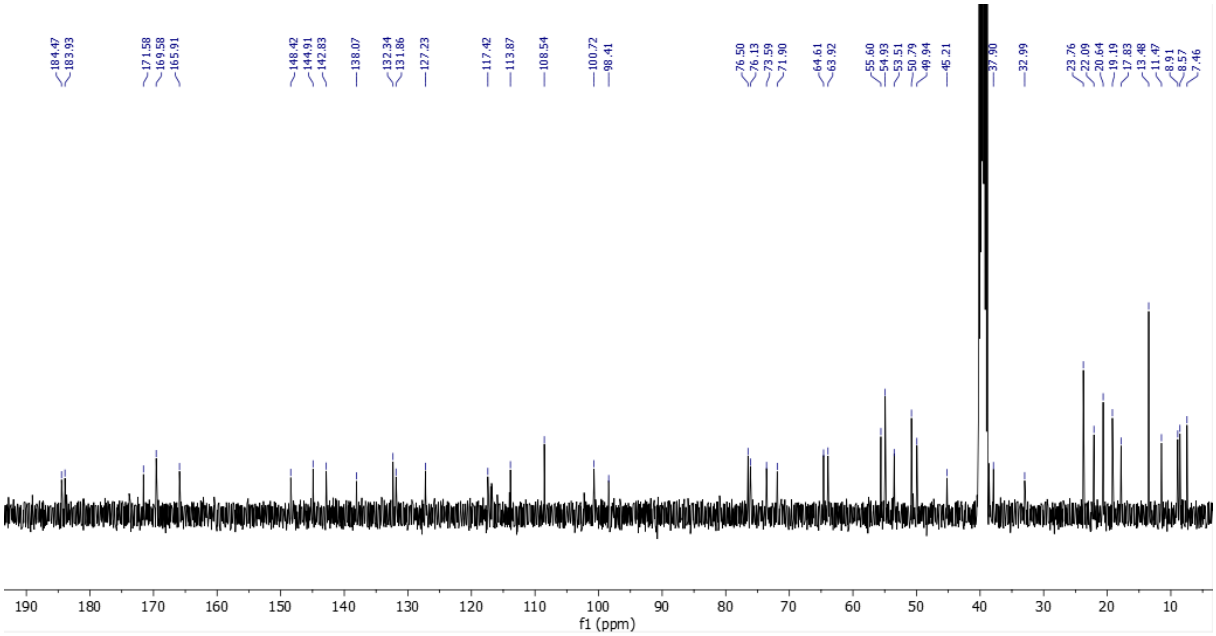

Appendix 36 - ^{13}C NMR spectrum of [$N_{1,1,4,2OH}$][Rif] in DMSO-*d_6*.

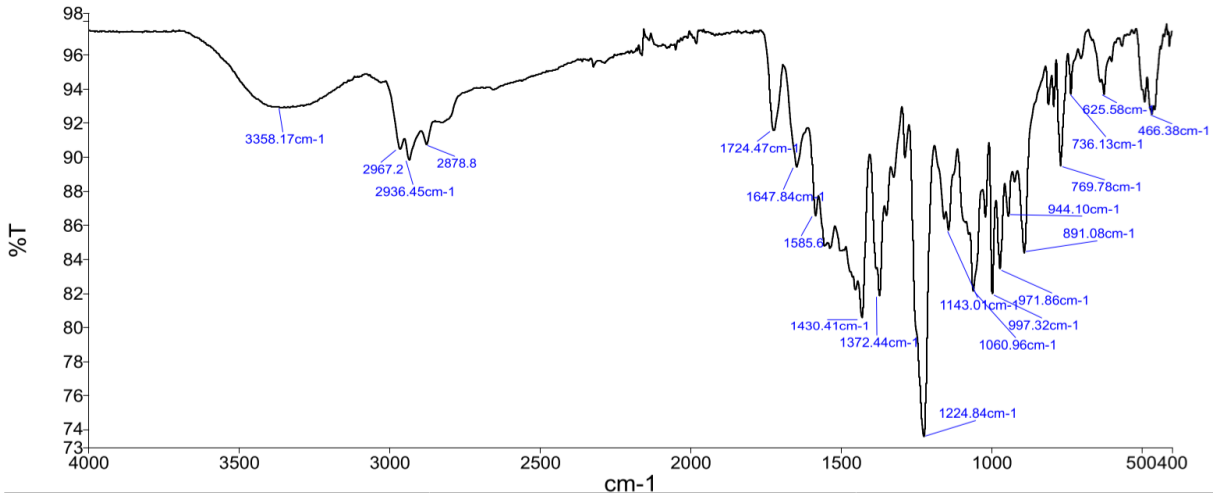

Appendix 37 - ATR-FTIR spectrum of [$N_{1,1,4,2OH}$][Rif].

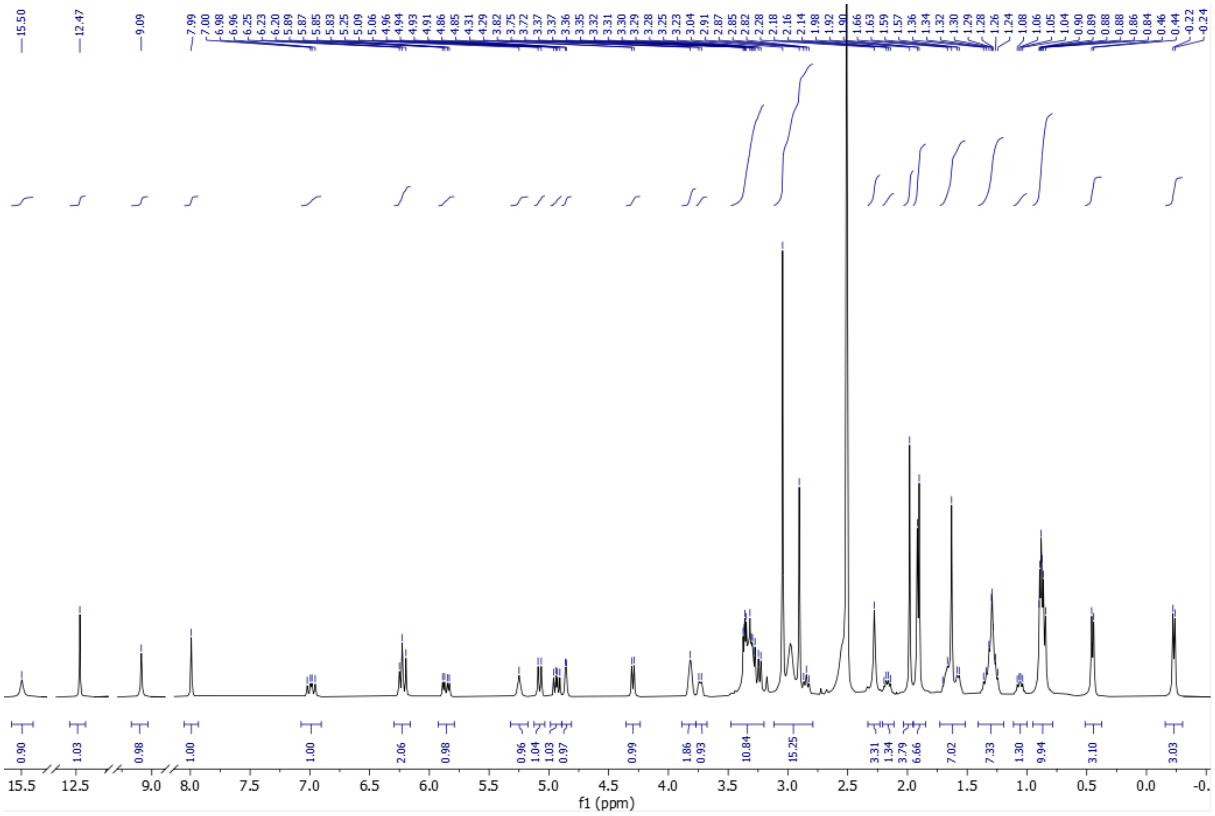

Appendix 38 - ^{1}H NMR spectrum of [$N_{1,1,6,2OH}$][Rif] in DMSO-*d_6*

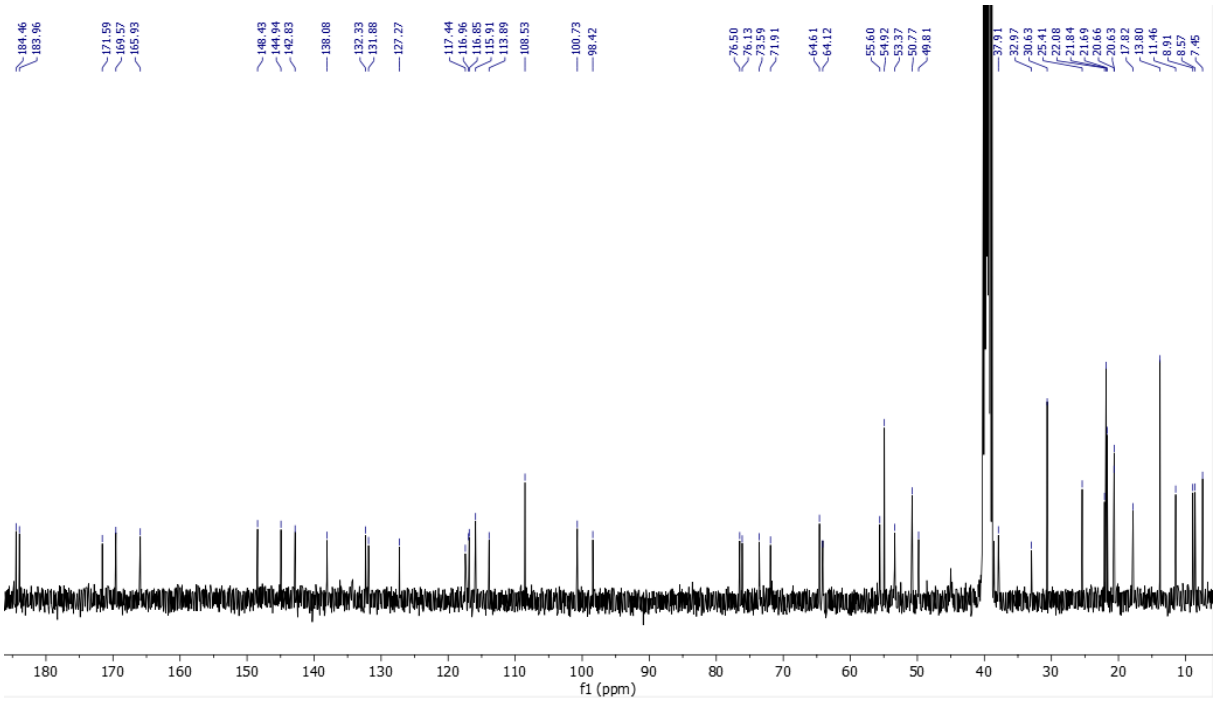

Appendix 39 - ^{13}C NMR spectrum of [$N_{1,1,6,2OH}$][Rif] in DMSO-*d_6*.

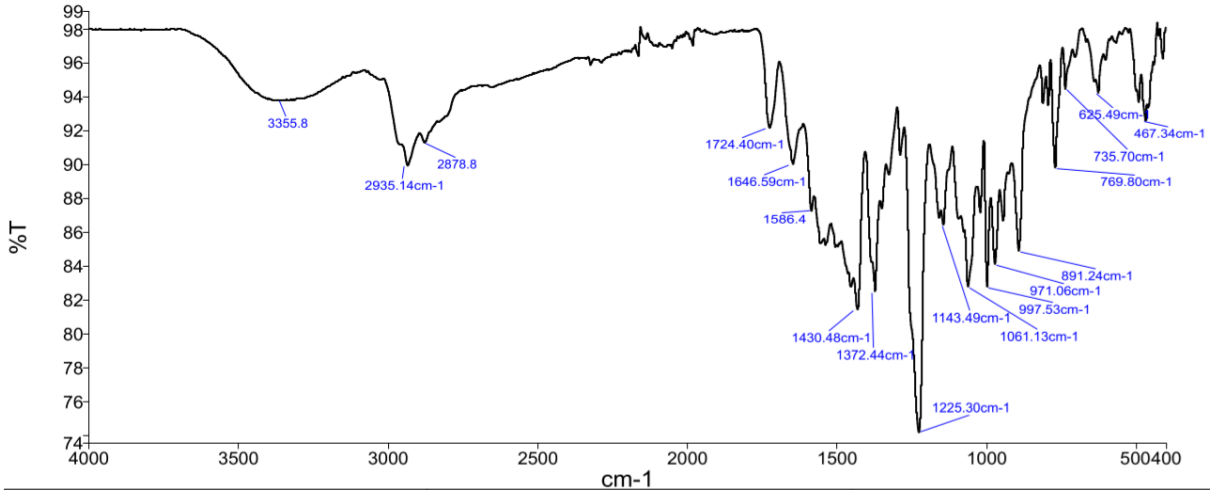

Appendix 40 - ATR-FTIR spectrum of [$N_{1,1,6,2OH}$][Rif].

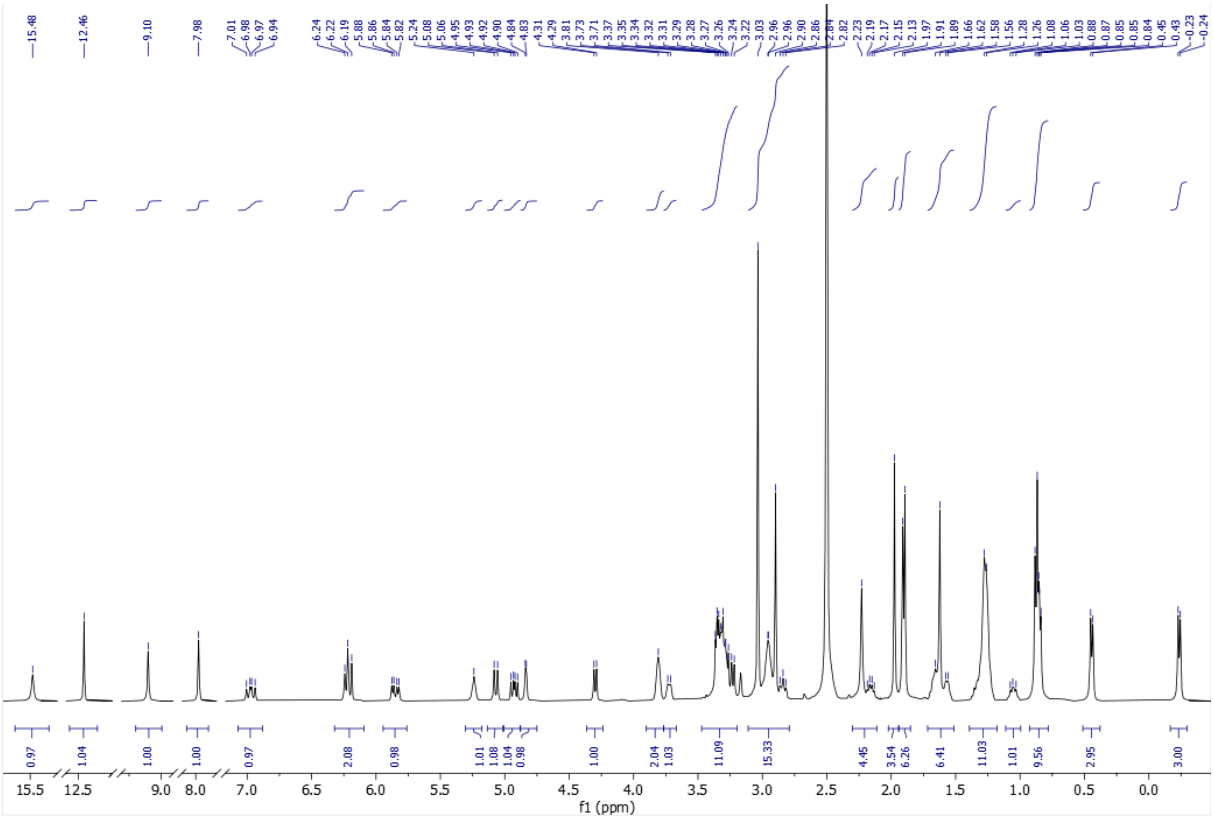

Appendix 41 - ^{1}H NMR spectrum of [$N_{1,1,8,2OH}$][Rif] in DMSO-*d*$_6$.

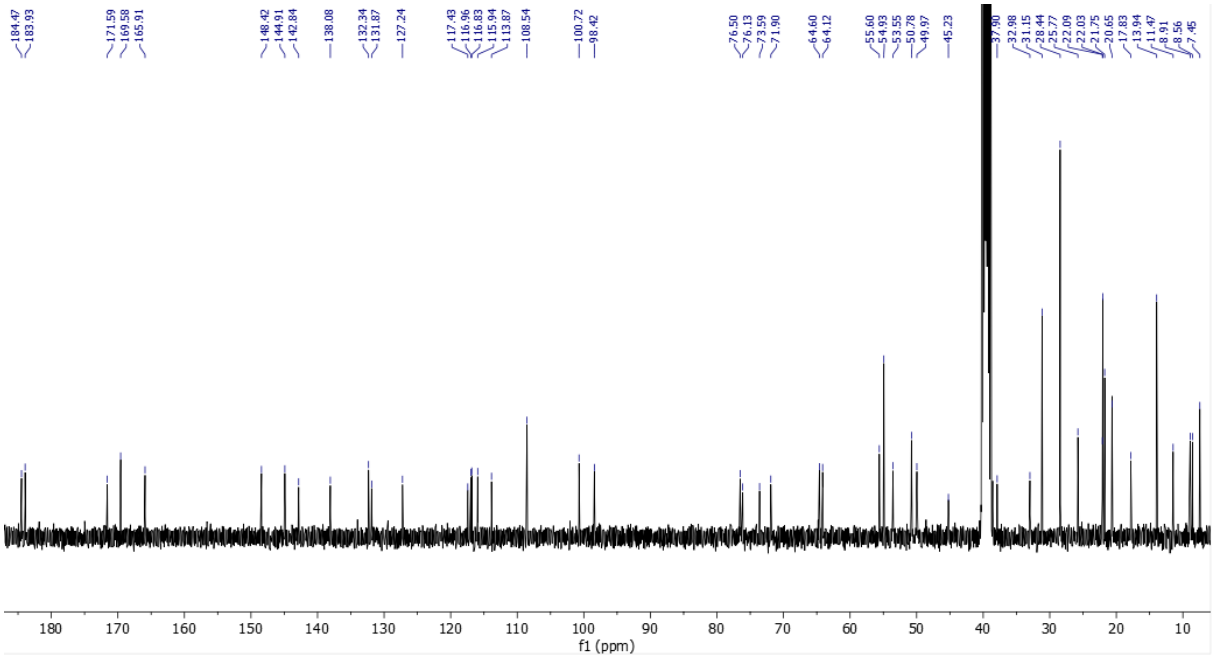

Appendix 42 - ^{13}C NMR spectrum of [$N_{1,1,8,2OH}$][Rif] in DMSO-*d_6*.

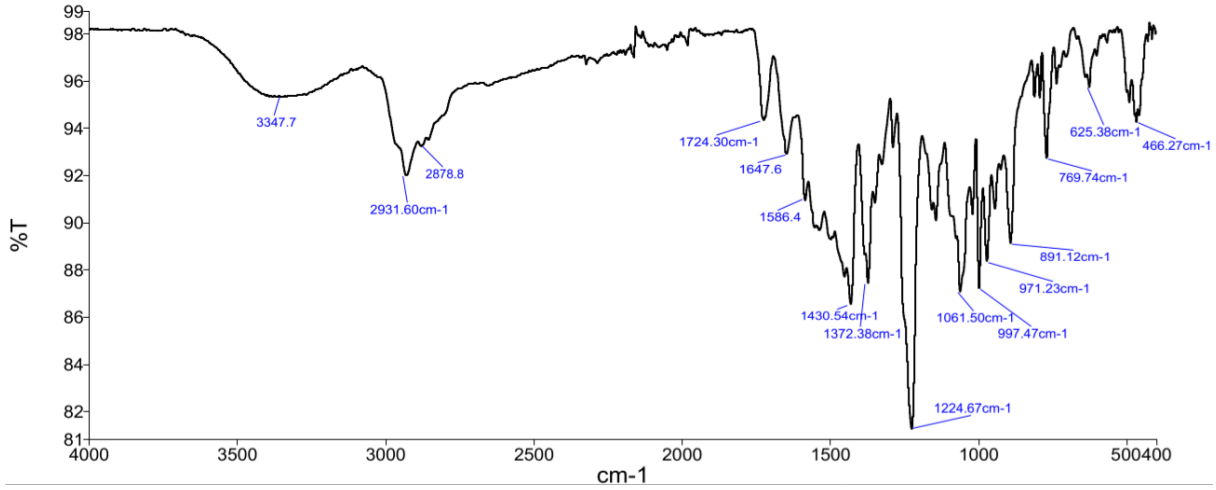

Appendix 43 - ATR-FTIR spectrum of [$N_{1,1,8,2OH}$][Rif].

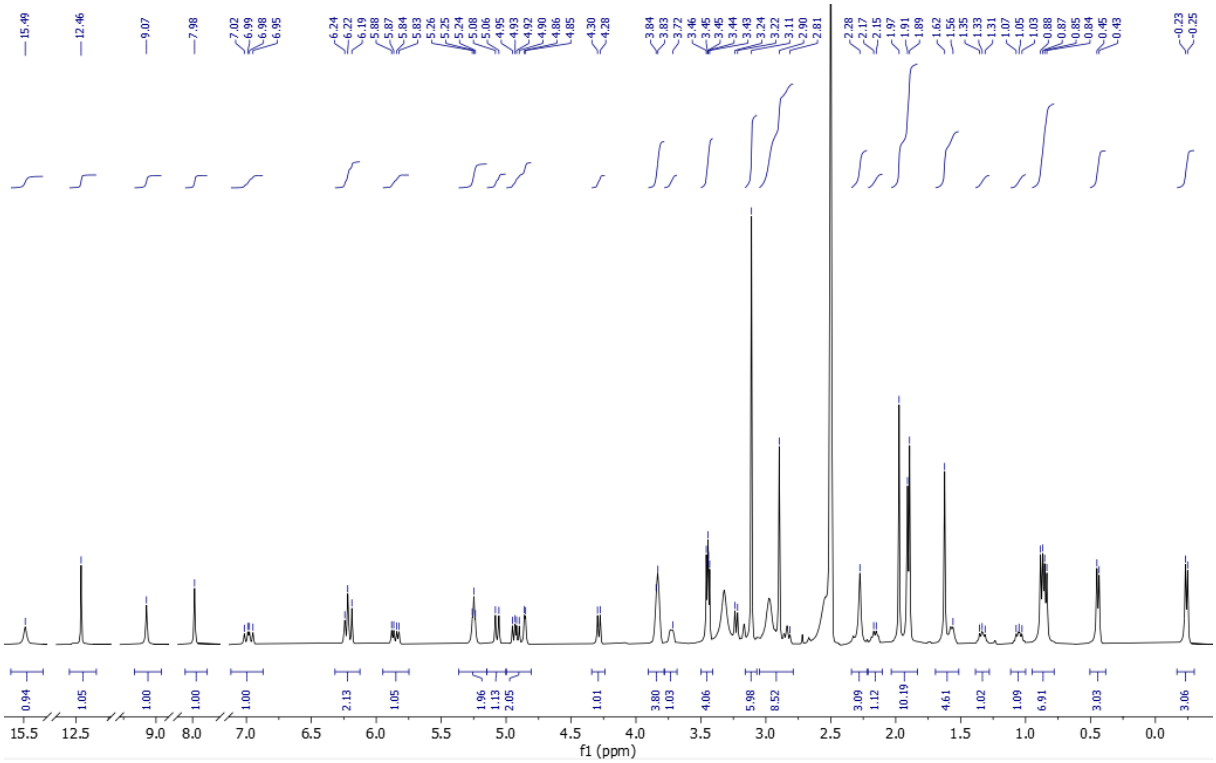

Appendix 44 - ^{1}H NMR spectrum of [N$_{1,1,2OH,2OH}$][Rif] in DMSO-*d6*.

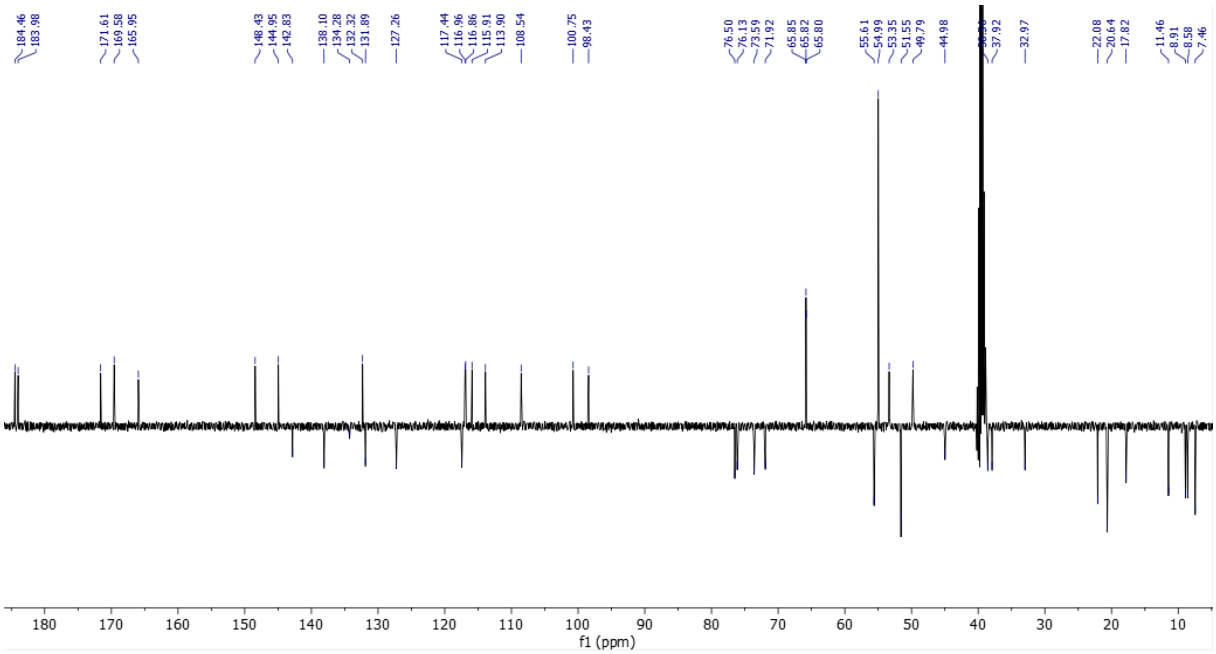

Appendix 45 - ^{13}C NMR spectrum of [N$_{1,1,2OH,2OH}$][Rif] in DMSO-*d6*.

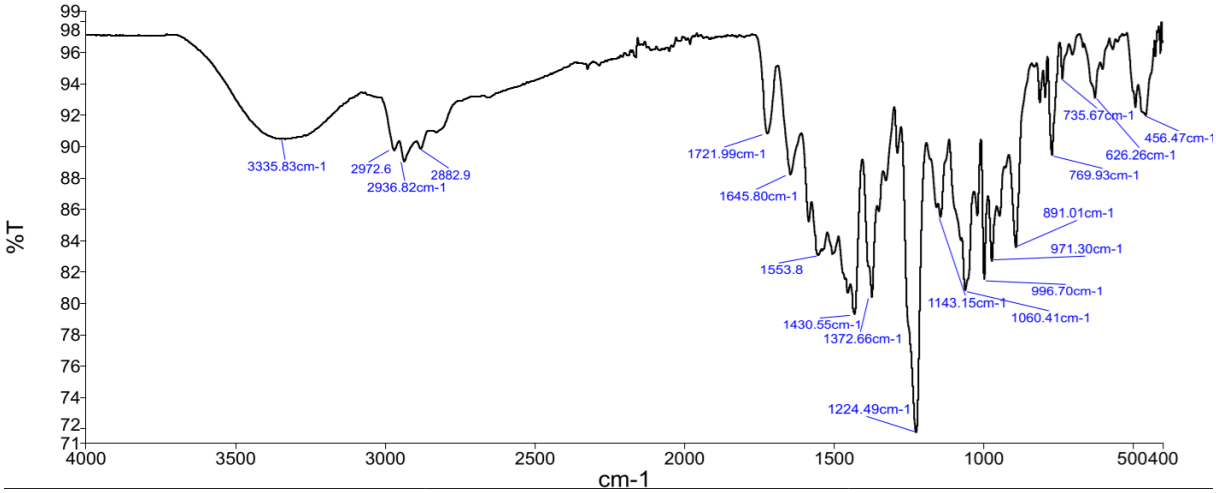

Appendix 46 - ATR-FTIR spectrum of [$N_{1,1,2OH,2OH}$][Rif].

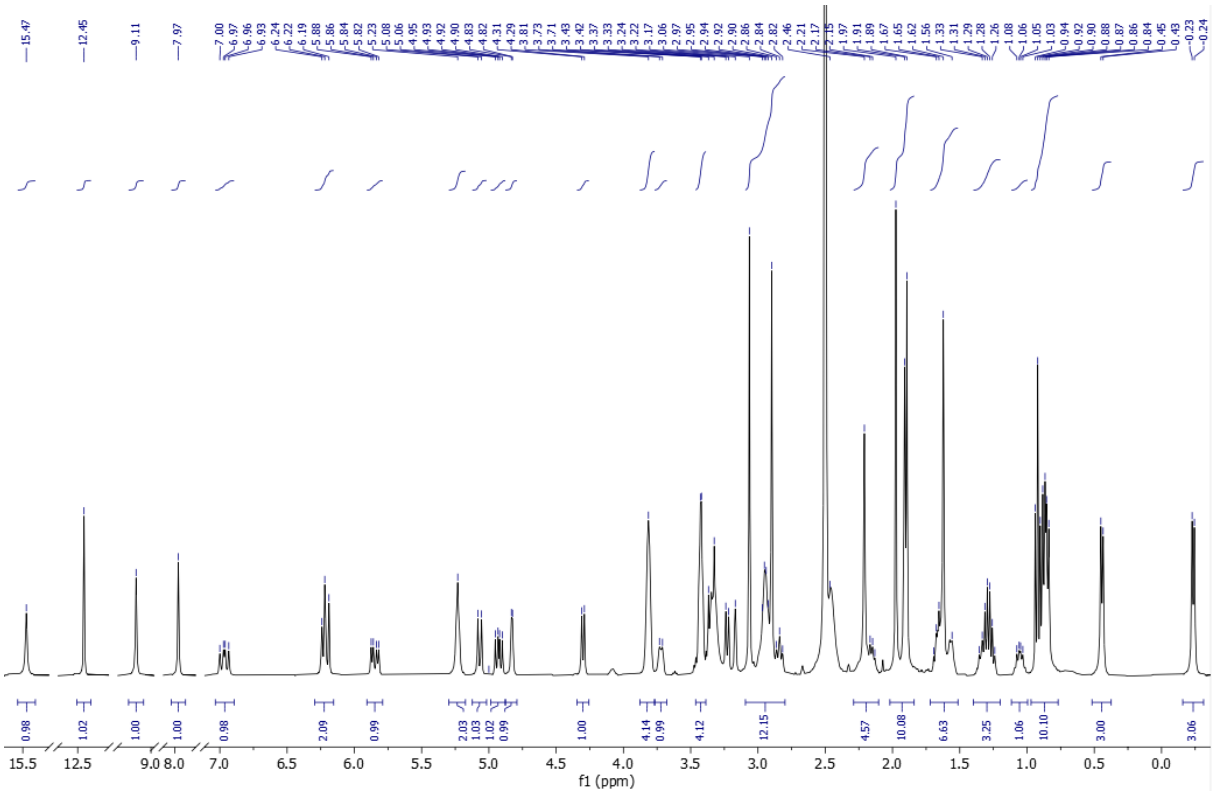

Appendix 47 - ^{1}H NMR spectrum of [$N_{1,4,2OH,2OH}$][Rif] in DMSO-*d*$_6$.

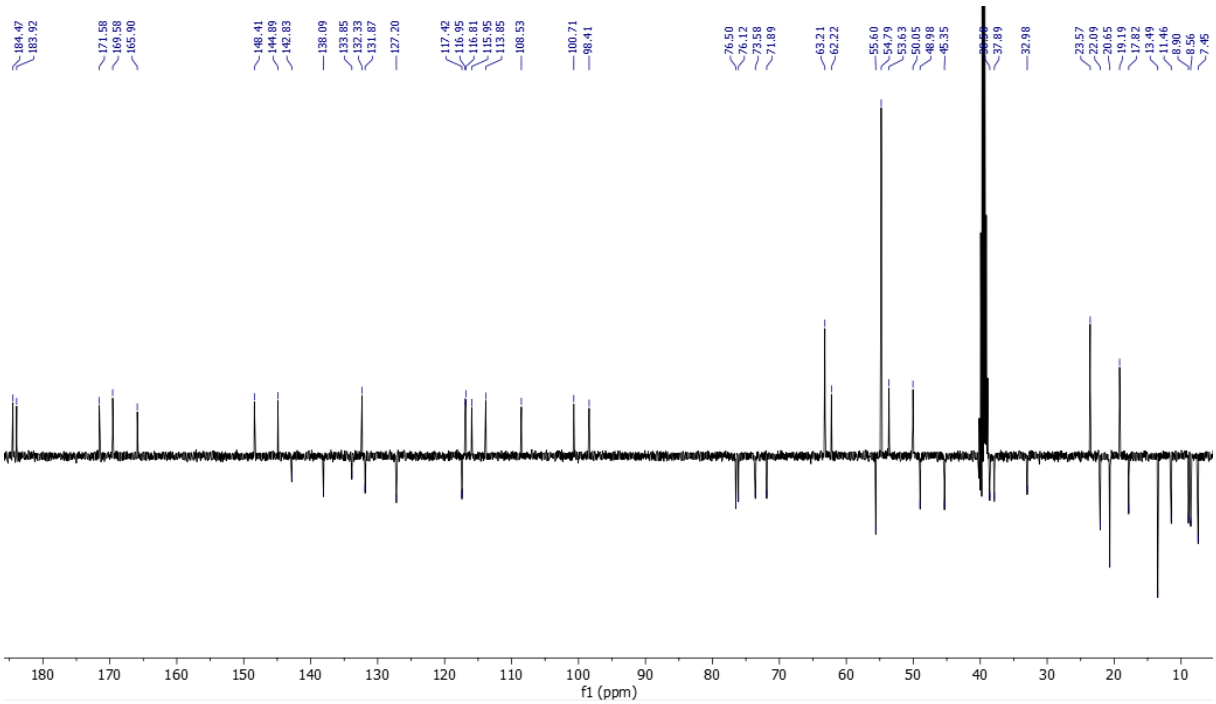

Appendix 48 - ^{13}C NMR spectrum of [$N_{1,4,2OH,2OH}$][Rif] in DMSO-*d_6*.

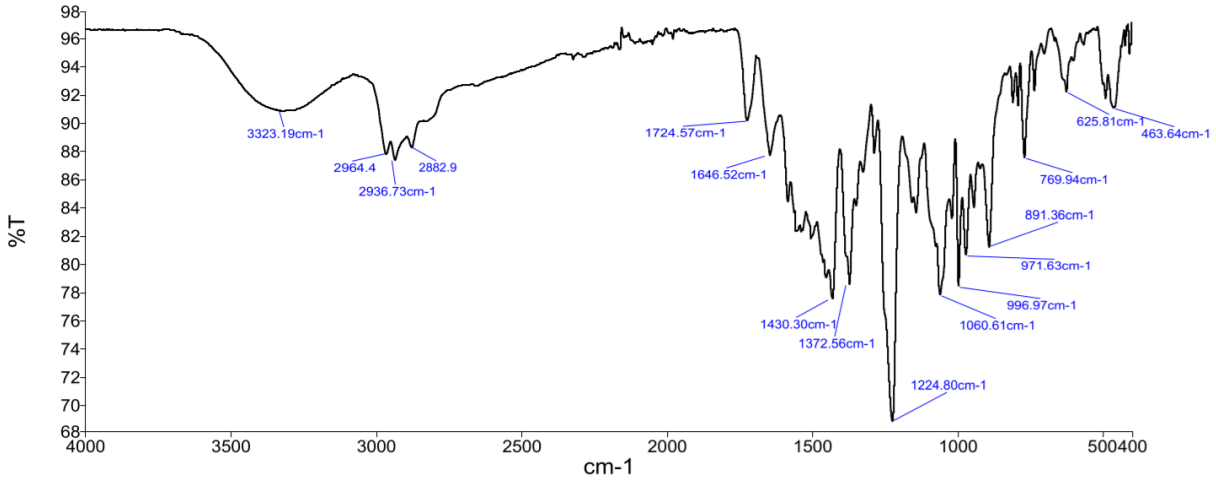

Appendix 49 - ATR-FTIR spectrum of [$N_{1,4,2OH,2OH}$][Rif].

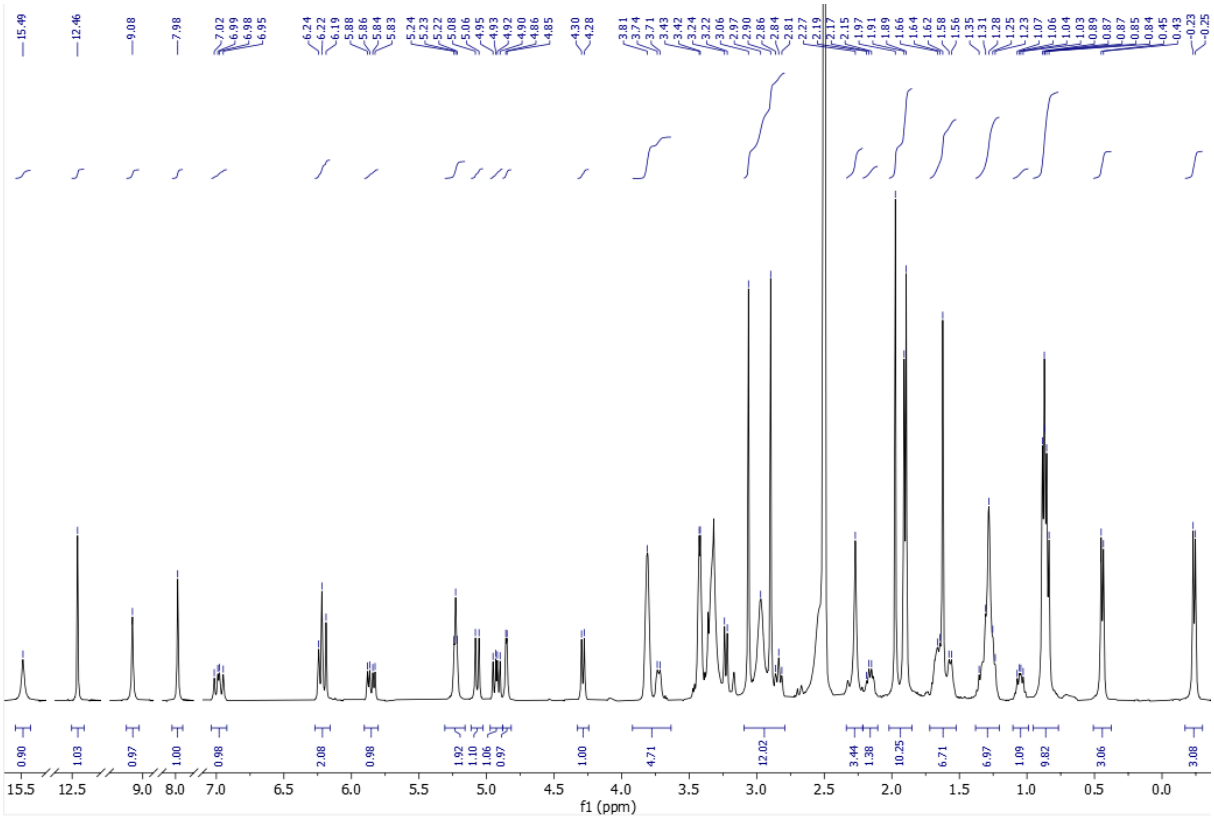

Appendix 50 - ^{1}H NMR spectrum of [N$_{1,6,2OH,2OH}$][Rif] in DMSO-*d6*.

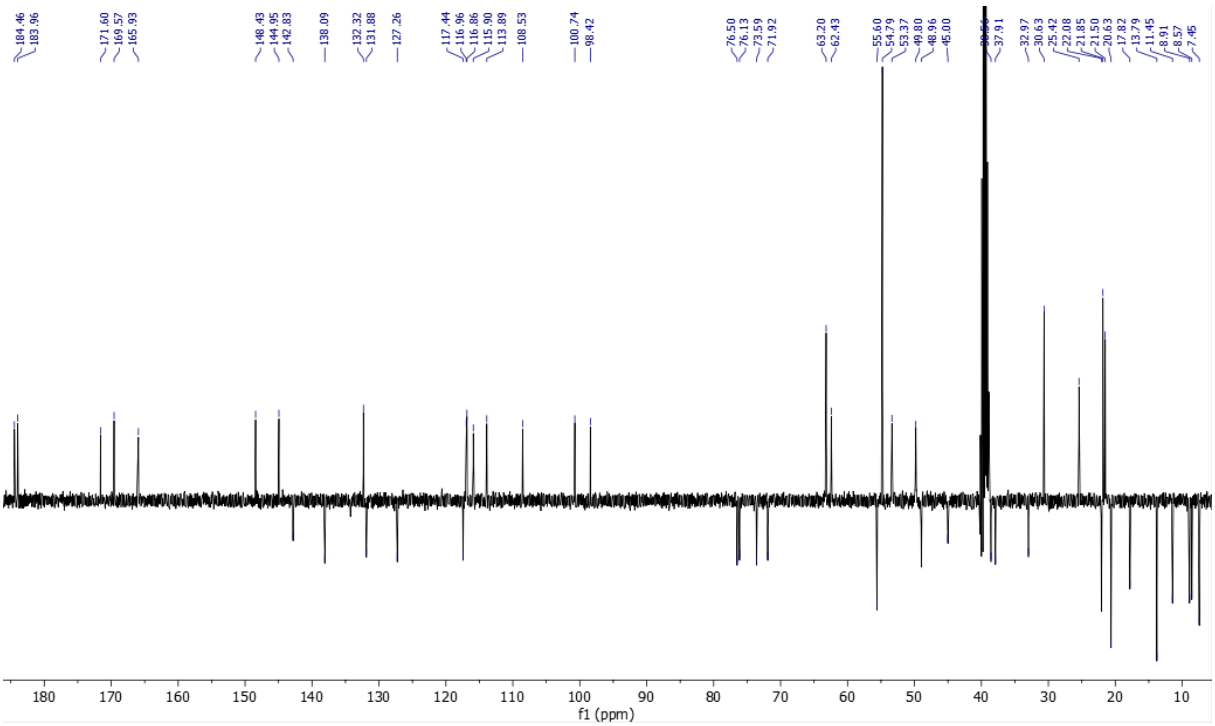

Appendix 51 - ^{1}H NMR spectrum of [N$_{1,6,2OH,2OH}$][Rif] in DMSO-d6.

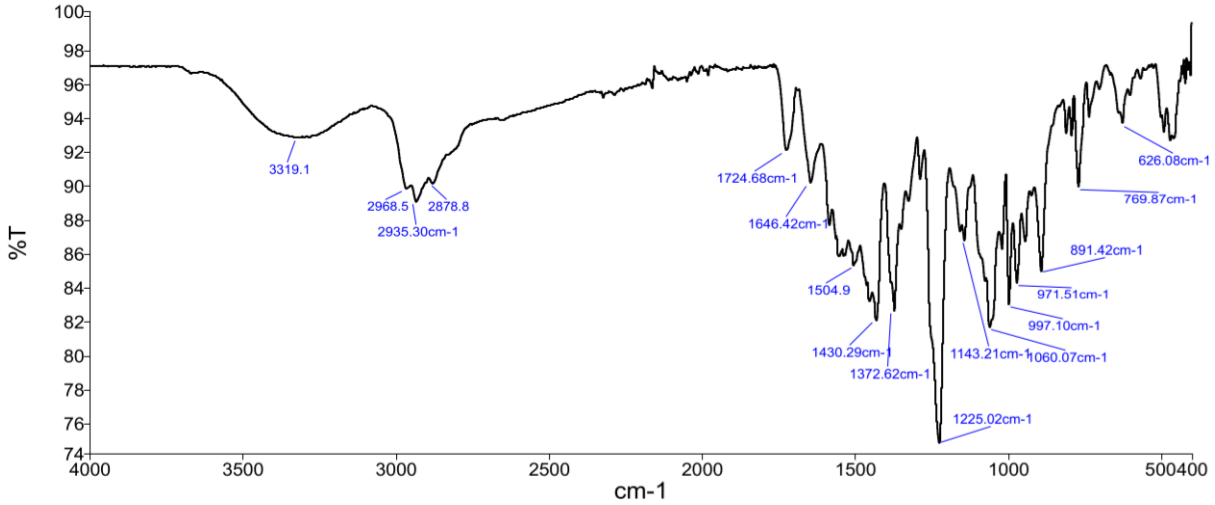

Appendix 52 - ATR-FTIR spectrum of [N1,6,2OH,2OH][Rif].

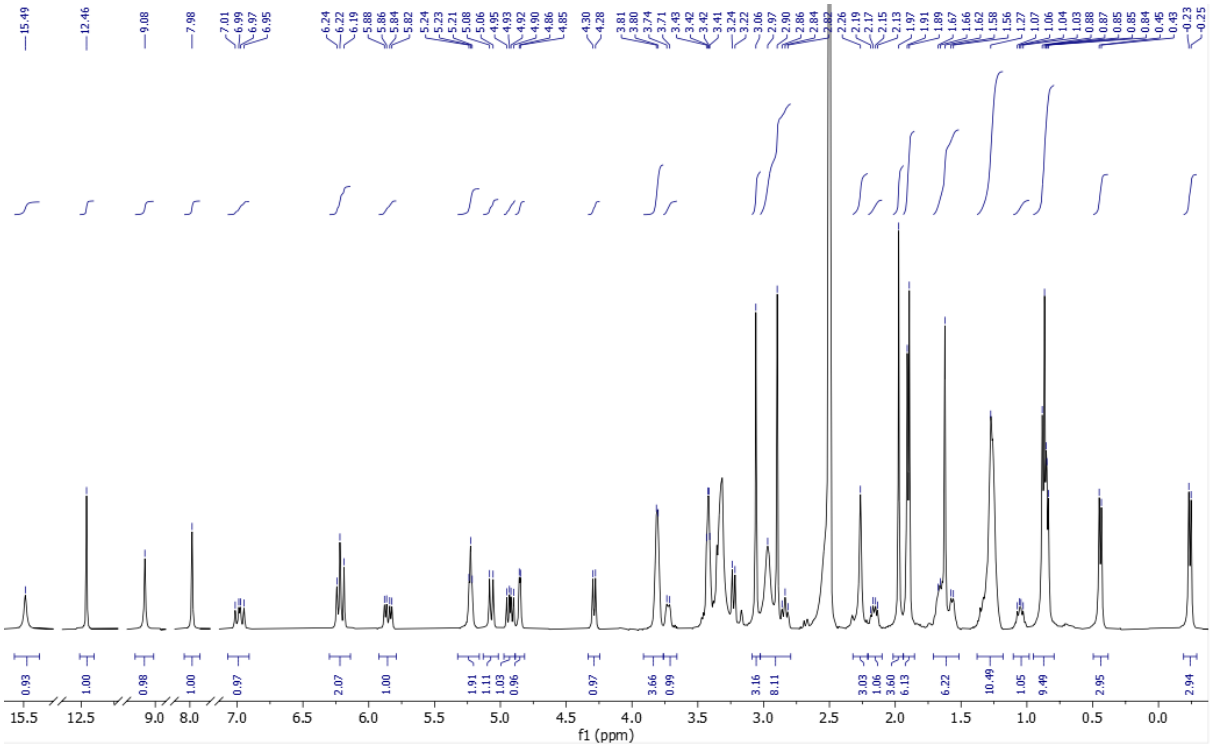

Appendix 53 - ^{1}H NMR spectrum of [N1,8,2OH,2OH][Rif] in DMSO-*d6*.

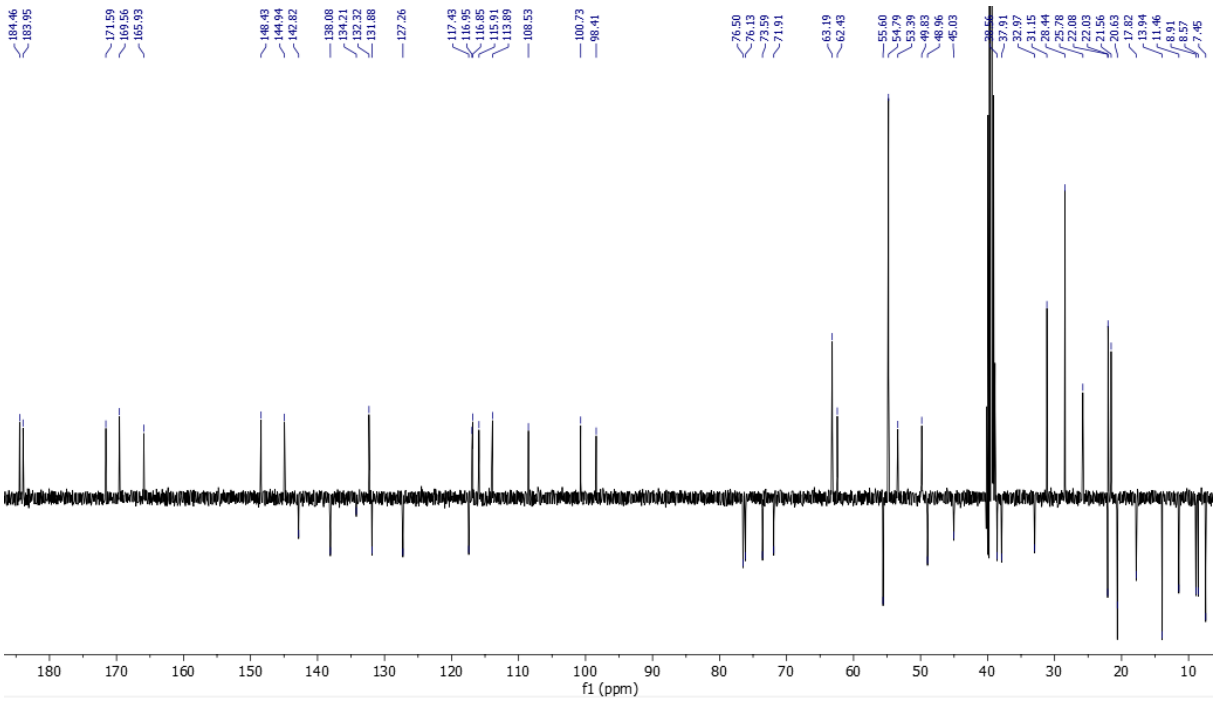

Appendix 54 - ^{13}C NMR spectrum of [N1,8,2OH,2OH][Rif] in DMSO-*d6*.

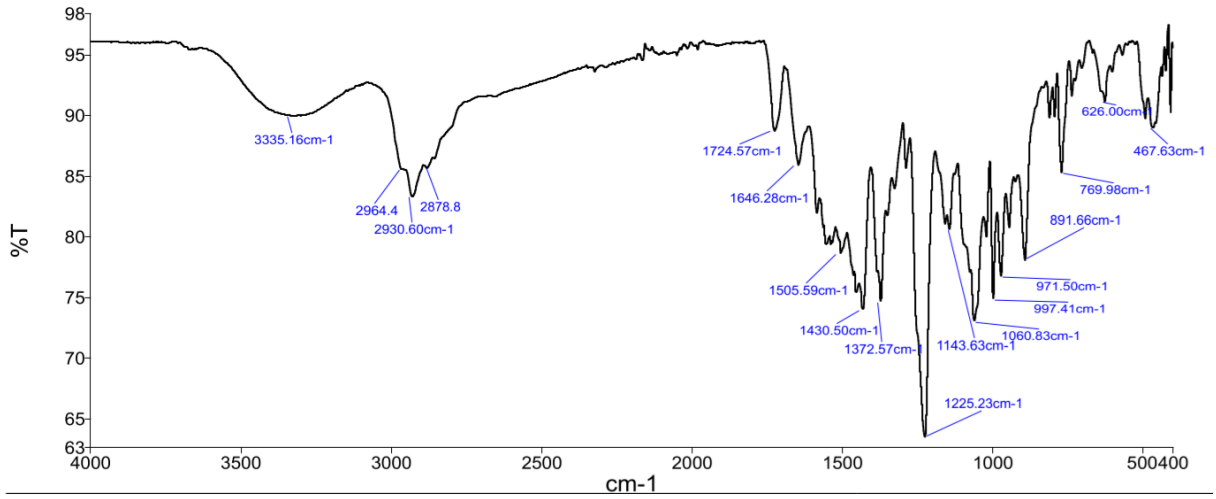

Appendix 55 - ATR-FTIR spectrum of [N1,8,2OH,2OH][Rif].

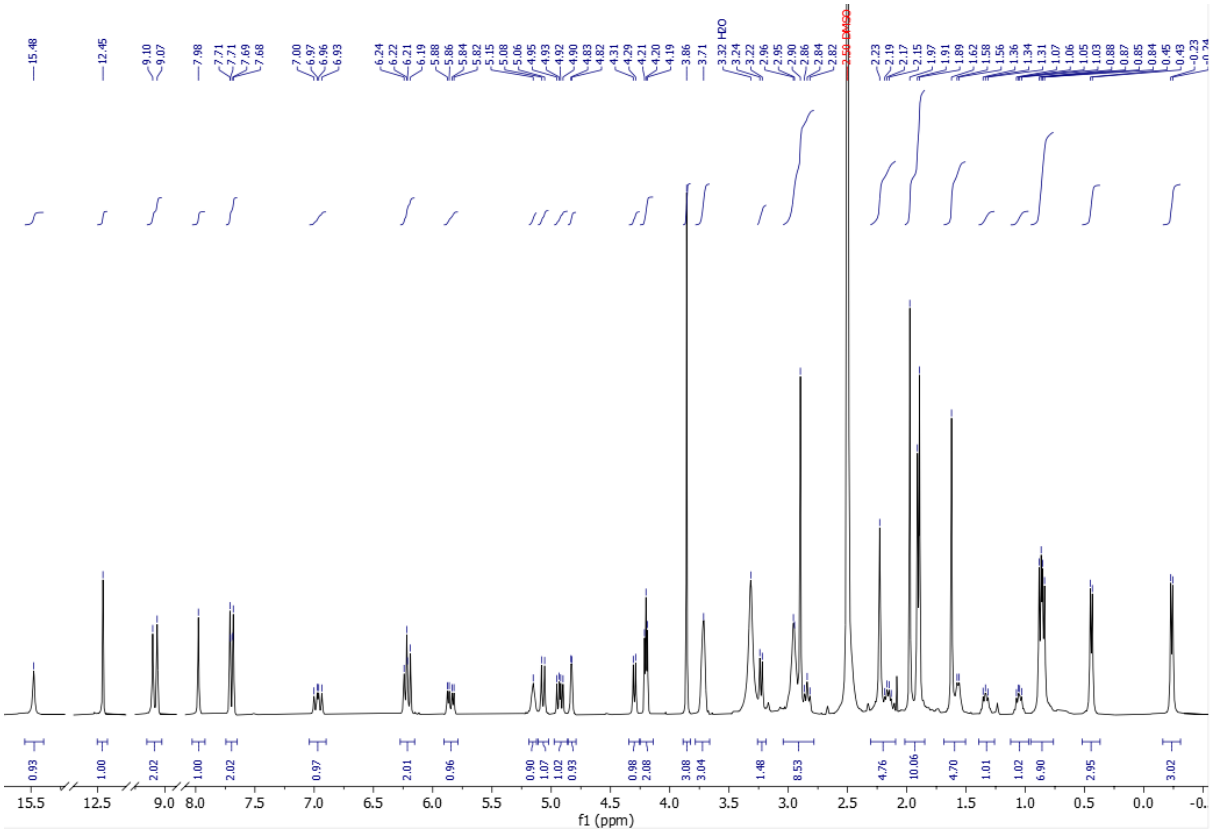

Appendix 56 - ^{1}H NMR spectrum of [C$_2$OHMIM][Rif] in DMSO-*d$_6$*.

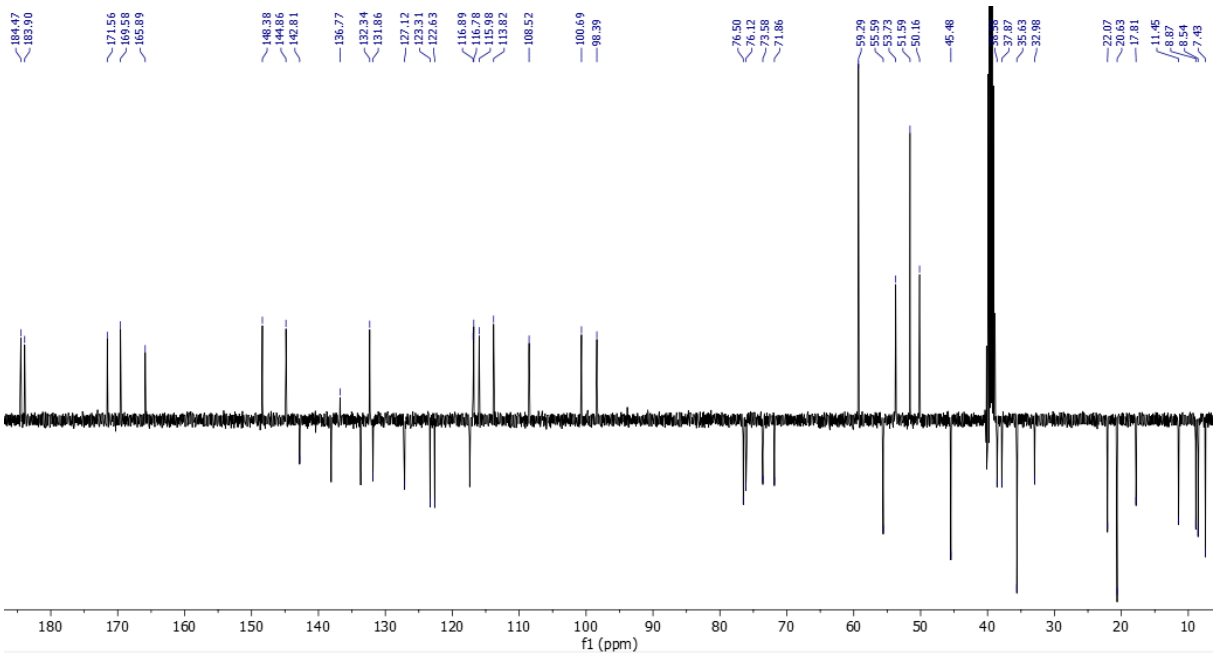

Appendix 57 – ^{13}C NMR spectrum of [C$_2$OHMIM][Rif] in DMSO-*d$_6$*.

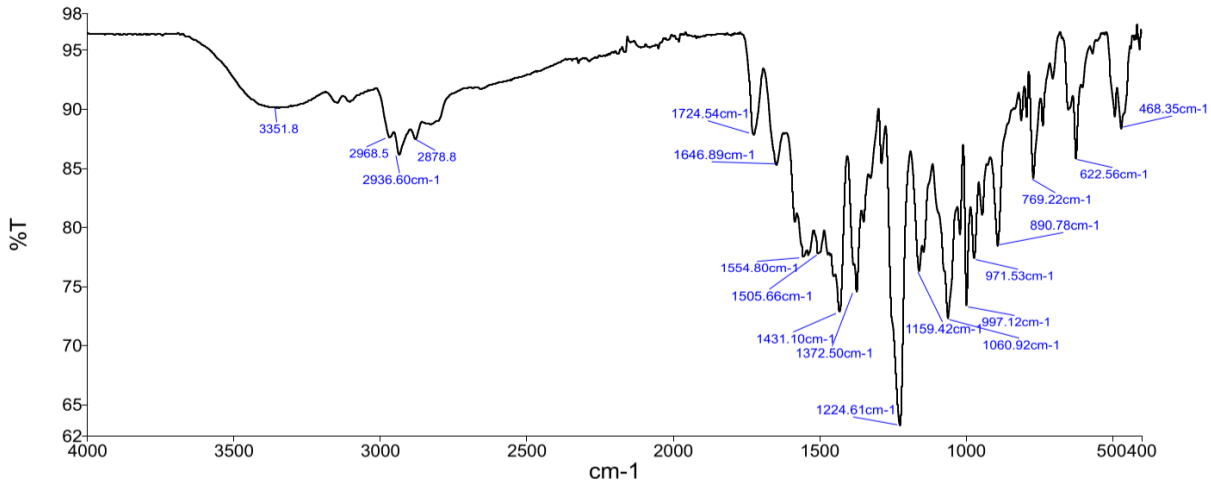

Appendix 58 – ATR-FTIR spectrum of [C2OHMIM][Rif].

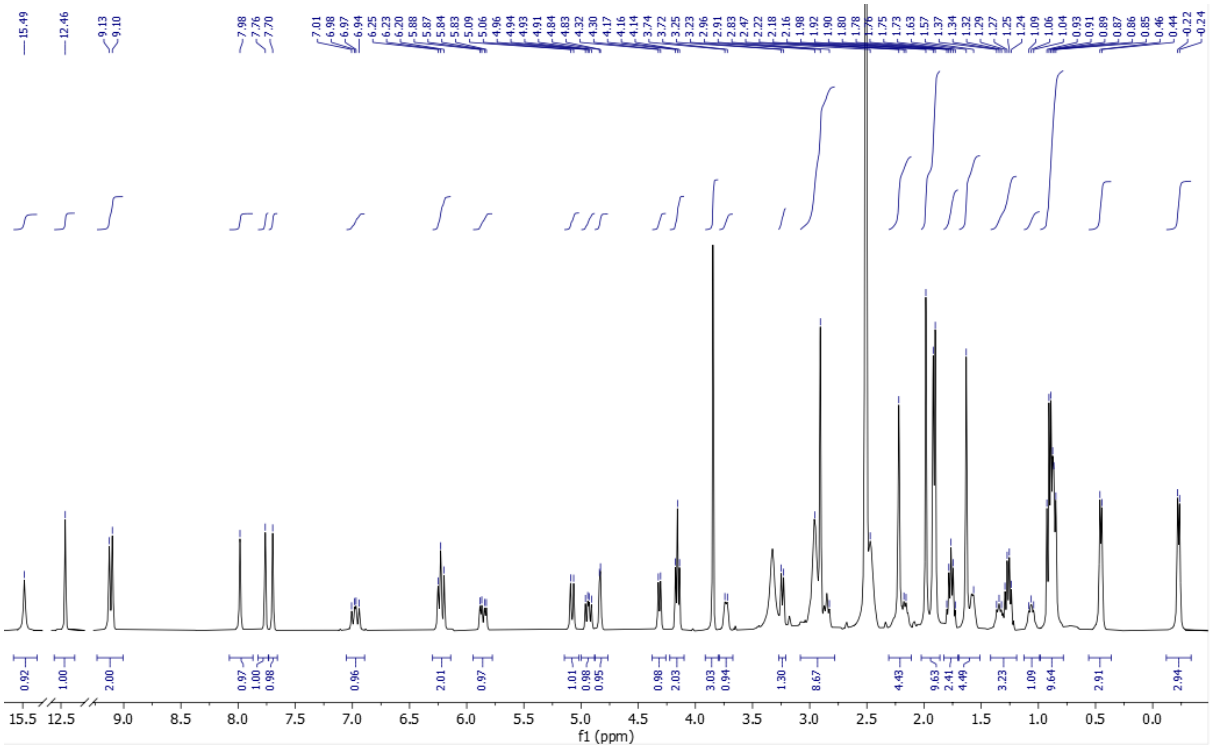

Appendix 59 - ^{1}H NMR spectrum of [C4MIM][Rif] in DMSO-*d6*.

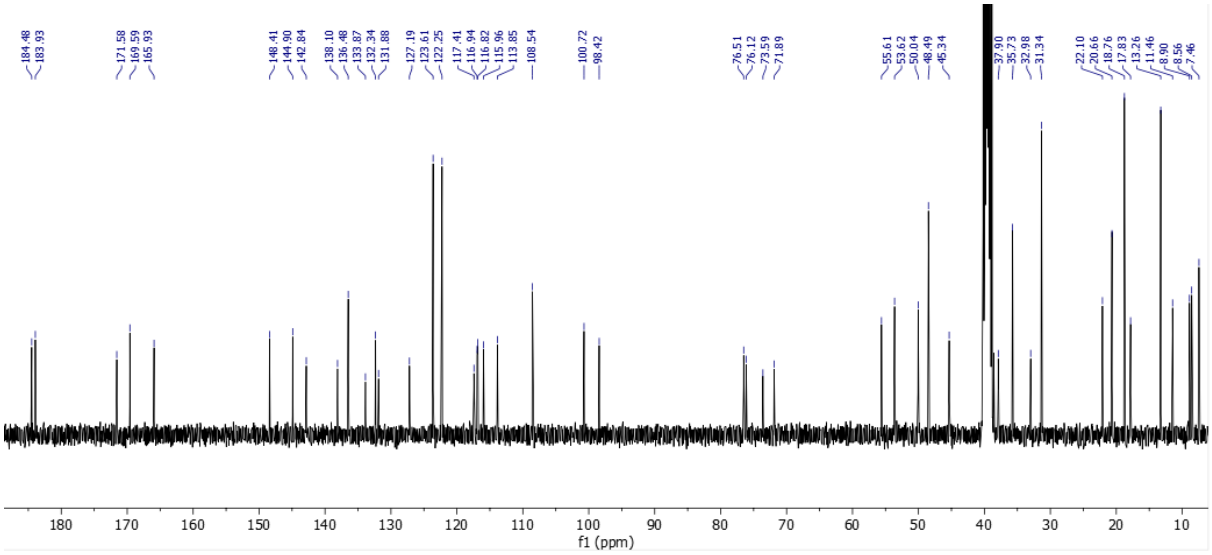

Appendix 60 - ^{13}C NMR spectrum of [C_4MIM][Rif] in DMSO-*d_6*.

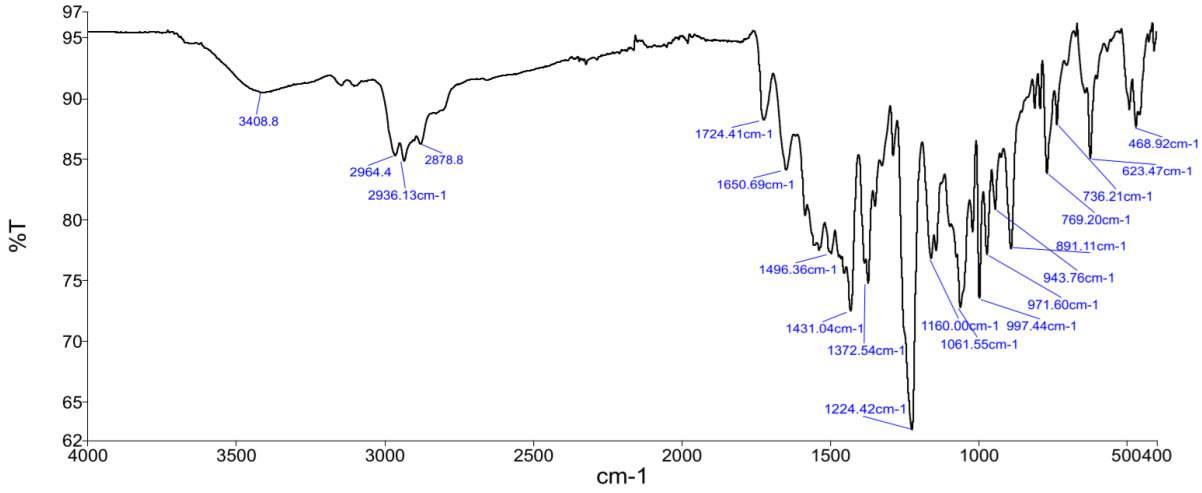

Appendix 61 - ATR-FTIR spectrum of [C_4MIM][Rif].

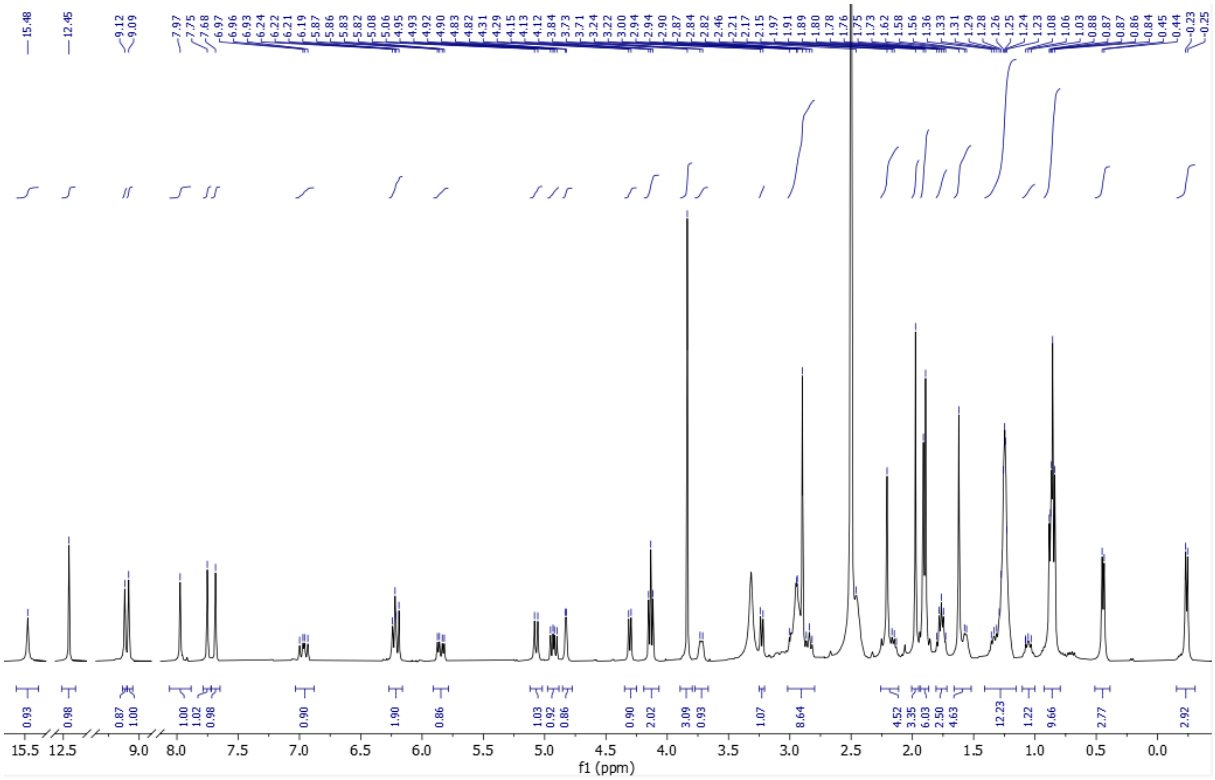

Appendix 62 - ^{1}H NMR spectrum of [C$_8$MIM][Rif] in DMSO-*d$_6$*.

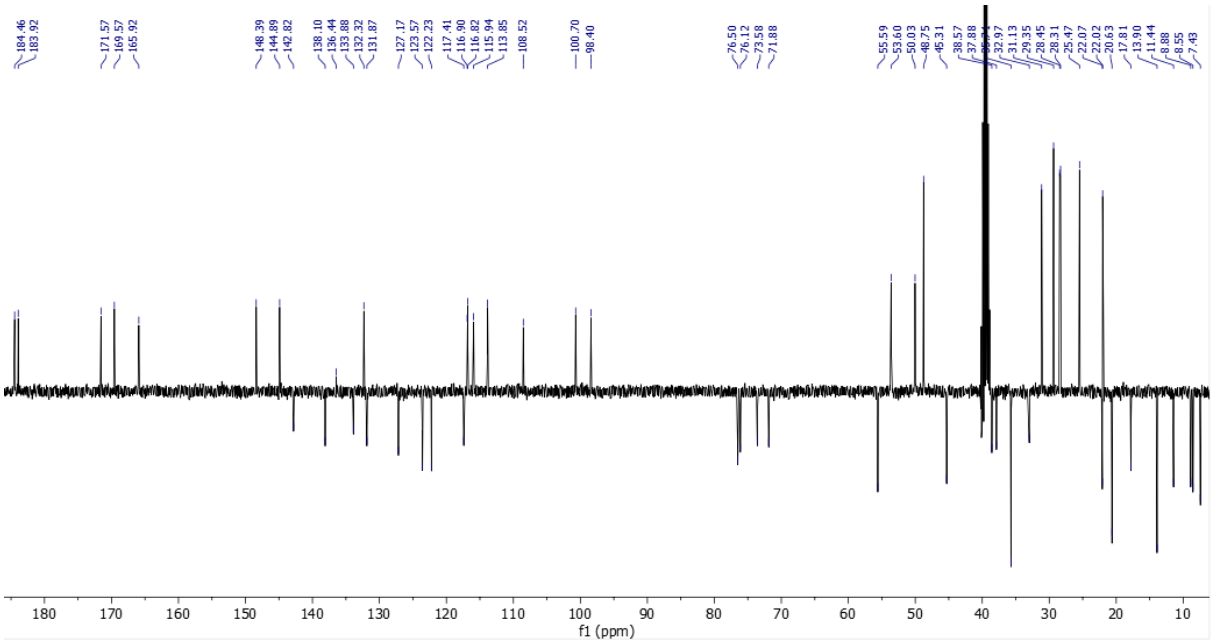

Appendix 63 - ^{13}C NMR spectrum of [C$_8$MIM][Rif] in DMSO-*d$_6$*.

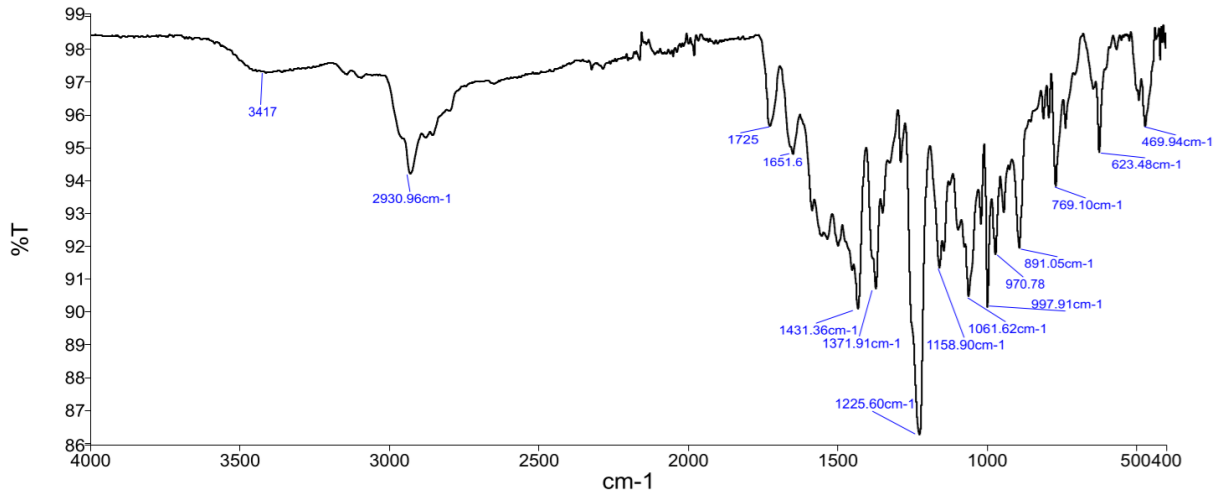

Appendix 64 - ATR-FTIR spectrum of [C_8MIM][Rif].

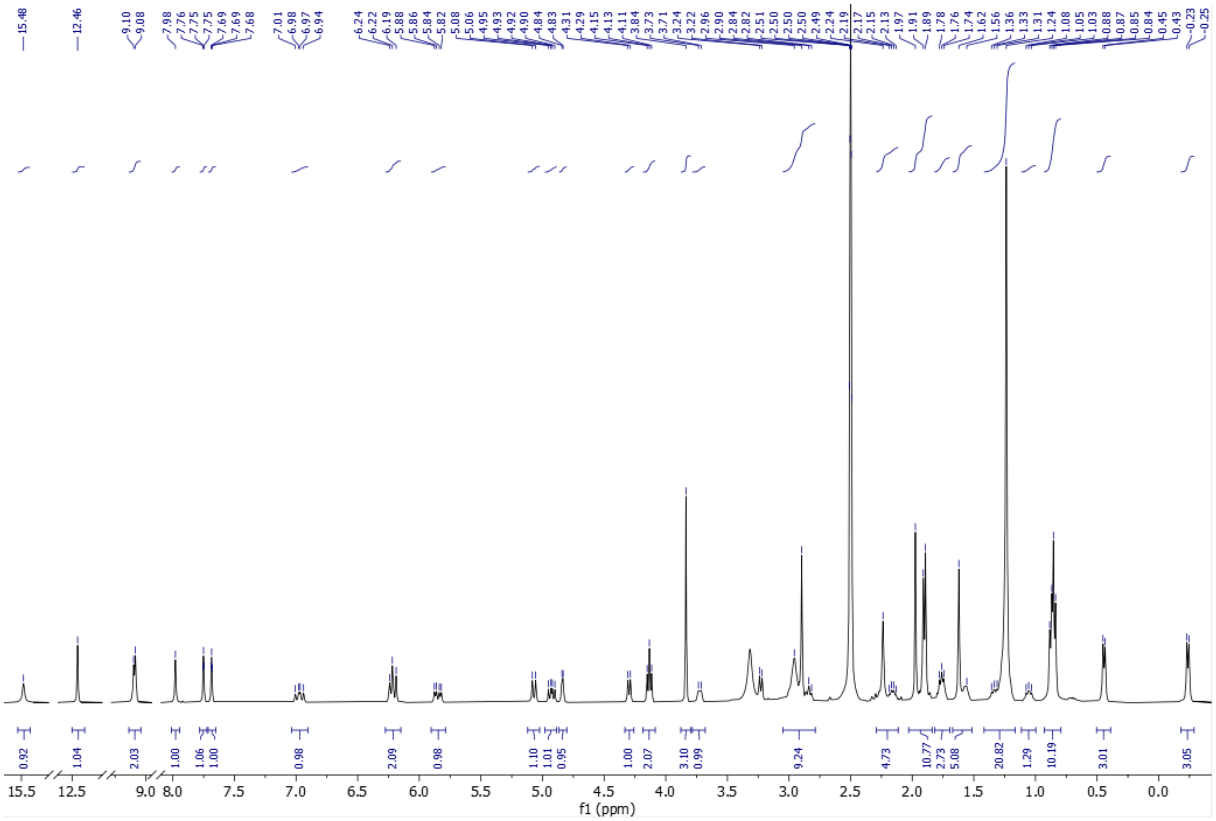

Appendix 65 - ^{1}H NMR spectrum of [C_{12}MIM][Rif] in DMSO-*d6*.

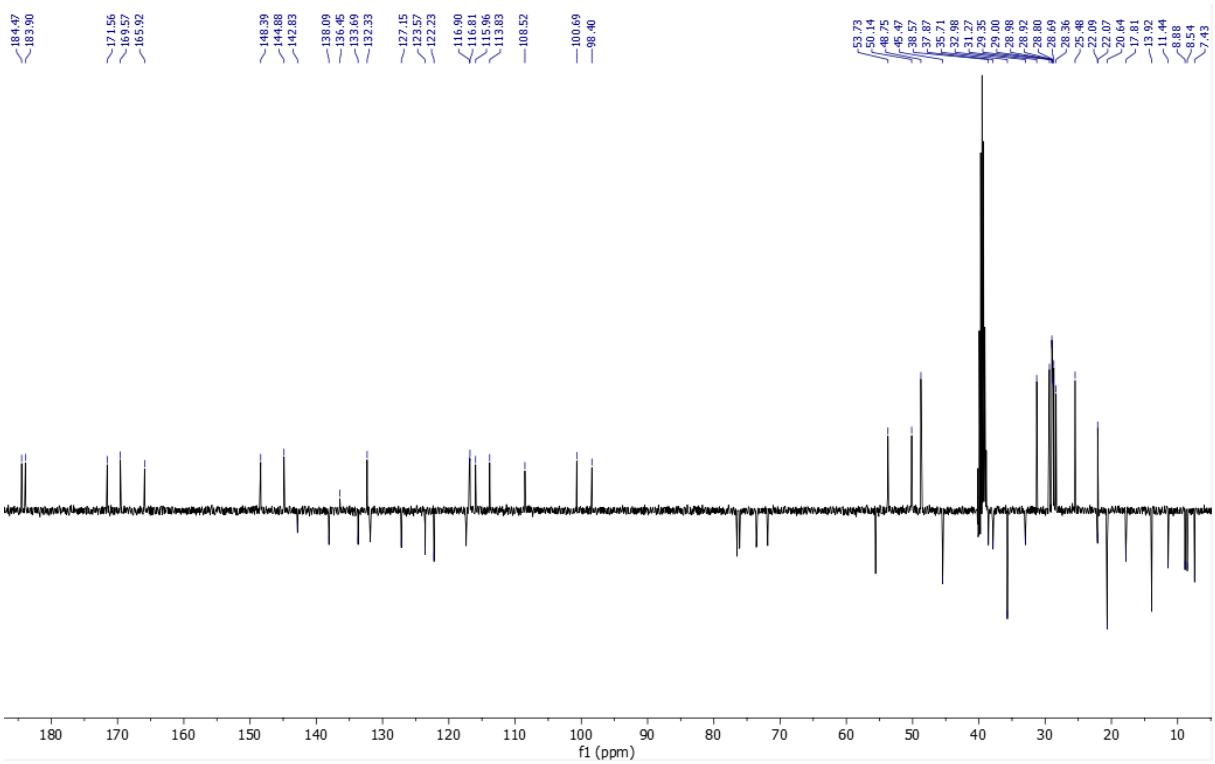

Appendix 66 – ^{13}C NMR spectrum of [C_{12}MIM][Rif] in DMSO-*d6*.

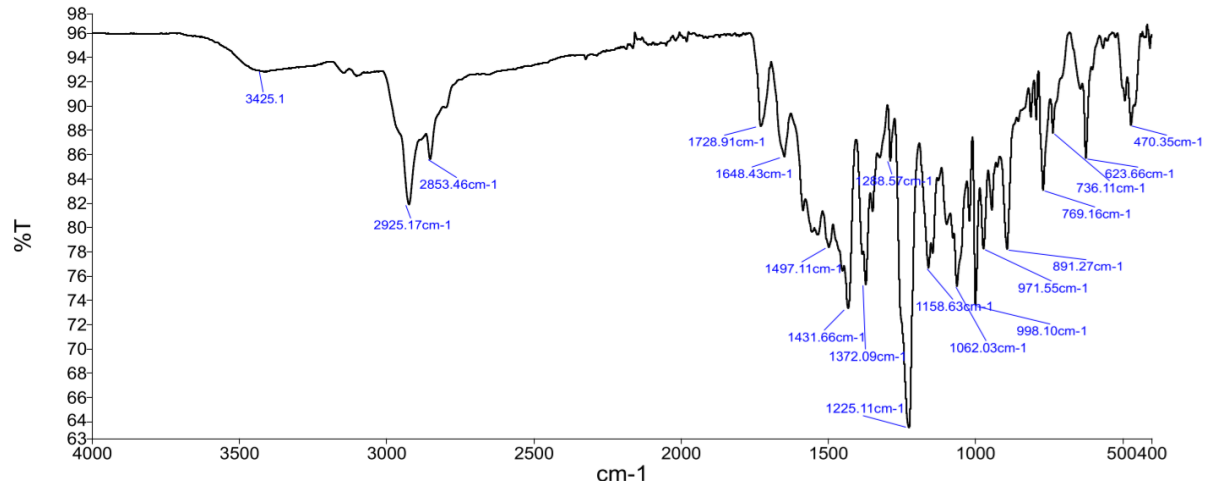

Appendix 67 - ATR-FTIR spectrum of [C_{12}MIM][Rif].

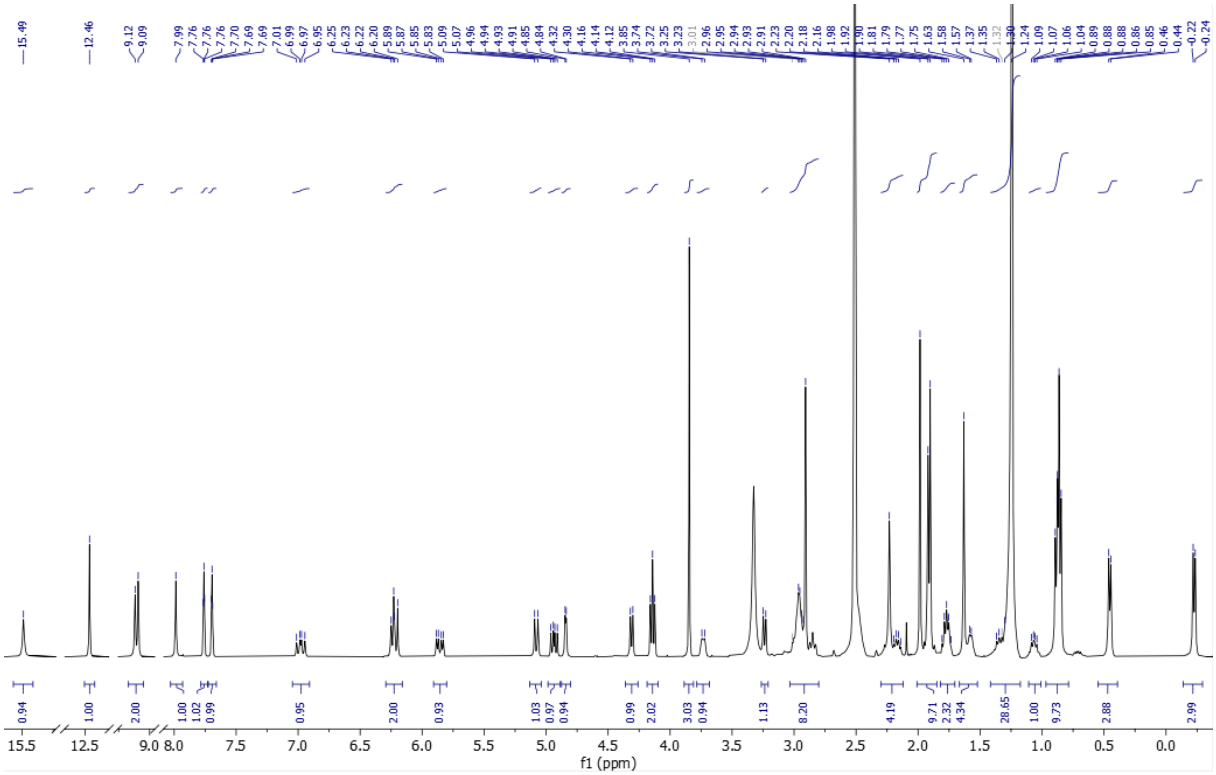

Appendix 68 - ^{1}H NMR spectrum of [C_{16}MIM][Rif] in DMSO-*d_6*.

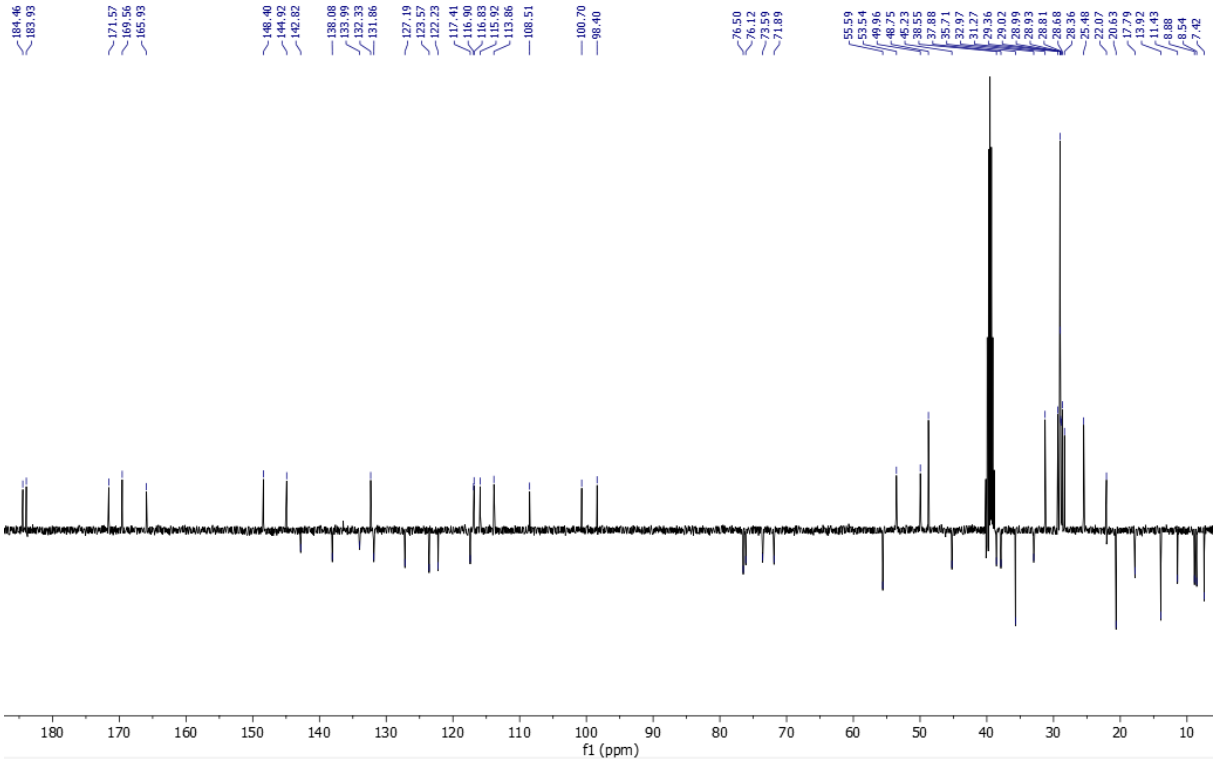

Appendix 69 – ^{13}C NMR spectrum of [C_{16}MIM][Rif] in DMSO-*d_6*.

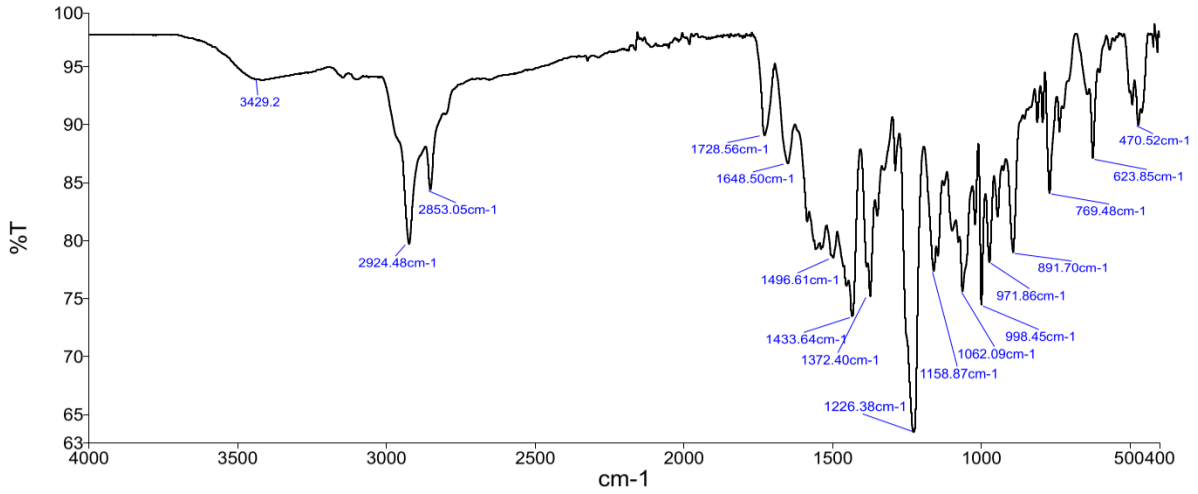

Appendix 70 - ATR-FTIR spectrum of [C_{16}MIM][Rif].

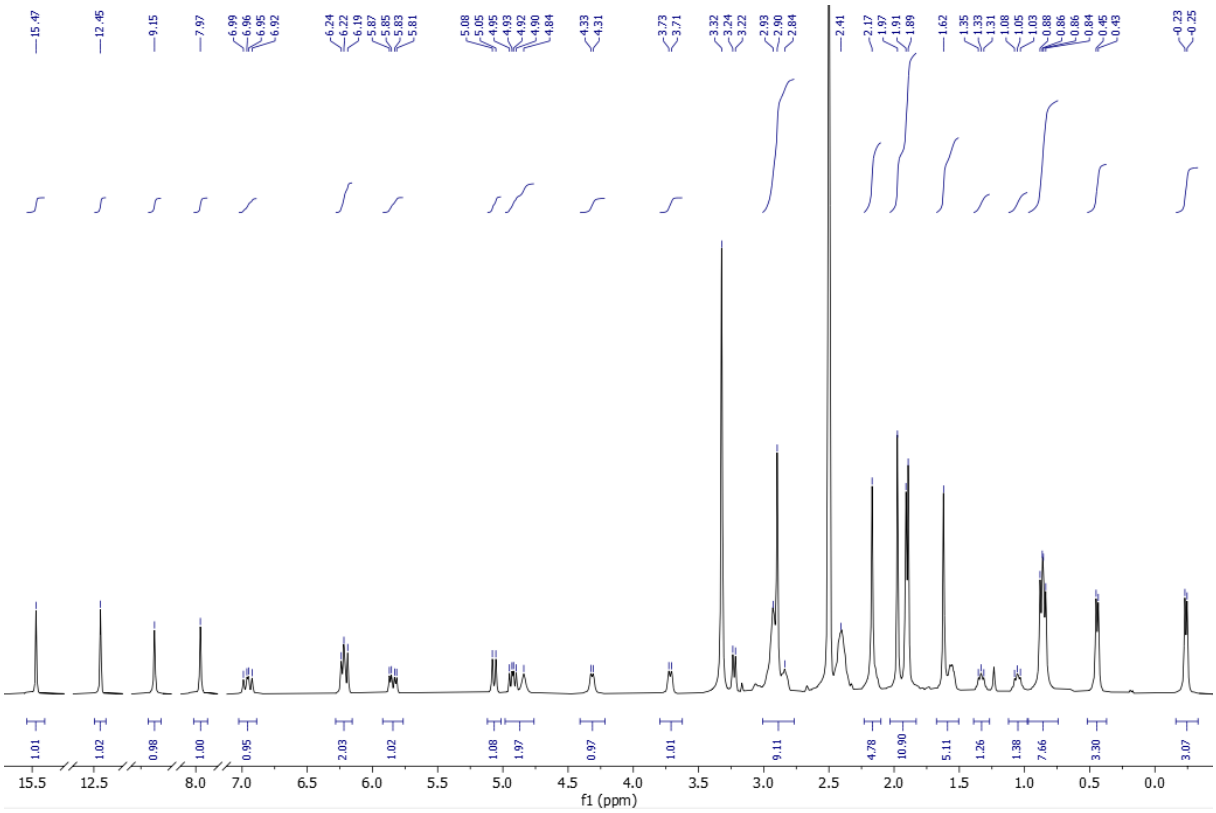

Appendix 71 - ^{1}H NMR spectrum of Na[Rif] in DMSO-*d6*.

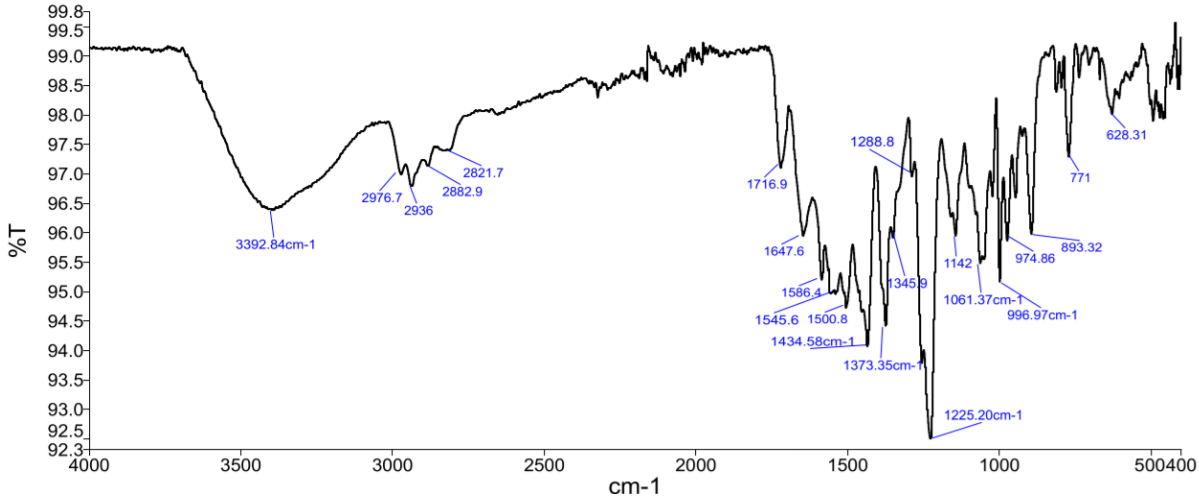

Appendix 72 - ATR-FTIR spectrum of Na[Rif].

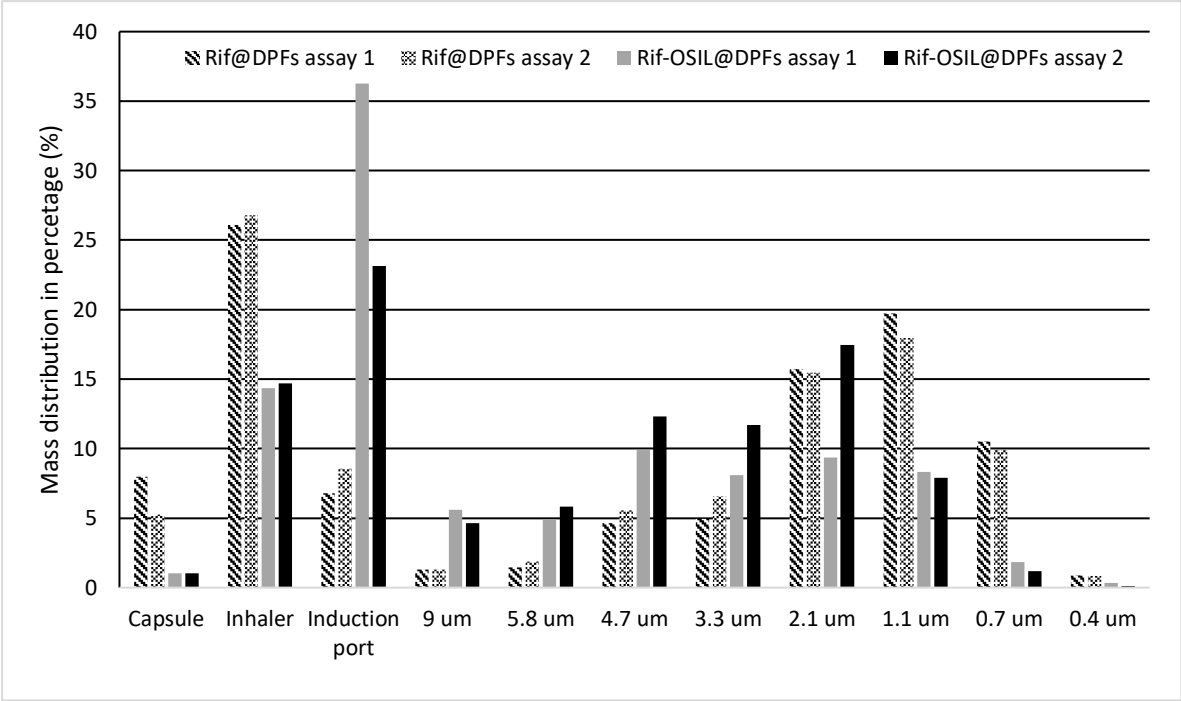

Appendix 73 - ACI mass distribution results.